

For Reference

NOT TO BE TAKEN FROM THIS ROOM

For Reference

NOT TO BE TAKEN FROM THIS ROOM

Ex libris
UNIVERSITATIS
ALBERTAE NSIS



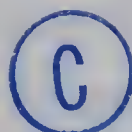
THE UNIVERSITY OF ALBERTA

SOME STUDIES ON TURBULENT WALL JETS

IN HYDRAULIC ENGINEERING

by

KANAKATTI SUBRAMANYA



A THESIS

SUBMITTED TO THE FACULTY OF GRADUATE STUDIES

IN PARTIAL FULFILMENT OF THE REQUIREMENTS FOR THE DEGREE OF

DOCTOR OF PHILOSOPHY

DEPARTMENT OF CIVIL ENGINEERING

EDMONTON, ALBERTA

OCTOBER, 1967

UNIVERSITY OF ALBERTA
FACULTY OF GRADUATE STUDIES

The undersigned certify that they have read, and recommend to the Faculty of Graduate Studies for acceptance, a thesis entitled "SOME STUDIES ON TURBULENT WALL JETS IN HYDRAULIC ENGINEERING" submitted by Kanakatti Subramanya, in partial fulfilment of the requirements for the degree of Doctor of Philosophy.

ABSTRACT

A few simplified flow situations from submerged outlets have been studied experimentally as an initial step towards understanding the mechanics of submerged flow from outlets. These are, the water wall jet, the reattached wall jet due to submerged flow from outlets situated over a drop, and the flow from outlets situated on the bed at a sudden symmetrical expansion in the width of a channel. The classical wall jet has been chosen as the basic flow model. In each of these problems the velocity profiles have been analysed for similarity and when similarity exists the variation of the length and velocity scales have been studied. The bed shear stress variation data have been obtained and correlated with the flow parameters. Some information on the boundary layer characteristics has also been obtained.

In connection with the study of the flow from finite size outlets on the bed at sudden width expansions, a characteristic length of the outlet has been defined and is found to be very useful in correlating the various data. This length parameter is found to be useful in correlating the available data for the maximum velocity decay of three-dimensional free jets also (Appendix B).

The gross characteristics of two types of hydraulic jumps occurring at a sudden symmetrical expansion in a channel have also been studied in detail and interesting results have been obtained.

The velocity and pressure field immediately below a deeply submerged sluice gate have been studied in Appendix A. A vena contracta

for the submerged flow has been defined and studied.

The profile of the hydraulic jump in a rectangular channel has been analysed for similarity and a single non-dimensional similarity profile, with simple scales, has been obtained, in Appendix C.

ACKNOWLEDGMENTS

The author wishes to express his sincere thanks to Professor T. Blench and Professor N. Rajaratnam for their guidance, advice and encouragement throughout the course of this work. Thanks are due to Professor A. W. Peterson for his keen interest and help in the construction of the test facilities.

The assistance of the Hydraulics laboratory staff in the construction of the apparatus is gratefully appreciated.

The author is grateful to the Canadian Commonwealth Scholarship and Fellowship Committee for providing him with a scholarship to pursue this study, and to the National Research Council of Canada for the financial support of this work.

TABLE OF CONTENTS

	Page
Title Page	i
Approval Sheet	ii
Abstract	iii
Acknowledgements	v
Table of Contents	vi
List of Tables	vii
List of Figures	viii
List of Symbols	xii
CHAPTER I INTRODUCTION	1
CHAPTER II EXPERIMENTAL FACILITIES	10
CHAPTER III STUDY OF WATER WALL JET	16
CHAPTER IV REATTACHED WALL JET	34
CHAPTER V WALL JETS ISSUING INTO WIDER CHANNELS	67
CHAPTER VI HYDRAULIC JUMPS BELOW ABRUPT SYMMETRICAL EXPANSIONS	91
CHAPTER VII CONCLUSIONS AND RECOMMENDATIONS	126
LIST OF REFERENCES	130
APPENDIX A FLOW IMMEDIATELY BELOW A SUBMERGED SLUICE GATE	A-1
APPENDIX B THREE-DIMENSIONAL FREE JETS	B-1
APPENDIX C PROFILE OF THE HYDRAULIC JUMP	C-1
APPENDIX D EXPERIMENTAL DATA	D-1

LIST OF TABLES

TABLE		Page
III-1	Classical Wall Jet--Coordinates of the Similarity Profile	17
III-2	Water Wall Jet--Summary of Data	20
IV -1	Reattaching Wall Jet (Nozzle Outlet)--Summary of Experimental Data	36
IV -2	Reattaching Wall Jet (Sluice Gate Opening)--Summary of Experimental Data	43
V -1	Wall Jets in Wider Channels--Summary of Experimental Data	70
A -1	Flow Immediately below a Submerged Sluice Gate--Summary of Experimental Data	A-3
A -2	Flow Immediately below a Submerged Sluice Gate--Velocity Profile Characteristics	A-10
A -3	Flow Immediately below a Submerged Sluice Gate--Boundary Layer Characteristics	A-11
C -1	Coordinates of the Similarity Profile of the Hydraulic Jump	C-3
D -1	Water Wall Jet Data--Velocity Profile Characteristics	D-1
D -2	Water Wall Jet Data--Variation of C_f	D-2
D -3	Reattached Wall Jet (Nozzle Outlet)--Velocity Profile Characteristics	D-3
D -4	Reattached Wall Jet (Sluice Gate Opening)--Velocity Profile Characteristics	D-4
D -5	Reattached Wall Jet--Bed Shear Stress Distribution Data	D-5
D -6	Wall Jets in Wider Channels--Centerline Velocity Distribution Characteristics	D-6
D -7	Experimental Data for R-Jumps	D-9
D -8	Experimental Data for S-Jumps	D-10

LIST OF FIGURES

FIG.		Page
I -1	Definition Sketch of a Wall Jet	9
II -1	Schematic Views of the Experimental Set-Up. Flume A	14
III-1	Velocity Scale for Classical Wall Jet	25
III-2	Length Scale Variation	26
III-3	Typical Velocity Distribution	27
III-4	Similarity Plot for the Water Wall Jet	28
III-5	Decay of Maximum Velocity in Water Wall Jet	29
III-6	Variation of C_f in Water Wall Jet	30
III-7	The Plane Free Jet and Wall Jet	31
III-8	Velocity Distribution	32
III-9	Study of the Velocity Scale	33
III-10	Study of the Length Scale	33
IV -1	Definition Sketch	49
IV -2	Variation of the Length of Eddy (Nozzle Outlet)	50
IV -3(a)	Pressure Coefficient in the Eddying Region	51
IV -3(b)	Pressure Coefficient Contours in the Eddying Region	51
IV -4	A Typical Plot of Pressure Head on the Bed	52
IV -5	Study of the Variation of C_{pm}	52
IV -6	A Typical Velocity Distribution Plot	53
IV -7	Dimensionless Velocity Profiles	54
IV -8	Study of Characteristic Lengths	55
IV -9	Decay of the Maximum Velocity	56

FIG.		Page
IV -10	Variation of the Length Scale	57
IV -11	Bed Shear Stress Plots	58
IV -12	Distribution of the Bed Shear Stress	59
IV -13	Study of the Shear Stress and Length Scales-- Nozzle Outlet	60
IV -14	Typical Velocity Distribution	61
IV -15	Contours of Constant C_p in the Separation Bubble and Impingement Region	62
IV -16	Variation of the Length of the Eddy	62
IV -17	Dimensionless Velocity Plot	63
IV -18	Variation of the Scales	64
IV -19	Bed Shear Stress Distribution	65
IV -20	Study of the Bed Shear Stress	66
V -1	Definition Sketch	78
V -2	Typical Velocity Distribution	79
V -3	Velocity Distribution in the Total Forward Flow	80
V -4(a)	Velocity Distribution--Free Mixing Region	81
V -4(b)	Velocity Distribution--Free Mixing Region	82
V -5	Velocity Distribution--Boundary Layer Region	83
V -6	Velocity Decay Results	84
V -7	Maximum Velocity Decay of Wall Jets in Wider Channels	85
V -8(a)	Length Scale Studies	86
V -8(b)	Length Scale Studies	87
V -9	Boundary Layer Growth	88
V -10	Boundary Shear Stress Studies	89
V -11	Variation of C_f with x/r' for Wall Jet in a Wider Channel	90

FIG.		Page
VI -1	Definition Sketch for R-Jump	108
VI -2	Variation of y_t/y_o with F_o for R-Jump	109
VI -3	Study of Kuznetsov's Parameter K	110
VI -4	Study of Consolidated Shear Coefficient C_s	111
VI -5	Length of Surface Roller of R-Jump	112
VI -6	Study of the Length L_1 of R-Jump	112
VI -7	Definition Sketch for S-Jump	113
VI -8	Typical Bed Pressure Profiles	114
VI -9(a)	Verification of Abramov's Equation	115
VI -9(b)	Verification of Unny's Equation	115
VI -9(c)	Verification of Eq. 6.15	115
VI -10	Study of the Ratio y_t/y_o for S-Jump	116
VI -11	Variation of y_t/r' with F'_o for S-Jumps	117
VI -12	Variation of y_3/r' with F'_o and α	118
VI -13	Length of S-Jump	118
VI -14	Energy Dissipation--S-Jumps	119
VI -15	Relative Energy Loss Studies--S-Jumps	120
VI -16	Typical Velocity Distribution along Centerline	121
VI -17	Velocity Distribution in S-Jumps	122
VI -18	Velocity Scale for S-Jumps	123
VI -19	Length Scale for S-Jumps	124
VI -20	Study of C_f for S-Jumps	125
A -1	(a) Free Flow and (b) Submerged Flow below a Sluice Gate	A-13
A -2	Typical Pressure Distributions	A-14

FIG.		Page
A -3	Generalised Pressure Distribution Plot	A-14
A -4	Excess Pressure on the Bed	A-15
A -5	Typical Velocity Distributions	A-16
A -6	Study of Forward Flow Depth	A-17
A -7	Vena Contracta for Submerged Flow	A-18
A -8	Free Jet Boundary Problem	A-19
A -9	Definition Sketch	A-19
A -10	Velocity Distribution in the Free Mixing Region	A-20
A -11	Study of the Length Scale	A-21
A -12	Spread of the Free Mixing Region	A-22
A -13	Variation of δ_p/x with a/x	A-23
A -14	Variation of y_f/x with a/x	A-23
A -15	Boundary Layer Velocity Distribution	A-24
B -1	Velocity Decay for Turbulent Jets--Conventional Plot	B-4
B -2	Velocity Decay for Turbulent Jets--Alternate Plot	B-5
B -3	Length Scale for Turbulent Jets	B-6
C -1	Definition Sketch	C-6
C -2	Dimensionless Surface Profiles of Hydraulic Jumps in Horizontal Channels (Bakhmeteff and Matzke)	C-7
C -3	Study of Rajaratnam's 1965 Data	C-8
C -4	Study of Scale Factor X/y_1	C-9
C -5	Study of Rajaratnam's 1961 Data	C-10
C -6	Study of the Data of Bakhmeteff-Matzke and Others	C-11
C -7	Study of Ortiz Data (B-Jumps at Abrupt Drops)	C-12
C -8	Scale Factor for Ortiz Data	C-13
PLATE II-1	Probes Used in the Investigation	15

LIST OF SYMBOLS

a	=	opening of the sluice gate; constant
A_1, A_2	=	constants
b	=	width of the jet; constant
C	=	constant
C_c	=	coefficient of contraction
C_f	=	bed shear stress coefficient
C_p	=	pressure coefficient
C_s	=	consolidated shear force coefficient
d	=	height of free jet
e	=	Naperian base
E	=	energy
E_L	=	energy loss
f	=	suffix for forward flow
F_o	=	Froude number = $U_o / \sqrt{gy_o}$
F'_o	=	modified Froude number = $U_o / \sqrt{g r'}$
g	=	acceleration due to gravity
h	=	height of step; pressure head
H	=	depth
H_o	=	total energy head
K, K_1, k	=	coefficients
L_e	=	length of eddy
L_j	=	length of jump
L_o	=	defined distance in R-jump

L_r	=	length of roller
m	=	suffix for maximum; a parameter
n	=	exponent
p, p_o	=	pressures
P_f	=	integrated bed shear stress
q	=	discharge intensity
r, r'	=	characteristic length of outlet
R, R_o	=	Reynolds number
t	=	suffix for tailwater
u	=	velocity at any point
u_m	=	maximum velocity at any section
U_o	=	initial velocity
U_t	=	mean velocity at tailwater section
x	=	longitudinal distance
\bar{x}	=	longitudinal distance from the reattachment line
X	=	length scale of jump profile
y	=	transverse distance
y_o	=	initial depth of the jet; depth of submerged flow at vena contracta
y_o^*	=	equivalent depth for sluice gate outlet
Y	=	depth scale of jump profile
α	=	contraction ratio = b/B
γ	=	specific weight
δ	=	boundary layer thickness
δ_1	=	length scale of the velocity profile similarity plot
δ_3	=	depth of free mixing region

δ_p	= distance to the top of the potential core
δ^*	= displacement thickness
ζ	= non-dimensionalised depth = y/Y
η'	= non-dimensional ordinate = $(y - \delta)/(\delta_1 - \delta)$
$\bar{\eta}$	= non-dimensional ordinate = $(y - \delta_p)/\delta_1$
θ	= constant; angle
θ_1	= bed shear stress scale
λ	= non-dimensionalised length = x/X
μ	= dynamic viscosity
ν	= kinematic viscosity
ρ	= mass density
τ_o	= bed shear stress
ψ	= ratio of relative energy loss

CHAPTER I

INTRODUCTION

1.1 General

Control gate structures, such as sluice gates, roller gates, radial gates, etc., are common features in any water resources development project. An understanding of the mechanics of flow from these structures is not only academically interesting but also has a great practical bearing on the design of efficient and economical structures, especially the energy dissipation components.

The submerged flow from an outlet can be analysed, in general, as a turbulent jet. If the boundaries are sufficiently far away, the jet can be analysed as a free turbulent jet, about which extensive information is readily available (Abramovich, 1963). If, on the other hand, the jet issues tangentially to the bed, the flow will have to be analysed as a wall jet. Of late, the study of wall jets has received considerable attention, especially in the disciplines of Aeronautical and Mechanical Engineering, and as a result of this, considerable information on plane (two-dimensional) turbulent wall jets under zero pressure gradients is available (Schwarz and Cosart, 1961; Myers et al., 1961). However, the flows from hydraulic structures which could be treated as wall jets, usually issue from outlets of finite breadth into spaces confined by vertical or inclined walls and may be situated right on the bed or at a finite height above the bed. Also, the water surface

downstream of the outlet may create adverse pressure gradients. These situations cause complex flow patterns below the outlet structures.

As a first step towards understanding the complex problem of flow from submerged outlets, experimental investigations of jets issuing from a few basic types of boundary configurations and outlet conditions were conducted. The data are analysed with the wall jet as the basic flow model, and the details are presented in this thesis.

A review of some of the important works on wall jets, pertinent to this study, is given in the following section.

1.2 The Wall Jet

The wall jet is described as a jet of fluid which impinges tangentially or at an angle, and grows along a wall. The plane turbulent wall jet issuing tangentially to a smooth wall, surrounded by the same fluid of infinite extent at rest, is known as the classical wall jet and is shown in Fig. I-1. The jet is of depth y_0 and has a uniform velocity U_0 at the nozzle. The boundary conditions of the jet are that the velocity at the wall and also at the end of the free mixing region is zero; hence the velocity profile must have a maximum. In Fig. I-1 is shown, schematically, a typical velocity distribution at a longitudinal distance x from the nozzle. The flow belongs to the class of "self-preserving" shear flows--such as jets, wakes and free jet boundary problems--characterised by non-dimensional velocity distributions that do not change (so are preserved) from section to section.

Historically, Forthmann (1936) was the first person to

undertake an experimental study of the two-dimensional wall jet. He found that for $x/y_0 > 20$, the flow reached a self-preserving state with respect to mean flow characteristics. On the basis of his experimental data, Forthmann (1936) defined the velocity profiles as

$$u = x^a f(y/x^b) \quad . \quad . \quad . \quad . \quad . \quad (1.1)$$

where y is the transverse distance, u is the turbulent mean velocity at any point (x,y) and a and b are constants. It was found that the maximum velocity, u_m , varies as x^a and a characteristic transverse dimension, to which y can be referred, varies as x^b . With this, the velocity profile took the similarity form of

$$u/u_m = f(y/\delta_1) \quad . \quad . \quad . \quad . \quad . \quad (1.2)$$

where δ_1 is a characteristic transverse dimension, known as the length scale and selected conventionally as the normal distance from the boundary to a point where $u = \frac{1}{2} u_m$ and the velocity gradient is negative (see Fig. I-1). The values of a and b were found to be 0.5 and 1.0 respectively. Further, the velocity distribution in the boundary layer was found to be given by the one-seventh power law.

Glauert (1956) was the first person to examine, theoretically, the similarity problem of laminar and turbulent wall jets. While a complete mathematical solution was easily obtained for the case of laminar wall jets, he found that for turbulent wall jets, there is no unique similarity solution for the entire flow. However, if the flow is considered as being divided into a boundary layer region and a free

mixing region, as shown in Fig. I-1, similarity conditions were found to be satisfied for each region treated individually. By a process of matching solutions, Glauert (1956) developed a theoretical method of predicting the nature of velocity distribution and rate of growth of wall jets.

Sigalla (1958-a, 1958-b) conducted an experimental investigation of plane turbulent wall jets and found that the flow is fully developed for $x/y_0 \geq 15$. In this fully developed region, in the entire practical range of y , the velocity profiles were found to be similar. Sigalla (1958-b) has given equations, based on his experimental data, for the variation of the shear stress on the bed, τ_0 , measured by the Preston tube technique (Preston, 1954), as

$$C_{fm} \equiv \frac{\tau_0}{\rho u_m^2 / 2} = \frac{0.0565}{(u_m \delta / \nu)^{1/4}} \quad . \quad . \quad (1.3)$$

where ρ = mass density of the fluid, ν = kinematic viscosity of the fluid and δ = thickness of the boundary layer.

Schwarz and Cosart (1961) showed, by an elegant analytical method, that the plane turbulent wall jet cannot, theoretically, have the same self-preserving character over the entire depth of the jet. However, if the small region immediately next to the wall--i.e., the viscous sub-layer--is neglected, the mean flow was shown to be self-preserving in the rest of the flow region. The variation of the length and velocity scales of the similarity profile were obtained as

$$\left. \begin{array}{l} \delta_1 \propto x \\ \text{and } u_m \propto x^a \end{array} \right\} \quad . \quad . \quad . \quad . \quad (1.4)$$

where a is a constant. Based on their experimental data, a well defined similarity curve--in the form of Eq. 1.2-- and equations for variation of velocity and length scales were derived. Further, they found that the velocity distribution in the boundary layer was of power law type with an exponent of $1/14$, against Forthmann's $1/7$.

Myers et al. (1961), developed analytical expressions for the plane wall jet characteristics by assuming the velocity distributions in the boundary layer and the free mixing regions. Also, they conducted an extensive experimental investigation. The similarity profiles of velocity and the distribution of velocity in the boundary layer were found to be in very good agreement with the findings of Schwarz and Cosart (1961). Empirical equations for the best fit curves of the velocity and length scale variation were derived. Further, Myers et al. (1961) measured the bed shear stress by the hot film technique and found that their measured values were about 15% higher than those given by Sigalla (1958-b), (Eq. 1.3).

1.3 Study of Wall Jets in Hydraulic Engineering

Glauert (1956), in his classical paper, mentioned the submerged flow below a sluice gate as an example of wall jet. Iwagaki and Tsuchia (1959) made an exploratory study of the wall jets from submerged outlets discharging into a channel, but analysed the data from a different point of view than that of wall jets. Rajaratnam (1965-c) has studied the submerged sluice gate flow as a wall jet. By defining a hypothetical depth

$$y_o^* = q/U_o \quad . \quad . \quad . \quad . \quad . \quad (1.5)$$

where q = discharge intensity entering the channel, and U_0 = the velocity in the potential core, he found that the flow was essentially of the same type as that of a plane wall jet issuing from a nozzle of height $y_0 = y_0^*$, and uniform velocity U_0 . The similarity profile, the length and velocity scales were essentially the same as found by Schwarz and Cosart (1961).

The free and submerged hydraulic jumps in a rectangular channel were studied by Rajaratnam (1965-a, 1965-b) as wall jet problems, where it was found that the velocity profiles in the forward flow are similar for all submergences and Froude numbers tested.

The flow from a sluice gate over rough boundaries was studied by Rajaratnam (1967). It was found that one similarity curve for the entire depth of flow was not possible. However, similarity was found to exist in the free mixing region for all roughness types tested.

1.4 The Present Investigation

The main aim of this investigation was to study the wall jet characteristics due to a jet of water entering a channel under high submergence and with one of the following boundary conditions:

- 1) a sudden drop in the bed directly below the jet outlet
- 2) a sudden symmetrical expansion of the channel at the jet outlet.

It was, however, found desirable to study, in addition, the characteristics of:--

- 3) a hydraulic jump occurring at a sudden symmetrical expansion of the channel at the jet outlet

- 4) a water wall jet, i.e., a jet of water issuing tangentially on to the bed of a channel, from a nozzle occupying the full width of the channel, under conditions of high submergence.

The test facilities and the limitations of the measurement techniques are described in Chapter II.

In Chapter III, the mean curves of the similarity plot, the velocity scale and the length scale of a classical wall jet are first established for purposes of reference. The experimental data on water wall jets are then studied and the results compared with those of the classical wall jet.

The following problems are studied in Chapters IV, V and VI respectively:--

- 1(a). Flow from a deeply submerged plane nozzle situated over an abrupt drop in the bed of a channel.

- 1(b). Flow from a deeply submerged sluice gate situated over an abrupt drop in the bed of a channel.

2. Characteristics of wall jet flow due to a nozzle discharging tangentially on to the bed of a wider channel, i.e., at a sudden symmetrical expansion, under high submergence.

3. The characteristics of hydraulic jumps at sudden symmetrical expansions.

In problems 1 and 2, the velocity profiles on the center line, measured at various sections along the channel, are analysed for similarity and the variations of length and velocity scales and the bed shear stress along the flow have been studied and compared with the

corresponding characteristics of the classical wall jet or the water wall jet, depending upon the case. In problem 3, however, only exploratory studies of the wall jet characteristics are made and the gross characteristics of the flow are studied in detail.

Chapter VII gives the general conclusions of the present investigation and recommendations for future studies on the topic of wall jets in hydraulic engineering.

During the course of this investigation, a few other interesting problems in hydraulic engineering were analysed with a novel approach. These studies, listed below, are reported in Appendices A through C:--

- A. Flow immediately below a submerged sluice gate.
- B. Three-dimensional free jets.
- C. Profile of the hydraulic jump.

Even though these studies are not directly related to the main topic of the present investigation, the idea for their analysis stemmed from the results of the present investigations.

The experimental investigation was carried out at the hydraulics laboratory of the University of Alberta, Edmonton, Canada, during the period 1965-1967.

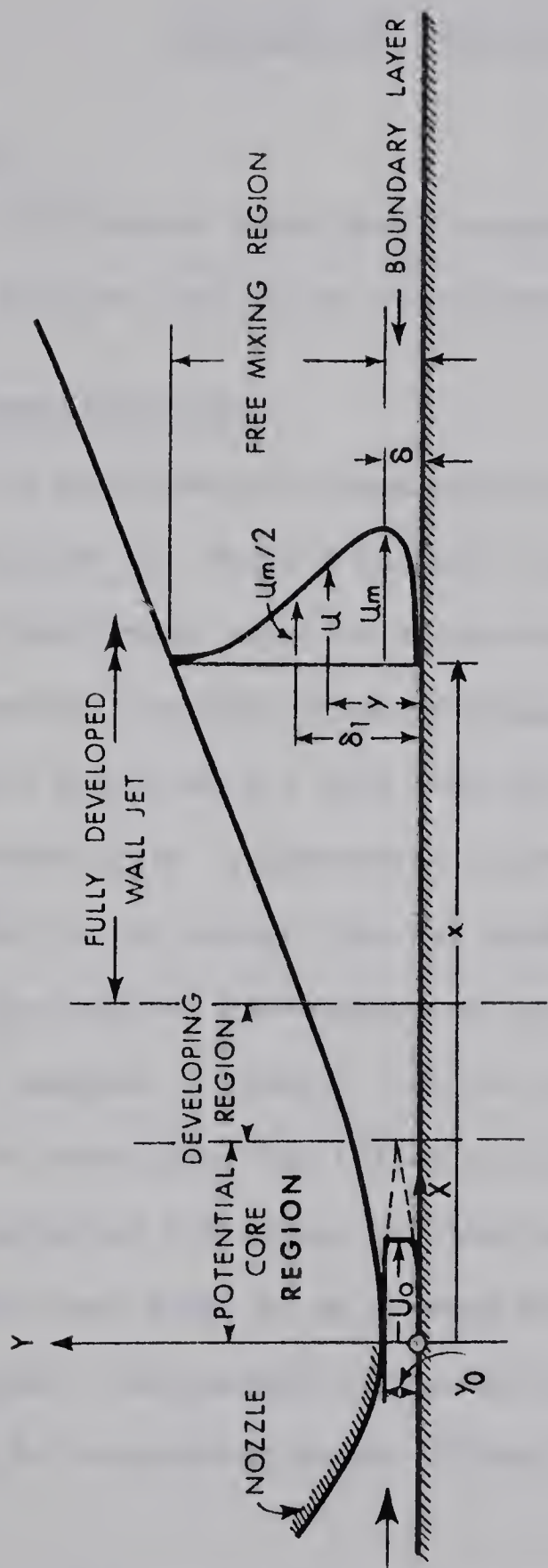


FIG. I-1. DEFINITION SKETCH OF A WALL JET

CHAPTER II

EXPERIMENTAL FACILITIES

2.1 General

This Chapter describes the experimental arrangement, instruments used and the limitations of the observed data.

2.2 Experimental Set-Up

The experimental investigation was carried out in two flumes, Flume A and Flume B. Flume A was 18 in. wide, 36 in. deep and 16 ft. long with a horizontal aluminum bottom and plexiglas sides. Fig. II-1 gives a schematic representation of Flume A. The set-up consisted of a recirculation system with a head tank with stilling arrangements, an upstream control gate, a downstream control gate and a sump. A calibrated orifice meter in the supply line was used to measure the discharge.

The upstream gate-slot was used to install any desired type of outlet, for example, a nozzle, a sluice gate, etc. The downstream gate was used for controlling the tailwater elevation. Two lines of 1/8 in. diameter piezometer holes were provided parallel to the center line of the flume, one on each side, at an average distance of 3 in. apart; the holes were staggered. Bed pressure heads were recorded by connecting the piezometers to a manometer board. Flume A was used in most of the experiments.

Flume B was used in only one investigation. It consisted of a horizontal flume, 12.25 in. wide, 24.0 in. high and 16 ft. long with glass

walls and smooth brass bed. This flume was fed by the laboratory main supply line and discharged into the laboratory sump. The tailwater level was controlled by a downstream flap gate. The discharge was measured by a calibrated orifice meter.

2.3 Measurements

The main instruments used in collecting the data are: point gauges for depth, Prandtl-type Pitot-static tubes for velocity, a screw driver probe (Girerd and Guienne, 1946) for pressure field, and Preston tube (Preston, 1954) for boundary shear measurements. Plate II-1 shows the various probes used in this study. The instruments were mounted on a traverse which could position the instrument with an accuracy of about 1/100 ft. in the longitudinal direction and 1/1000 ft. in the transverse direction.

2.3.1 Depth

The depth measurements were made by use of simple point gauges which could be read to an accuracy of 1/1000 ft. The water surface elevations were normally measured along the center line.

2.3.2 Velocity

The velocity observations were made with commercial Prandtl-type Pitot-static tubes of 3mm. external diameter. No corrections were made for turbulence, displacement and viscous effects.

It is known that a Pitot-static tube is insensitive to angle of attack less than about 5° and gives an error of about 3% at 10° . In the diffusion process of a wall jet, the velocity vectors are inclined to

the bed and may reach an angle of about 10° at the outer edge. However, a study of the Schwarz and Cosart (1961) data on plane wall jets indicates that, within a depth of δ_1 from the bed (the velocity vector at which place makes an angle of about 4.0° with the wall) 74% of mass, 87.5% of momentum and 94.5% of kinetic energy at that section is passed. It is, therefore, believed that the error due to angle of attack affects only the outer region, $y > \delta_1$, and the resulting error is too small to affect the characteristics of the measured velocity profile. Hence, no corrections were made for the angle of attack.

In all cases of submerged fluid flows of finite depth, for reasons of continuity of flow, a reversed flow zone is created over the forward flow. In the present investigation the measurements of the velocities in the reversed flow were not made.

2.3.3 Pressure Field

The streamlined static pressure probe is sensitive to angle of attack and cannot be used to measure pressure fields in zones of appreciable angle of attack (Rosenhead, 1963). For example, for an angle of attack of 10° , the error in the static pressure is about 2.5% of the velocity head at that point and this error increases to about 10% at an angle of attack of 20° . On the other hand, the screw driver probe studied by Girerd and Guienne (1949) is very insensitive to angle of attack. For example, at an angle of attack of 10° (in the vertical plane), the error is only 0.75% and increases to only 3% at 20° . Such a screw driver probe, with a tube diameter of 3mm., was prepared and used for measuring the pressure fields in regions of appreciable angle of attack.

2.3.4 Bed Shear Stress

The method of bed shear measurement was that due to Preston (1954), which is based on the fact that in all types of shear flows past a wall there is a region of local dynamical similarity near the wall such that when a tube of small dimensions is placed on its surface the reading of the tube is related to the local shear stress and other characteristics of the wall region. A Preston tube of 3mm. external diameter, and a ratio of internal to external diameter of about 0.6, was used. The calibration curve used was that given by Patel (1965).

2.4 Flow Visualization

Colour injection and a tuft probe--a probe with a small coloured woollen thread at the end--were used for flow visualisation and qualitative description.

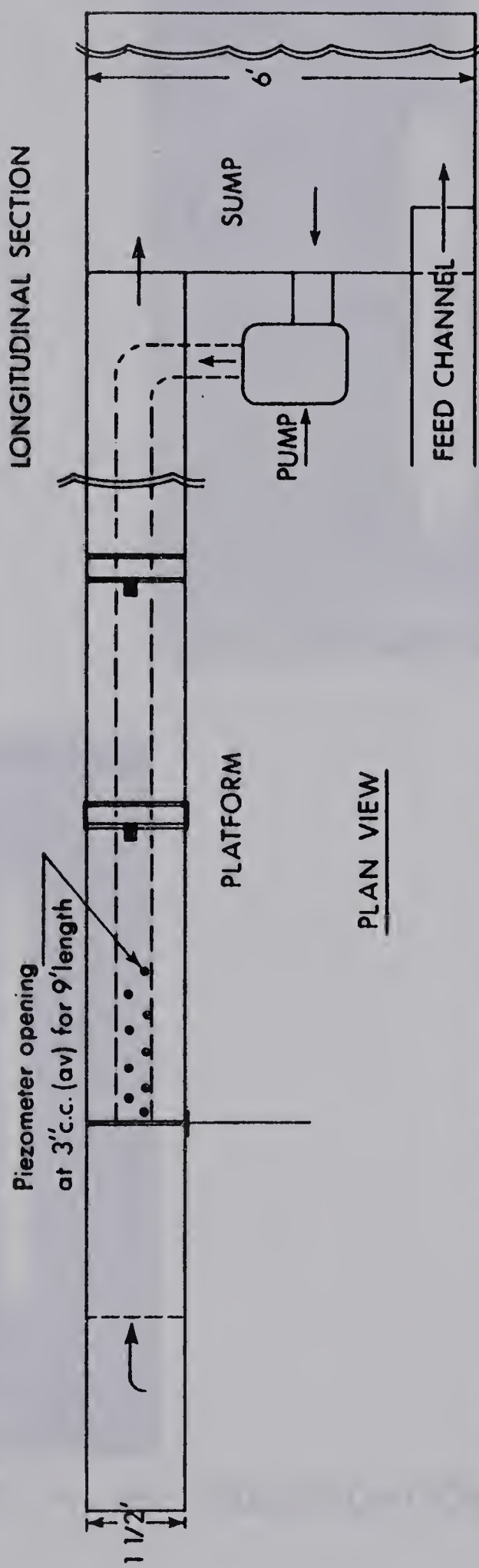
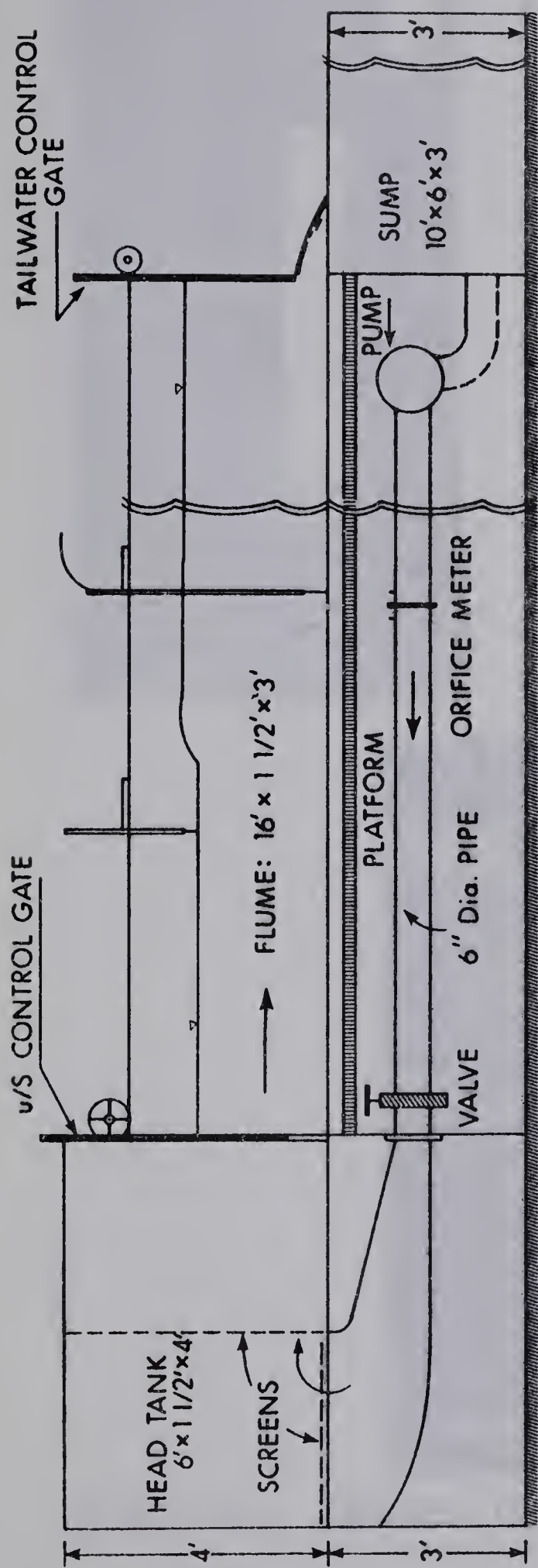


FIG.II-1. SCHEMATIC VIEWS OF THE EXPERIMENTAL SET-UP
FLUME : A.



PLATE: II-1. PROBES USED IN THE INVESTIGATION

CHAPTER III

STUDY OF WATER WALL JET

3.1 The Classical Wall Jet

3.1.1 General

The available information on the variation of the mean characteristics of the plane turbulent wall jets in stagnant ambient fluid is in terms of numerous experimental data, with air as the working fluid, and empirical formulae deduced therefrom. For purposes of comparison and reference, the mean curves drawn through available data of similarity profile, velocity scale and length scale, respectively, will be considered to represent the corresponding characteristics of the classical wall jet.

3.1.2 Similarity Profile

The experimental data on the velocity profiles of Forthmann (1936), Sigalla (1958-b), Schwarz and Cosart (1961) and Myers et al. (1961) were plotted in the form u/u_m vs. y/δ_1 and a mean curve was drawn through them. The scatter of the data was very little. The coordinates of the mean curve, which will be called the similarity profile of the classical wall jet, is given in Table III-1.

Regarding the velocity distribution in the boundary layer region, a power law

$$u/u_m = (y/\delta)^{1/n} \quad . \quad . \quad . \quad . \quad . \quad (3.1)$$

TABLE III-1

CLASSICAL WALL JET

CO-ORDINATES OF SIMILARITY PROFILE

y/δ_1	u/u_m	y/δ_1	u/u_m
0.00	0.00	1.10	0.450
0.02	0.79	1.20	0.405
0.05	0.90	1.30	0.360
0.08	0.95	1.40	0.310
0.10	0.98	1.50	0.260
0.16	1.00	1.60	0.215
0.20	0.995	1.70	0.170
0.30	0.950	1.80	0.125
0.40	0.890	1.90	0.085
0.50	0.825	2.00	0.055
0.60	0.760	2.10	0.030
0.70	0.690	2.20	0.005
0.80	0.625	2.25	0.000
0.90	0.560		
1.00	0.500		

is considered to adequately represent the velocity distribution. The value of n has been found to be 14 by Schwarz and Cosart (1961) and Myers et al. (1961). Sridhar and Tu (1966) found $n = 12$. Neglecting the rather low value of $n = 7$ found by Forthmann (1936) a value of $n = 14$ would be a reasonable value for the power law exponent.

3.1.3 Velocity and Length Scales

The variation of the velocity scale, u_m , is shown plotted as u_m/U_0 vs. x/y_0 in Fig. III-1. The scatter of the data seems acceptable in terms of the various sources. The mean curve through the plotted data is used to define the velocity scale of the classical wall jet.

The length scale is plotted in the non-dimensional form, δ_1/y_0 vs. x/y_0 , in Fig. III-2. The Schwarz and Cosart (1961) equation:--

$$\delta_1/y_0 = 0.76 + 0.068 x/y_0 \quad . \quad . \quad . \quad (3.2)$$

can be used to smooth the data and hence to define the length scale of the classical wall jet.

3.2 Water Wall Jet

3.2.1 General

The jet of water issuing tangentially on to the bed of a channel, from a nozzle occupying the full width of the channel, under conditions of high submergence is termed a water wall jet. It differs from the classical wall jet by the ambient fluid being of finite extent

with a free surface. In a water wall jet, for reasons of continuity, a backward flow is created over the forward flow, as shown in the inset of Fig. III-4.

There appears to be no detailed study of the water wall jet. Experimental data collected in the course of the present investigation are analysed to compare a water wall jet with the classical wall jet.

3.2.2 Experiments

Three experiments--two in Flume A and one in Flume B --were conducted. The nozzle was formed by attaching a curved hood to a sliding gate. The flow from the nozzle was two-dimensional, at least in the middle 40% of the flume. All the experiments were conducted under conditions of high submergence, so that the tailwater was essentially level for considerable distance below the nozzle. Table III-2 gives the summary of the experiments and the detailed data are given in Appendix D (Tables D-1 and D-2).

3.2.3 Similarity

Fig. III-3 is a plot of velocity distributions in a typical run. The gradual growth of the boundary layer and the free mixing region is clearly seen in this Figure. The velocity profiles are reduced to the similarity profile co-ordinates and are shown plotted in Fig. III-4. It is seen that the scatter of the data is small and not systematic. In the range of $y/\delta_1 < 1.1$, the data agree very well with the classical wall jet curve. In the range of $y/\delta_1 > 1.1$ the data somewhat deviate from the classical wall jet curve. It is believed that this deviation is not significant in view of the high turbulent

TABLE III-2
WATER WALL JET
SUMMARY OF DATA

Run	Width of Flume B in.	y_o in.	U_o ft./sec.	Tail-Water Depth y_t in.	$R = U_o y_o / \nu$ $\times 10^4$
II-E-1	12.25	1.063	7.87	18.90	6.60
I-E-1	18.00	1.375	8.50	26.80	9.30
I-E-1	18.00	0.875	8.50	27.40	5.60

intensities and low intermittency values at the outer region of free shear flows (Schubauer and Tchen, 1961). Thus it can be said that the velocity distribution in a water wall jet is similar and the similarity profile is essentially the same as for the classical wall jet.

3.2.4 Velocity and Length Scales

Fig. III-5 shows the plot of u_m/U_o against x/y_o . Also plotted is the corresponding curve for the classical wall jet and its limits of scatter. The present data are well described by the classical wall jet curve.

The variation of the dimensionless length scale is studied in Fig. III-2. The present data, from all three runs, are well described by a straight line given by

$$\delta_1/y_o = 0.65 + 0.095 x/y_o \quad . \quad . \quad . \quad (3.3)$$

However, it is interesting to note that the water wall jet grows about 1.4 times faster than the classical wall jet. The reversed flow in the

recirculating zone is possibly responsible for this faster growth. For very high submergences, the recirculating flow may become very weak, and as a result the rate of growth of the water wall jet may approach that of the classical wall jet. However, this aspect could not be tested in the present test facility.

3.2.5 Boundary Shear Stress

The bed shear stress coefficient, C_f , defined as

$$C_f = \frac{\tau_o}{\rho U_o^2 / 2} \quad (3.4)$$

was calculated for all three runs and the variation of C_f with x/y_o plotted in Fig. III-6. The data are well correlated. The variation of C_f within the range $10.0 < x/y_o < 80.0$ can be expressed as

$$C_f = 0.0044 e^{-0.02436(x/y_o)} \quad (3.5)$$

Regarding the corresponding variation of C_f for the classical wall jet, information from only two sources was available. The variation of C_f with x/y_o was calculated, for a value of Reynolds number $R = U_o y_o / \nu = 10^5$, by the use of equations given by Sigalla (1958-b) and Myers et al. (1961), and is shown plotted in Fig. III-6. The variation of bed shear stress in the water wall jet is essentially the same as in the classical wall jet.

3.3 Plane Free Jet and Classical Wall Jet

3.3.1 General

One way of looking at the classical wall jet is to consider it as a half of a free jet created by inserting a 'wall' at the plane

of symmetry of the jet. Under such a model, it is interesting to study the effect of the wall on the velocity profile. In this section, a half of a plane turbulent free jet is compared with a classical wall jet regarding the three important characteristics, viz., the velocity distribution and the variation of the velocity and length scales, in the region of developed flow.

3.3.2 The Free Jet

Fig. III-7 shows a plane free jet of thickness $2y_0$ with an uniform velocity U_0 diffusing in an infinite surrounding. It has been found that the length of the potential core--i.e., the wedge shaped zone into which turbulent diffusion has not yet penetrated--is about 11.8 to 13.2 y_0 (Yevdjevich, 1966). For $x/y_0 > 20$, the mean velocity distribution is similar and is satisfactorily described by the theoretical solutions, given by Tollmien and Goertler, respectively (Abramovich, 1963; Newman, 1961).

The similarity profile of the velocity distribution is shown in Fig. III-8. In this plot y is the normal distance and δ_1 is the length scale as shown in Fig. III-7. Some of the well known experimental results for the decay of maximum velocity, u_m , taken from Abramovich (1963), Newman (1961), Zignen (1957), and Albertson et al. (1950) are shown in Fig. III-9. If the curve-2 of Zignen (1957), which is comparatively low, is left out, then Zignen's curve-1 is a good average for the others. Regarding the length scale, the variation of δ_1 given by Abramovich (1963) and Newman (1961) are plotted in Fig. III-10.

3.3.3 Comparison of Wall Jet with Free Jet

The similarity curve of the classical wall jet is shown in Fig. III-8. It is seen that except in the boundary layer region and a very small portion of the free mixing region, the classical wall jet profile agrees well with that of the free jet, especially with the curve of Tollmien.

Since for wall jets on rough boundaries (Rajaratnam, 1967), and those with adverse pressure gradients (Rajaratnam, 1965-b) and those with co-flowing streams (Eskinazi and Kruka, 1962, 1964) it has been found that the flow has to be considered as being divided into boundary layer region and free mixing region, the similarity velocity profile in the free mixing region is compared with the free jet curve in Fig. III-8. This curve, for which the abscissa is $\frac{(y - \delta)}{(\delta_1 - \delta)}$ is found to be slightly different from others, but still, for practical purposes this difference could possibly be neglected.

Regarding the velocity scale, the limits of scatter of the classical wall jet, taken from Fig. III-1, is shown plotted in Fig. III-9. It is seen that the mean curve for the free jet describes the wall jet data satisfactorily except for values $7.0 < x/y_0 < 20.0$, as the length of the potential core for the wall jet is only about $7.0 y_0$ (Myers et al., 1961).

The variation of the length scales of the free jet, classical wall jet and water wall jet are shown in Fig. III-10. It is interesting to see that the classical wall jet grows only about 0.70 times as fast as the free jet and the water wall jet grows as fast as the free jet.

3.4 Conclusions

From the comparative study of the characteristics of the classical wall jet and the water wall jet it is concluded that, both the flow situations are essentially the same except for the growth rate of the length scale which is 1.4 times faster in the water wall jet.

Similarly, the chief difference between the diffusion of the half of a plane free jet and the classical wall jet is in the rate of growth of the length scale only.

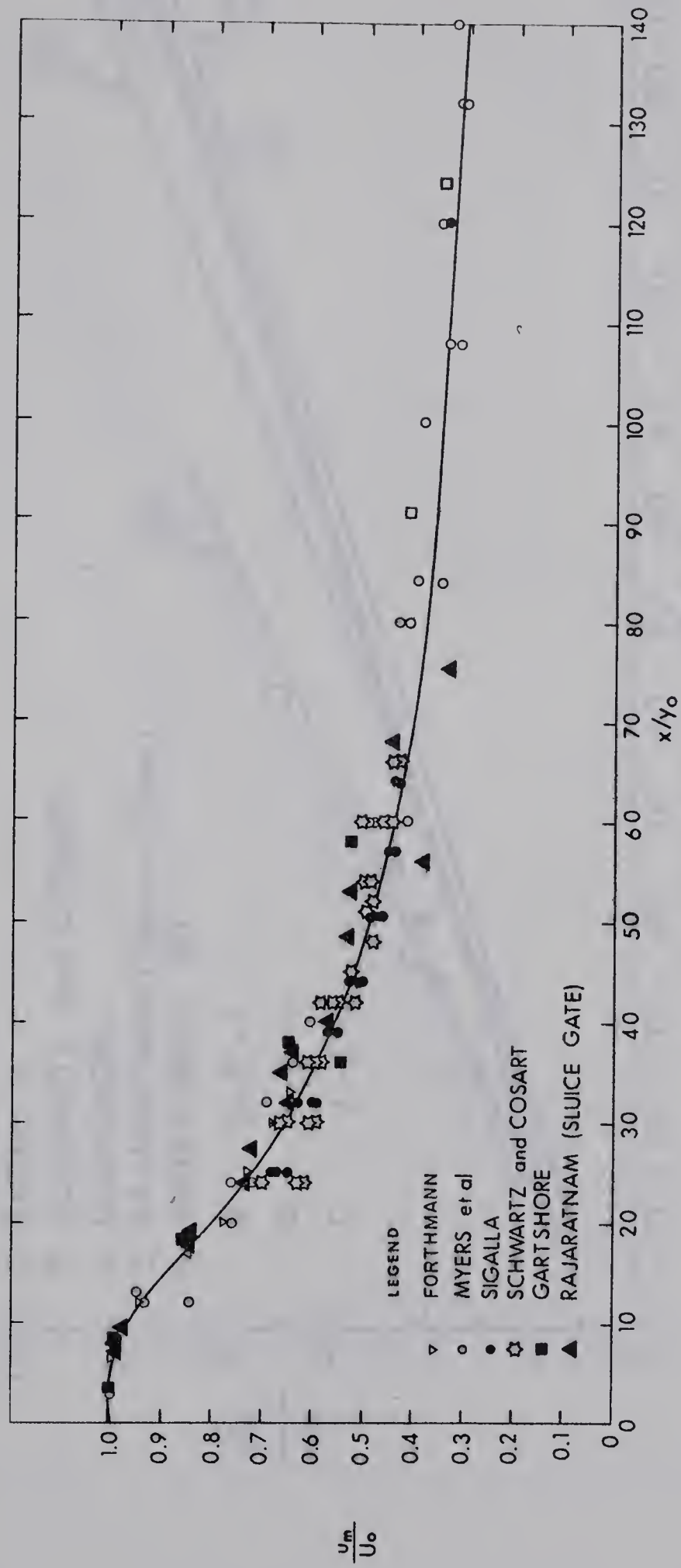


FIG. III - 1. Velocity Scale for Classical Wall Jet

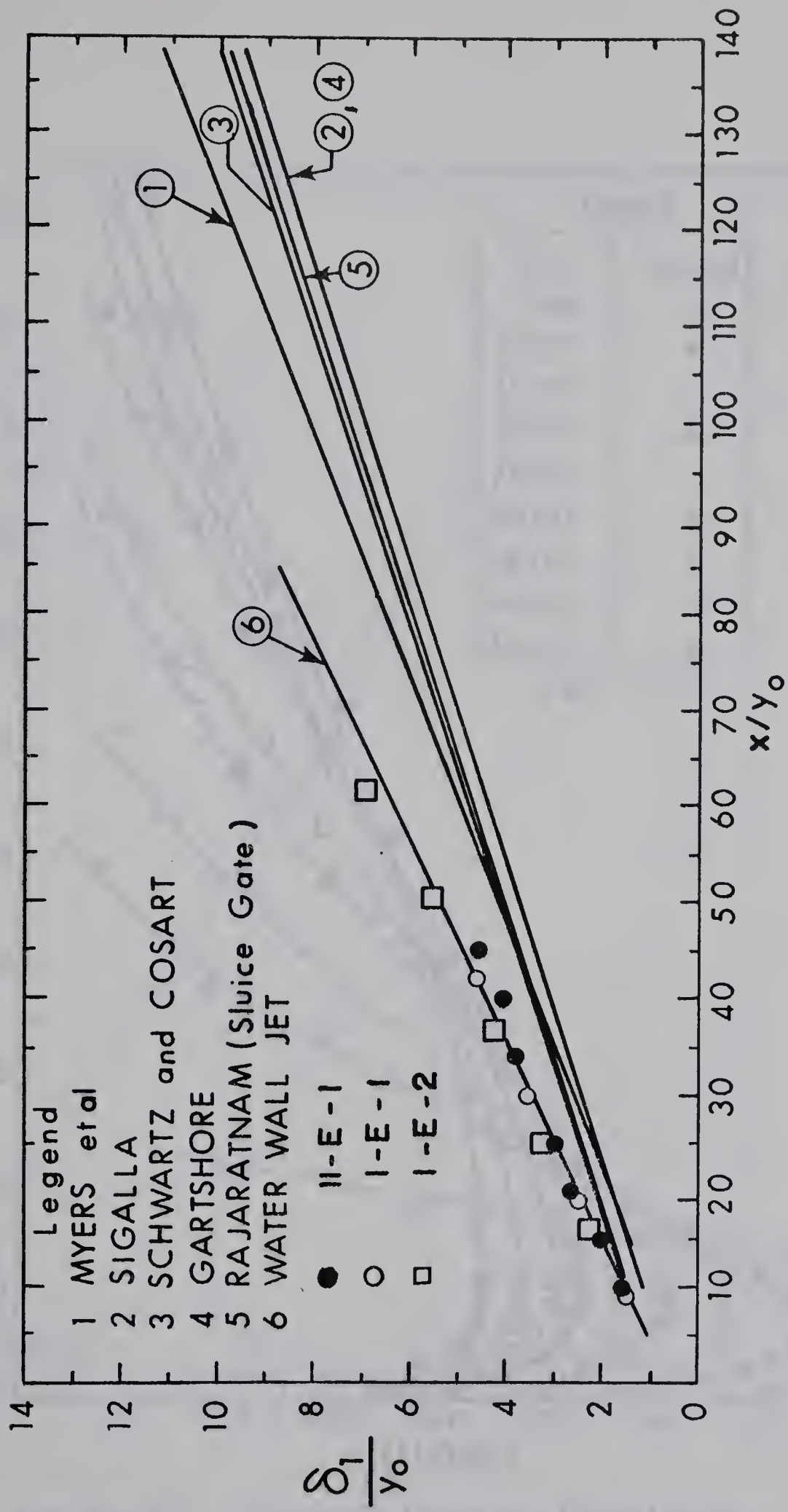


FIG. III - 2. LENGTH SCALE VARIATION

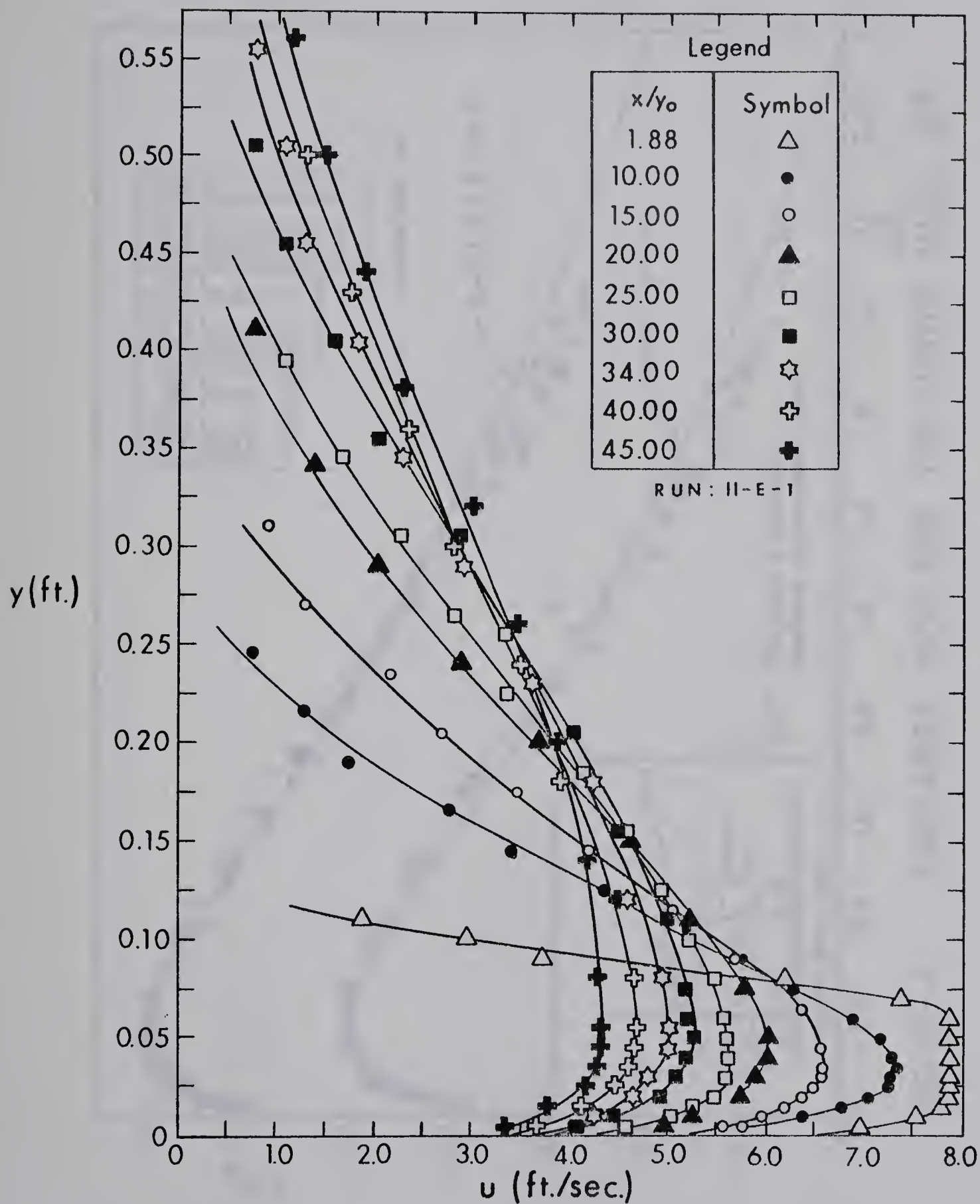


Fig. III - 3. Typical Velocity Distribution

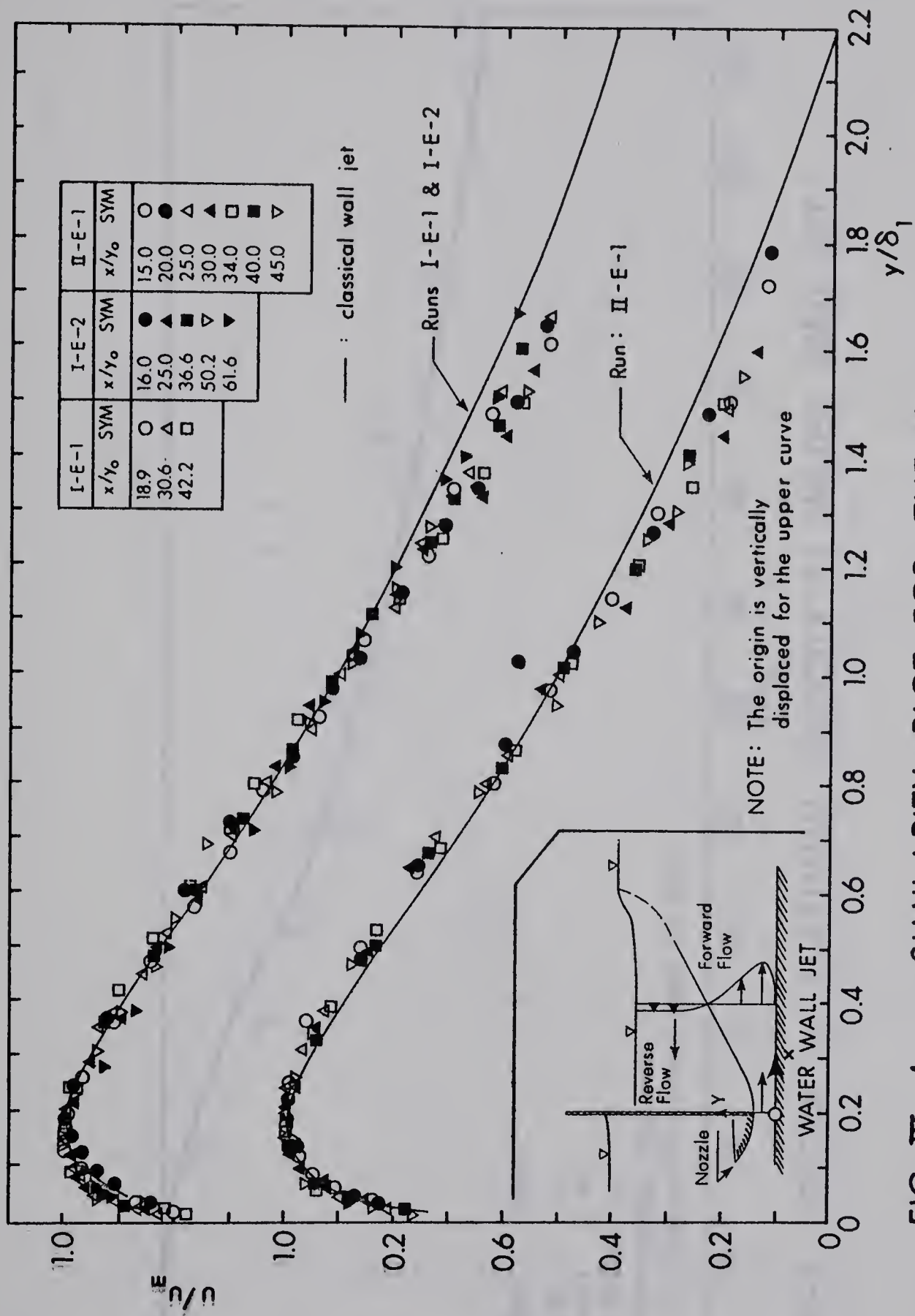


FIG. III-4. SIMILARITY PLOT FOR THE WATER WALL JET

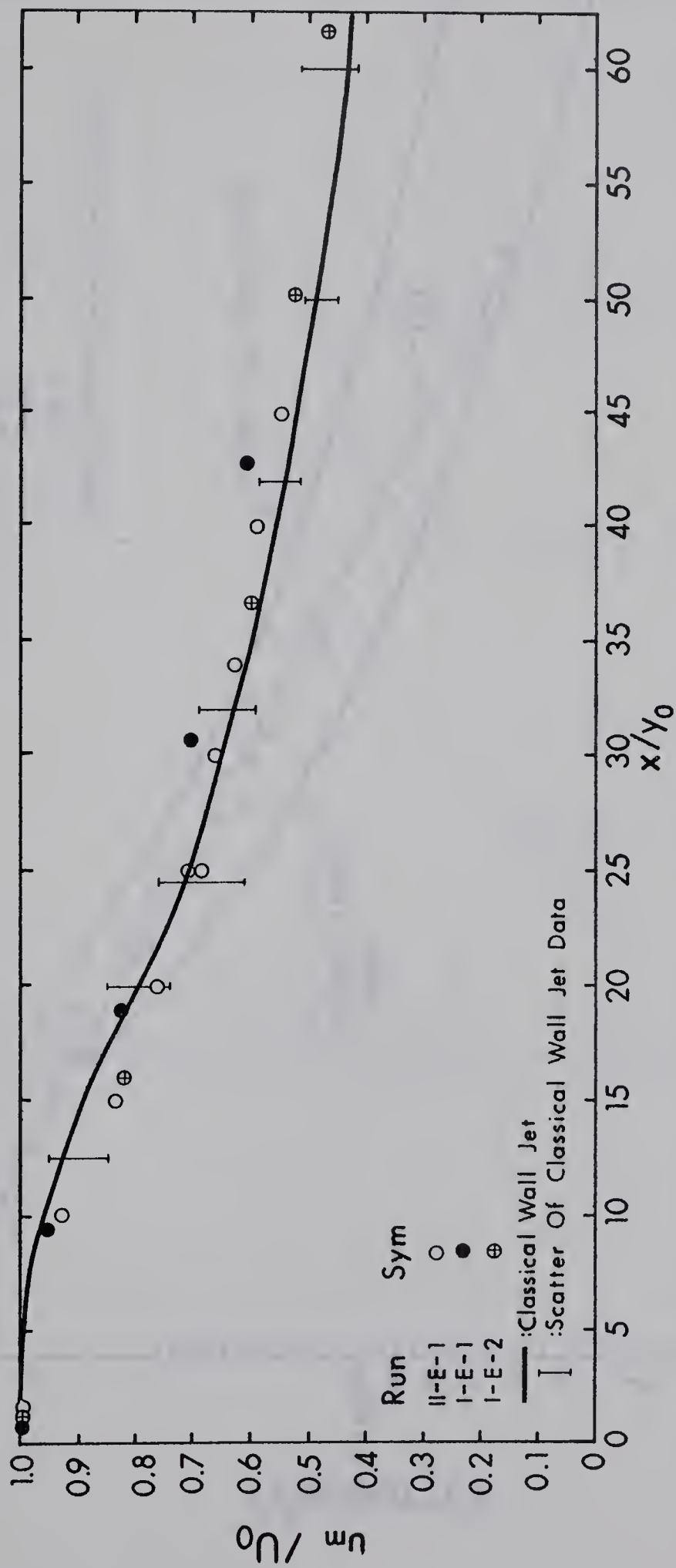


FIG. III-5. DECAY OF MAXIMUM VELOCITY IN WATER WALL JET

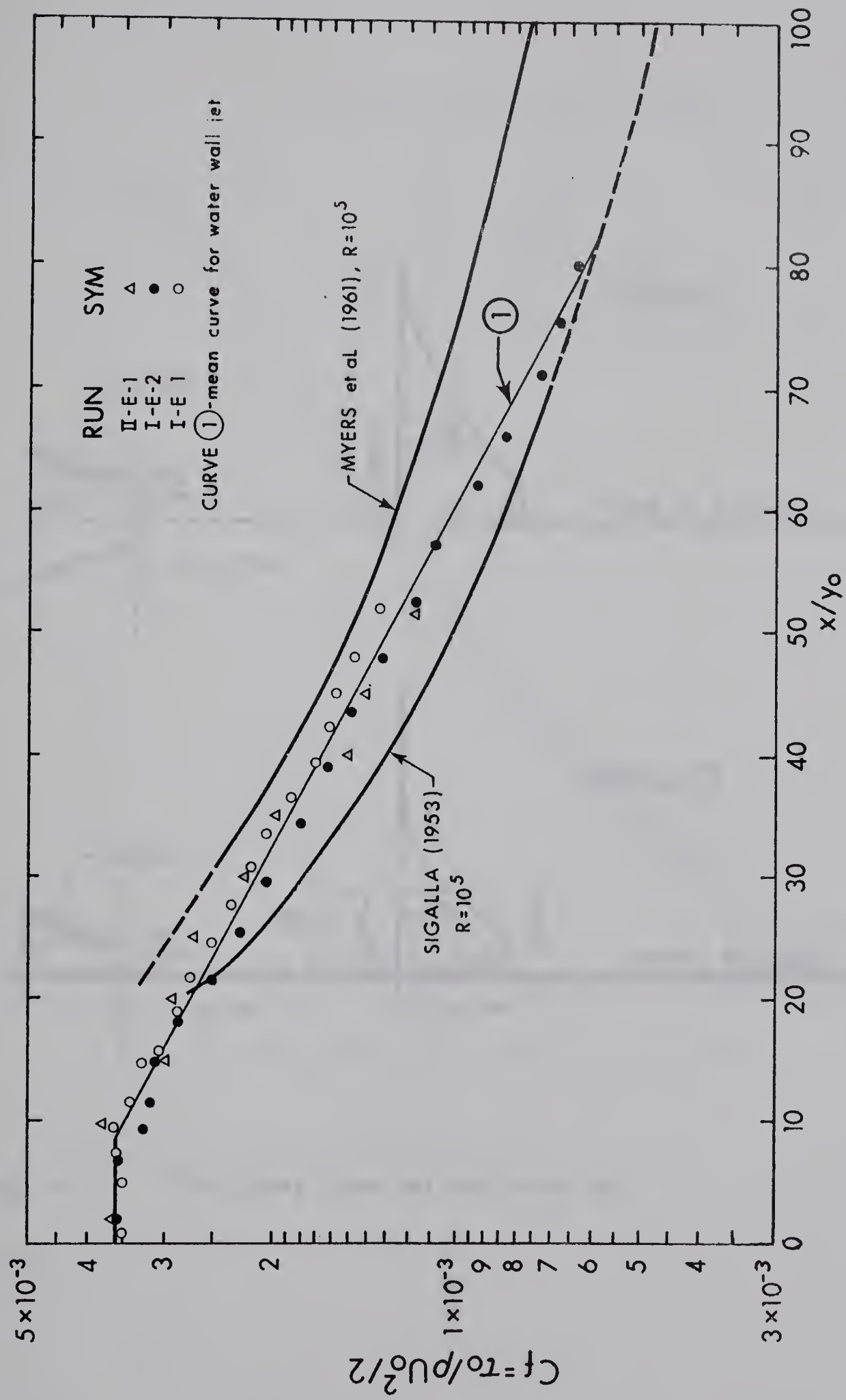


FIG. III-6. VARIATION OF C_f IN WATER WALL JET

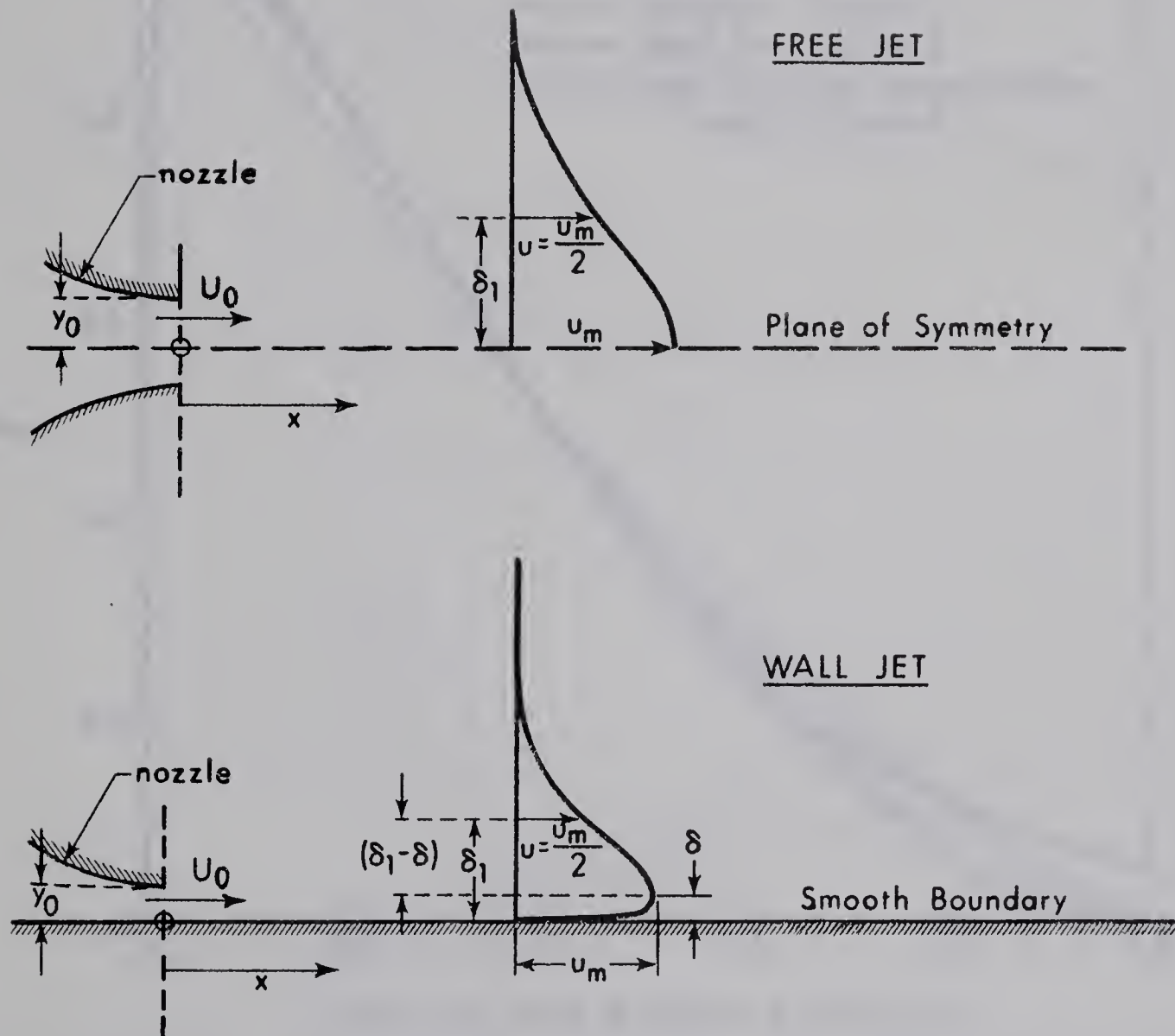


Fig. III - 7. The Plane Free Jet and Wall Jet

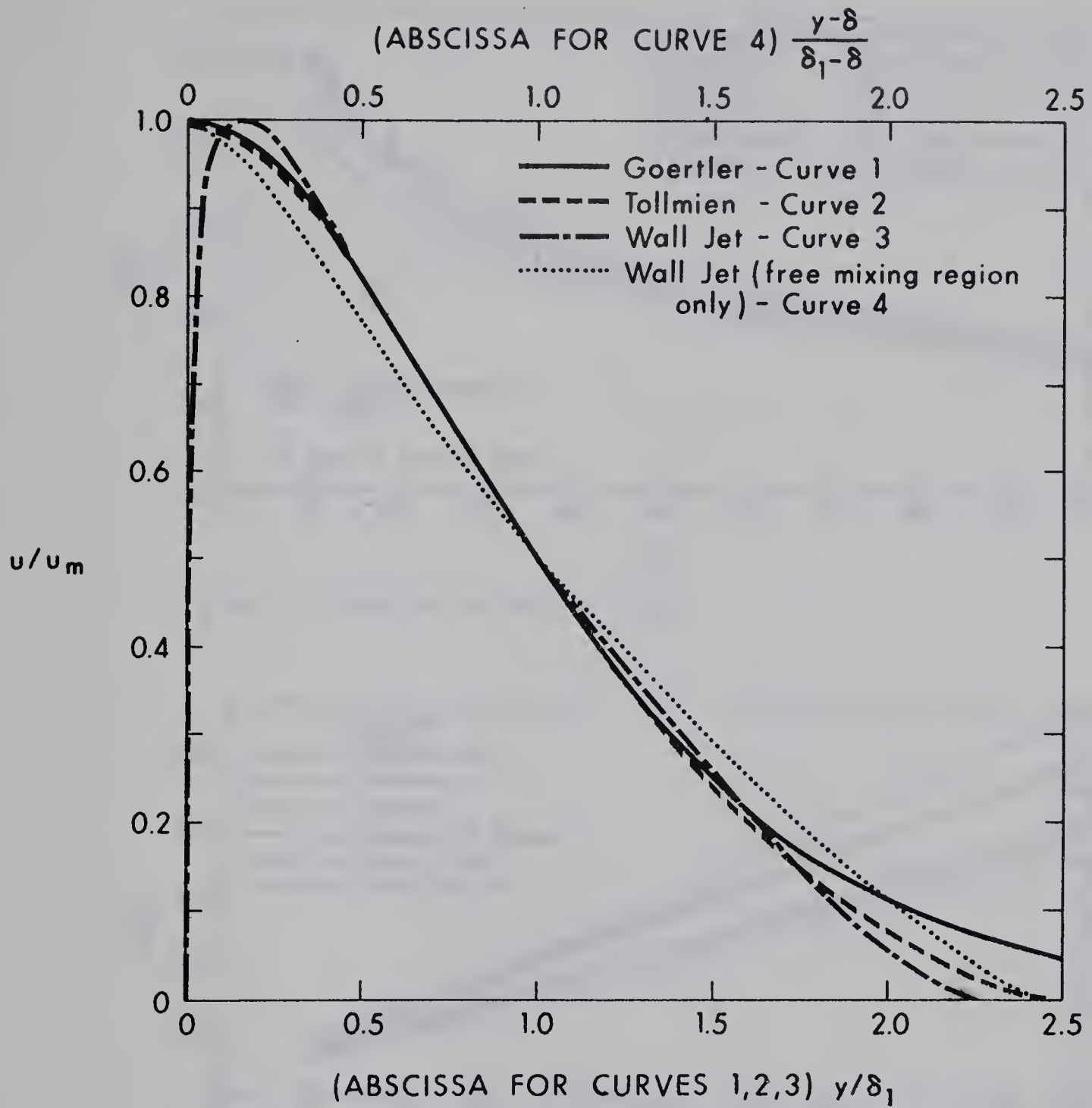


Fig. III- 8. Velocity Distribution

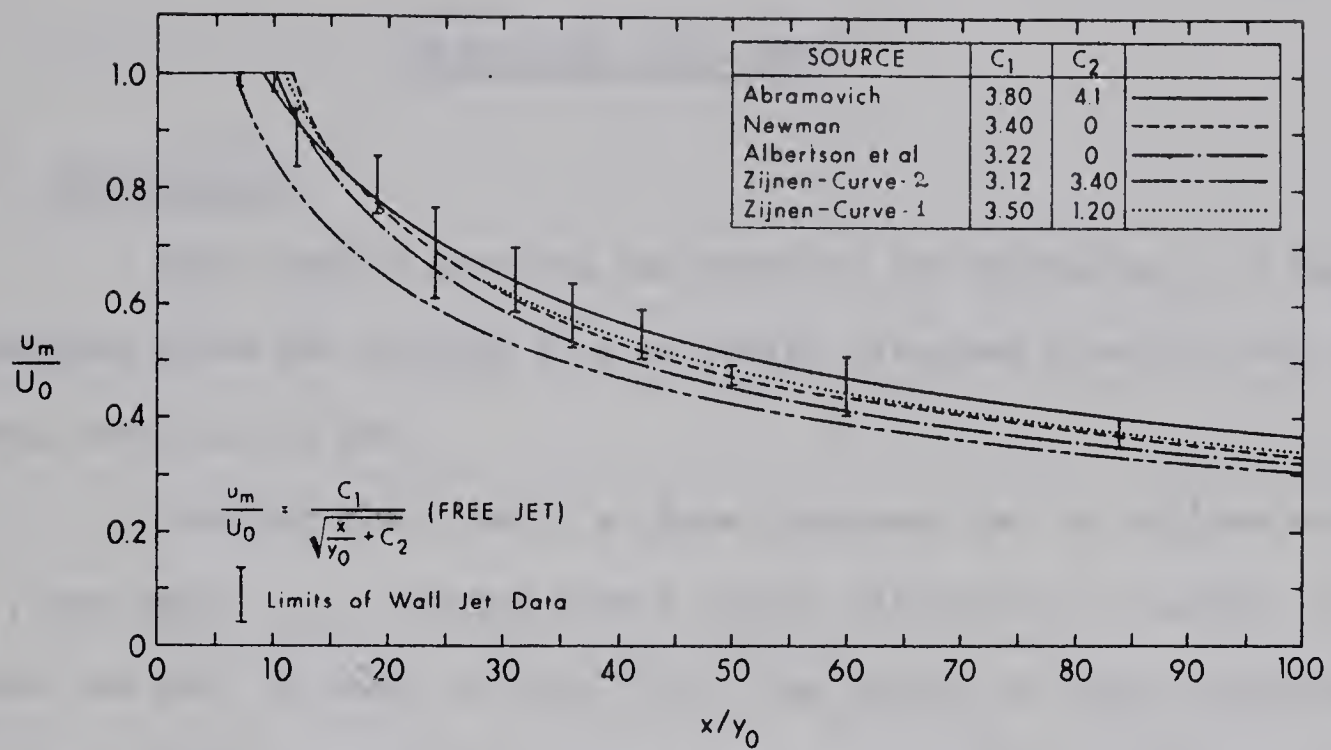


Fig. III-9. Study of the Velocity Scale

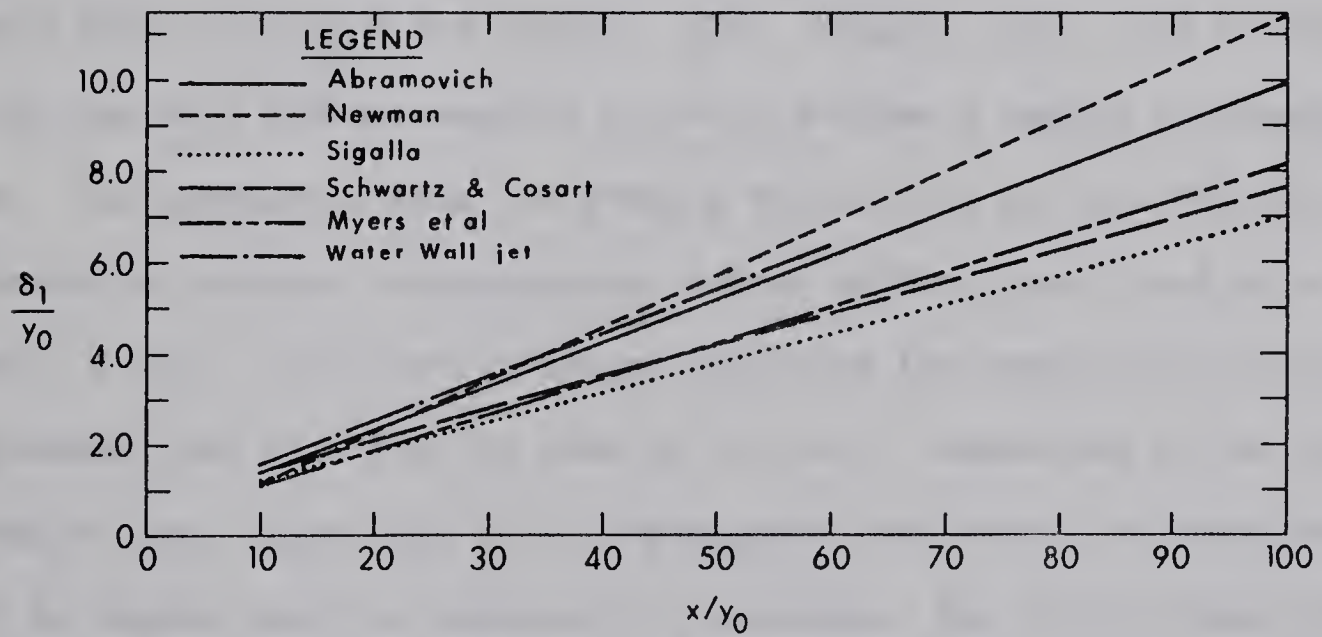


Fig. III-10. Study of Length Scale

CHAPTER IV

REATTACHED WALL JETS

4.1 Introduction

This chapter presents the study of the diffusion of a deeply submerged plane jet issuing from an outlet situated directly over an abrupt drop in the bed.

Consider the case of a plane turbulent jet of uniform velocity U_0 , and depth y_0 , issuing from a nozzle situated at a height h above the bed, as shown in Fig. IV-1. The outlet is deeply submerged. The jet, after leaving the nozzle, curves toward the solid boundary due to the reduction of the pressure below the jet--this is known as the Coanda effect (Bourque and Newman, 1960; Newman, 1961)--and reattaches to the bed at a certain section so as to enclose a region of separate flow. The pressure inside the eddy region will be less than the hydrostatic pressure corresponding to free surface level, and as a result of this, for given upstream conditions the mass rate of flow will be greater than that for the case of no step. Downstream of the reattachment line, there will be an impingement zone where the pressures will be higher than the hydrostatic pressures. Due to the steep favourable pressure gradients existing in the impingement zone, the flow is accelerated and the high velocity filaments will be in the neighbourhood of the bed. At the end of the impingement zone, the acceleration ceases. Beyond the end of the impingement zone the high velocity stream undergoes turbulent diffusion analogous to that of a plane turbulent wall jet.

This forward flow, which has the characteristics of a wall jet, is called the "Reattached Wall Jet."

4.2 Review of Previous Work

Certain gross characteristics of the flow over a drop situated downstream of a sluice gate have been studied by Escande (1946) and Jaegar (1957). However, there appears to be no detailed study of the diffusive flow--viz., the study of velocity and bed shear stress distribution--due to a submerged reattaching jet, in hydraulic engineering literature.

The problem of the reattaching jets has received considerable attention in Aeronautical and Mechanical engineering, especially in connection with the study of the Coanda effect. Bourque and Newman (1960) and Sawyer (1960, 1963) have studied the length of the eddy, L_e , and the minimum and maximum pressures, due to a reattaching jet, for values of h/y_0 greater than 3.50. Regarding the reattached wall jet region, Bourque and Newman (1960) in connection with their study of reattachment of a plane jet on to an inclined plate, found that the velocity distribution well downstream of the reattachment line was similar and agreed well with Glauert's theory (Glauert, 1956). There appears to be no other investigation on the subject, so no information is available on the variation of the length scale, velocity scale and bed shear stress of a reattached wall jet.

4.3 Present Study

An experimental study of the diffusion of a plane turbulent submerged jet situated over an abrupt drop was undertaken with the main

aim of studying the velocity and bed shear stress characteristics of the reattached wall jet. Data on the length of the eddying region and the maximum pressure on the bed were also obtained to supplement the available information. The investigation was limited to small values of h/y_o , which are of interest in the field of Hydraulic engineering.

The gross characteristics of the flow like discharge coefficient and tailwater elevation were not studied.

Two types of outlets-- 1) Nozzle outlet (data: Group-I) and 2) Sharp edged sluice gate (data: Group-I(S))--were studied.

4.4 Nozzle Outlet over an Abrupt Expansion

4.4.1 Experiments

The experiments were conducted in Flume A under conditions of high submergence. A total of 10 runs with h/y_o varying from 0 to 6 were conducted. The summary of experimental data is given in Table IV-1

TABLE IV-1

REATTACHING WALL JET (NOZZLE OUTLET)

Data: Group-I Summary of Experimental Data

Expt. No.	q cfs/ft	y_o in.	h in.	L_e in.	ΔH in.	\bar{y}_t in.	U_o fps.	$\frac{U_o y_o}{v}$ $\times 10^4$
I-A-1	0.677	1.00	3.312	9.50	11.8	25.2	8.14	7.10
A-2	0.683	1.00	3.312	9.75	11.9	25.5	8.23	7.17
A-3	0.810	1.00	3.312	9.75	16.6	26.0	9.73	8.50
B-1	0.411	0.55	3.312	8.00	14.6	20.8	9.00	4.31
B-2	0.480	0.55	3.312	7.50	21.9	19.3	10.90	5.04
C-1	0.604	0.75	1.344	4.50	17.0	20.2	9.85	6.34
D-1	0.945	1.34	1.344	5.00	12.1	26.0	8.47	9.92
D-2	0.875	1.34	1.344	5.00	10.7	27.1	8.00	9.20
E-1	0.885	1.375	0	0	13.3	26.8	8.50	9.30
E-2	0.534	0.875	0	0	13.3	27.4	8.50	5.60

and the detailed data are given in Appendix D (Tables D-3 and D-5). One run, (I-A-1), was devoted to measuring the pressure field in the eddy. The length of the eddy was measured, by colour injection, in all the runs.

4.4.2 Length of the Eddying Region

The length of the eddying region, L_e , for submerged flow can be represented as

$$L_e = f(U_o, y_o, h, \rho, \mu) \quad (4.1)$$

By dimensional analysis,

$$L_e/h = f_1\left(\frac{\rho U_o y_o}{\mu}, \frac{h}{y_o}\right) \quad (4.2)$$

For large values of Reynolds number, $R = \rho U_o y_o / \mu$, viscosity is known to have negligible effect on turbulent flow, and hence

$$L_e/h = f_1(h/y_o) \quad (4.3)$$

The present data are plotted as L_e/h vs. h/y_o in Fig. IV-2, along with the data of Bourque and Newman (1960) and Sawyer (1960) in the range of $h/y_o < 10.0$. It is seen that the present data are in good agreement with the results of other investigators. The data of Tani et al.'s study on flow separation of a stream associated with a step, plotted in Fig. IV-2, serve as a reference point in extrapolating the mean curve to small values of h/y_o .

4.4.3 Pressures in the Eddying Region

Designating the difference between the pressure at a point and the corresponding hydrostatic pressure at the same point as Δp , a

pressure coefficient C_p is defined as $C_p = \Delta p / (\rho U_o^2 / 2)$. The variation of C_p in the eddying region, for run I-A-1, is shown in Fig. IV-3(a). Using this figure, the contours of C_p in the eddying region are plotted in Fig. IV-3(b). Even though no great accuracy can be claimed for this figure, it is helpful in indicating the true nature of the pressure distribution in the eddying region. The contours resemble the pressure distribution in a point vortex situated off-center in the eddying region. Also, it is interesting to note that while the pressure on the bed falls from the corner towards the center and rises, the minimum pressure recorded by a series of piezometers in the bed is not the overall minimum pressure in the eddy.

4.4.4 Impingement Region

The deflected jet impinges on the bed in a region surrounding the reattachment line and as a result of this, pressures in excess of the hydrostatic pressures are built up over the bed. A typical plot of piezometer readings is shown in Fig. IV-4. A smooth curve through the piezometer readings, as in Fig. IV-4, was used to read the maximum pressure. It was observed that the position of reattachment line coincides fairly well with the position of the maximum pressure. A similar observation has been recorded by Sawyer (1960).

If Δp_m is the maximum value of Δp in the impingement region, a pressure coefficient C_{pm} is defined as $C_{pm} = \Delta p_m / (\rho U_o^2 / 2)$. By dimensional analysis, it can be shown that for high values of R ,

$$C_{pm} = f(h/y_o) \quad . \quad . \quad . \quad . \quad . \quad (4.4)$$

The present data and all other available data on C_{pm} are plotted in Fig. IV-5 as C_{pm} vs. h/y_o . It is seen that there is considerable scatter in the region $4.0 < h/y_o < 7.0$. However, if the dotted line

in Fig. IV-5 is considered to indicate approximately the variation of C_{pm} with h/y_0 , it can be seen that C_{pm} decreases very slowly with h/y_0 .

4.4.5 Analysis of Velocity Profiles in the Reattached Wall Jet

(a) Similarity

Fig. IV-6 is a plot of the velocity profiles measured in a typical run, (I-A-2). From a study of this figure it can be observed that at sufficient distance beyond the reattachment line the velocity profiles have the characteristic shape of a wall jet. The velocity profiles in the downstream region of the reattachment line, at various values of x/y_0 , were analysed for similarity. The velocity profile at a given x/y_0 is non-dimensionalised as u/u_m against y/δ_1 . Fig. IV-7 shows such a dimensionless plot for the various runs. In this plot, for a given h/y_0 , the velocity profiles beyond a certain value of x/y_0 have all collapsed into one single curve. Further, the dimensionless velocity distribution curve is seen to be in good agreement with the corresponding classical wall jet curve, for all h/y_0 tested. Thus in the reattached wall jet, the velocity profiles beyond a certain value x_1/y_0 are similar and the similarity profile itself is independent of h/y_0 and is the same as that of the classical wall jet (see Fig. IV-7). The variation of x_1/y_0 with h/y_0 is shown in Fig. IV-8, where it is seen that x_1/y_0 varies linearly with h/y_0 and is given by the relation

$$x_1/y_0 = 13.5 + 2.83 h/y_0 \quad . \quad . \quad . \quad (4.5)$$

(b) Velocity Scale

The variation of the maximum velocity, u_m , is shown plotted, as u_m/U_0 vs. x/y_0 for various values of h/y_0 , in Fig. IV-9. It can be seen that, in general, the length of the potential core is very small and u_m/U_0 decreases very fast till reattachment, as in this region the emerging stream is a curved plane free jet. After the reattachment there is a slight recovery of u_m/U_0 and then onwards there is a decay at a rate less than that of the classical wall jet. Further, the recovery and the decay rate after the reattachment depend upon h/y_0 . It is interesting to note that, for a given h/y_0 , after a certain distance x_2 , the decay of u_m/U_0 with x/y_0 follows the same curve as that of the classical wall jet. In this region, so far as the velocity decay is concerned, the flow seems to become oblivious of the nozzle location. For a given h/y_0 , $x_2/y_0 > x_1/y_0$ and the variation of x_2/y_0 with h/y_0 is shown in Fig. IV-8.

Thus the maximum velocity decay of a reattached wall jet can be considered to be made up of two portions:-- 1) the region between x_1 and x_2 , where for a given x/y_0 the value of u_m/U_0 and its decay rate are dependent upon the value of h/y_0 , i.e., a characteristic decay region 2) the region beyond x_2 where the value of u_m/U_0 at any x/y_0 is the same as that of the classical wall jet and this region can be termed the classical wall jet decay region.

(c) Length Scale

In Fig. IV-10, δ_1/y_0 is plotted against x/y_0 for the various runs. The curve of water wall jet ($h/y_0 = 0$) is used as a reference for

comparison purposes. For each h/y_o the variation is linear in the initial portion and exhibits a tendency to join the line of $h/y_o = 0$ at a certain relative distance x_3/y_o . The variation of x_3/y_o with h/y_o is shown in Fig. IV-8, from which it is seen that $x_3/y_o > x_2/y_o > x_1/y_o$. Since the data in Fig. IV-10 are insufficient to delineate accurately the limits of the characteristic growth region in the different curves, the curve-3 in Fig. IV-8 should be considered only approximate.

4.4.6 Study of Bed Shear Stress

The velocity distribution in the boundary layer portions beyond the zone of impingement was of the power law type with the power of about $1/12$. Thus the use of Preston tube to measure τ_o in those sections is valid. Even though its use in the impingement region is questionable, the Preston tube is used to get at least the order of magnitude of the bed shear stress in that region. The bed shear stress variation in the various runs is shown in Fig. IV-11. τ_o is zero at the reattachment line, reaches a maximum and then decreases gradually with x . The variation of τ_o is analysed in terms of the similarity of shear stress profiles analogous to the study of velocity profiles discussed earlier. In Fig. IV-12, τ_o/τ_{om} is plotted against \bar{x}/θ_1 , where (as in the definition sketch of Fig. IV-11) \bar{x} = longitudinal distance measured from the reattachment line, τ_{om} = maximum value of τ_o for a given τ_o vs. x profile, θ_1 = distance from the reattachment line to the point where $\tau_o = \tau_{om}/2$ and $d\tau_o/d\bar{x}$ is negative. It can be seen that the scatter of the data is very small and a single curve, independent of h/y_o , can be drawn through the data. Thus the longitudinal variation of bed shear stress can be considered similar.

The variation of τ_{om} is studied by plotting $C_{fm} = \tau_{om}/(\rho U_o^2/2)$ against h/y_o in Fig. IV-13. It is found that C_{fm} decreases, quite appreciably, with increase in h/y_o . Also shown in Fig. IV-13, is the variation of the length scale θ_1 , which is plotted as θ_1/h vs. y_o/h . The variation is linear and is given by the expression

$$\theta_1/h = 3.2 + 31.2 (y_o/h) . \quad . \quad . \quad . \quad (4.6)$$

4.5 Sluice Gate Outlet over a Drop

4.5.1 General

While the nozzle outlet studied above (sec. 4.4) represents one limit of idealised outlet situation, a sharp edged sluice gate can be considered as another limit of an idealised outlet and probably a nearer approximation to many situations existing in practice. The flow from a sluice gate situated over an abrupt drop is slightly different from the nozzle outlet case for the reason that the jet initially undergoes a contraction due to action of inertial forces and then expands due to turbulent diffusion. This could be expected to affect the various characteristics of the flow. Further, there is the problem of selecting a depth parameter which would adequately represent the length characteristic of the jet.

An exploratory study of the submerged flow from a sharp edged outlet situated over an abrupt drop was conducted--on essentially the same lines as that of the nozzle outlet case--to find the modification of the flow due to change in the nature of the outlet.

4.5.2 Experiments and Data

The experiments were conducted in Flume A and consisted of six series. The summary of experimental data (Group: I(S)) is given in Table IV-2 and the detailed data used in the analysis are in Appendix D (Tables D-4 and D-5). A definition sketch is given in the inset of Fig. IV-14.

TABLE IV-2

REATTACHING WALL JET (SLUICE GATE OPENING)

Data: Group-I(S) Summary of Experimental Data

Expt. No.	q cfs/ft.	a in.	h in.	ΔH in.	y_t in.	U_o ft./sec.	L_e in.	y_o^* in.
I(S)-A-1	0.586	1.344	1.344	12.20	24.60	8.23	3.25	0.856
A-2	0.715	1.344	1.344	18.30	23.10	10.06	8.00	0.852
B	0.775	2.000	1.344	9.70	25.60	7.20	3.50	1.290
C	0.490	1.000	3.312	14.80	25.00	9.14	5.75	0.643
D	0.773	1.677	3.312	13.30	25.00	8.62	6.25	1.080
E	0.720	1.550	3.312	13.20	19.50	8.56	5.75	1.010

4.5.3 Effective Depth of the Outlet

Fig. IV-14 shows the velocity distributions at various sections in a typical run. Referring to the velocity distribution at section $x = 1.0$ in., in this figure, it can be seen that the jet from the sluice gate opening has undergone a noticeable contraction and has a potential core. Such potential cores existed in all the other runs. If U_o is the velocity of the potential core it could be expressed as

$$U_o = k \sqrt{2g \Delta H} \quad . \quad . \quad . \quad . \quad . \quad (4.7)$$

where ΔH = difference in water level on either side of the gate, and k is a coefficient whose value varied from 1.00 to 1.021 in the various runs. For the case of $h = 0$ the value of k was 1.0 (see Appendix A).

For purposes of correlating the data, a hypothetical depth y_o^* --designated as the equivalent depth of the outlet--is defined as

$$y_o^* = q/U_o \quad . \quad . \quad . \quad . \quad . \quad (4.8)$$

where q is the discharge intensity emerging from the sluice gate. If "a" is the gate opening, in the six runs of the present study the value of y_o^*/a varied from 0.636 to 0.651 with an average value of 0.642 .

4.5.4 Eddying and Impingement Region

In run I(S)-E , a survey of the pressure field in the eddying and impingement region was conducted by using the screw driver probe. The contours of the pressure coefficient C_p are shown in Fig. IV-15. The pressure distribution in the eddying zone is similar to that of the nozzle outlet (Fig. IV-3(b)) but with the difference that the pressure coefficient rises rapidly on the downstream of the eye of the eddy. This figure very clearly illustrates the fact that while the overall minimum pressure is inside the eddy and hence cannot be measured by surface piezometers, the overall maximum is on the surface and can be measured by the surface piezometers.

The variation of the length of the eddy is studied by plotting L_e/h vs. h/y_o^* in Fig. IV-16. It is seen that the variation is similar

to that of the nozzle outlet case, but the values are about 30% smaller.

The pressure coefficient C_{pm} was calculated for all the runs and the plot of C_{pm} vs. h/y_o^* showed some scatter. An average value of $C_{pm} = 0.32$ was obtained for the range of h/y_o^* from 1.0 to 5.0.

4.5.5 Analysis of Velocity Profiles

The velocity profiles, for runs A through D, in the reattached wall jet region are tested for similarity in Fig. IV-17 by plotting u/u_m against y/δ_1 . As in the nozzle outlet case, here also, beyond a certain value of relative distance x_1/y_o^* , the velocity profiles are similar and agree well with that of the classical wall jet.

The variation of the velocity scale is studied, in Fig. IV-18, by plotting u_m/U_o against x/y_o^* . Also plotted is the curve of $h/y_o^* = 0$ (Rajaratnam, 1965-c), which is essentially the same as that of the classical wall jet (see Fig. III-1). The data clearly show the existence of a characteristic decay region which transforms to the classical wall jet decay region beyond a certain relative distance, x_2/y_o^* , as found in Sec. 4.4.5. However, the present data are insufficient to find the variation of the characteristic distances x_1 and x_2 .

The variation of length scale is studied in Fig. IV-18. The line $h/y_o^* = 0$ is due to Rajaratnam (1965-c) and is essentially the same as that of the classical wall jet case (see Fig. III-2). It is interesting to see that the length scale does not exhibit any characteristic growth region in the range of h/y_o^* tested, and grows essentially at the same rate as the classical wall jet.

4.5.6 Study of Bed Shear Stress

The profiles of bed shear stress, τ_o , measured by Preston tube, are shown in Fig. IV-19. These measurements are subject to the same limitation as mentioned in Sec. 4.4.6. These profiles are tested for similarity, by plotting τ_o/τ_{om} against \bar{x}/θ_1 , in Fig. IV-20(a). As before, the data lie on one single curve, indicating the similarity of bed shear stress profiles. Further, this curve is found to be essentially the same as the one obtained for the nozzle outlet (Fig. IV-12).

The scales of the shear stress similarity plot are studied in Fig. IV-20(b). The shear stress scale C_{fm} is well correlated with h/y_o^* . The value of $C_{fm} = 0.0055$ for $h/y_o^* = 0$, as plotted in Fig. IV-20(b), was obtained from the study of Rajaratnam (1965-c). The values of C_{fm} in the present case are found to be about 30% more than the corresponding case of the nozzle outlet.

The length scale, θ_1 , is seen to have a linear variation with y_o^*/h , given by

$$\theta_1/h = 1.0 + 25.0 y_o^*/h \quad . \quad . \quad . \quad . \quad (4.8)$$

as compared to Eq. 4.6 for the case of the nozzle outlet.

The variation of the bed shear stress studied in this chapter could possibly be used advantageously, in conjunction with some reasonable relation for the initiation of motion--for example, Shield's curve (Henderson, 1965)--to predict the length of protection below a submerged outlet situated over an abrupt drop in the channel.

4.6 Sluice Gate Outlet with $h/y_o^* = 0$

The submerged flow from a sluice gate outlet situated on the bed of a channel has been studied, as the case of a wall jet, by Rajaratnam (1965-c). His investigation is mainly in the region of developed flow, i.e., $x/y_o^* \geq 15$. There appears to be no information available on the nature of flow in the immediate vicinity of the sluice gate, i.e., small values of x/y_o^* . Hence an experimental investigation was conducted on the nature of flow in a zone located immediately below a submerged sluice gate on the bed of a channel and the results are presented in Appendix A.

4.7 Similarity Methods of Analysing the Profiles

The success with which the velocity profiles and the bed shear stress profiles in this study were reduced to corresponding simple dimensionless similarity profiles was encouraging enough to examine the possibility of reducing some of the important rapidly varied flow profiles, commonly occurring in Hydraulic engineering, into simple non-dimensional plots. This was tried, successfully, in the case of the profile of the hydraulic jump in rectangular channels and is reported in Appendix C.

4.8 Conclusions

From this study of the characteristics of submerged plane jets issuing from nozzles and sluice gate openings situated over an abrupt drop in the bed, the following significant conclusions are drawn:

- 1) After a certain distance downstream of the reattachment line, the velocity profiles in the reattached wall jet are similar and the similarity profile is the same as that of the classical wall jet.

- 2) The maximum velocity decay of the reattached wall jet is composed of a well defined characteristic decay region and a classical wall jet decay region.
- 3) The profiles of the bed shear stress distribution could be reduced to one dimensionless similarity plot. The non-dimensional shear stress and length scales of this plot depend upon the relative height of the drop, h/y_o .
- 4) For the sluice gate outlet, the effective depth y_o^* is adequate as a length characteristic of the outlet in correlating the data.
- 5) For the sluice gate outlet, the length scale of the reattached wall jet is the same as for the classical wall jet, in the range of h/y_o^* studied.

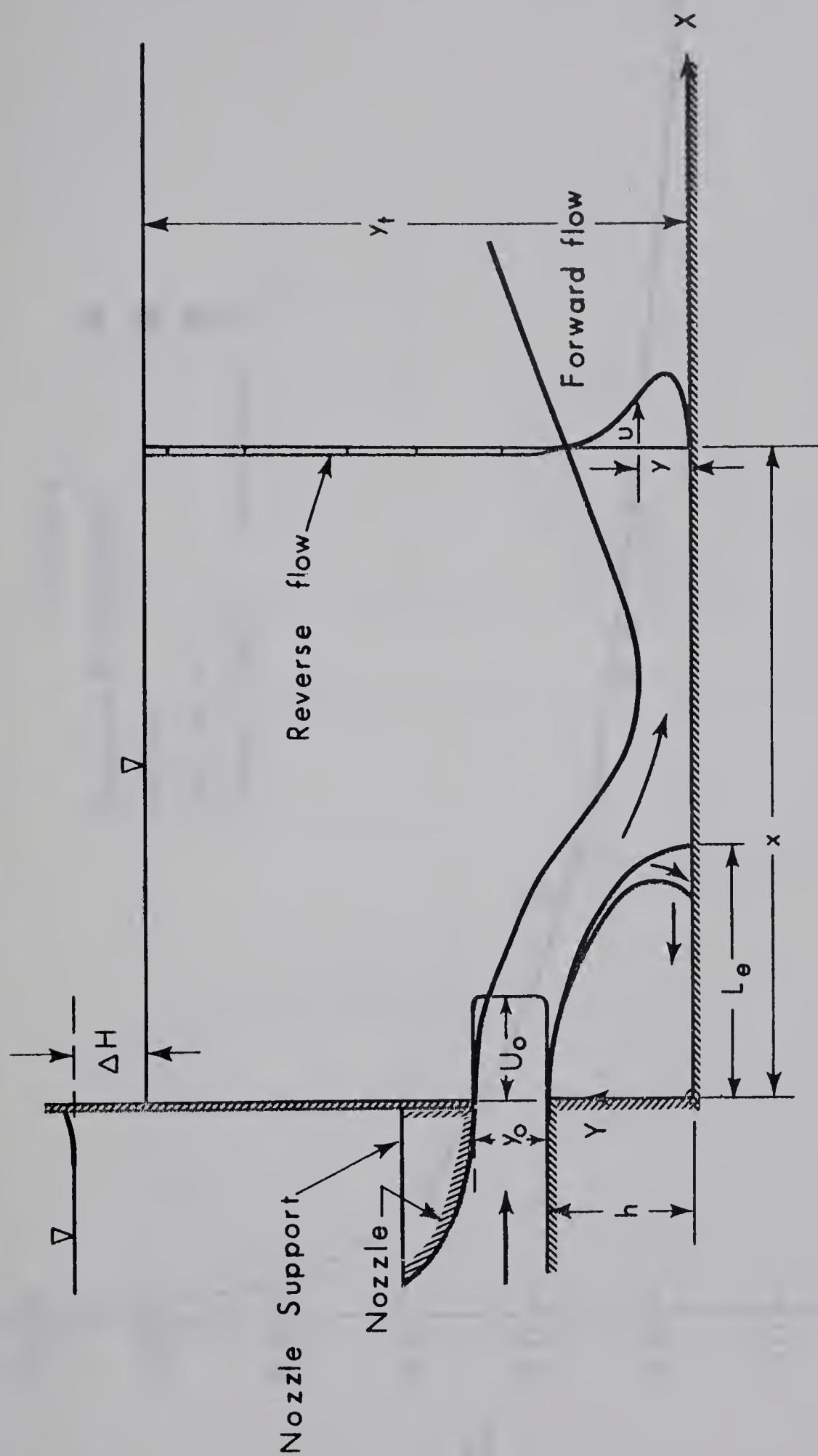


FIG.IV-1. DEFINITION SKETCH

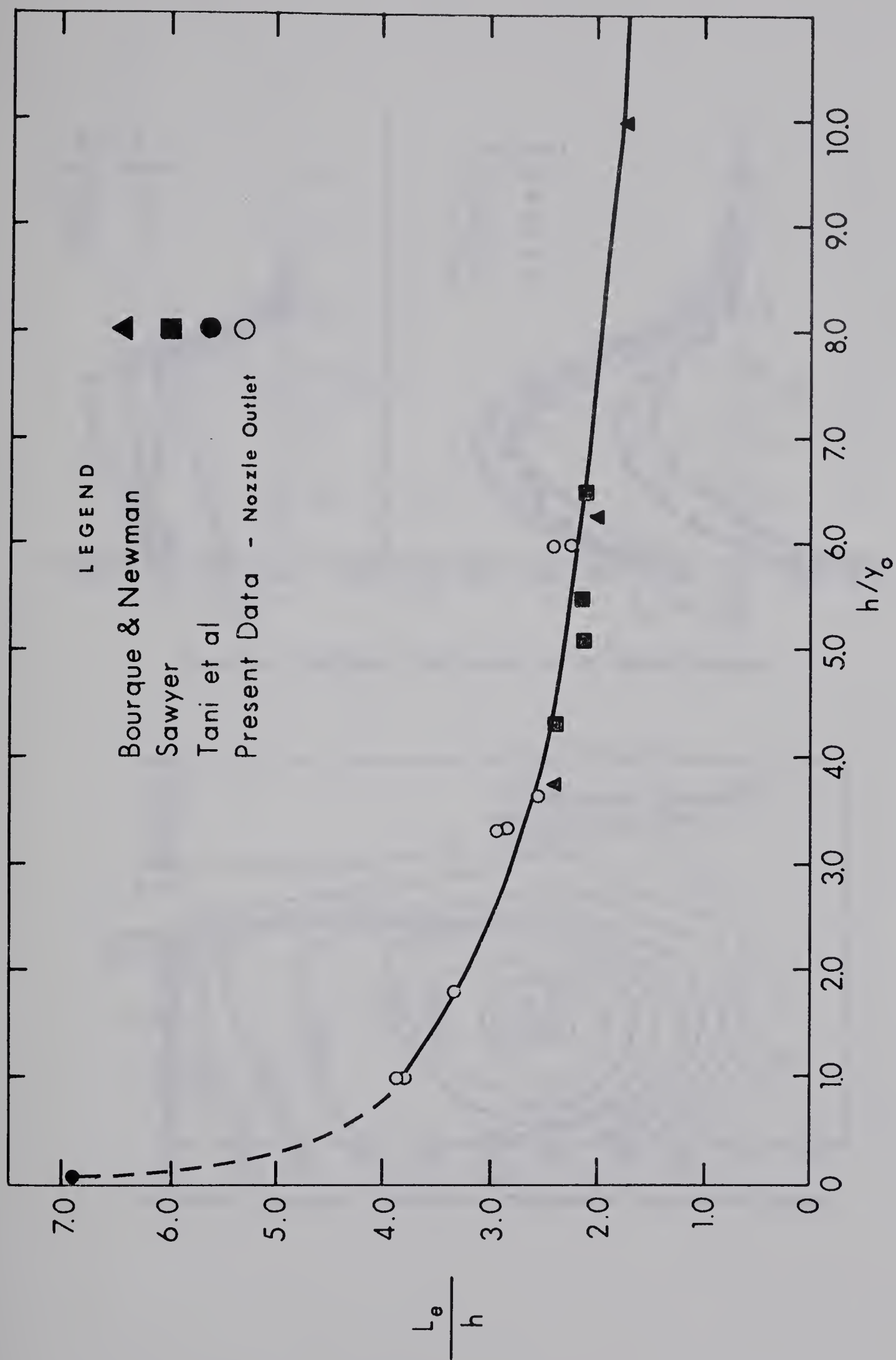


FIG.IV-2. VARIATION OF THE LENGTH OF EDDY (Nozzle Outlet)

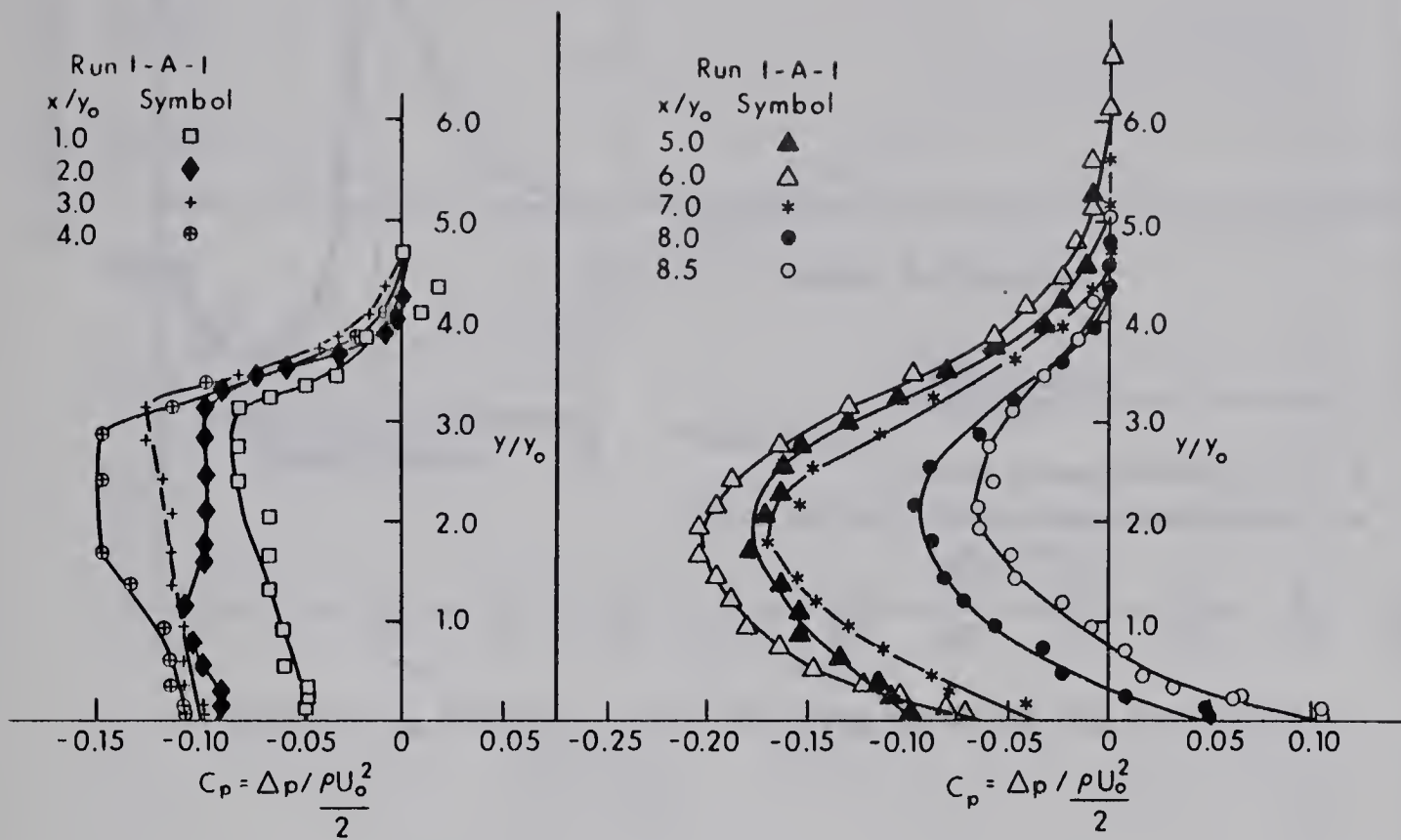


FIG. IV-3 (a). PRESSURE COEFFICIENT IN THE EDDYING REGION

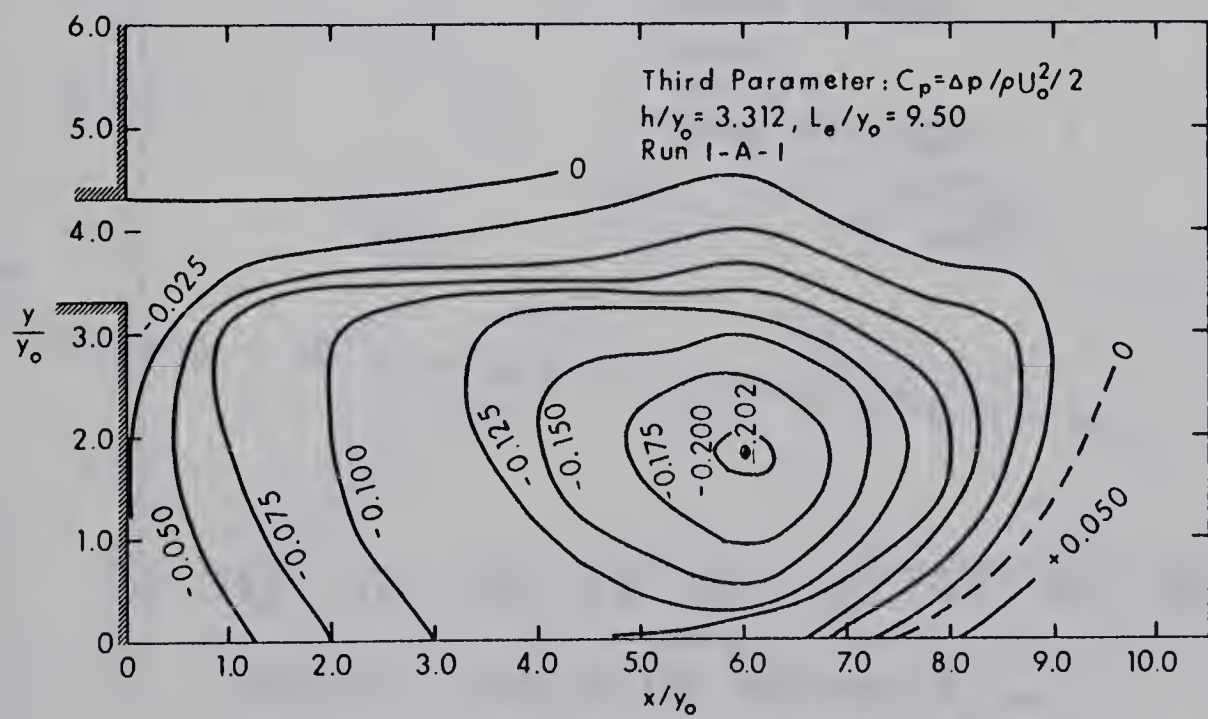
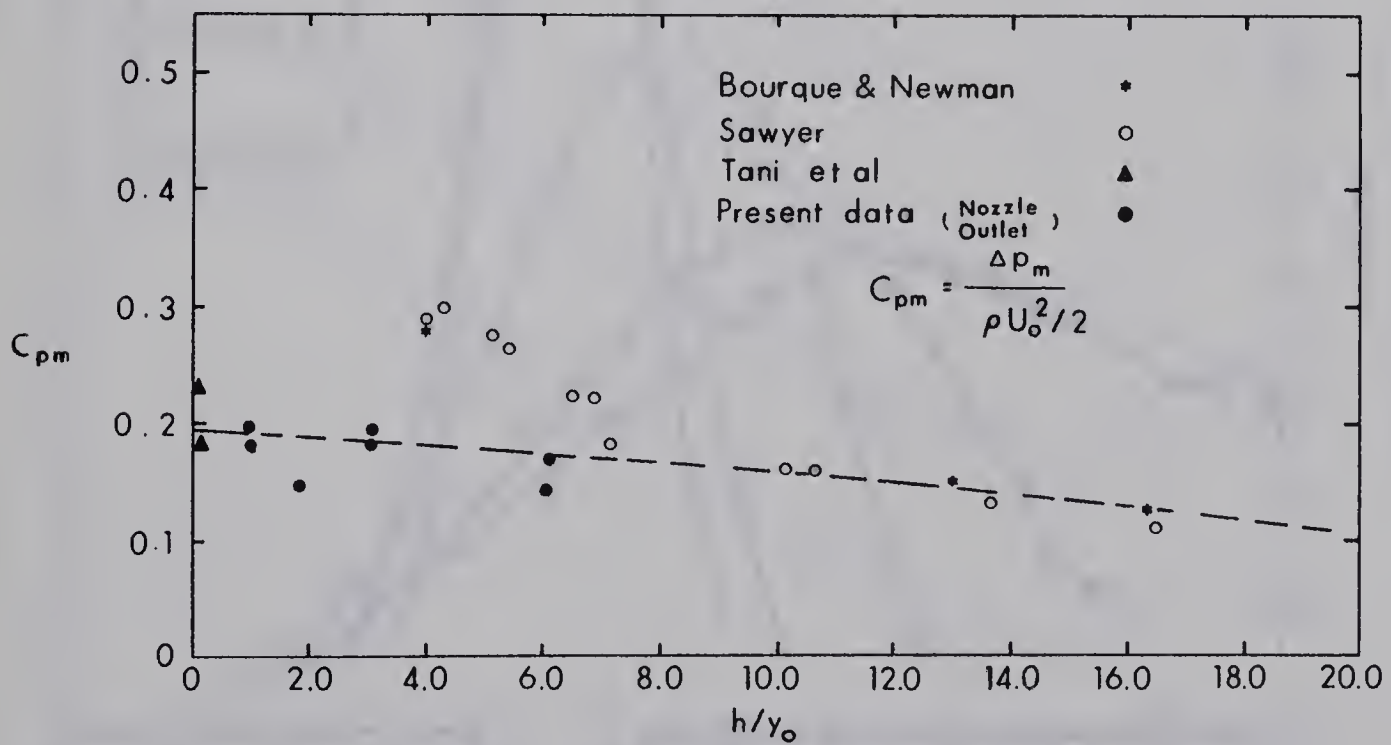
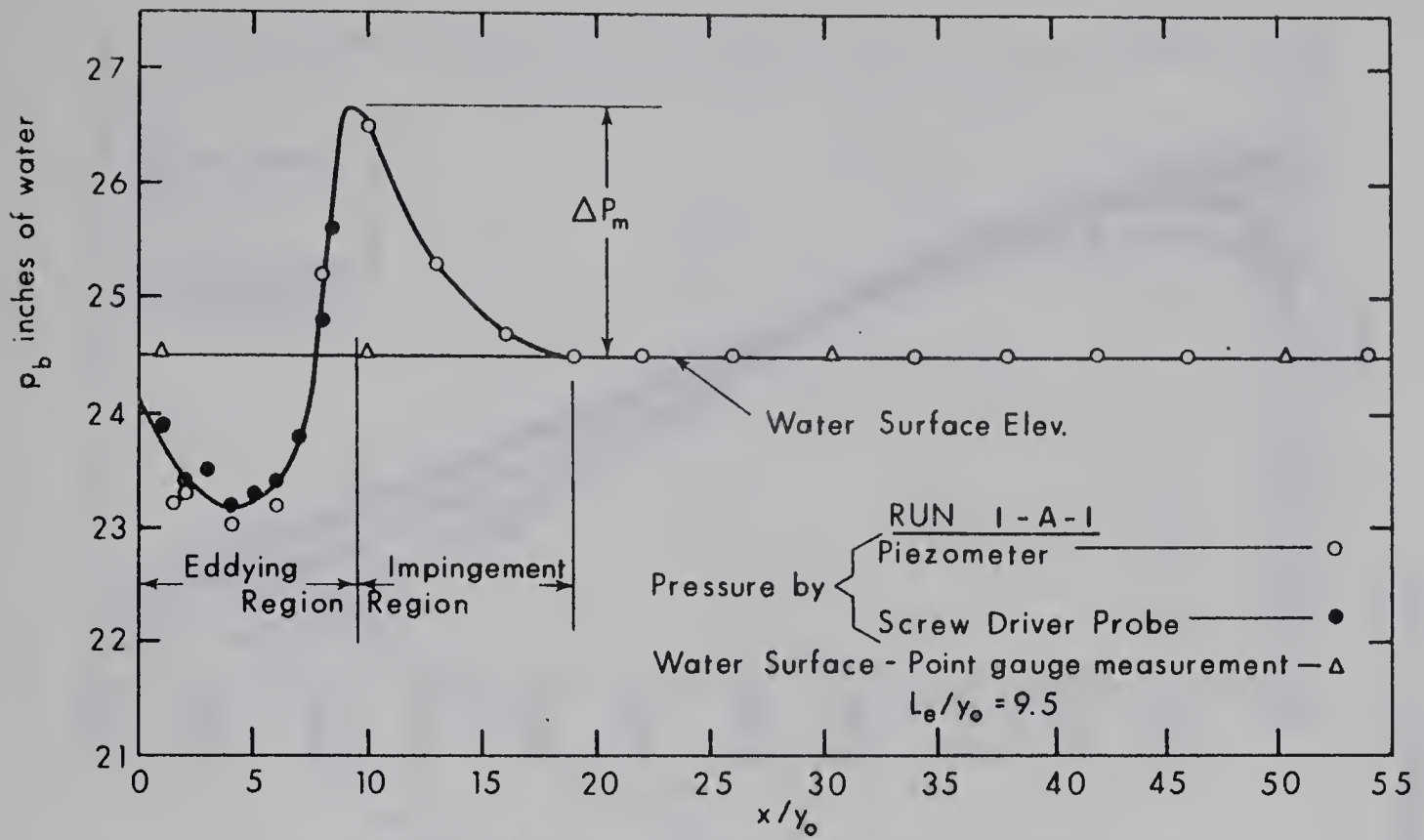


FIG. IV-3 (b). PRESSURE COEFFICIENT CONTOURS IN THE EDDYING REGION



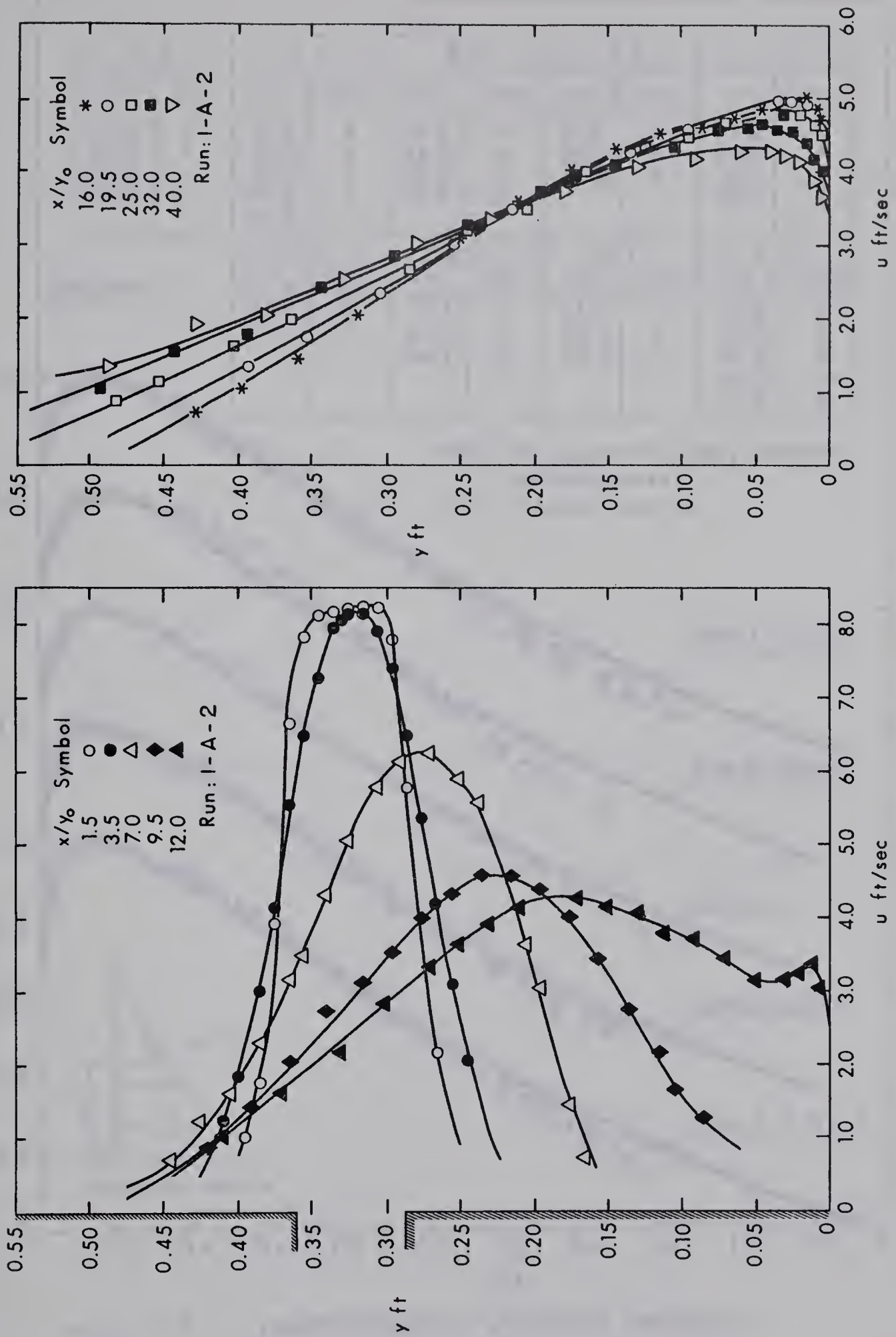


FIG. IV - 6. A TYPICAL VELOCITY DISTRIBUTION PLOT

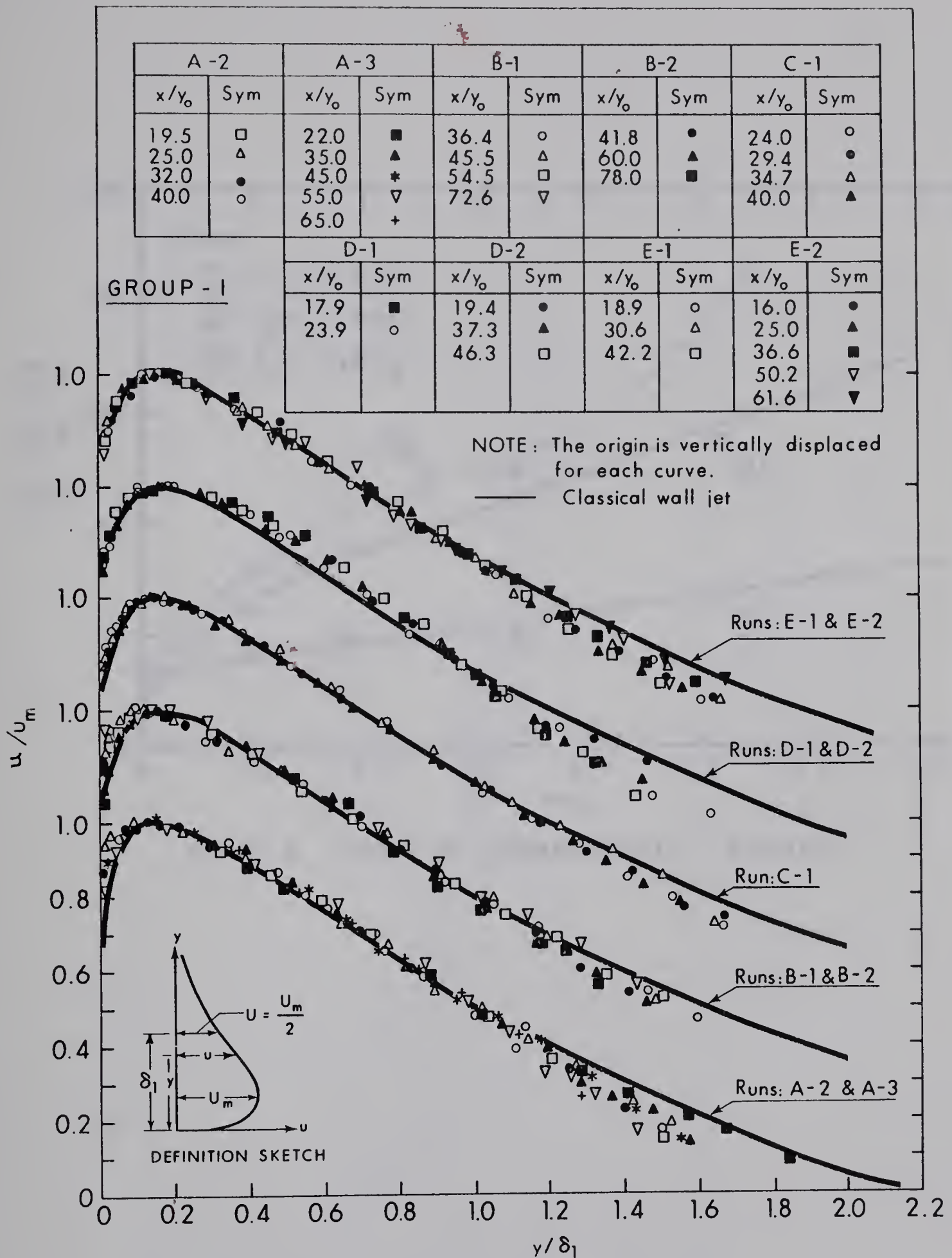


FIG. IV-7. DIMENSIONLESS VELOCITY PROFILES

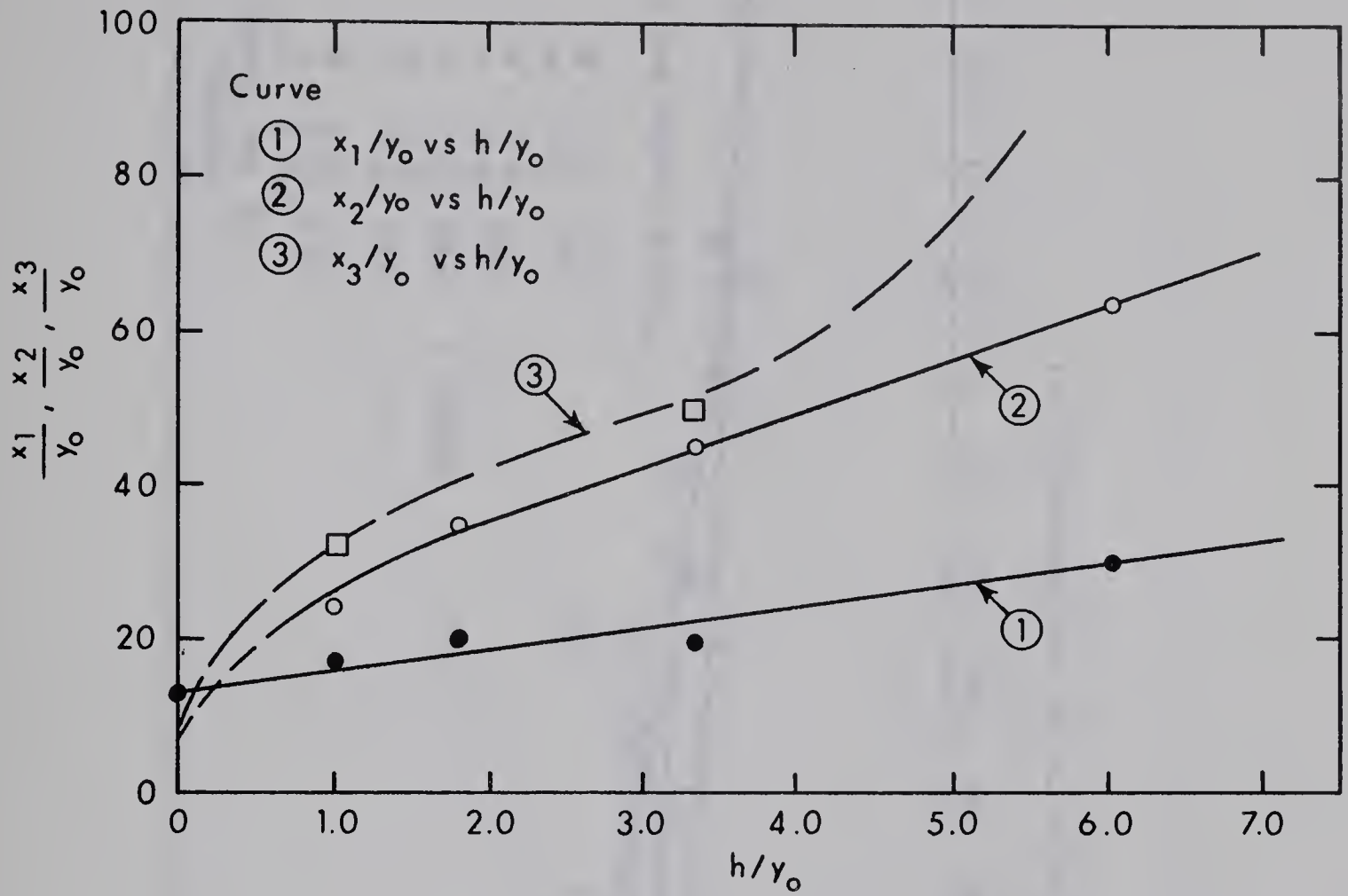


FIG. IV-8. STUDY OF CHARACTERISTIC LENGTHS

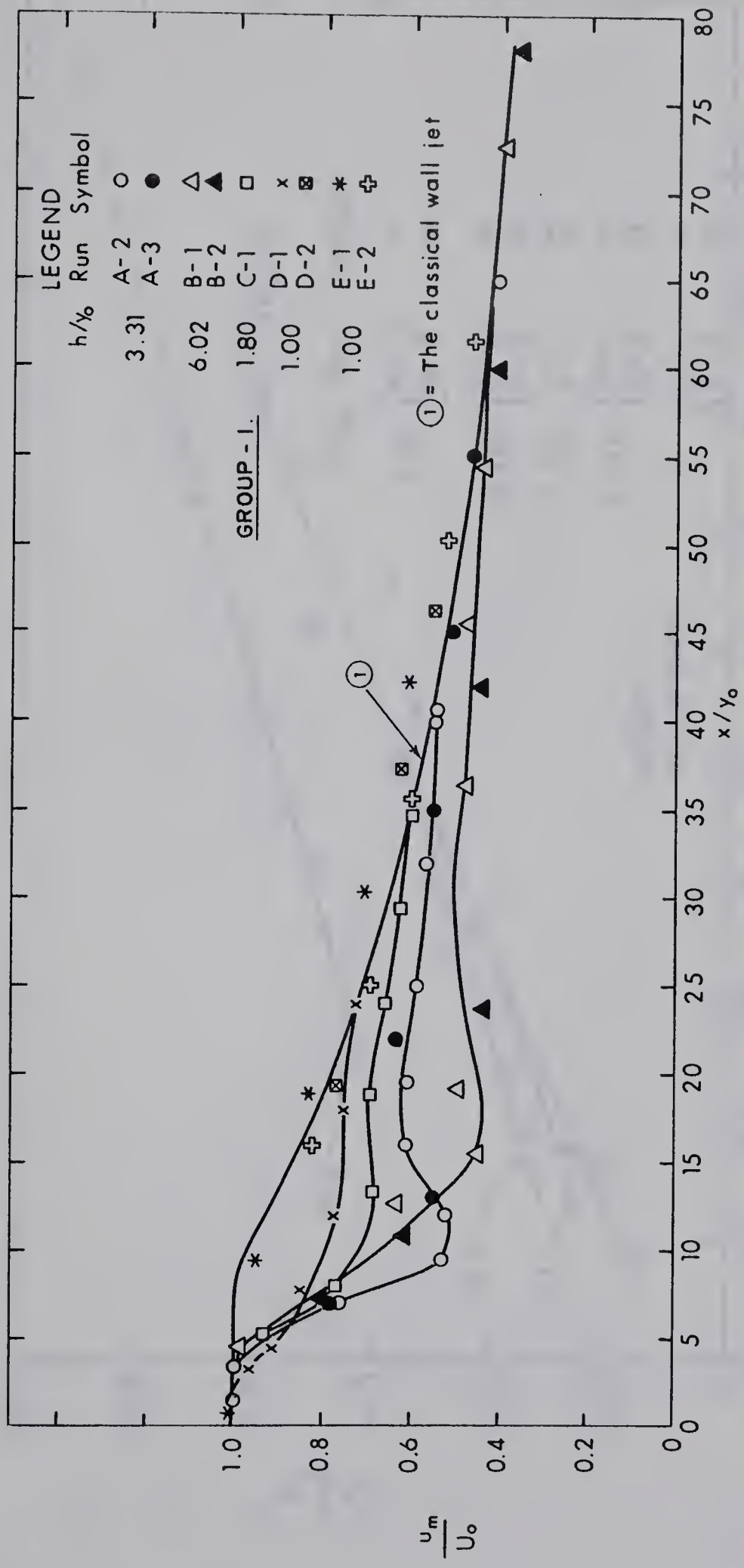


FIG. IV-9. DECAY OF THE MAXIMUM VELOCITY

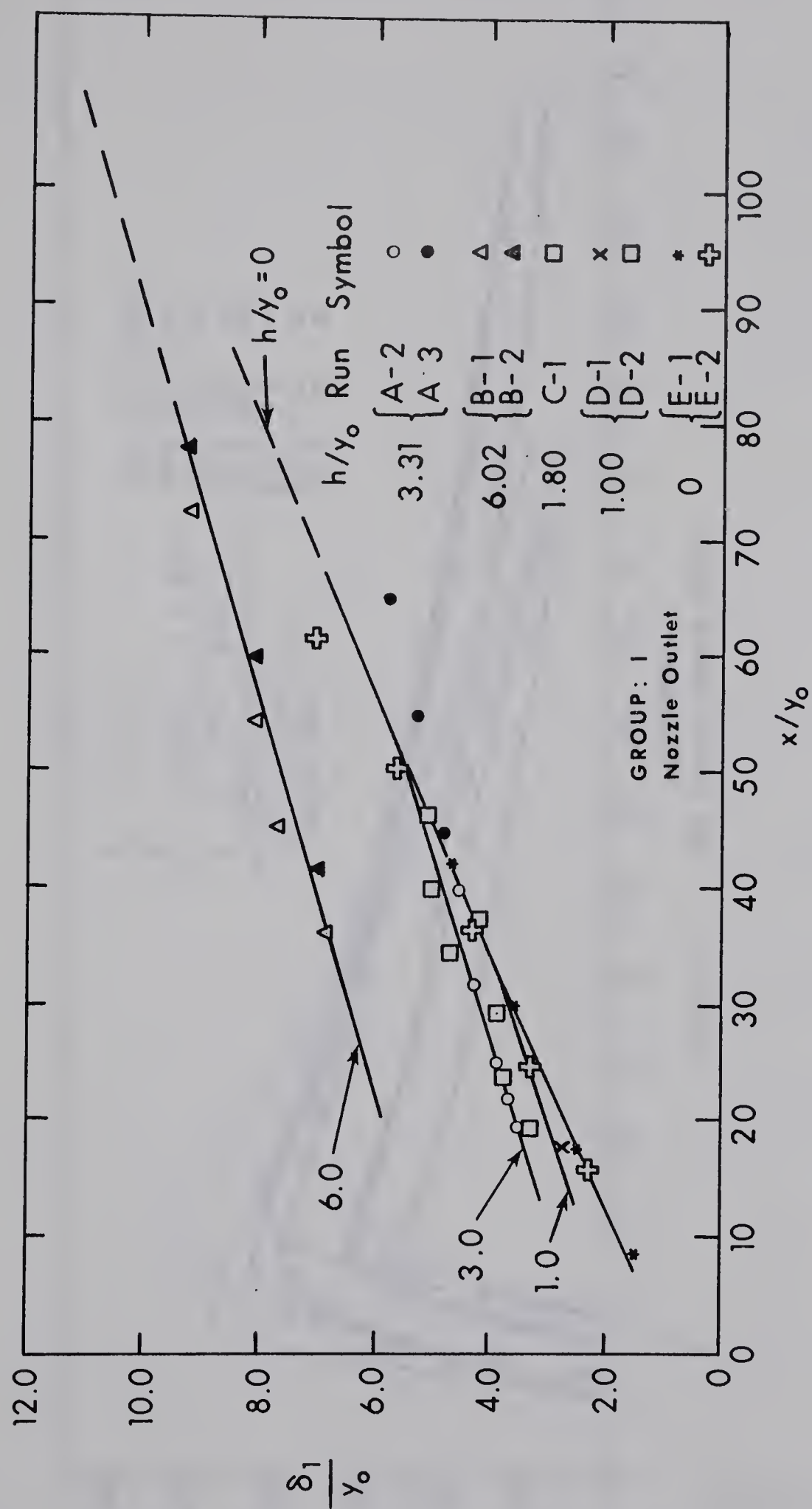


FIG. IV-10. VARIATION OF THE LENGTH SCALE

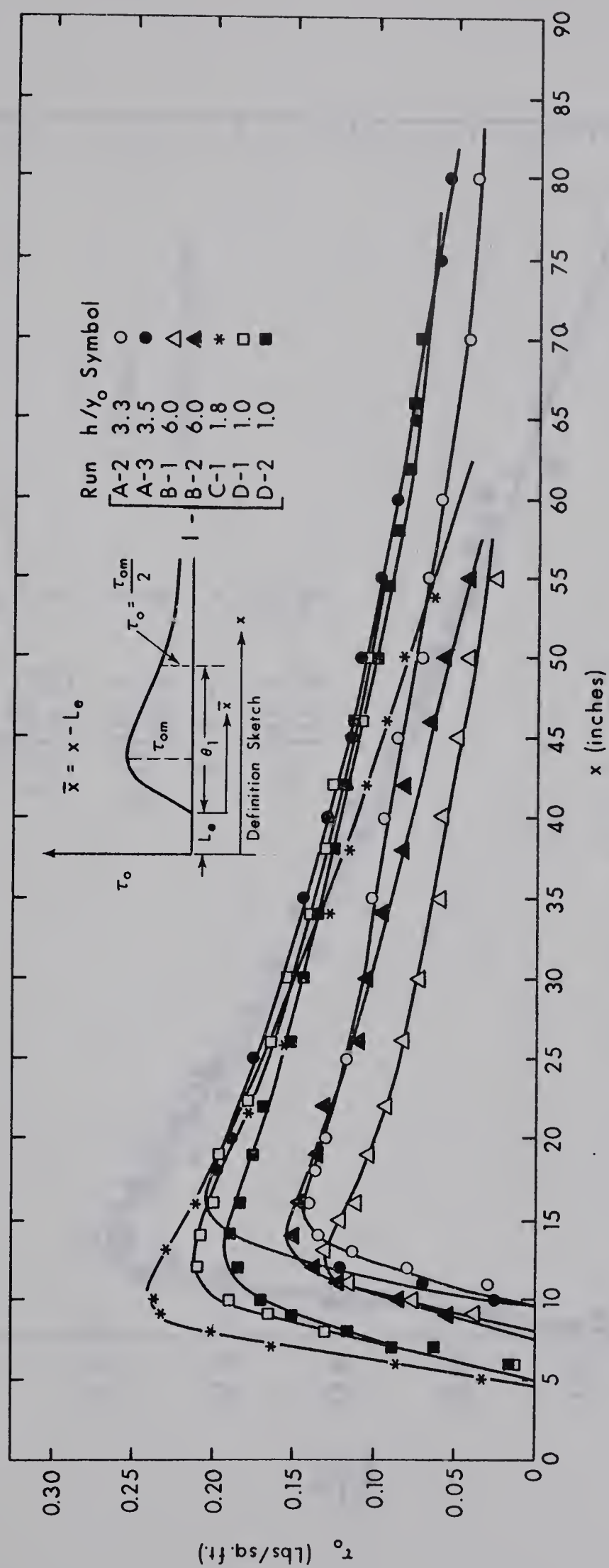


FIG. IV-11. BED SHEAR STRESS PLOTS

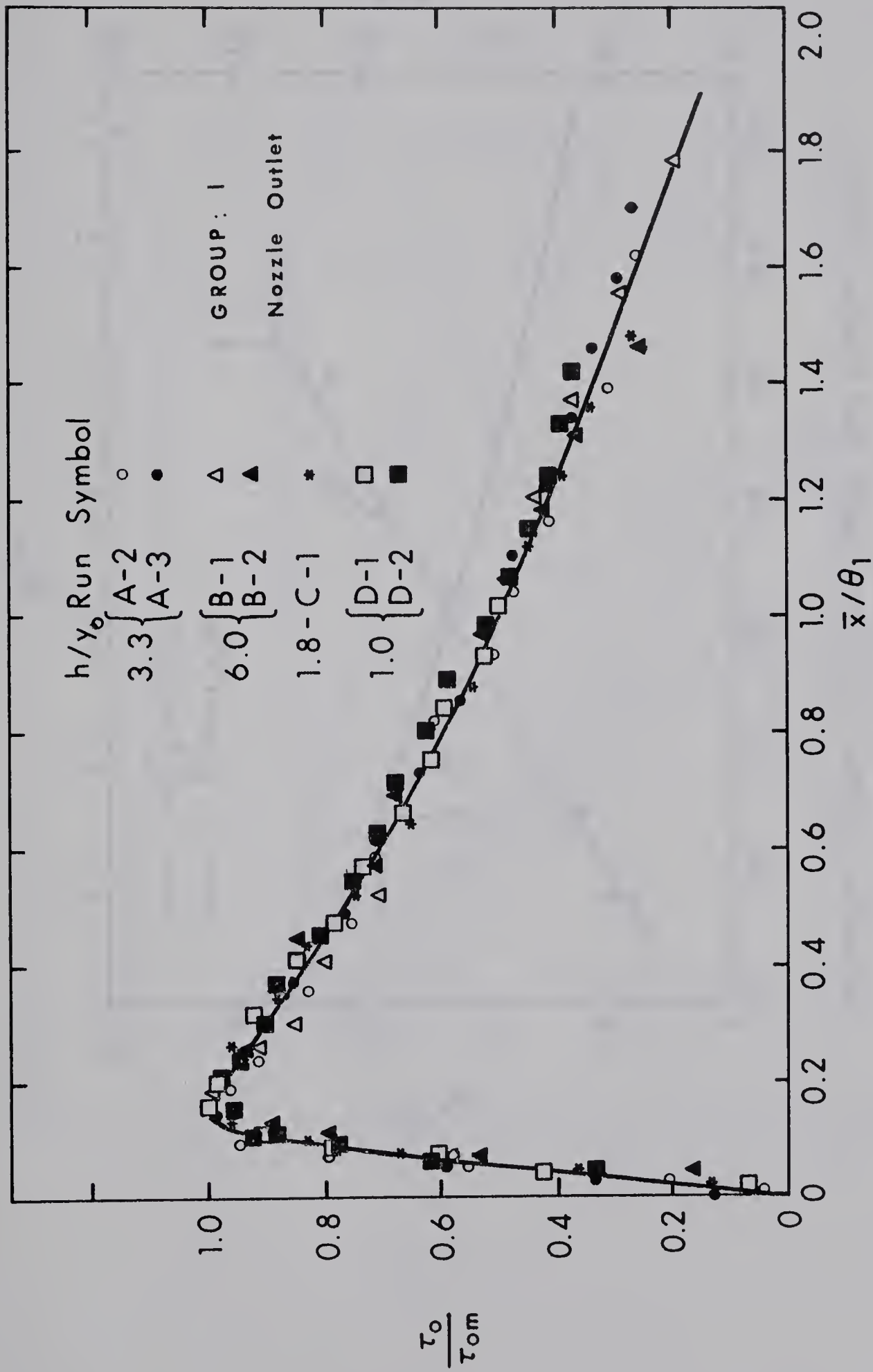


FIG. IV-12. DISTRIBUTION OF THE BED SHEAR STRESS

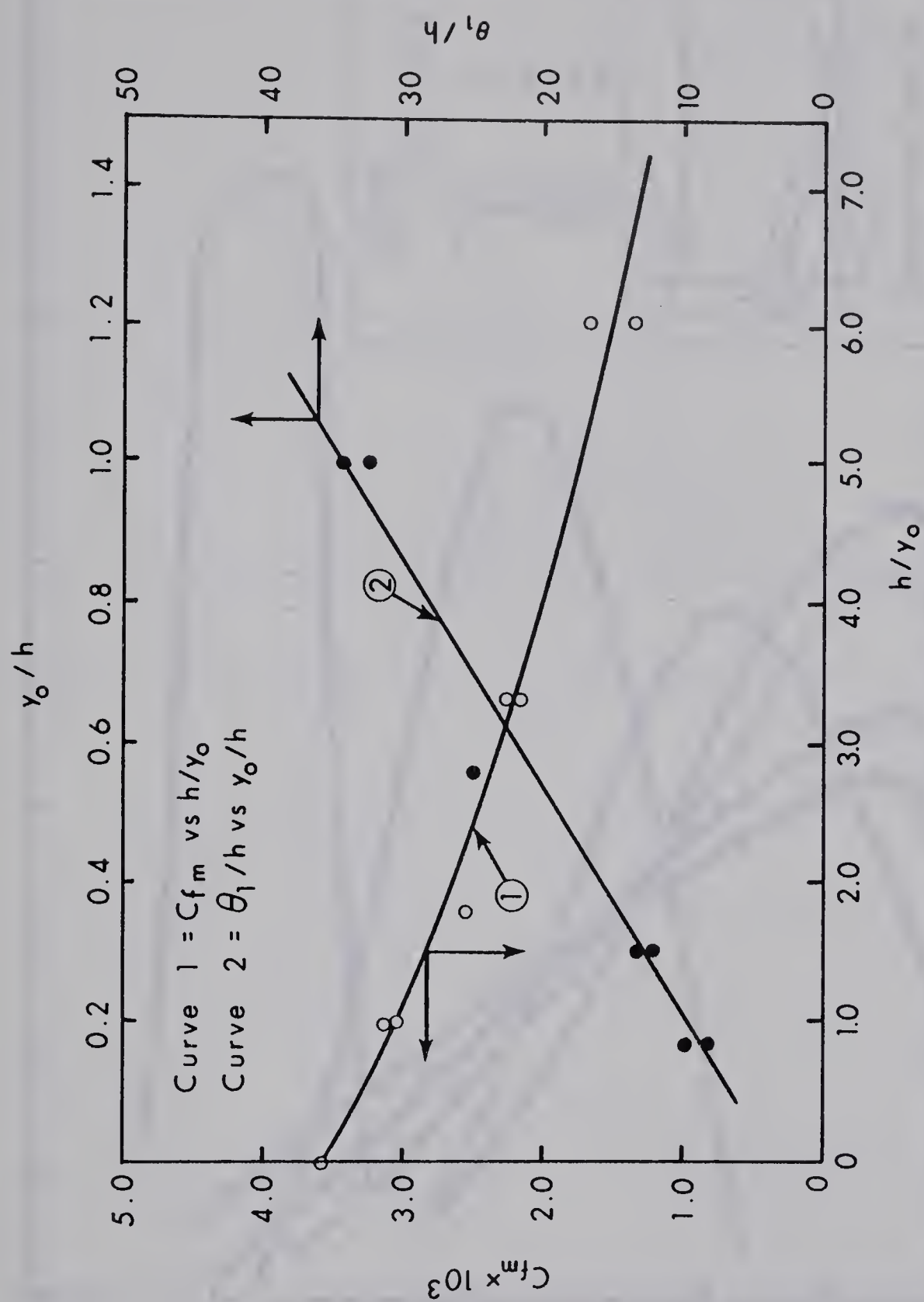


FIG. IV-13. STUDY OF SHEAR STRESS AND LENGTH SCALES
- NOZZLE OUTLET

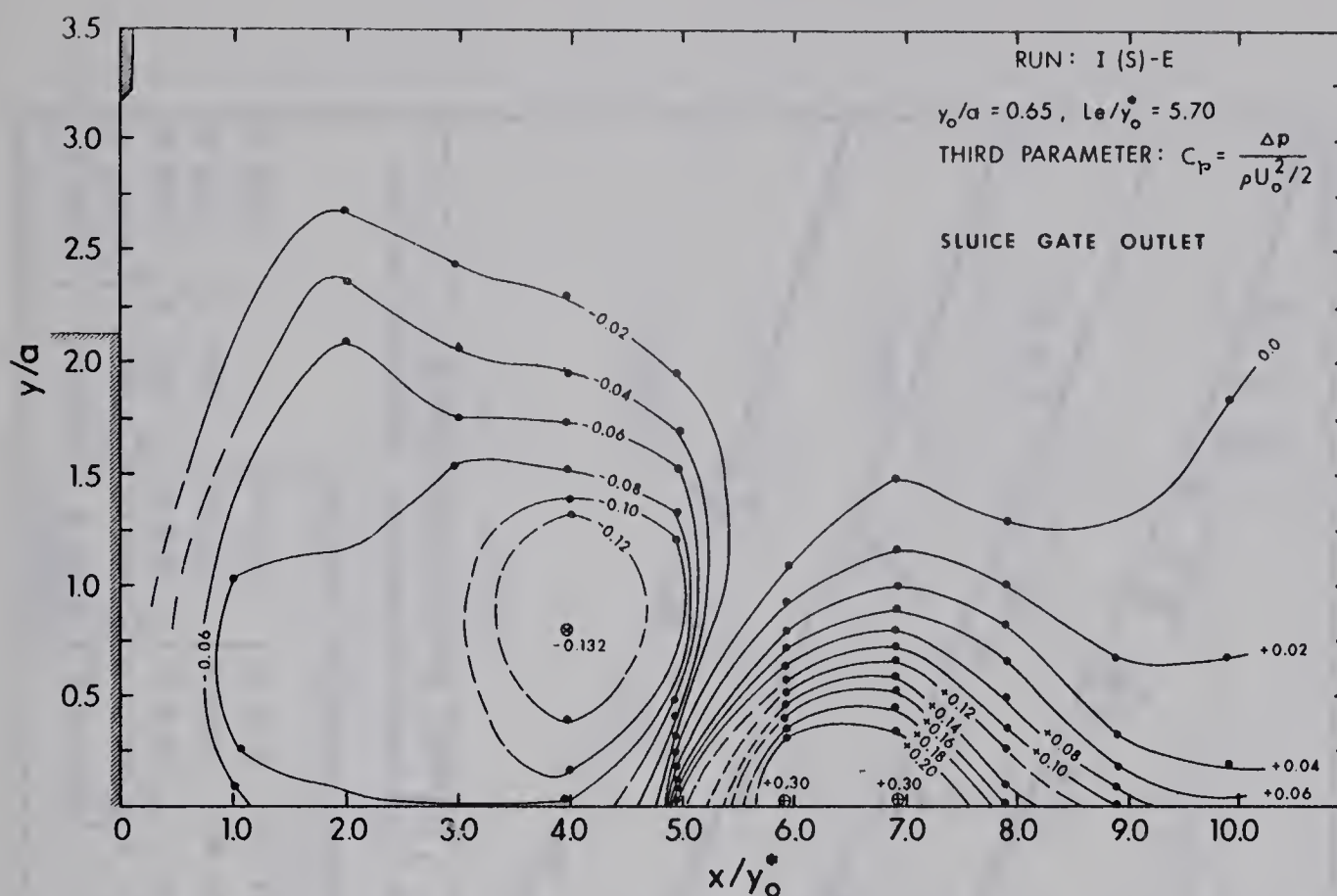


FIG. IV-15. Contours of Constant C_p in the Separation Bubble and Impingement Region

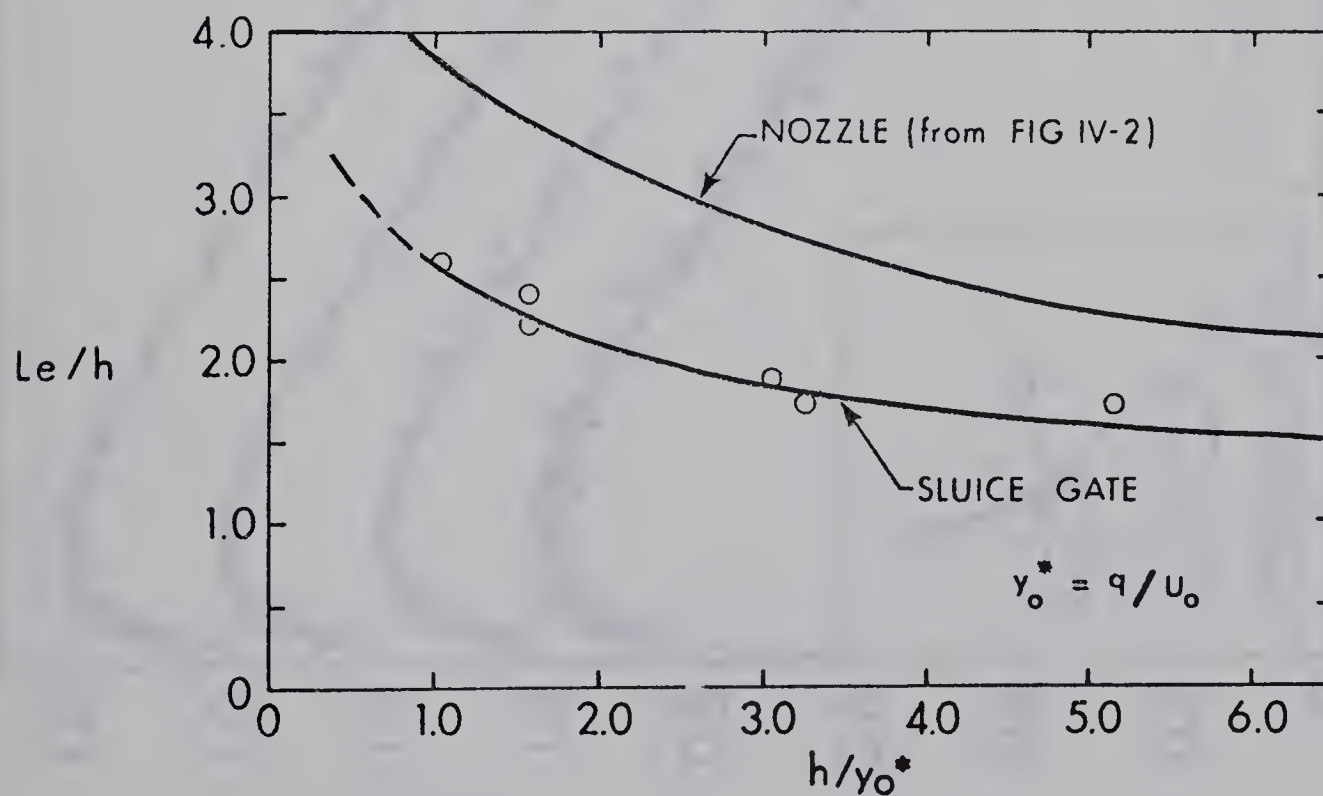


FIG. IV-16. VARIATION OF THE LENGTH OF THE EDDY

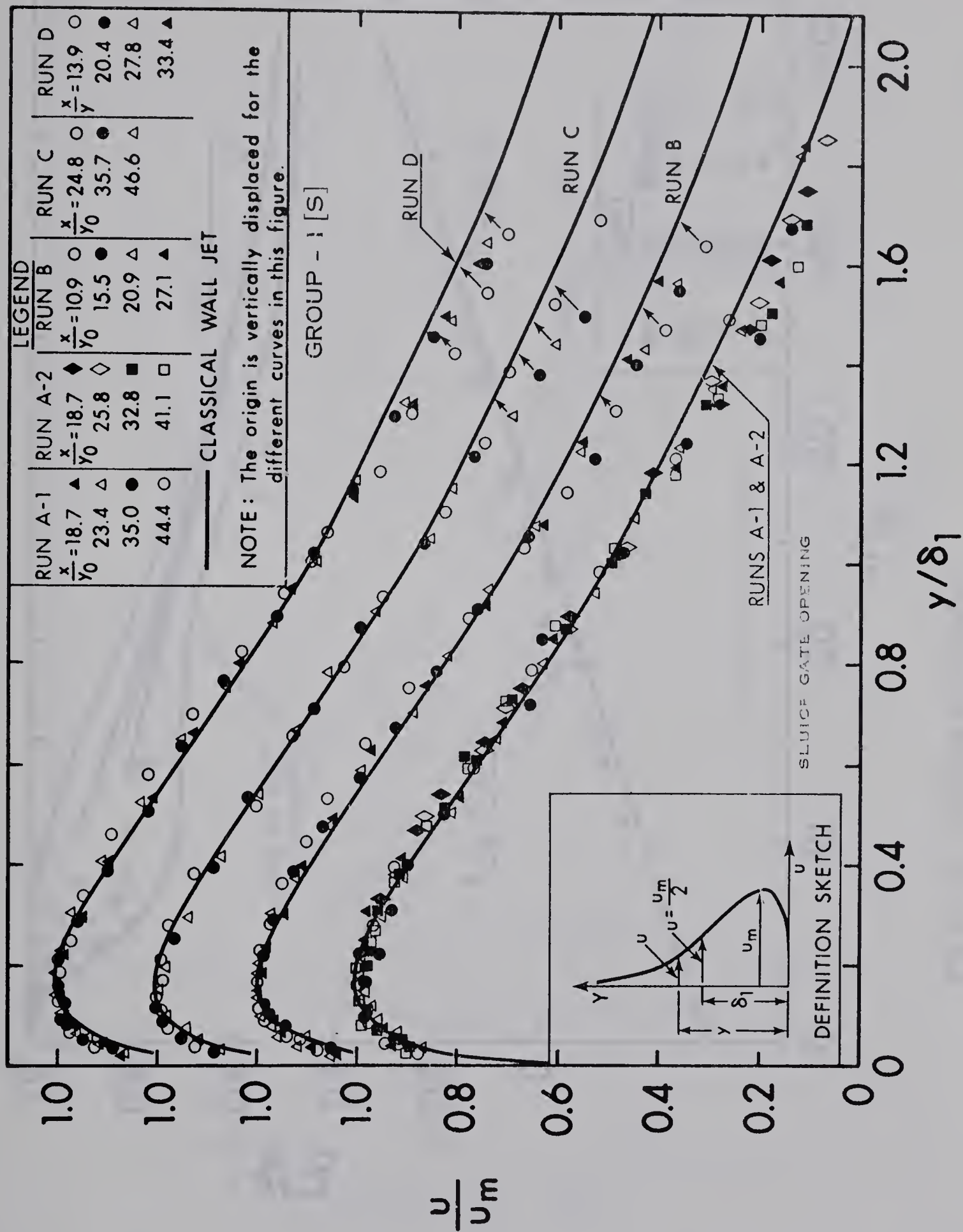


Fig IV . 17 Dimension less Velocity Plot

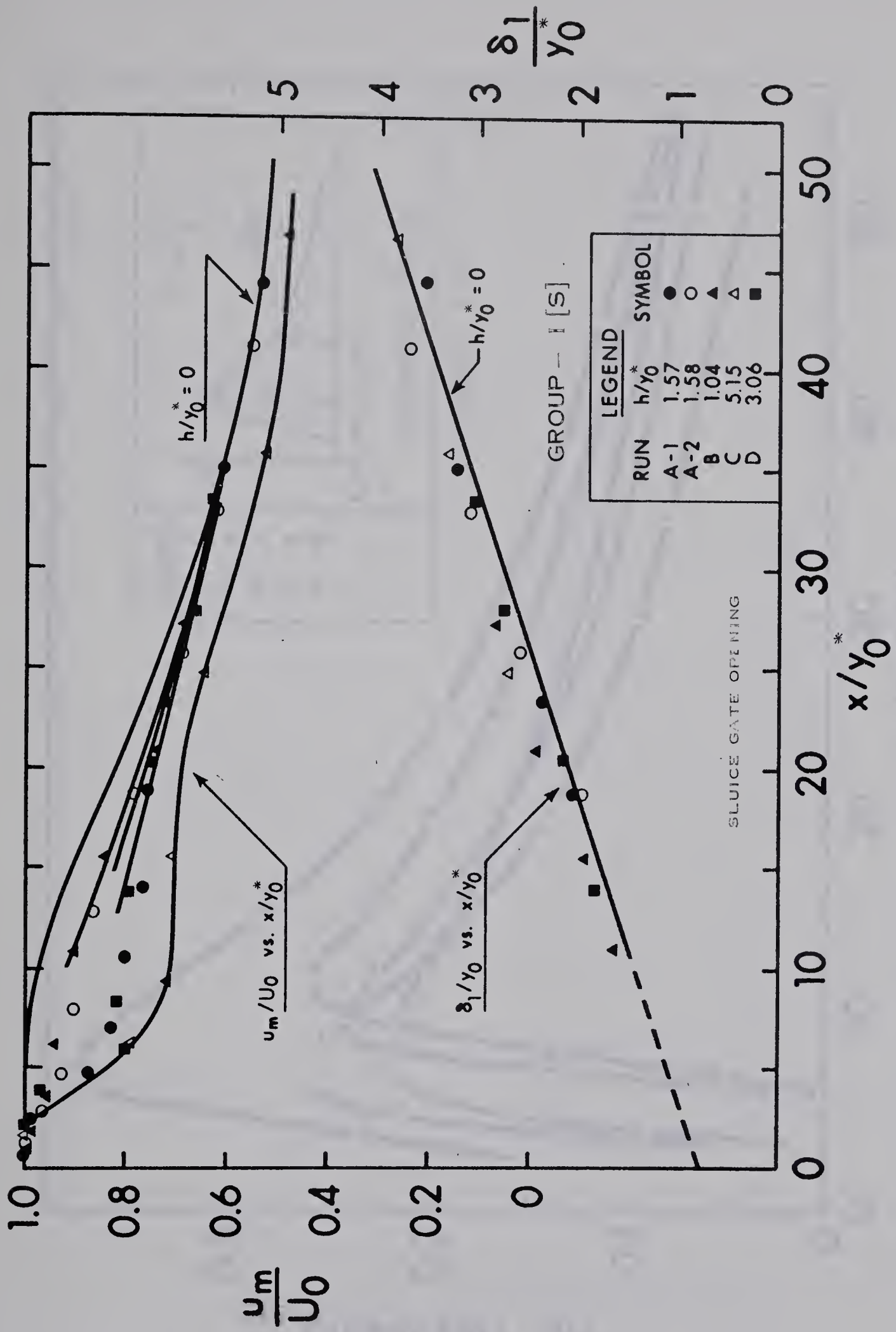


Fig IV - 18 Variation of the Scales

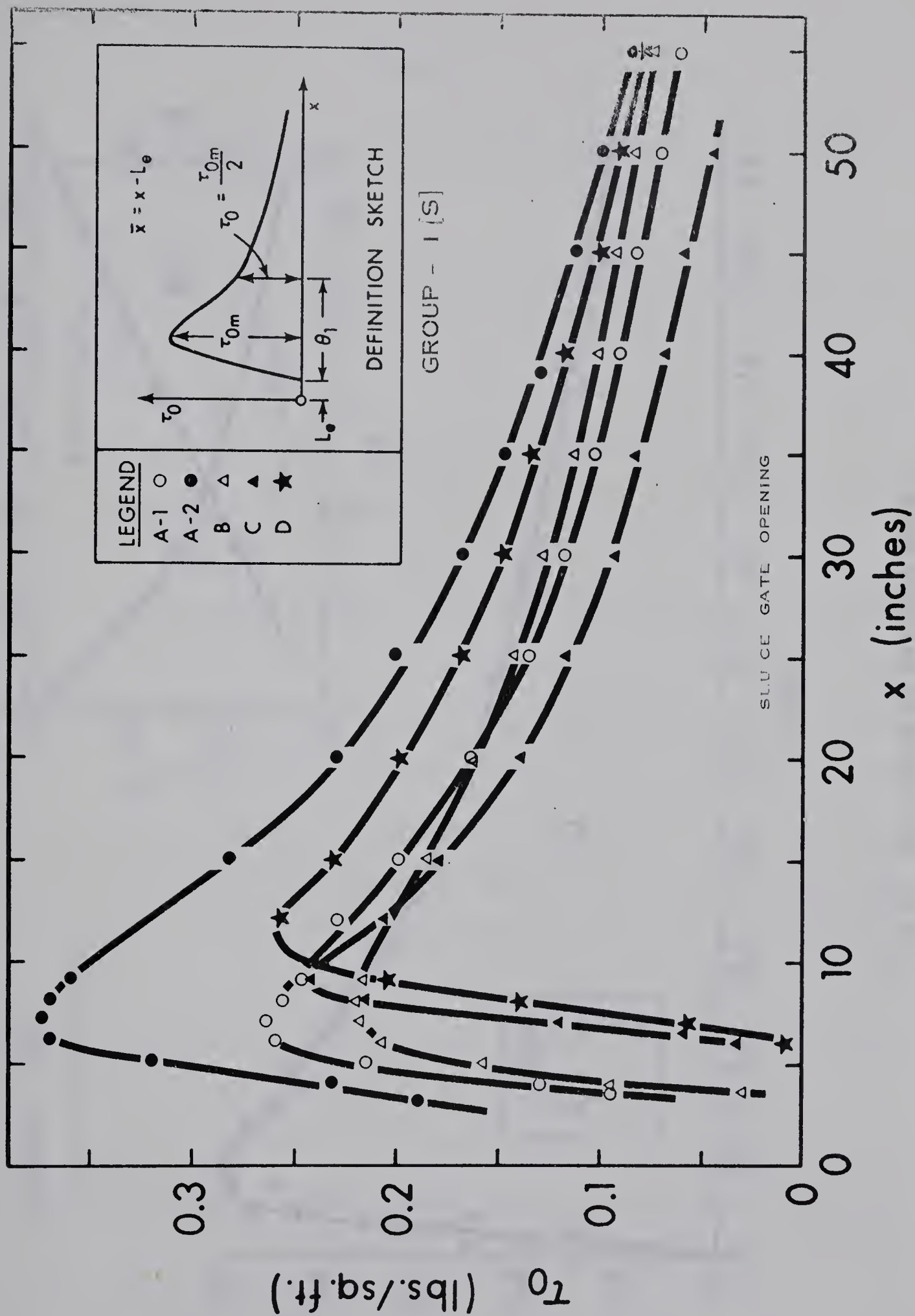


Fig IV 19 Bed Shear Stress Distribution

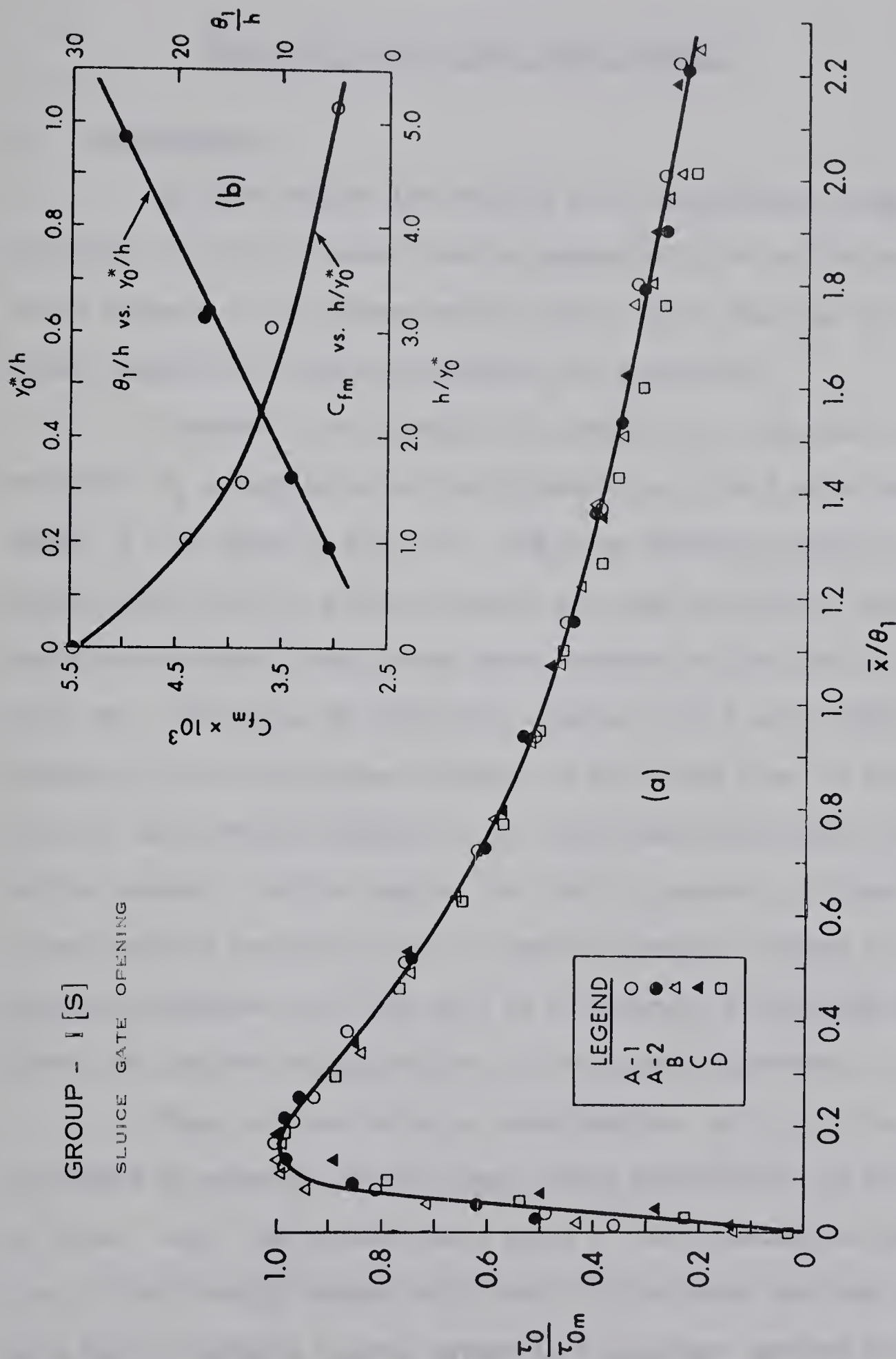


Fig IV - 20 Study of the Bed Shear Stress

CHAPTER V

WALL JETS ISSUING INTO WIDER CHANNELS

5.1 Introduction

In this chapter the results of an experimental study of the diffusion of a jet of water issuing tangentially on to the bed of a wider channel, i.e., between walls further apart than the jet width, under conditions of high submergence, are presented.

Consider a jet of width b , depth y_0 , and almost uniform velocity U_0 , issuing under high submergence, into a wider channel of width B , as shown in Fig. V-1. The flow situation--which is essentially a wall jet in a wider channel and under negligible pressure gradient--is highly complicated when compared to the case of a plane wall jet. Since the jet initially occupies only a part width of the channel, the jet undergoes diffusion on the sides also, in addition to that in the vertical direction, till the forward flow fills the width of the channel. In this region the flow, in general, is three dimensional and the boundary layer is skewed. However, because of the symmetrical expansion, the flow will be collateral, in both the boundary layer and the free mixing region, in the plane of symmetry.

There appears to be no investigation, so far, on the characteristics of velocity and bed shear stress distribution of this type of flow. Also, the related basic topic of three dimensional wall jets--i.e., a jet issuing tangentially from a finite size slot and expanding on a bed of infinite lateral extent in a quiescent ambient surrounding

of the same fluid--is, surprisingly, almost unexplored. The first, and apparently the only investigation, so far, on three dimensional wall jets is the exploratory study of Viets and Sforza (1966). They conducted one experiment on a three dimensional wall jet of aspect ratio, b/y_0 , of 10 and found that the velocity decay could be considered to be made up of a potential core, a characteristic decay region and the radial wall jet decay region. The velocity profiles along the centerline were found to be similar in both the characteristic decay and radial wall jet decay regions and the similarity profile was the same as that given by Glauert (1956). No bed shear stress measurements were reported.

An examination of the velocity similarity plots of Viets and Sforza (1966) shows that, while the agreement of the data with the Glauert's curve (1956) in the free mixing region is good, there is an acute paucity of data in the boundary layer region--about four points in each plot--and hence their conclusion of one similarity profile for the entire wall jet depth lacks conclusive support.

The present problem under study, even though not a strict three dimensional wall jet, can be considered as a restricted form of three dimensional wall jet, and finds application in Hydraulic engineering practice. As a first step towards understanding the phenomenon of wall jets in wider channels, an experimental study with measurements of velocity and bed shear stress restricted to the plane of symmetry was undertaken and the results are presented in the following sections.

5.2 Wall Jets in Wider Channels under Zero Pressure Gradient

5.2.1 Experiments

The experiments were conducted in Flume B. A total of 12 runs

with the ratio b/B varying from 0.087 to 1.00 were made. The data of this investigation are designated as Group-II. A summary of experimental data is presented in Table V-1 and the detailed data are given in Appendix D (Table D-6).

5.2.2 Similarity of the Entire Velocity Profile

Fig. V-2 shows the velocity distribution on the plane of symmetry of the jet at various positions along the channel in a typical run, (II-D-1), for which b/B was 0.087. It is seen that the velocity profiles have the characteristic shape of the wall jet, but the diffusion rate in comparison with Fig. III-3 of the water wall jet appears to be very fast.

First of all, it was attempted to find whether the centerline velocity distribution is similar and if so, how it compares with that of the classical wall jet. The non-dimensional similarity plot u/u_m vs. y/δ_1 for runs A-1, A-2 and A-3 of Group II, is shown in Fig. V-3. In the major part of the flow there is a strong indication of similarity. However, there is appreciable scatter, especially in the boundary layer region, indicating that one similarity profile for the entire depth of forward flow is not feasible. This differs from the conclusion of one similarity profile for three-dimensional jets found by Viets and Sforza (1966). Similar results were found for the various runs with $b/B < 0.75$.

It is believed that the inability to have one similarity profile for the entire flow depth is the effect of the three dimensionality of the overall flow. Johnston (1960-a, 1960-b) has shown that in three-dimensional

TABLE V-1

WALL JETS IN WIDER CHANNELS

SUMMARY OF EXPERIMENTAL DATA

Data: Group-II

B = Width of Channel = 12.25"

Run	b in.	y_o in.	r^* in.	U_o ft./sec.	y_t in.	b/B	$\frac{b}{y_o}$	$\frac{B}{y_o}$	$\frac{y_o}{r^*}$	$R = U_o y_o / \nu$
II-A-1	6.0	1.125	0.818	8.46	17.50	0.49	5.33	10.9	1.38	7.47×10^{-4}
II-A-2	6.0	1.125	0.818	9.13	17.50	0.49	5.33	10.9	1.38	8.06
II-A-3	6.0	1.125	0.818	6.86	17.83	0.49	5.33	10.9	1.38	6.05
II-B-1	6.0	1.625	1.052	6.03	18.10	0.49	3.69	7.5	1.54	7.70
II-B-2	6.0	1.625	1.052	8.87	18.80	0.49	3.69	7.5	1.54	11.32
II-C-1	3.09	1.125	0.653	6.43	16.80	0.252	2.75	10.9	1.72	5.69
II-C-2	3.09	1.125	0.653	9.08	17.20	0.252	2.75	10.9	1.72	8.02
II-D-1	1.06	1.125	0.360	5.92	14.30	0.087	0.945	10.9	3.12	5.25
II-D-2	1.06	1.125	0.360	8.58	16.40	0.087	0.945	10.9	3.12	7.60
II-E-1	12.25	1.060	--	7.87	18.90	1.00	11.60	11.5	--	6.56
II-F-1	9.06	1.060	0.860	6.57	18.40	0.74	8.55	11.5	1.23	5.47
II-F-2	9.06	1.060	0.860	8.37	18.85	0.74	8.55	11.5	1.23	6.96×10^{-4}

boundary layer flow, the velocity distribution in the plane of symmetry, though collateral, is different from the corresponding two-dimensional flow case because of the skewed boundary layer and the main flow divergence in the surrounding region.

Departure from the similarity plot in the boundary layer region, as in the present case, has been observed in other studies on plane wall jets, in coflowing streams (Eskinazi and Kruka, 1962, 1964), on rough boundaries (Rajaratnam, 1967) and on rough boundaries with suction (Lau, 1963). In most of these cases, it is found that if the profile is considered in two parts, viz., boundary layer and free mixing regions, each of the parts exhibits similarity. This procedure was adopted in the present case and the similarity of the free mixing and boundary layer regions are studied separately.

5.2.3 Similarity in the Free Mixing Region

The free mixing region of the centerline velocity profiles was non dimensionalised and plotted as $f(\eta') = u/u_m$ vs. $\eta' = (y - \delta)/(\delta_1 - \delta)$, in Figs. V-4(a) and V-4(b), in which δ is the thickness of the boundary layer. The data for all the runs, II-A-1 through II-E-2, are plotted and compared with the corresponding classical wall jet curve. It can be observed that the agreement is quite satisfactory for all the runs. Hence, it can be concluded that in the plane of symmetry, the velocity distribution in the free mixing region is similar for all b/B ratios and the similarity profile is the same as that of the classical wall jet.

5.2.4 Velocity Distribution in the Boundary Layer

The velocity distribution in the boundary layer, in the plane of symmetry, was found to be satisfactorily given (for practical purposes) by a power law type of relation

$$u/u_m = (y/\delta)^{1/n} \quad . \quad . \quad . \quad . \quad . \quad (5.1)$$

Fig. V-5 shows the variation of u/u_m with y/δ for series II-A and II-D. From this and similar plots it was found that $n = 12$ for series II-A, II-B, II-E and II-F (i.e., $b/B \geq 0.50$) and $n = 10$ for series II-C and II-D (i.e., $b/B \leq 0.25$).

5.2.5 Velocity Scale

The maximum velocity, u_m , is the velocity scale for the similarity plots of both the free mixing region and the boundary layer region. It can be expressed as

$$u_m = f(U_o, y_o, b, B, \nu, x) \quad . \quad . \quad (5.2)$$

By dimensional analysis

$$u_m/U_o = f_1(U_o y_o/\nu, b/y_o, B/y_o, x/y_o) \quad . \quad (5.3)$$

Since the Reynolds number $R = U_o y_o/\nu$ has negligible influence on turbulent diffusion, Eq. 5.3 can be written as

$$u_m/U_o = f_2(b/B, B/y_o, x/y_o) \quad . \quad . \quad (5.4)$$

The term B/y_o can be expected to affect the pattern of diffusion, due to side wall effects, only at small values.

The experimental results on the decay of maximum velocity are plotted in Fig. V-6 as u_m/U_o vs. x/y_o with b/B as the third parameter. It is seen that the data are well correlated. In series II-A and II-B, b/B was kept constant at 0.49 and B/y_o had values of 10.9 and 7.5 respectively. The data for both the series can be considered to be described well by one curve. Thus the effect of B/y_o seems to be insignificant at this range. The Fig. V-6 illustrates well the effect of b/B on the maximum velocity decay.

At this stage, it was thought, intuitively, that the diffusion process of jets from finite slots of given area (and, of course, given momentum) depend upon the perimeter exposed to the diffusion process. Based on this hypothesis, a characteristic length of the outlet, r' , is defined as

$$\begin{aligned} r' &= \frac{\text{area at the outlet}}{\text{perimeter exposed to diffusion at the outlet}} \\ &= \frac{b y_o}{b + 2 y_o} \end{aligned} \quad (5.5)$$

$$\text{Then } r'/y_o = \frac{1}{2/(b/y_o) + 1} \quad (5.6)$$

Now, by using r'/y_o in place of b/y_o , Eq. 5.4 can be written as

$$u_m/U_o = f_3 (r'/y_o, B/y_o, x/r') \quad (5.7)$$

The present data are plotted in Fig. V-7, as u_m/U_o against x/r' . It can be seen that the correlation is surprisingly good. All the data fall on one line, independent of r'/y_o and B/y_o , in the

range of the tests. It is interesting to note that in these tests y_o/r' was varied from 1.23 to 3.12 and this corresponds to a variation in the slot aspect ratio, b/y_o , of 0.95 to 11.60. In Fig. V-7, the velocity decay curve of the classical wall jet is plotted (by assuming $y_o = r'$) for comparison purposes. The present curve, of wall jet in wider channels, is initially slightly above the classical wall jet curve and seems to join it at $x/y_o \geq 75$.

Encouraged by the good correlation of u_m/U_o , obtained by use of r' in the place of y_o , the concept of the characteristic length of outlet was used to correlate the available data of three-dimensional free jets of triangular, square, rectangular, elliptical and circular cross section, and interesting results were obtained. This study on three-dimensional free jets is reported in Appendix B.

5.2.6 Length Scales

Since the similarity of velocity profiles are considered in two parts, the length scale for the mixing region is $(\delta_1 - \delta)$. The variation of $(\delta_1 - \delta)$ is studied in Fig. V-8(a) by plotting $(\delta_1 - \delta)/y_o$ vs. x/y_o . Even though there is some scatter of data, it could be said that $(\delta_1 - \delta)/y_o$ varies linearly with x/y_o for a given b/B and the variation can be expressed as

$$(\delta_1 - \delta)/y_o = m (x/y_o) + C \quad . \quad . \quad . \quad (5.8)$$

where $m = f(b/B)$ and $C \approx 0.35$ and is essentially the same for all b/B . The variation of m with b/B is shown in Fig. V-8(b).

Regarding the boundary layer thickness δ along the centerline,

by a rough analogy with the two dimensional boundary layer growth on a flat plate, the variation was considered as

$$\delta/x = f(U_o x/\nu, x/y_o) \quad . \quad . \quad . \quad . \quad (5.9)$$

$$= f(U_o y_o/\nu, x/y_o) \quad . \quad . \quad . \quad . \quad (5.10)$$

Hence for high values of R ,

$$\delta/x = f(x/y_o) \quad . \quad . \quad . \quad . \quad . \quad (5.11)$$

The variation of δ/x with x/y_o is shown in Fig. V-9. In this figure b/B appears to have a small effect. The difficulty of determining exactly the value of δ from the measured velocity profiles, is probably responsible for the scatter of the data. However, it is believed that the Fig. V-9 is useful, in knowing, at least the order of magnitude of δ .

5.2.7 Bed Shear Stress on the Centerline

The bed shear stress, measured along the centerline, was expressed as the shear stress coefficient $C_f = \tau_o/(\rho U_o^2/2)$. The variation of C_f with x/y_o is shown in Fig. V-10. The distribution of the data indicates that in addition to b/B , the Reynolds number, R , may also be a significant parameter. However, a very good correlation of data was obtained when C_f was plotted against x/r' , as shown in Fig. V-11. It is seen that there is no noticeable effect of Reynolds number and the scatter is random. The mean curve through the data could be considered to represent the variation of bed shear stress fairly well. In the range of the present data the variation of C_f can

be expressed as

$$C_f = 0.005145 e^{-0.0262 (x/r')} \quad . \quad . \quad (5.12)$$

In Fig. V-11 is plotted the curve of water wall jet with the assumption $y_o = r'$. It is interesting to see that the difference is just like the one in Fig. V-7.

5.3 Conclusion

From the study of the characteristics of the velocity distribution and bed shear stress along the centerline of a wall jet in a wider channel under high submergence, as discussed in this chapter, the following conclusions are drawn:

- 1) The velocity profiles along the centerline in the free mixing region are similar and the similarity profile is the same as that of the classical wall jet.
- 2) The velocity distribution in the boundary layer can be expressed as a power law with the power varying from 1/10 to 1/12 depending upon b/B .
- 3) The concept of the characteristic length of the outlet, r' , is very useful in correlating the maximum velocity decay data and the bed shear stress data.

Even for quite exaggerated orifice and b/B between 0.1 and 0.75, the decay of the maximum velocity is close to that for a standard shape of the same hydraulic radius r' , with r' substituted for y_o , as in Fig. V-7; it does not differ seriously from that of a classical wall jet. This should help engineering estimations.

- 4) The dimensionless length scale of free mixing region $(\delta_1 - \delta)/y_0$, varies linearly with x/y_0 , the rate of growth being dependent on b/B .
- 5) The relative boundary layer thickness δ/x is correlated with x/y_0 and b/B has small effect on the correlation.

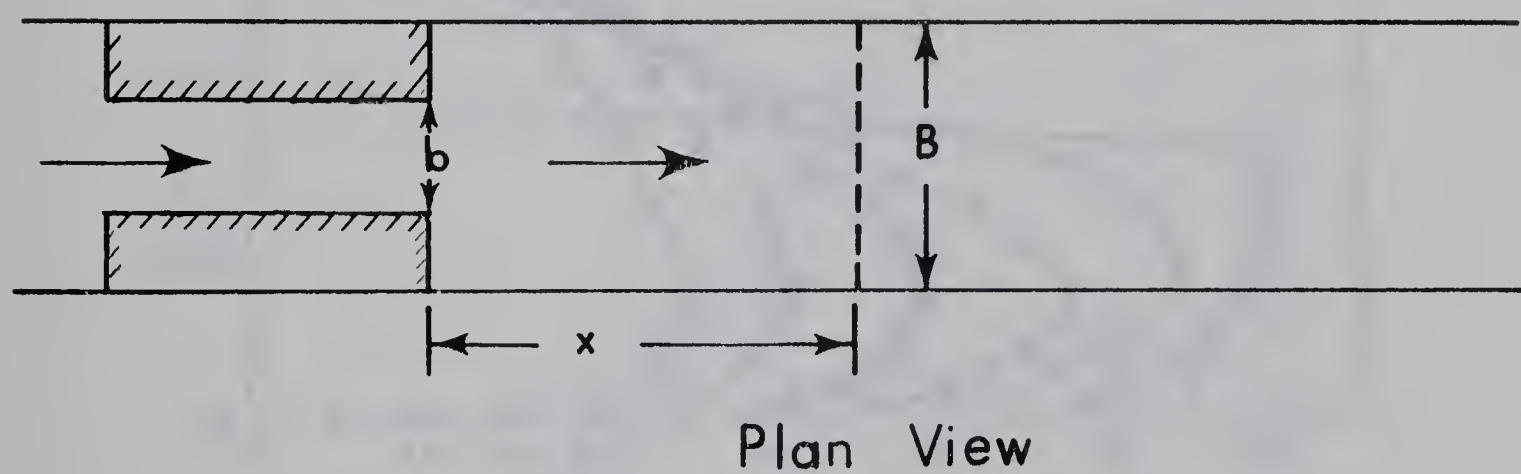
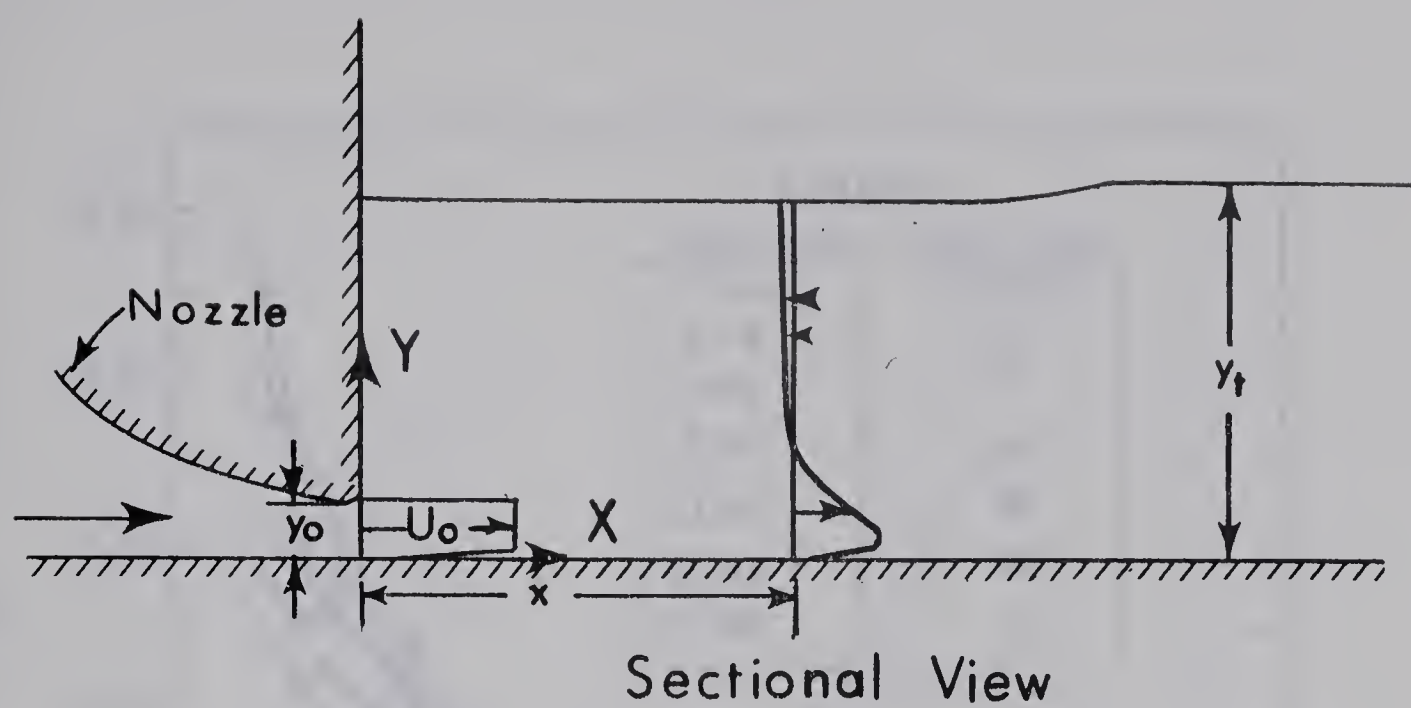


FIG. V-1. Definition Sketch

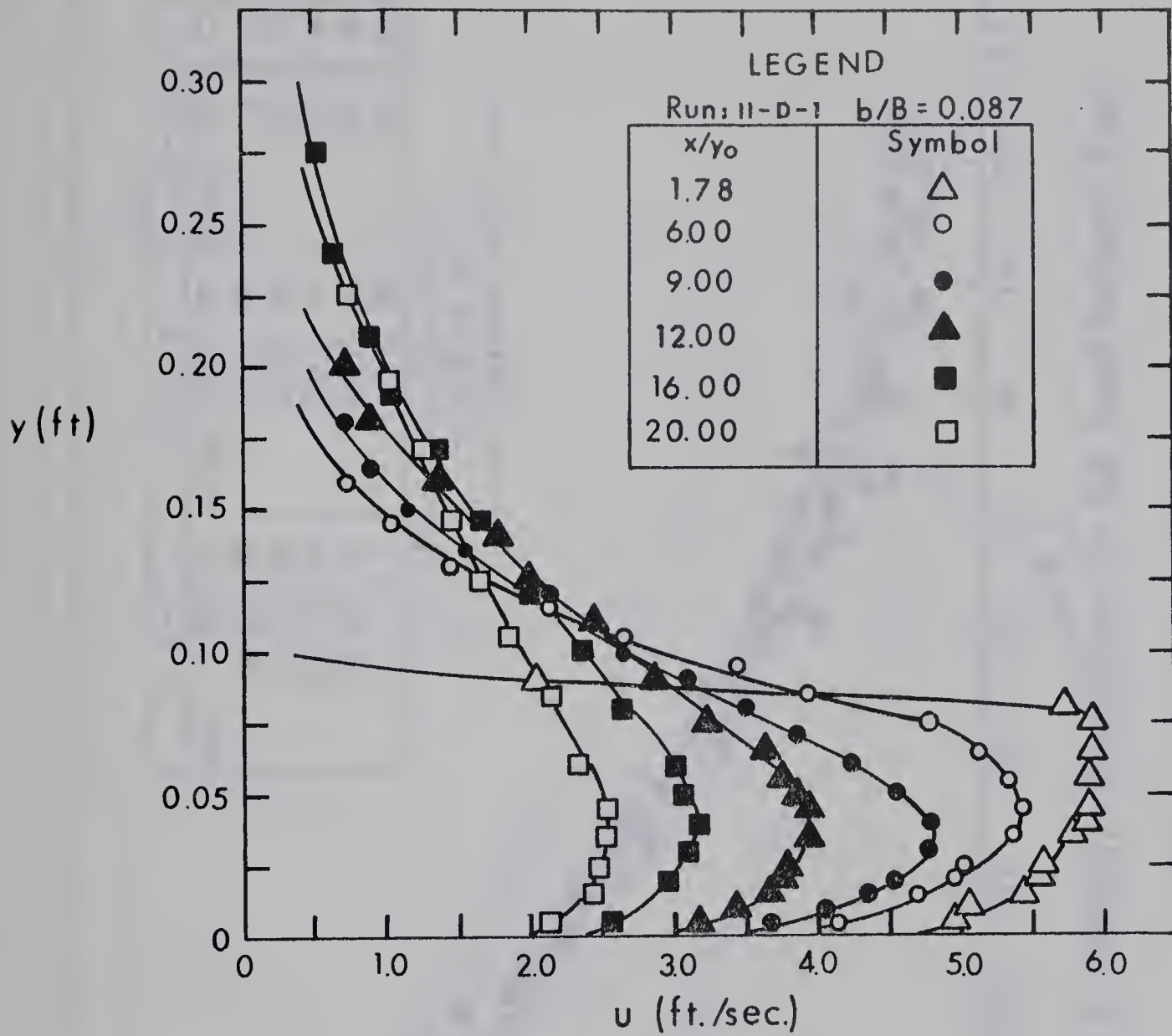


Fig. V-2. Typical Velocity Distribution

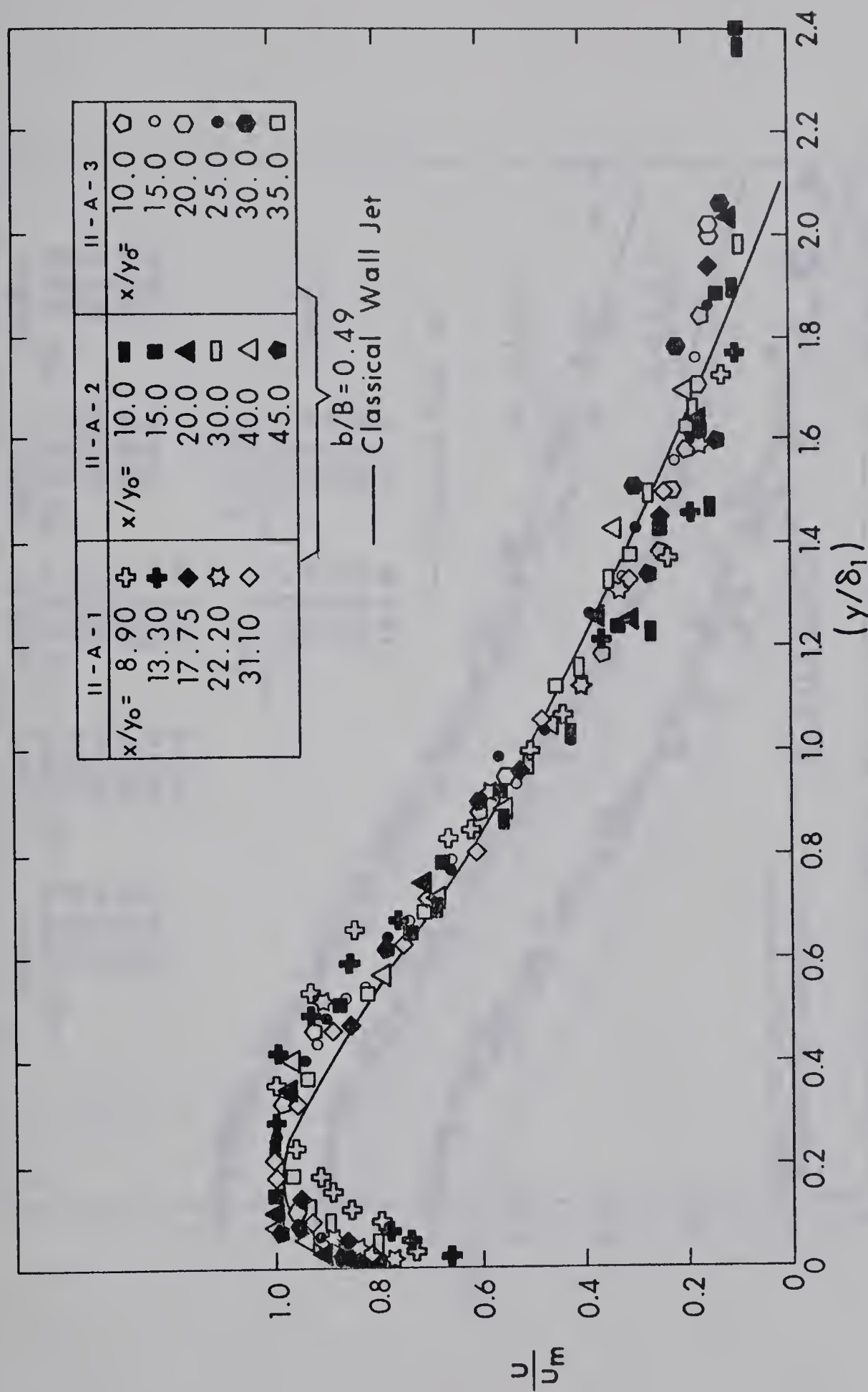


FIG. V-3. Velocity Distribution in the Total Forward Flow

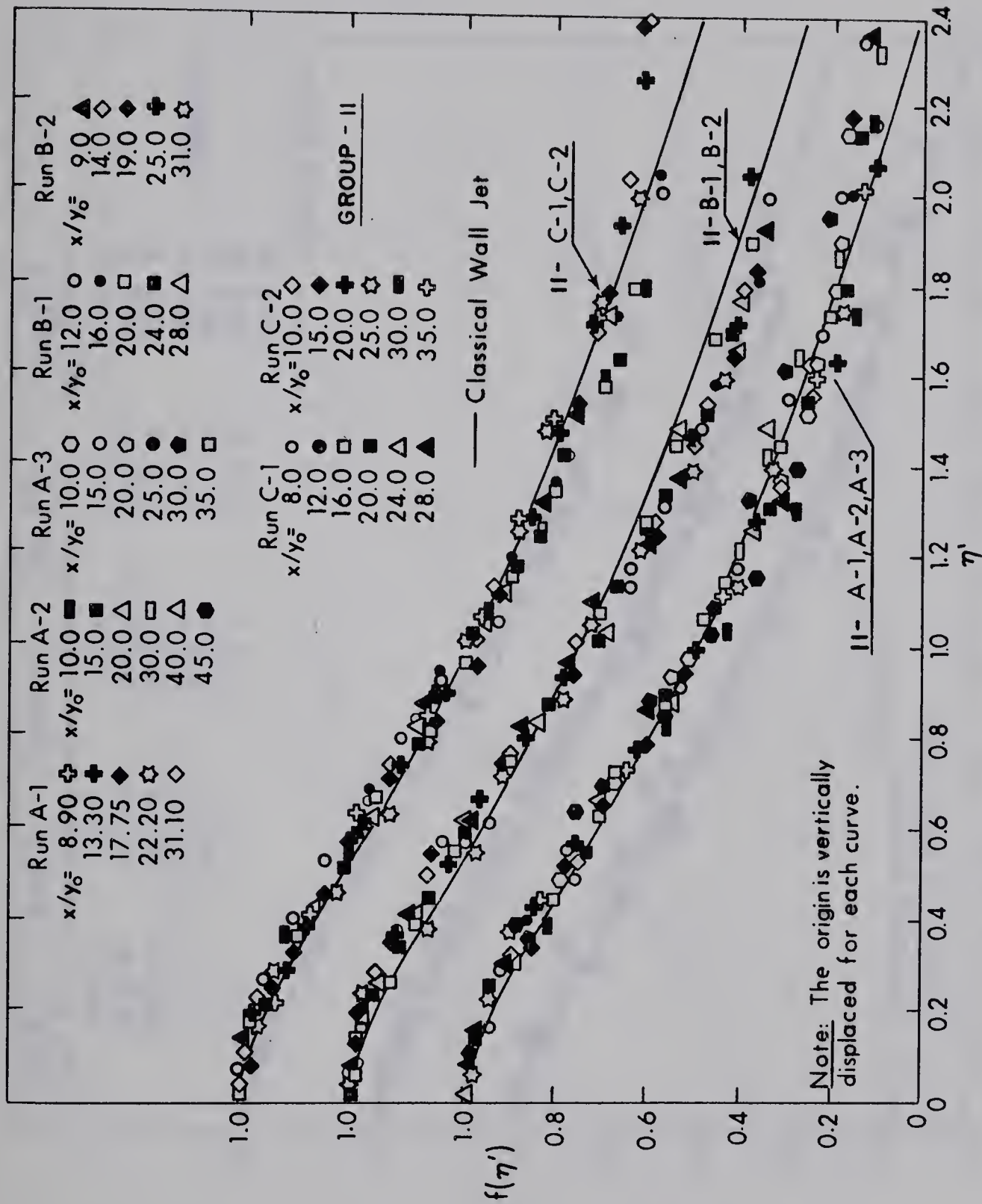


Fig. V-4(a). Velocity Distribution-Free Mixing Region

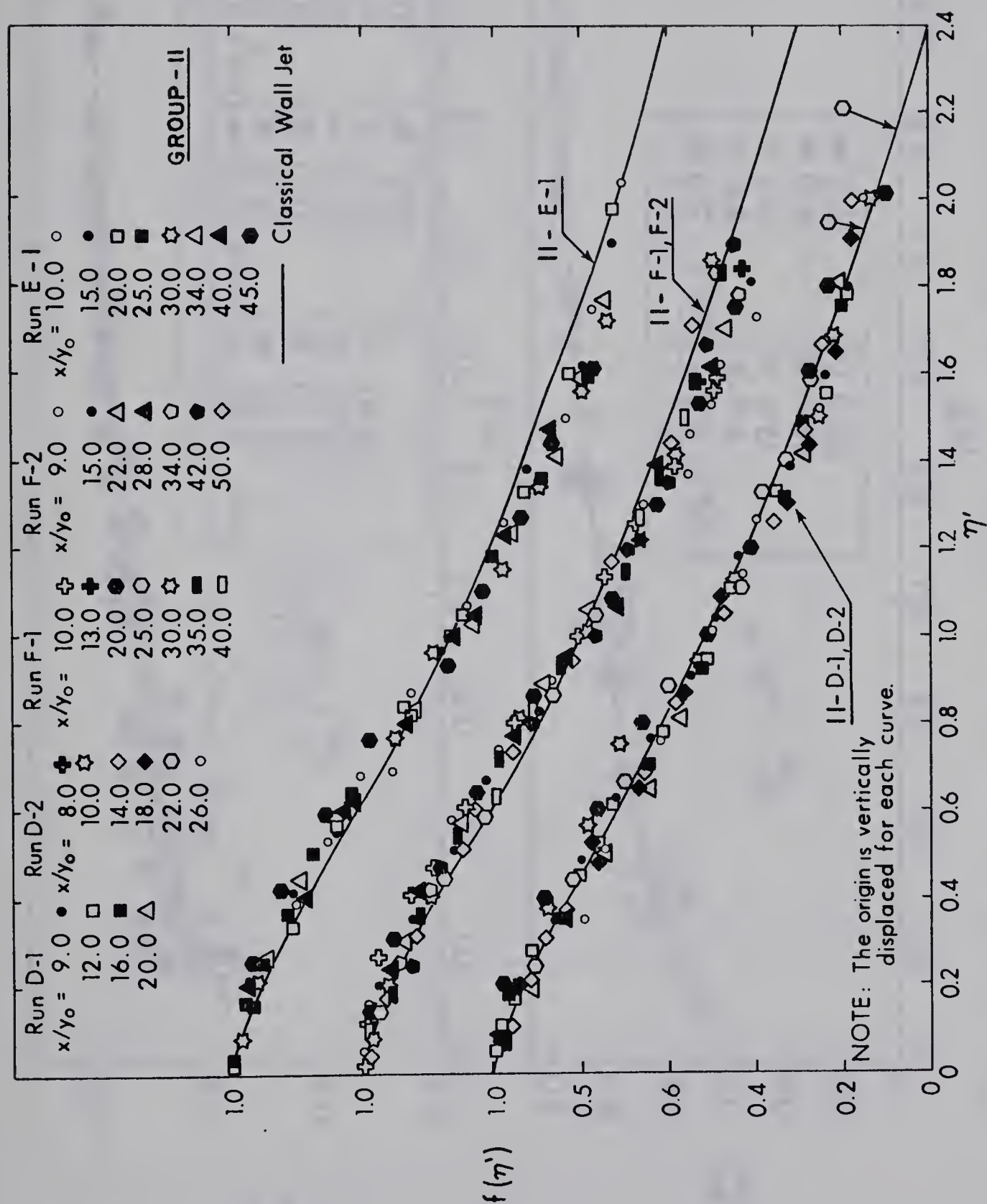


Fig. V-4 (b). Velocity Distribution - Free Mixing Region

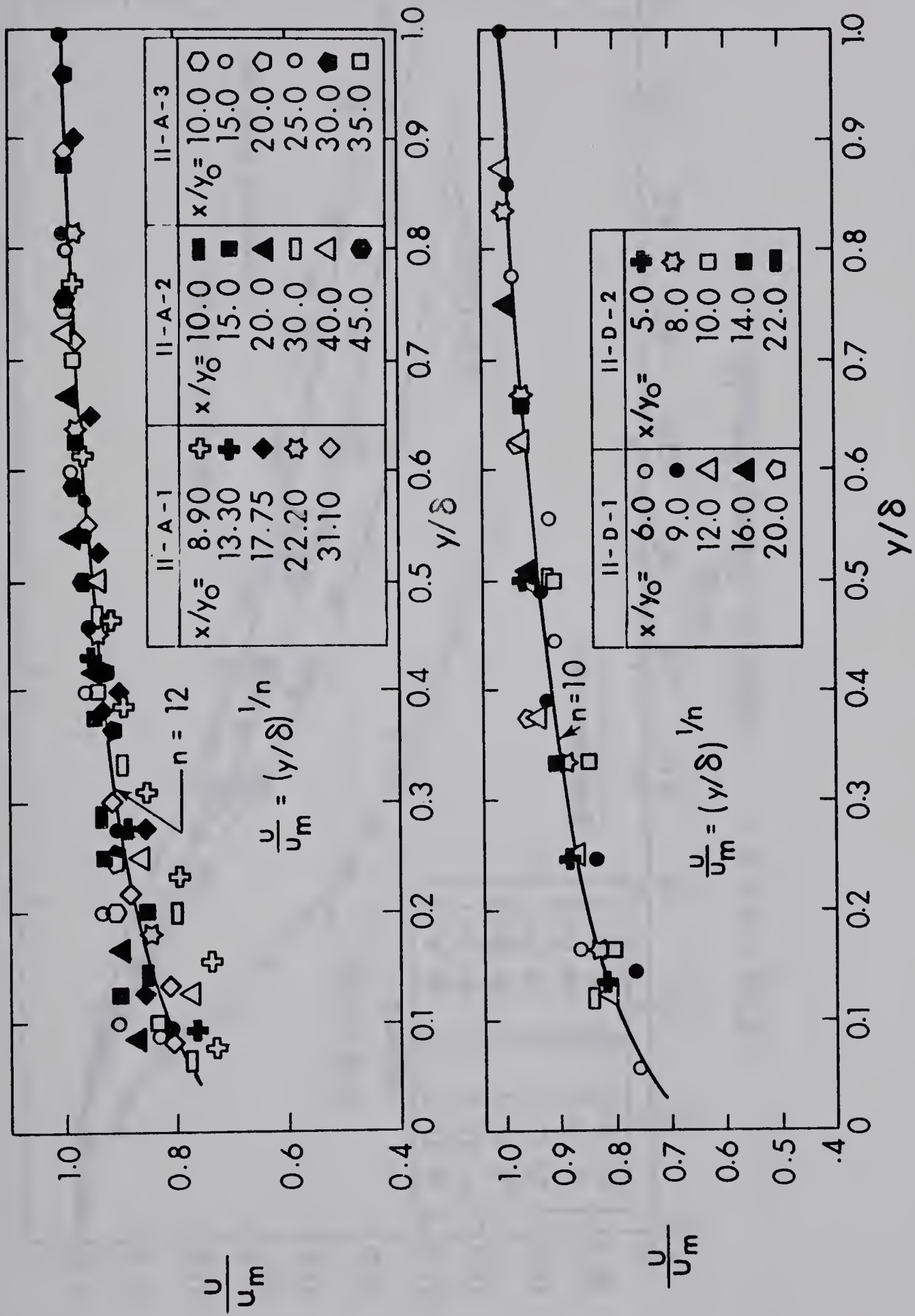


Fig. V - 5. Velocity Distribution - Boundary Layer Region

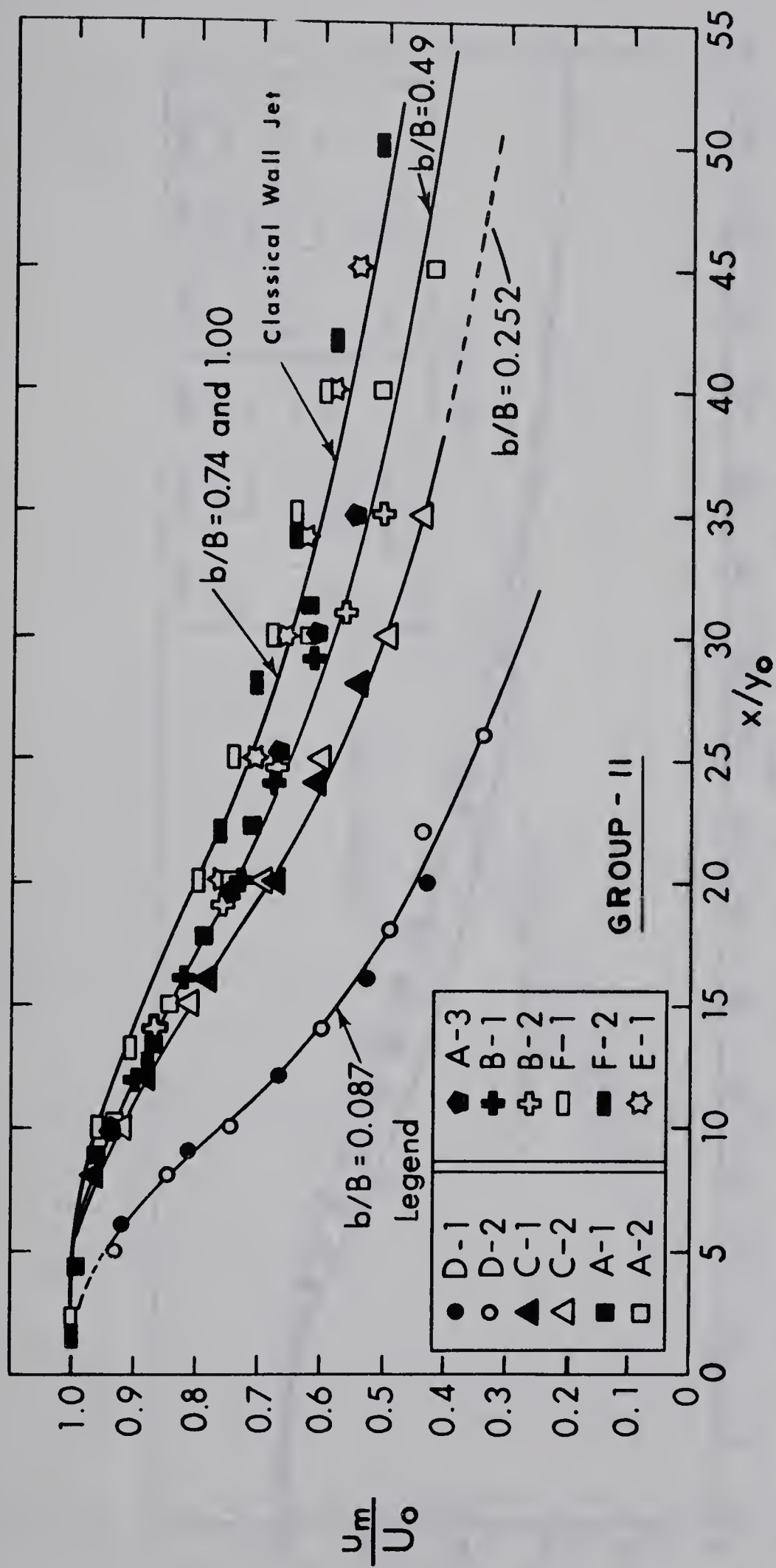


Fig. V - 6. Velocity Decay Results

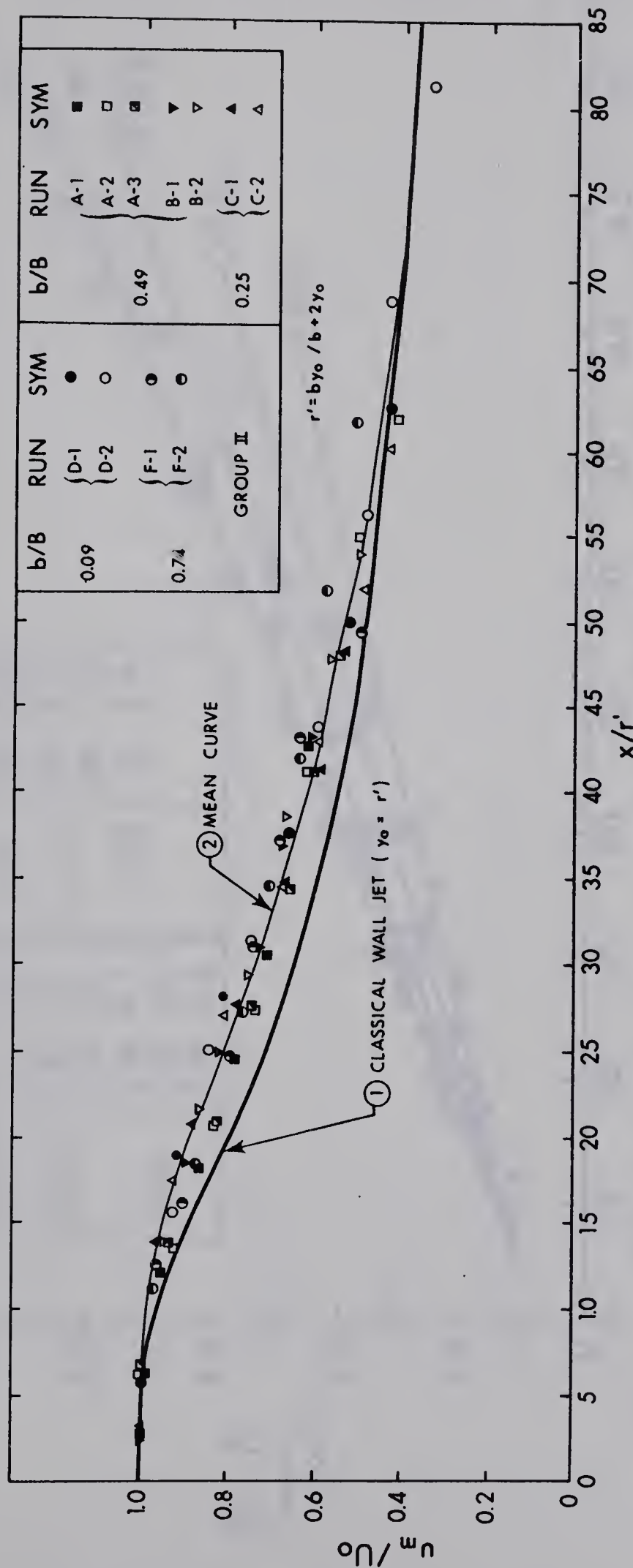


FIG. V-7. MAXIMUM VELOCITY DECAY OF WALL JETS IN WIDER CHANNELS

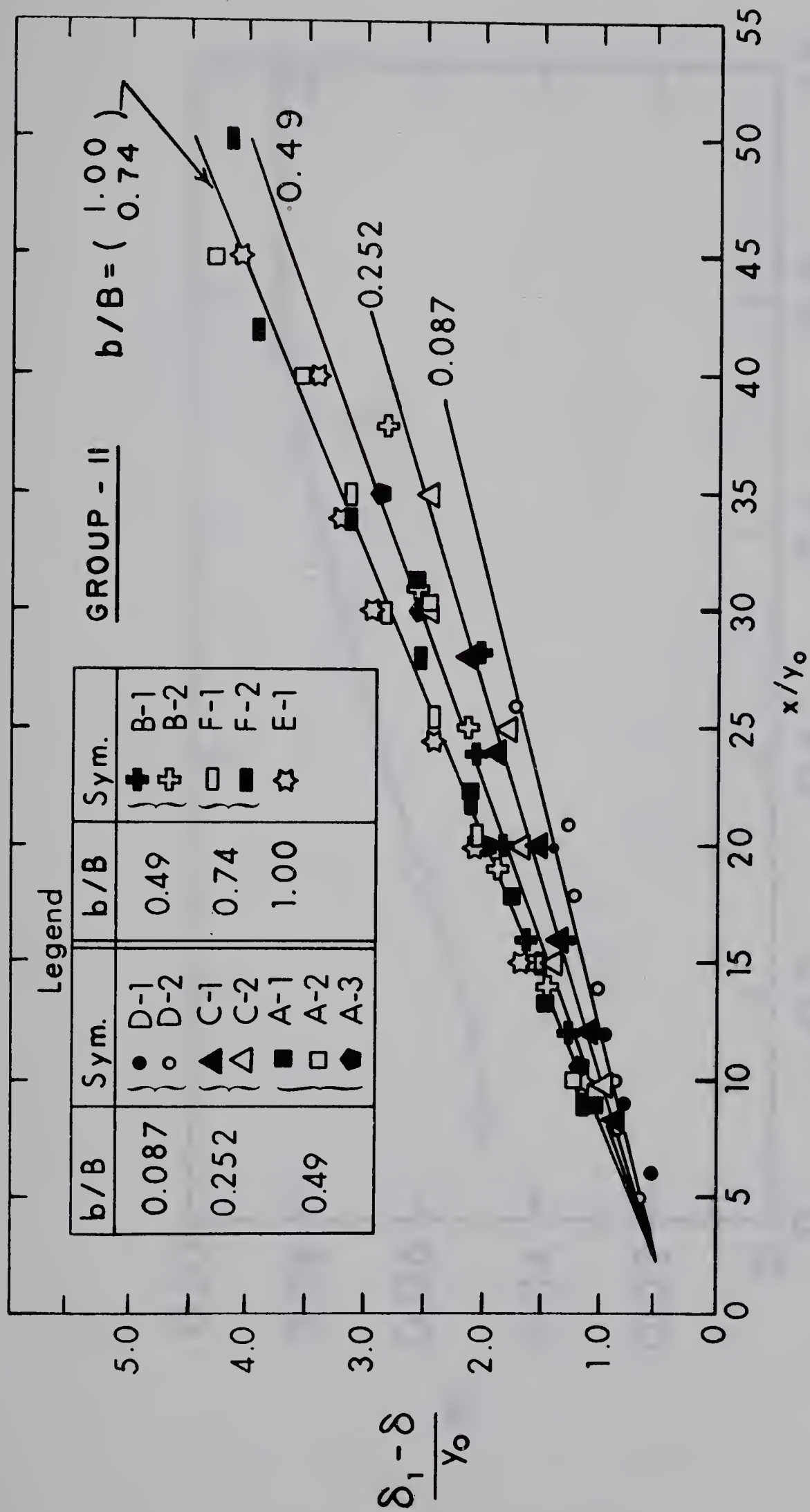


Fig. V-8 (a). Length Scale Studies

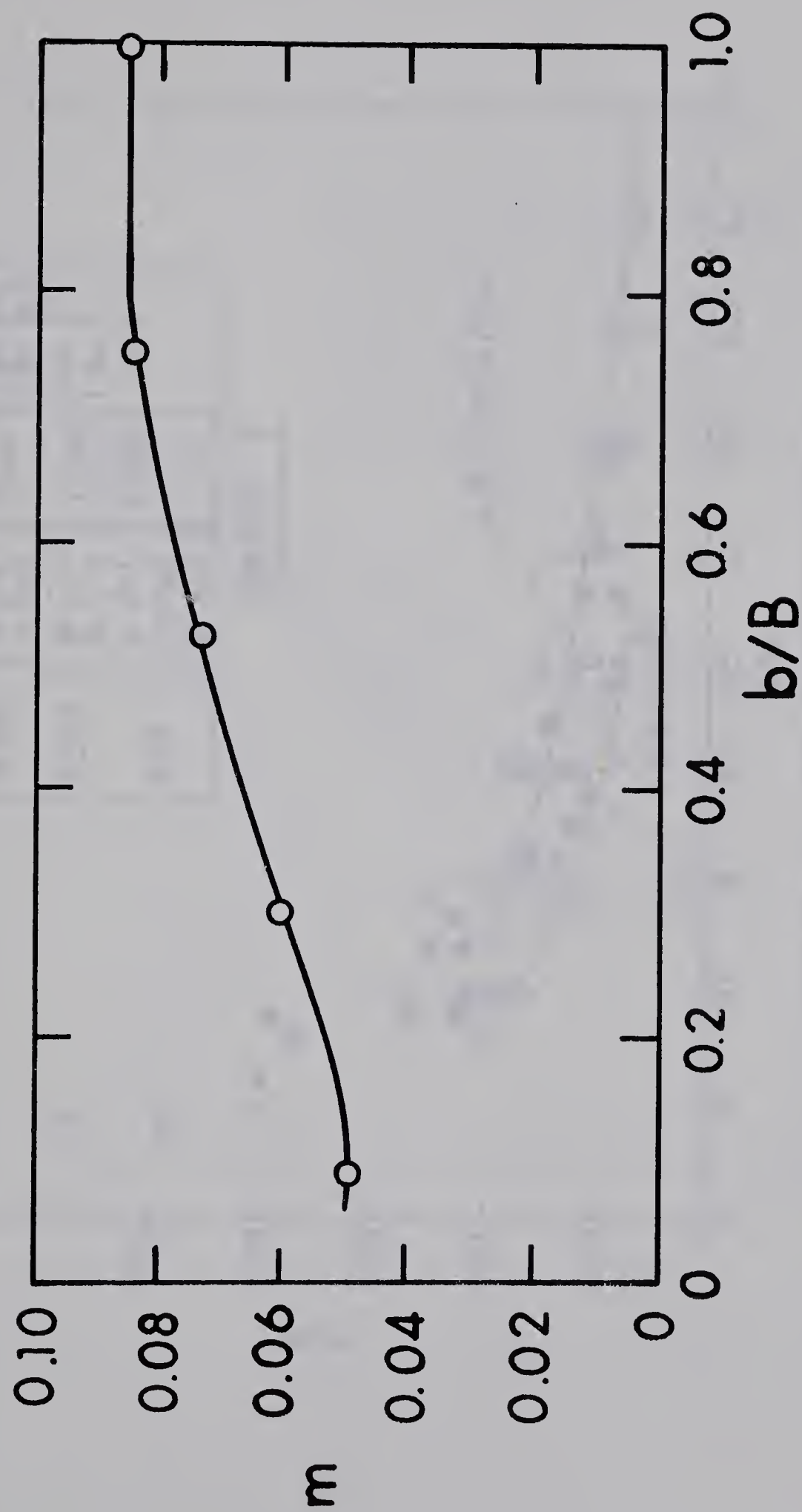


Fig. V-8(b). Length Scale Studies

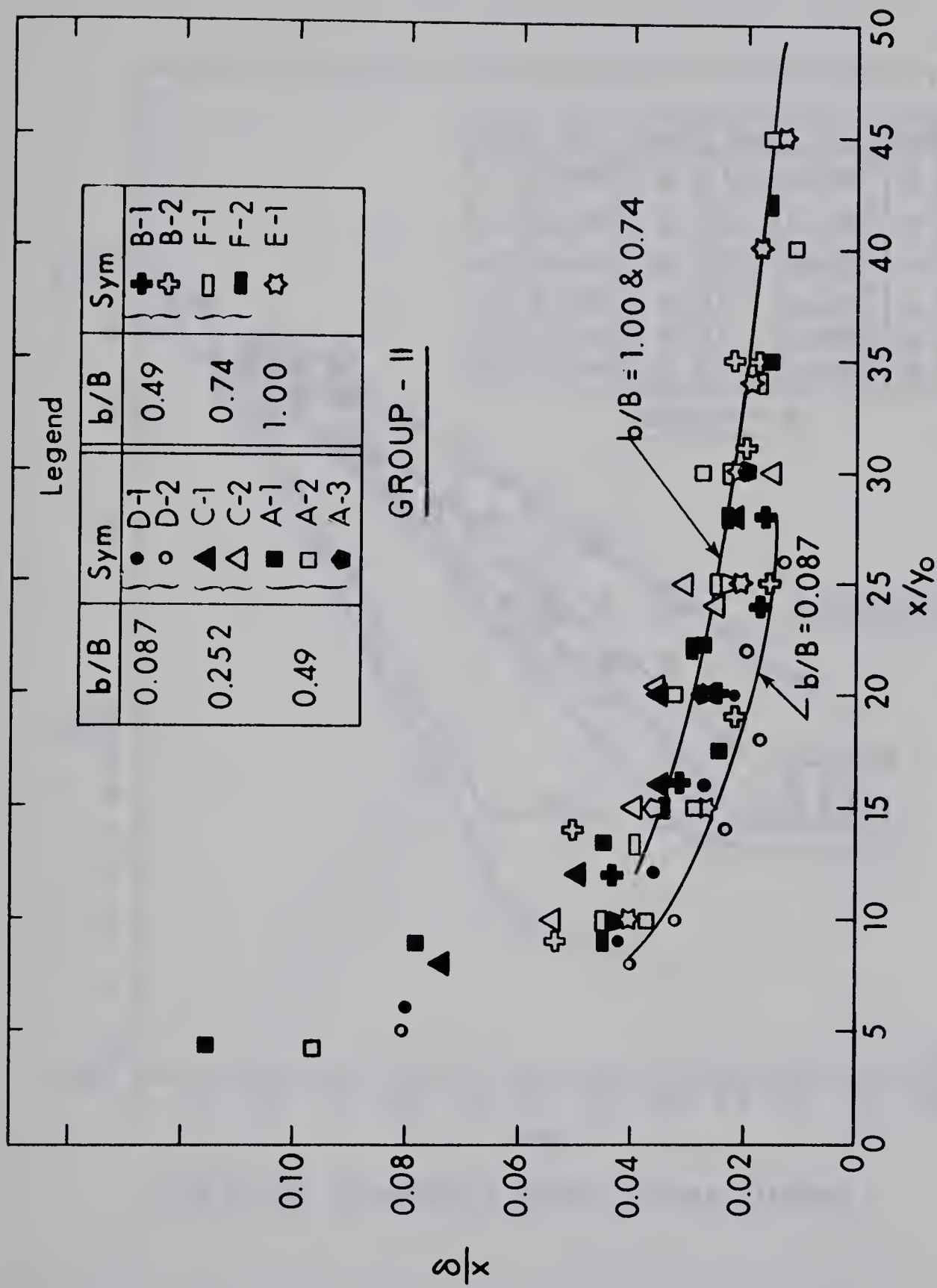


Fig. V-9. Boundary Layer Growth

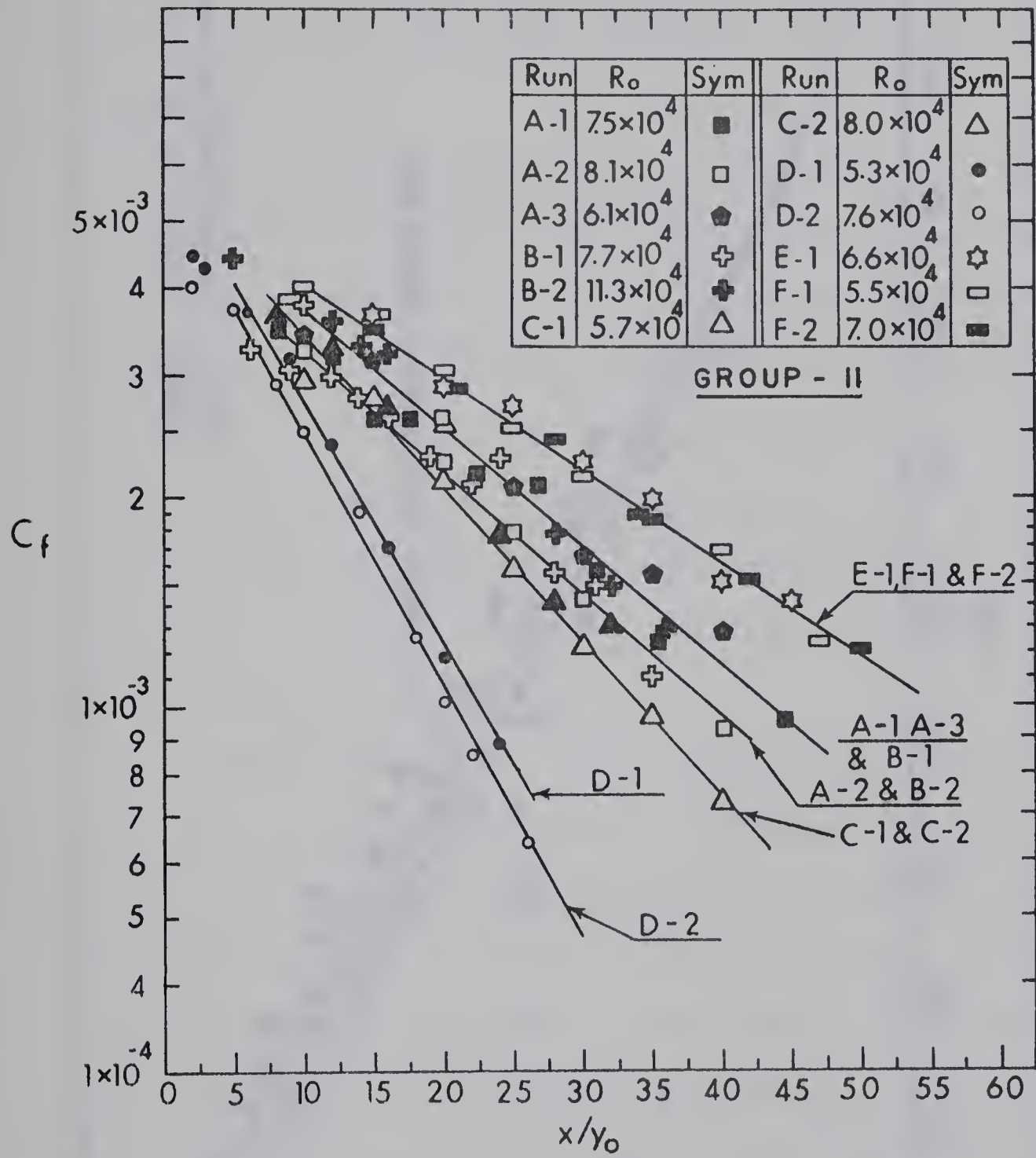


Fig.V-10. Boundary Shear Stress Studies

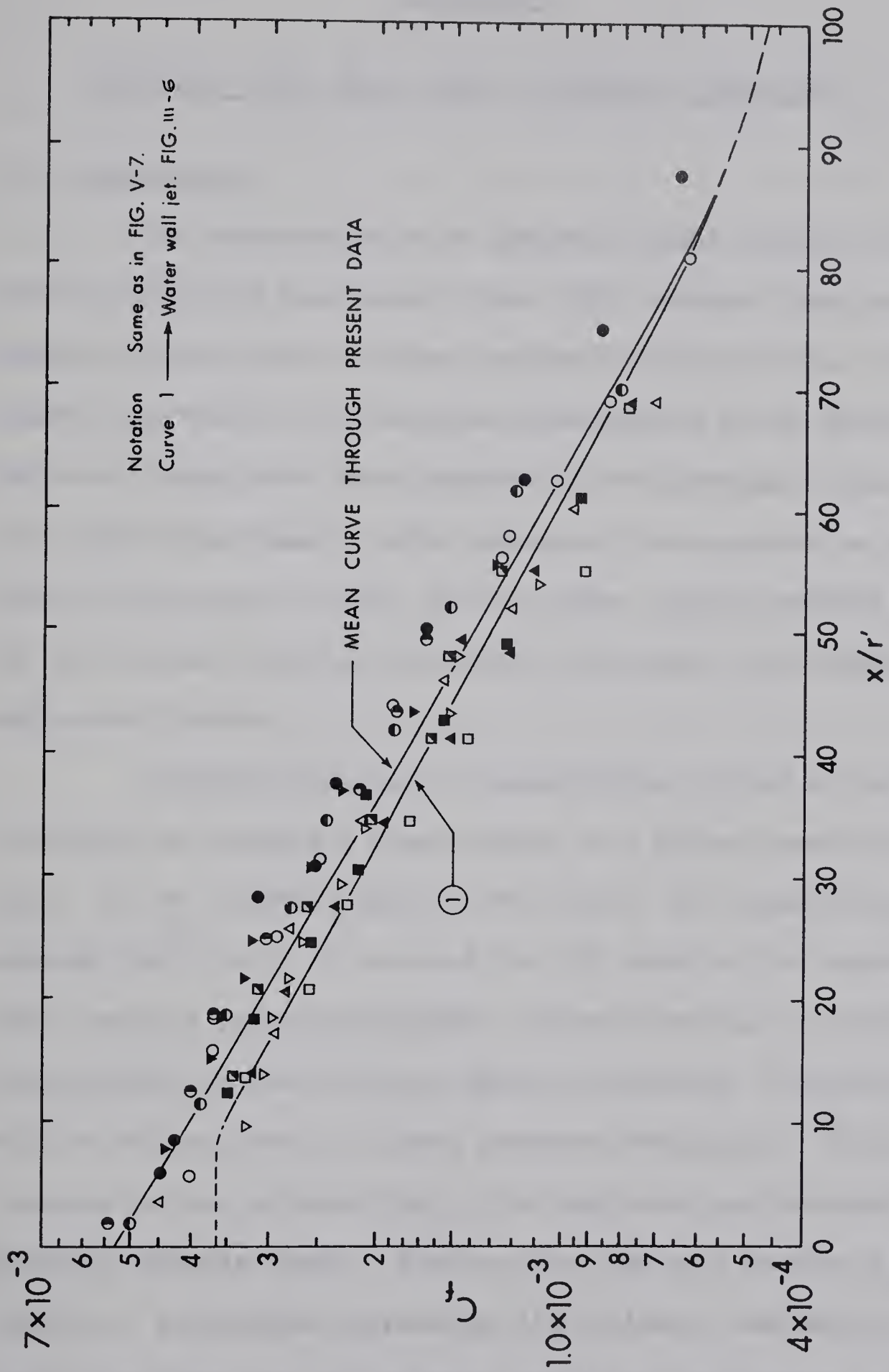


FIG. V-11. VARIATION OF C_f WITH x/r' FOR WALL JET IN A WIDER CHANNEL.

CHAPTER VI

HYDRAULIC JUMPS BELOW ABRUPT SYMMETRICAL EXPANSIONS

6.1 Introduction

The characteristics of hydraulic jumps formed in channels of constant width are well known (Chow, 1959), whereas jumps occurring at sudden expansions have not been analysed satisfactorily. In this chapter the results of a detailed investigation of the gross characteristics of jumps below abrupt expansions are discussed. Also, the case of a stable jump below a sudden expansion is recognised as an extreme limit of the case of a wall jet in a wider channel (studied in Chapter V), and the wall jet characteristics of the jump are studied in an exploratory manner.

Consider (Fig. VI-1) a supercritical stream of rectangular cross-section entering a wider channel at a sudden symmetrical expansion. If the tailwater depth is very small, the supercritical stream expands freely until it occupies the full width of the channel and then creates a system of diagonal surface waves due to successive reflections. As the tailwater depth is increased, a hydraulic jump with an oblique front is formed somewhere downstream. With an increase in the tailwater depth, the jump moves upstream and its front gradually becomes normal. However, the jump soon reaches a limiting position. Any further increase in the tailwater elevation causes the jump to collapse and the tailwater spills on the upstream supercritical flow on one side. The jump formed under this limiting tailwater

condition is termed the repelled jump and is designated the R-jump.

If the tailwater is slightly greater than the sequent depth of the R-jump, the jet gets twisted and deflected to one side due to the tailwater occupying the other side of the outlet. The jet undergoes subsequent reflections on its travel downstream and creates a very unstable and non-uniform flow situation. With further increase in the tailwater level, the outlet gets gradually submerged on both sides, but the jet will still be unstable, oscillating rather violently. However, at a certain higher tailwater level, the jet ceases to oscillate, the flow becomes stable and the phenomenon resembles the familiar hydraulic jump with small submergence. Further increase of tailwater causes greater submergence and the flow resembles a submerged jump. The minimum tailwater situation at which the stable flow takes place, after the collapse of the R-jump, is designated the stable jump or S-jump.

The results of an experimental study of the characteristics of R-jump and S-jump are discussed in the following sections.

6.2 The R-Jump

6.2.1 Theoretical Analysis

Fig. VI-1 is a schematic representation of the R-jump where B is the width of the channel, b is the width of the supercritical stream at the nozzle outlet, y is the depth and U the mean velocity with the subscripts 0 , 1 and t referring to the nozzle outlet, toe of the jump and tailwater respectively. L_1 is the distance of the toe of the jump from the outlet.

For a given supercritical stream of known y_o , U_o and b and channel width B , the problem is to predict the required tailwater depth y_t for a R-jump to form and also to predict L_1 and other flow characteristics.

To predict the tailwater depth y_t , the momentum equation could be written for the outlet section and the end of the jump. The two roughly triangular areas formed at the corners of the sudden expansion by the expanding stream do not contain any water. The pressure distribution at the two sections could be assumed to be hydrostatic and the momentum correction factors could be taken as unity. The momentum equation is then written as

$$\frac{1}{2} \gamma b y_o^2 - \frac{1}{2} \gamma B y_t^2 - P_f = \rho Q U_t - \rho Q U_o \quad (6.1)$$

where P_f is the integrated bed shear stress between the two sections under consideration and Q is the discharge. If P_f is neglected, Eq. (6.1) can be written

$$y_t/y_o = \frac{1}{2} \left[\sqrt{\alpha^2 + 8 F_o^2 \alpha} - \alpha \right] \quad (6.2)$$

in which F_o is the Froude number of the supercritical stream at the outlet section, namely,

$$F_o = Q/b \sqrt{gy_o^3} \quad (6.3)$$

and $\alpha = b/B$.

Kuznetsov (1964) introduced a coefficient K in Eq. 2, apparently to account for the neglect of the integrated bed shear stress, and gave

the following equation for the calculation of the sequent depth of the R-jump;

$$y_t/y_o = K^{1/2} [\sqrt{\alpha^2 + 8 F_o^2 \alpha} - \alpha] \quad . \quad . \quad (6.4)$$

where K is given by the expression

$$K = 0.665 + 0.15 \alpha \quad . \quad . \quad . \quad . \quad (6.5)$$

6.2.2 Experiments

The experiments were conducted in Flume A, and five values of α in the range of 0.17 - 0.83 were tested. The detailed data are given in Table D-7 in Appendix D.

For the four series, having $\alpha \geq 0.33$, in the entire range of F_o tested, the R-jump had an essentially normal front with a strong surface roller. The jump was stable and the stability improved with increase in the Froude number, F_o . However, for the CR series ($\alpha = 0.17$) it was very difficult to obtain the R-jump, as the jump was very unstable. Only two observations could be made in this series and in view of the difficulty of establishing a fairly stable jump, no great accuracy is attached to the two runs.

6.2.3 Sequent Depth Ratio

The variation of the sequent depth with F_o and α for all the runs of the present study is shown in Fig. VI-2. For a given value of F_o , the relative sequent depth, y_t/y_o , decreases with a decrease in the value of α . In the BR series the value of α was kept at 0.33 and the aspect ratio, b/y_o , varied from 2.0 to 4.8. The points

corresponding to these series all follow one line, indicating the insignificant effect of aspect ratio, for a given α , in the range tested.

The present data were used to check the relation for the correction factor K , given by Kuznetsov (1964) and the results are shown in Fig. VI-3. It is seen that K is a function of both F_o and α , and only beyond a certain value of F_o does K become independent of F_o . Also, the present values of K are considerably larger than those predicted by Eq. 6.5.

For practical purposes, the experimental results shown in Fig. VI-2 were used to construct a simple expression

$$\frac{(y_t/y_o) - 0.75}{F_o - 0.85} = \alpha + 0.30 \quad . \quad . \quad . \quad (6.6)$$

It is believed that this relation will be good for values of α in the range 0.30 to 0.90.

6.2.4 Shear Force on the Bed

A knowledge of the shear force on the bed between the initial and tailwater section is essential for writing an accurate momentum equation between the two sections. However, the two-dimensional nature of the shear stress on the bed precludes the use of simple Preston tube technique and necessitates a very laborious and time consuming procedure to get the bed shear field. Hence, an indirect method was devised to compute the total shear force.

$$\text{Let } P_f = C_s Q U_o \quad . \quad . \quad . \quad . \quad (6.7)$$

in which C_s is a consolidated shear force coefficient. Introducing Eq. 6.7 in Eq. 6.1 and simplifying

$$\left[\frac{y_t}{y_o}\right]^3 - \left[\frac{y_t}{y_o}\right] [2F_o^2\alpha (1 - C_s) + \alpha] + 2F_o^2\alpha = 0 \quad (6.8)$$

Using Eq. 6.8, the values of C_s were calculated for all the runs and the results are shown in Fig. VI-4. It is interesting to find that for a given value of α , C_s increases with F_o up to a certain value beyond which it is constant. The constant value of C_s increases with decrease in the value of α .

6.2.5 Length Characteristics

The variation of the length of the roller, L_r , is plotted in Fig. VI-5. The scatter of the data can be attributed to the difficulty of accurately fixing the fluctuating roller length. The mean curve through the data shows that L_r/y_t reaches a constant value of 3.6 for values of $F_o \geq 7.0$. Regarding the length of the jump, L_j , a plot of L_j/y_t vs. F_o showed considerable scatter and it could be roughly said that for the R-jump, L_j/y_t is about 15% larger than L_j/y_2 of the corresponding classical jump ($\alpha = 1.0$) where y_2 is the subcritical sequent depth.

The variation of the distance of the toe of the R-jump from the outlet, L_1 , is studied in Fig. VI-6, by plotting $L_1/(B - b)$ against F_o . It is interesting to find that the data are very well correlated and a single curve could be drawn to describe the variation in the full range of the variables studied. Similarly, the distance of

the section of first noticeable wave reflection at the side wall, L_o , was found to be given by the expression

$$L_o / (B - b) = 0.31 F_o \quad . \quad . \quad . \quad . \quad (6.10)$$

which agrees fairly well with an expression given earlier by Kuznetsov (1964).

6.3 The S-Jump

6.3.1 Review of Previous Work

The S-jump appears to have received considerable attention from Russian research workers, as could be gathered from a recent summary of the problem by Sharma (1966). A critical study has been conducted by Unny (1961). In these works, the S-jump has been called the Spatial jump.

The main aim of most of the previous works appears to be the development of a theoretical equation to predict the sequent depth of a S-jump for given values of y_o , F_o and α . With reference to the definition sketch of the S-jump shown in Fig. VI-7, if the momentum equation is to be written for the outlet section and the end of the jump, one should initially know the backed up depth y_3 at the outlet, the width of the flow and the nature of the velocity distribution at the end of the jump and also the integrated bed shear stress. Different assumptions have been made by the various investigators regarding the above factors and as a result a large number of empirical formulae exist.

A typical formula in the Russian Hydraulics literature for the determination of the sequent depth in a S-jump, is that of Abramov, which

is given as (Sharma, 1966):

$$\frac{y_t}{y_o} = \frac{K_1 + 14}{10 (K_1 + 2)} \left[\sqrt{1 + 600 \frac{K_1 + 2}{(K_1 + 14)^2} F_o^2} - 1 \right] \quad (6.11)$$

where K_1 is an empirical factor which could be taken as 3.0 to 4.0 for $B/b < 10.0$ and 5.0 to 6.0 for $B/b > 10.0$. Unny (1961) has obtained a semi-empirical formula for the case of $\alpha = 0.50$ as:

$$\frac{y_t}{y_o} = \frac{1}{2} \left[1 + 2.2 \frac{y_1}{b} F_o^2 \right] \left[\sqrt{1 + \frac{8 F_o^2}{\left(1 + 2.2 \frac{y_1}{b} F_o^2\right)^2}} - 1 \right] \quad (6.12)$$

6.3.2 Experiments

The experiments were conducted in Flume A. There were four main series of experiments with the values of $\alpha = 0.33, 0.50, 0.67$, and 0.83 . For the series $\alpha = 0.33$ and 0.50 , additional experiments were conducted to study the effect of the aspect ratio (b/y_o) of the supercritical stream. The experimental data are given in Table D-8, Appendix D.

Fig. VI-8 gives a few typical bed pressure profiles obtained by means of piezometer tapings in the bed. In a few runs the water surface profiles were also obtained and they were essentially the same as the bed pressure profiles. For a few selected runs (shown by an asterisk in Table D-7), the velocity distribution along the centerline was measured at a number of sections. Also, for these runs the distribution of bed shear stress along the center line was measured by a Preston tube. While the length of the jump, L_j , was measured fairly

accurately in all runs, it was not possible to measure the length of the roller, with sufficient accuracy, as in any run it fluctuated over a fairly large range.

6.3.3 Verification of the Formulae of Abramov and Unny

Abramov's formula [Eq. 6.11] by selecting a value of $K_1 = 3.5$ for the range of α involved in the present work, becomes:

$$\frac{y_t}{y_o} = 0.318 \left[\sqrt{1 + 10.8 F_o^2} - 1 \right] . \quad (6.13)$$

Eq. 13 was evaluated for all the runs and is compared with the experimental results in Fig. VI-9(a). It can be seen that only the results of the BS-series, with the lowest values of α agree well with Eq. 6.13 in the range of $y_t/y_o > 5.0$. In general, however, the experimental values of y_t/y_o are higher than the theoretically predicted values.

Unny's equation (Eq. 6.12) is compared with the results of AS1 and AS2 series in Fig. VI-9(b). The experimental values are very much larger than those given by Eq. 6.12.

6.3.4 Simple Momentum Equation

In the course of the present work, it was found by visual observation, that the forward flow occupied the whole width of the channel at the end of the jump. Further, the backed-up depth at the outlet was almost constant in the lateral direction. With these observations and neglecting the integrated bed shear stress, the momentum equation between the outlet and the end of the jump is written as

$$\frac{\gamma y_3^2}{2} B - \frac{\gamma y_t^2}{2} B = \frac{\gamma Q}{g} \left[\frac{Q}{By_t} - \frac{Q}{by_o} \right] \quad \dots (6.14)$$

In Eq. 6.14 the momentum coefficients at both sections are assumed to be unity. If $y_3 = \theta y_o$, Eq. 6.14 could be reduced to

$$\left[\frac{y_t}{y_o} \right]^3 - \left[\frac{y_t}{y_o} \right] \left[\theta^2 + 2 F_o^2 \alpha \right] + 2 F_o^2 \alpha^2 = 0 \quad \dots (6.15)$$

Based on the experimental results, as a first approximation θ was given an average value of 4.0 and Eq. 6.15 was evaluated for all the runs and is compared with the experimental results in Fig. VI-9(c). The agreement with Eq. 6.15 is as bad (or as good) as that with the other two equations previously tested. From this performance, it is suggested that to be able to write a reasonably correct equation one should be able to predict the backed-up depth, the width and nature of the forward flow at the end of the jump and the shear force on the bed. As an alternate method, for practical use, a simple formula based on dimensional analysis and using the present experimental results is developed in the next section.

6.3.5 Empirical Equation for the Sequent Depth of S-Jump

For the sequent depth of a S-jump, one could write

$$y_t = f_1 (U_o, y_o, b, B, \rho, g, \mu) \quad \dots (6.16)$$

By dimensional analysis, Eq. 6.16 could be reduced to

$$\frac{y_t}{y_o} = f_2 \left[F_o = \frac{U_o}{\sqrt{gy_o}}, R = \frac{U_o y_o}{\nu}, \alpha = \frac{b}{B}, \frac{b}{y_o} \right] \quad (6.17)$$

For large values of R the effect of the fluid ^{viscosity on} diffusion is very small and hence Eq. 6.17 becomes

$$\frac{y_t}{y_o} = f_3 \left[F_o, \alpha, \frac{b}{y_o} \right] \quad (6.18)$$

Experimental results plotted as y_t/y_o against F_o in Fig. VI-10, show a relation as given by Eq. 6.17. Also, it appears that b/y_o is having a stronger influence than b/B on the variation of y_t/y_o with F_o .

Introducing the characteristic length of the outlet, r' , (Sec. 5.2) given by

$$r'/y_o = \frac{1}{1 + 2(y_o/b)} \quad (5.2)$$

into the dimensional analysis, the Eq. 6.18 can be written as

$$\frac{y_t}{r'} = f_4 \left[F'_o = \frac{U_o}{\sqrt{gr'}}, \alpha, \frac{b}{y_o} \right] \quad (6.19)$$

The experimental data are plotted as y_t/r' against F'_o in Fig. VI-11. It is interesting to see that all the data are correlated by one straight line, independent of α and b/y_o . The equation of this straight line is

$$y_t/r' = 1.08 F'_o + 1.40 \quad (6.20)$$

6.3.6 The Backed-Up Depth

A knowledge of the backed-up depth, y_3 , is necessary for writing an accurate momentum equation and also for estimating the water surface profile. It could be written

$$\text{that } y_3 = f_5 [U_o, y_o, b, g, \rho, \mu] \quad . \quad . \quad . \quad (6.21)$$

By dimensional analysis, similar to that of y_t ,

$$\frac{y_3}{r'} = f [F'_o, \alpha, \frac{b}{y_o}] \quad . \quad . \quad . \quad (6.22)$$

Fig. VI-12 shows that y_3/r' is a function of F'_o and α only and separate curves are drawn for each value of α .

6.3.7 Length of the S-Jump

Various plots were made regarding the variation of the jump length, L_j , and the best possible correlation was obtained in the plot of L_j/r' versus F'_o shown in Fig. VI-13. Also shown in Fig. VI-13 is the corresponding length of a classical jump, i.e., the hydraulic jump in a level rectangular channel (Chow, 1959). It can be seen that in general the S-jump is longer than the corresponding classical jump.

6.3.8 Energy Loss Characteristics

If E_o is the energy of the supercritical stream at the outlet,

$$E_o = y_3 + U_o^2 / 2g \quad . \quad . \quad . \quad . \quad (6.23)$$

and E_t is the energy at the end of the jump,

$$E_t = y_t + U_t^2 / 2g \quad . \quad . \quad . \quad . \quad (6.24)$$

the energy loss in the S-jump is

$$E_L = E_o - E_t \quad . \quad . \quad . \quad . \quad (6.25)$$

and the relative energy loss is

$$\frac{E_L}{E_o} = \frac{(y_3 - y_t) + (U_o^2 / 2g - U_t^2 / 2g)}{y_3 + U_o^2 / 2g} \quad . \quad . \quad (6.26)$$

For the present data, E_L/E_o was calculated using Eq. 6.26 and is plotted against F_o in Fig. VI-14. This plot shows that the relative energy loss, E_L/E_o , is a function of F_o , α and b/y_o . However, when the experimental results are re-plotted with E_L/E_o against F_o' , as in Fig. VI-15, all the points follow one single curve proving once again the usefulness of the characteristic length r' in correlating the S-jump characteristics.

Since, from Fig. VI-15, E_L / E_o is a function of F_o' only, it could be said that the relative energy loss will be a maximum when for a given area of the supercritical stream (and of course for a given momentum) the perimeter of the fluid boundary is a maximum, i.e., the characteristic length r' is a minimum. For a rectangular supercritical stream, for such a condition

$$\left. \begin{aligned} b &= 2 y_o \\ \text{and } r_m' &= \text{minimum value of } r' = y_o/2 \end{aligned} \right\} \quad . \quad . \quad (6.27)$$

Using this value of r_m' and Fig. VI-15, the maximum relative energy loss in a S-jump was calculated as a function of F_o and is shown plotted in Fig. VI-14. If a ratio ψ is defined as

$$\psi = \frac{(E_L/E_o)_{\text{max}} \text{ for S-jump}}{(E_L/E_o) \text{ for Classical jump}} \quad . \quad . \quad (6.28)$$

the variation of ψ with F_o is also shown in Fig. VI-15. It is seen that ψ decreases rapidly from about 6.0 at $F_o = 1.8$.

6.3.9 Wall Jet Characteristics of S-Jump

The S-jump can be considered as a rectangular wall jet in a wider channel under an adverse pressure gradient, i.e., a limiting case of the wall jet in wider channel studied in Chapter V. A comparative study of the wall jet characteristics of a S-jump and the classical jump is useful in knowing the effect of the sudden expansion on the diffusion character of the jump.

The velocity distribution along the centerline of a typical S-jump (Run: BS1-7) is shown in Fig. VI-16. The velocity profiles show the characteristic shape of a wall jet. The growth of the boundary layer and the free mixing region are clearly seen in this Figure. The velocity profiles, obtained in the various runs, were tested for similarity by plotting in the standard form u/u_m vs. y/δ_1 , in Fig. VI-17. Also shown in this Figure are the similarity curves of the classical

wall jet and the free mixing region of the classical jump (Rajaratnam, 1965-b), plotted with the same coordinates, u/u_m vs. y/δ_1 . There is slight scatter of the data in the boundary layer region but in the free mixing region the data agree very well with the similarity curve of the classical jump. Thus the velocity profiles can be considered to be similar, at least in the free mixing region. In the boundary layer region, for the present data, the velocity distribution was found to be approximately represented by a power law type of equation with the power varying from about $1/10$ to $1/12$.

Regarding the variation of the maximum velocity, u_m/U_o is plotted against x/r' in Fig. VI-18, along with the curves of the classical jump (Rajaratnam, 1965-b), classical wall jet (Fig. III-1) and wall jet in wider channel (Fig. V-7). It is seen that for values of $\alpha = 0.33$ and 0.50 , the experimental points lie on the curve of the wall jet in wider channel, indicating that the adverse pressure gradient due to S-jump is too small to have any effect on the velocity decay for these small values of α . As the value of α increases, the experimental points shift towards the curve-1. It is interesting to note that the reduction of maximum velocity is fastest in the classical jump.

Fig. VI-19 shows the variation of the dimensionless length scale δ_1/y_o with x/y_o . The present results agree very well with the curve of the classical jump (Rajaratnam, 1965-b) which itself is not much different from the curve of the classical wall jet in all regions except near the end of the surface roller.

6.3.10 Study of the Bed Shear Stress

The skin friction coefficient, C_f , is plotted against x/r' in Fig. VI-20. Even though there is considerable scatter, it is not systematic and for practical purposes the mean curve through the points can be considered to represent the variation of C_f . It is seen that the centerline bed shear stress decreases faster in a S-jump than in the corresponding deeply submerged case, as can be expected.

6.4 Conclusions

Hydraulic jumps taking place below abrupt symmetrical expansions have been classified as R-jumps and S-jumps. The study of the gross characteristics of R- and S-jumps and the exploratory study of the wall jet characteristics of S-jumps, lead to the following conclusions:

- 1) For the R-jump, the available equation, i.e., Kuznetsov's equation, cannot satisfactorily predict the sequent depth. For practical purposes, the empirical equation to predict the sequent depth and the length characteristics, as in Sec. 6.2, can be used advantageously.
- 2) For the S-jump, the equations of Abramov, Unny and the simple momentum equation (Eq. 6.15) have all been found to be unsatisfactory for predicting the sequent depth.
- 3) The concept of the characteristic length of the outlet, has been found to be very useful in correlating the characteristics of the S-jump. A simple empirical formula for the sequent depth of S-jumps is developed.

- 4) Interesting results have been obtained regarding the energy loss in S-jump. Relative energy loss in a S-jump of maximum efficiency is predicted and compared with the corresponding classical jump.
- 5) Regarding the wall jet characteristics of a S-jump, it has been found that the velocity distribution along the centerline is similar, at least in the free mixing region. The similarity plot and the variation of the length scale are essentially the same as that for a classical jump. The decay of maximum velocity is fastest in the classical jump. The variation of the centerline bed shear coefficient has also been studied.

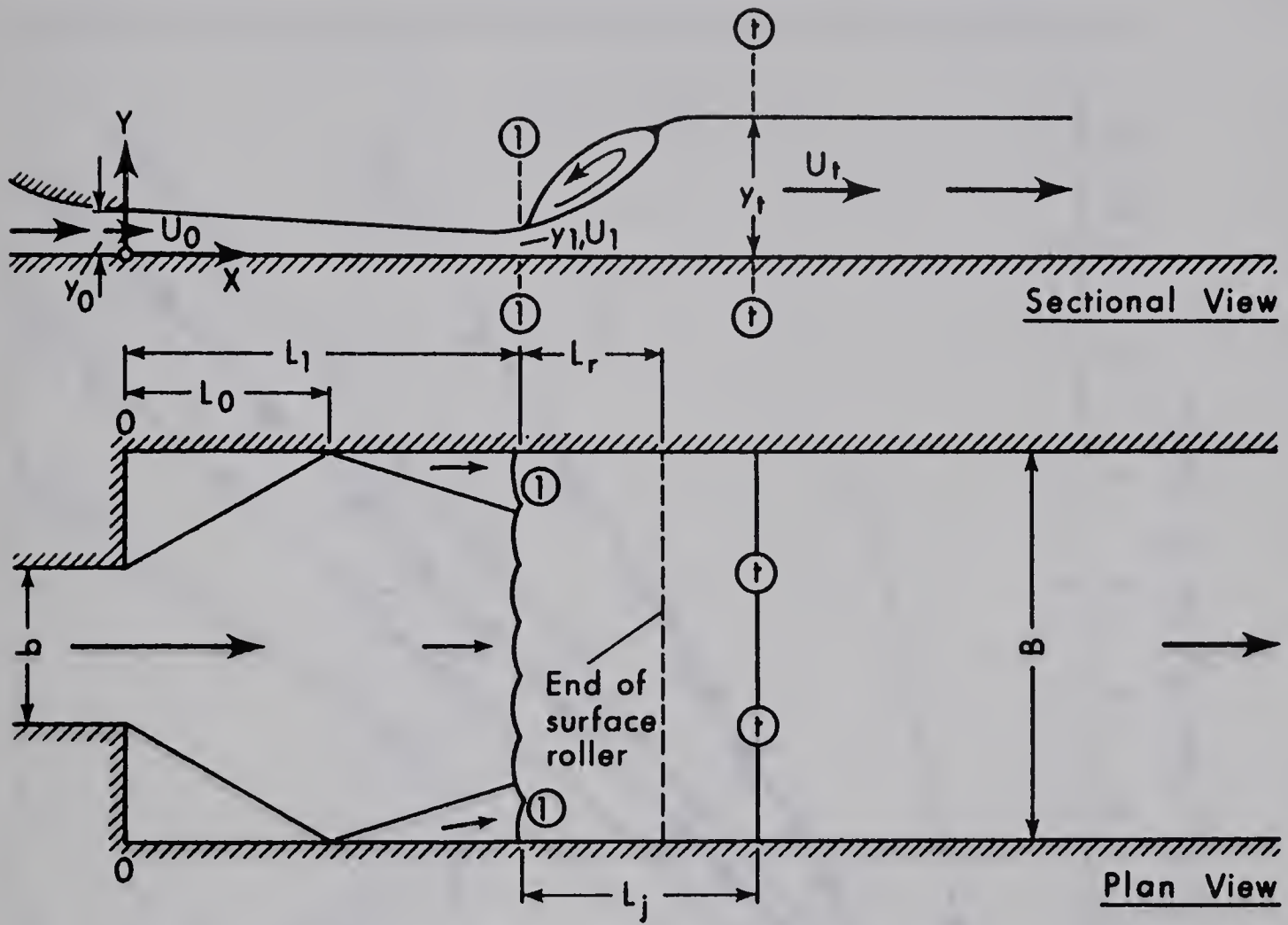


Fig. VI-1. Definition Sketch for R - Jump

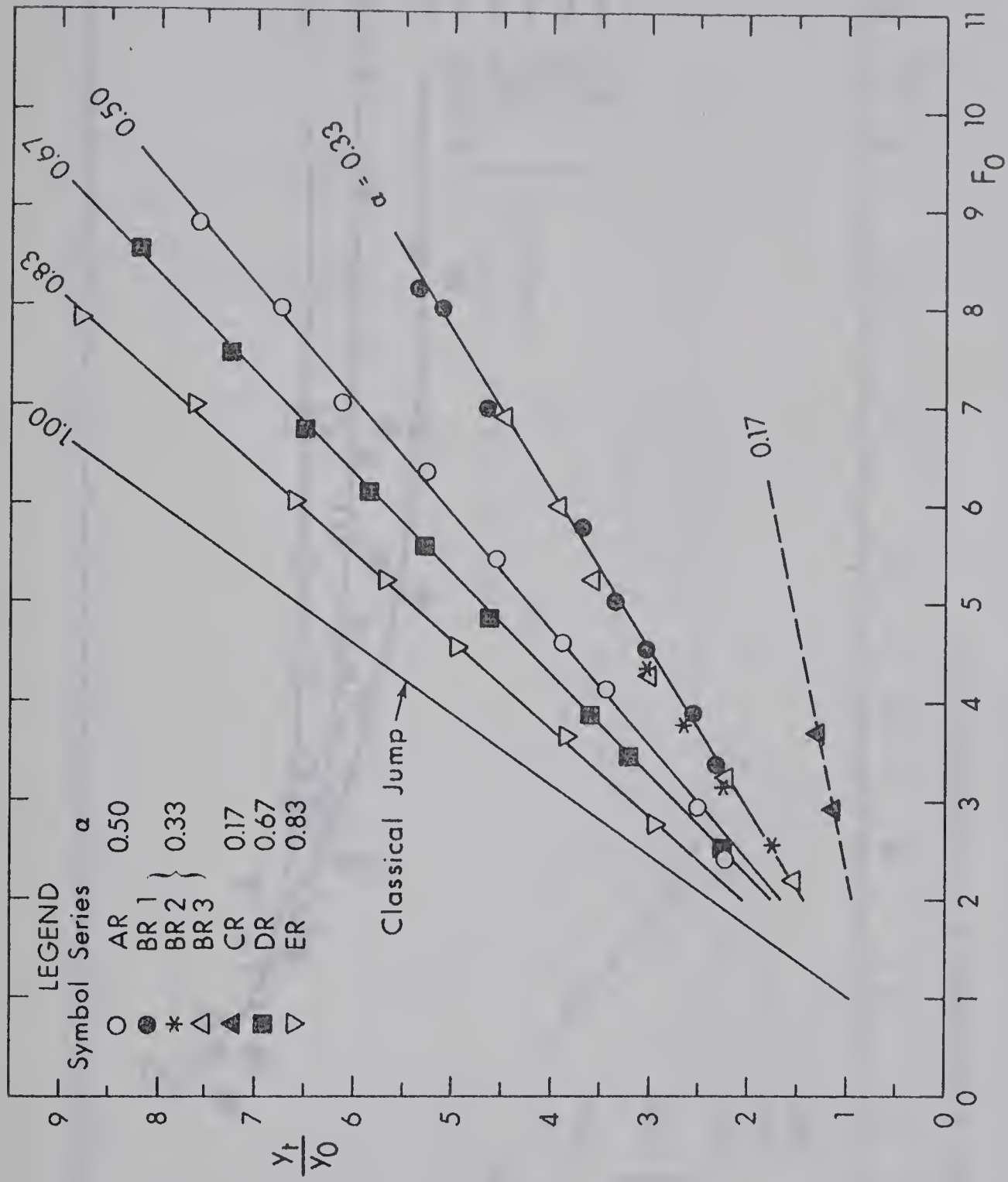


Fig.VI-2. Variation of γ_t/γ_0 with F_0 for R-Jump

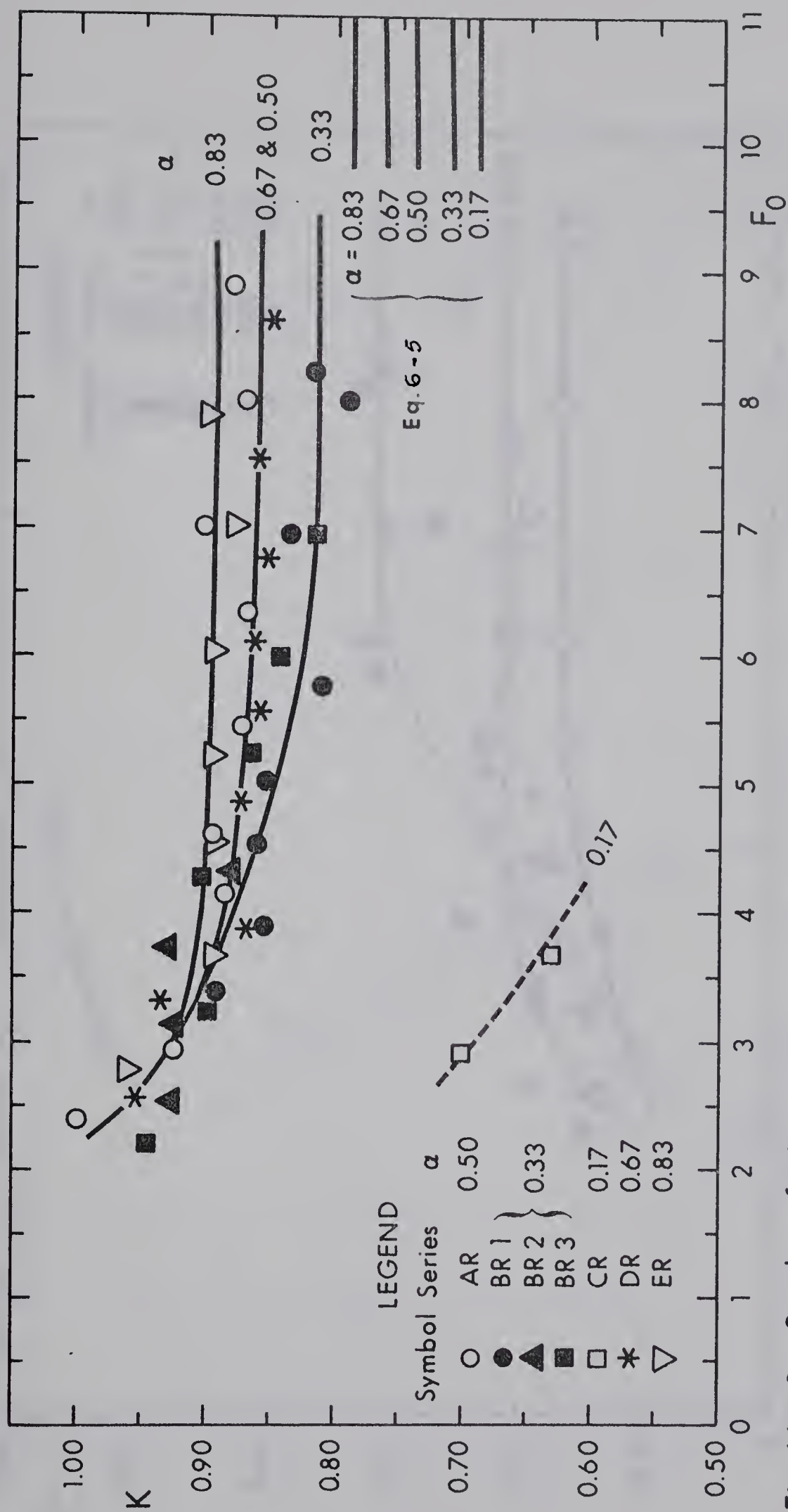


Fig. VI-3. Study of Kuznetsov's Parameter K

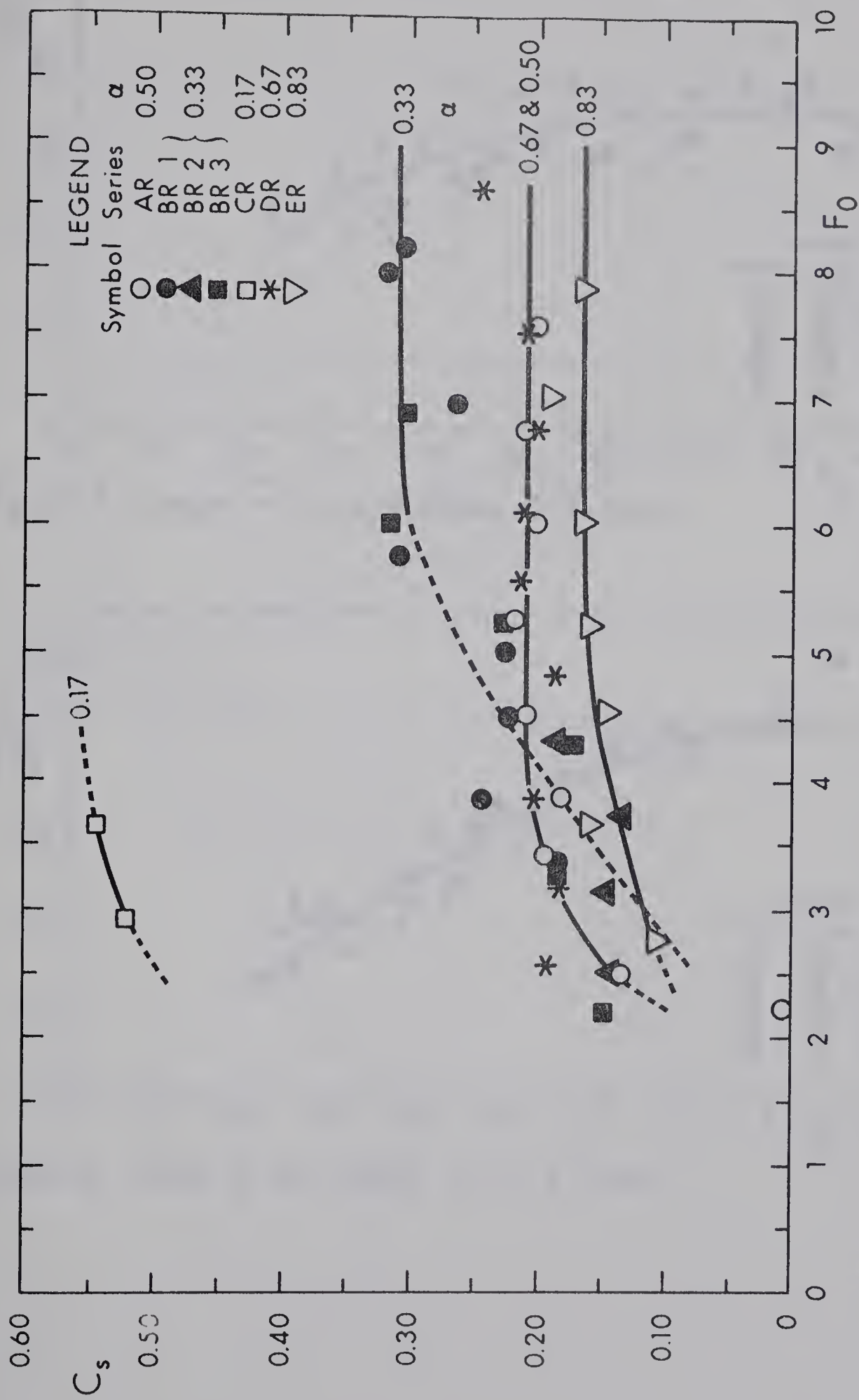


Fig. VI-4. Study of the Consolidated Shear Force Coefficient C_s

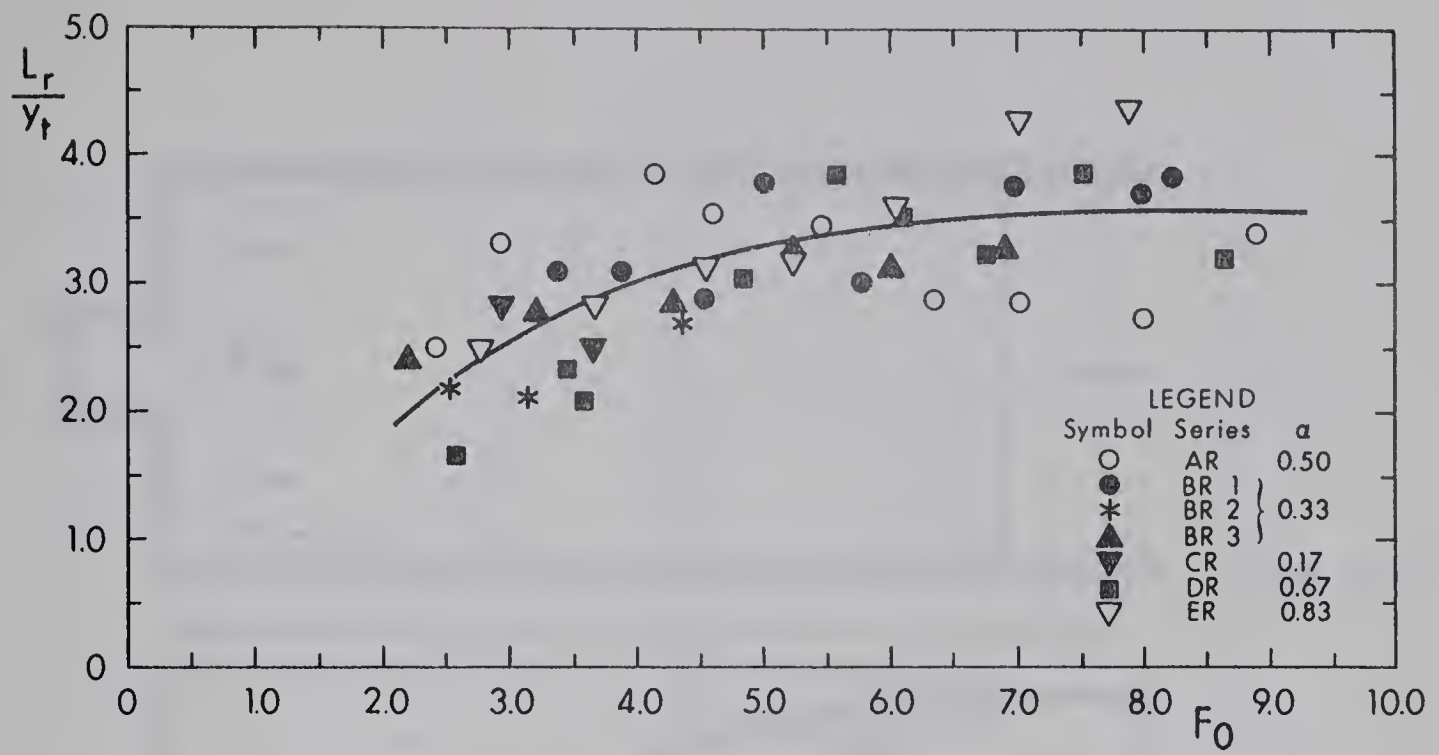


Fig. VI-5. Length of Surface Roller of R-Jump

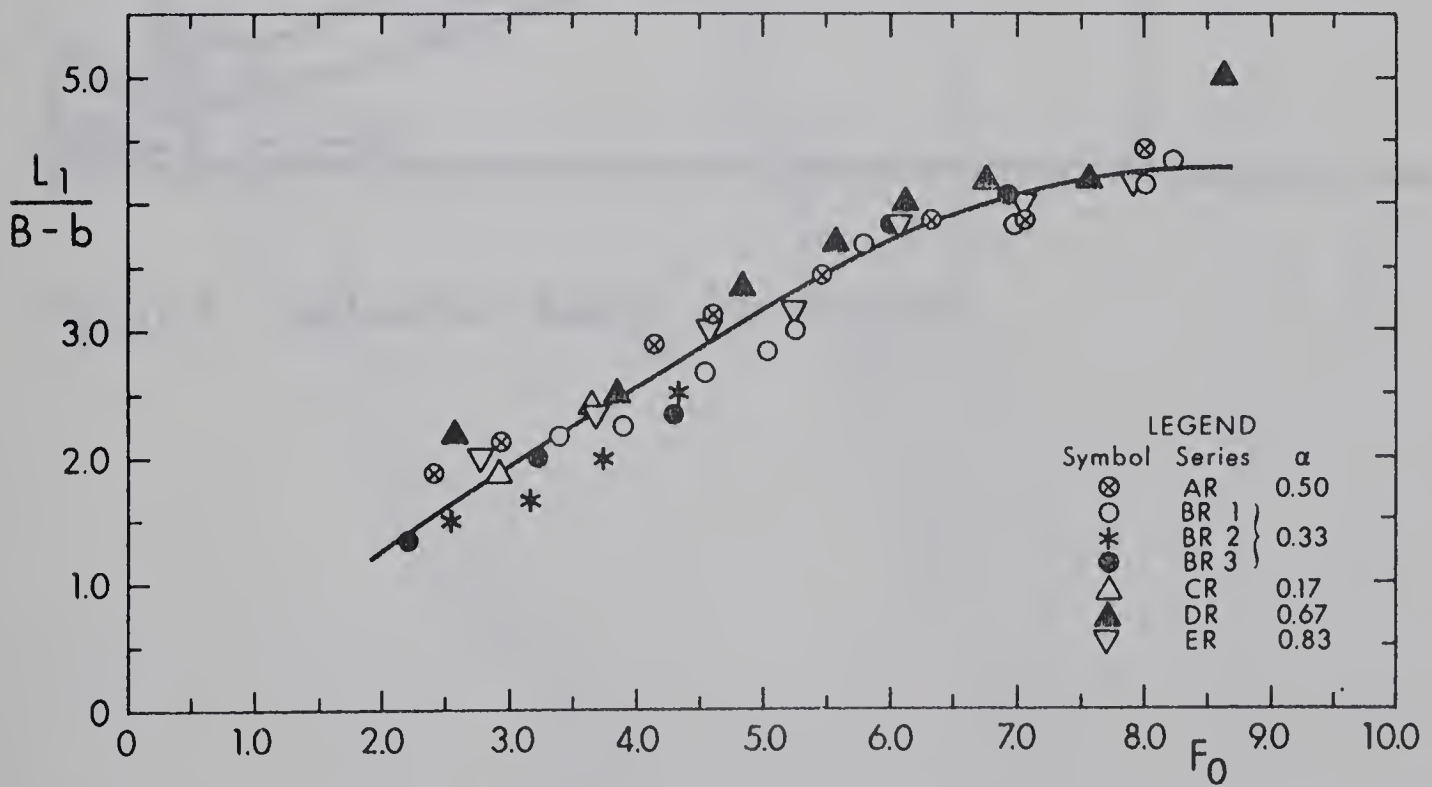


Fig. VI-6. Study of the Length L_1 of R-Jump

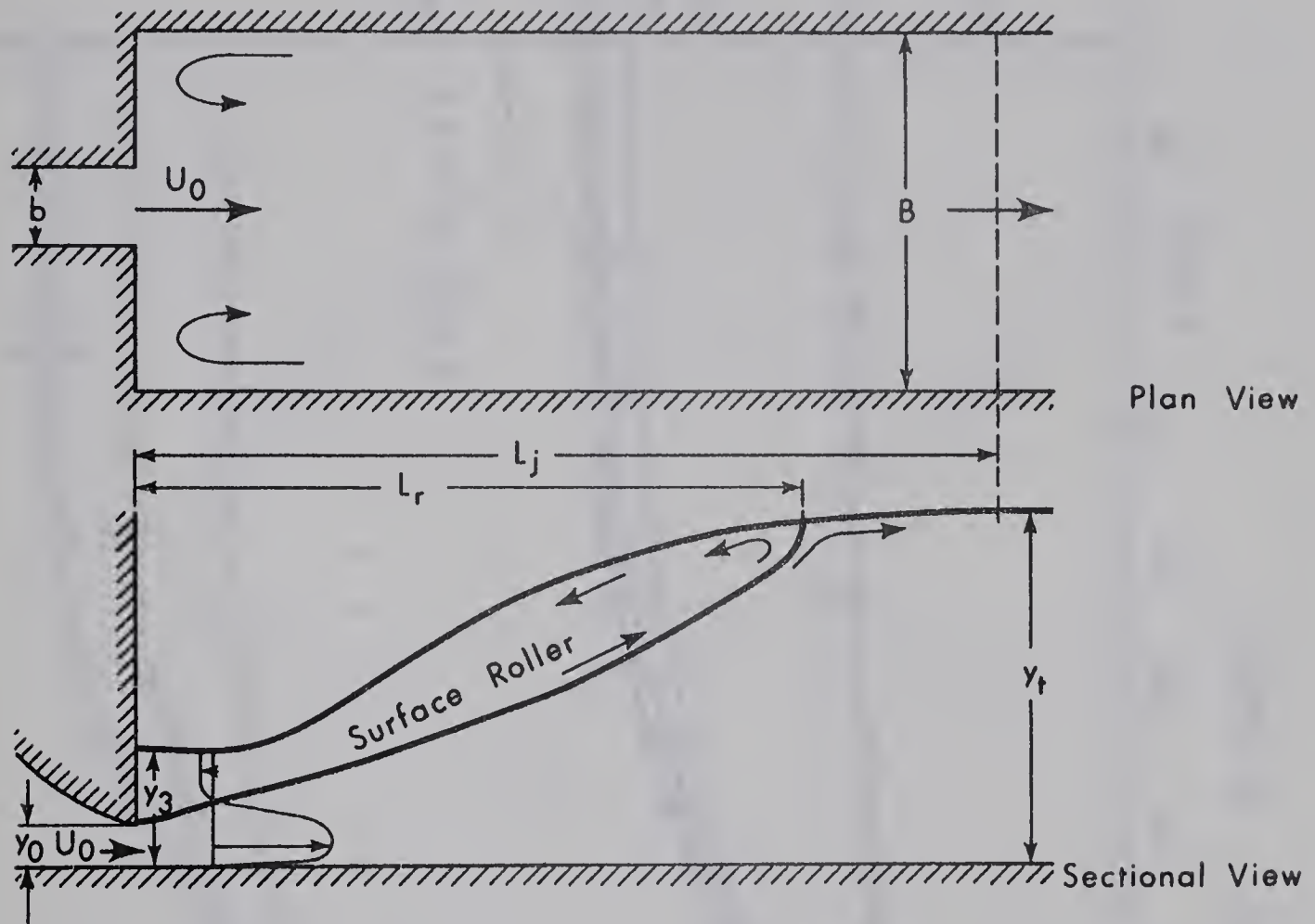


Fig. VI-7. Definition Sketch for S-Jump

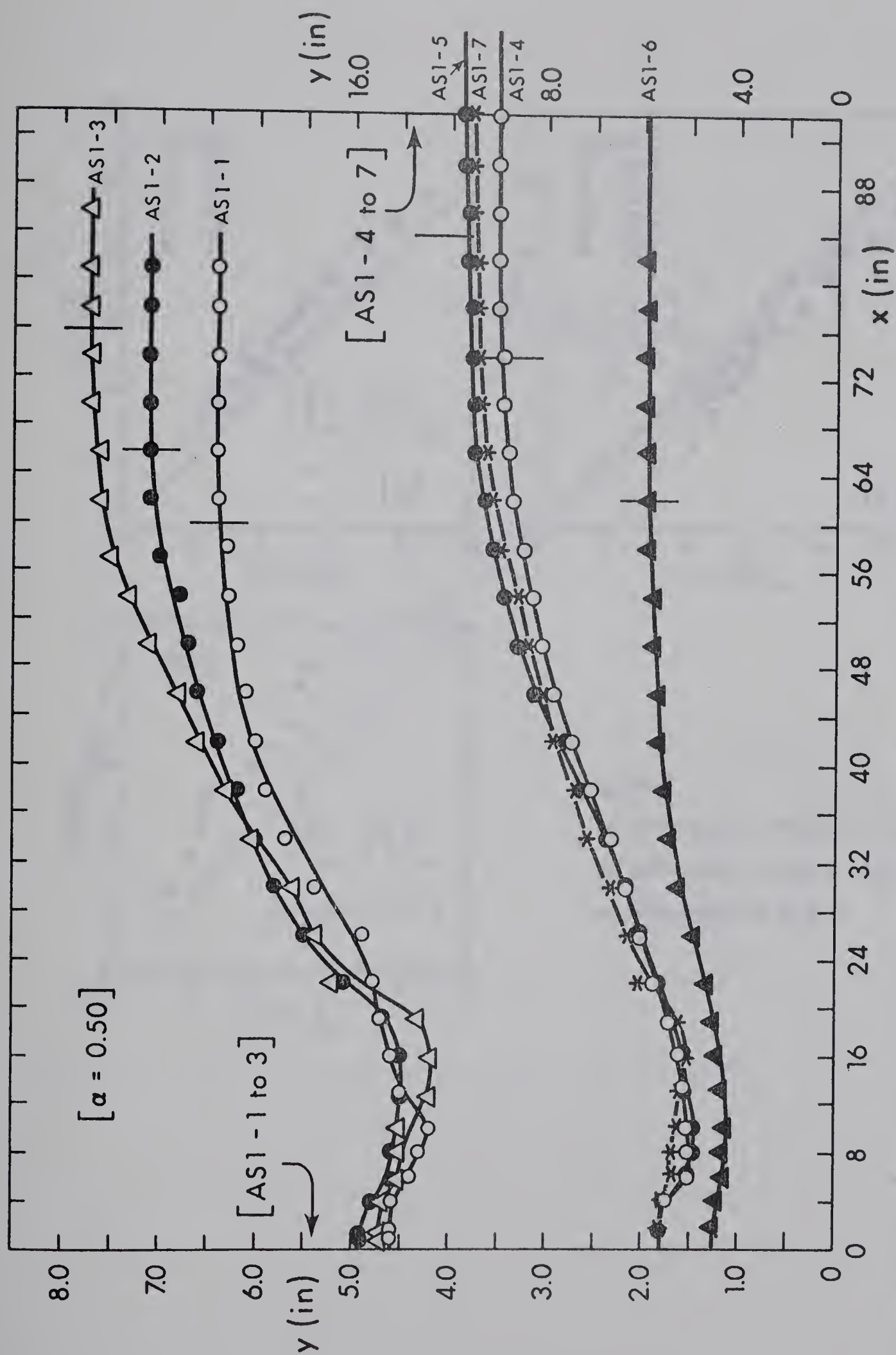


Fig. VI-8. Typical Bed Pressure Profiles - S-Jump

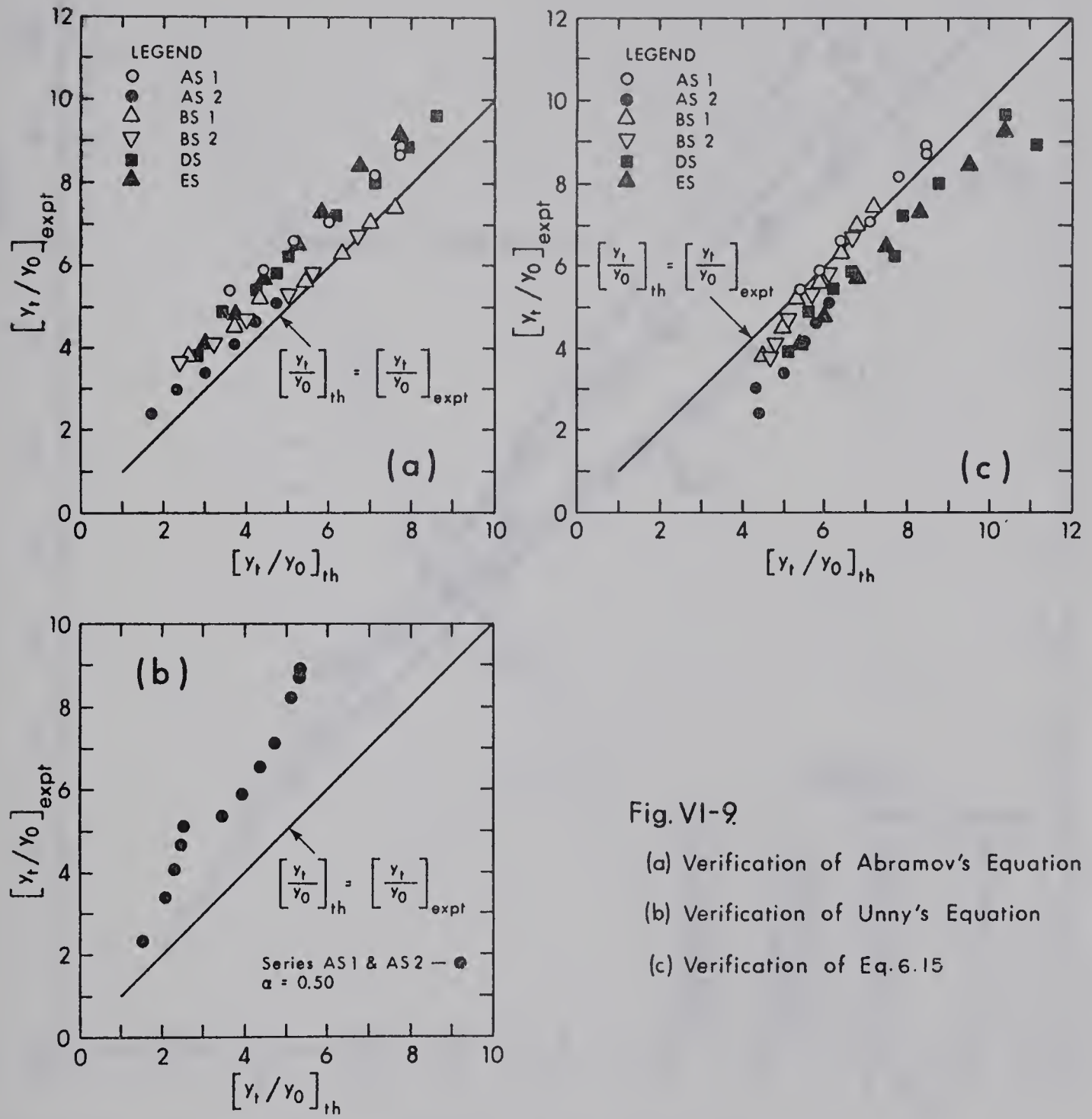


Fig. VI-9

(a) Verification of Abramov's Equation

(b) Verification of Unny's Equation

(c) Verification of Eq. 6.15

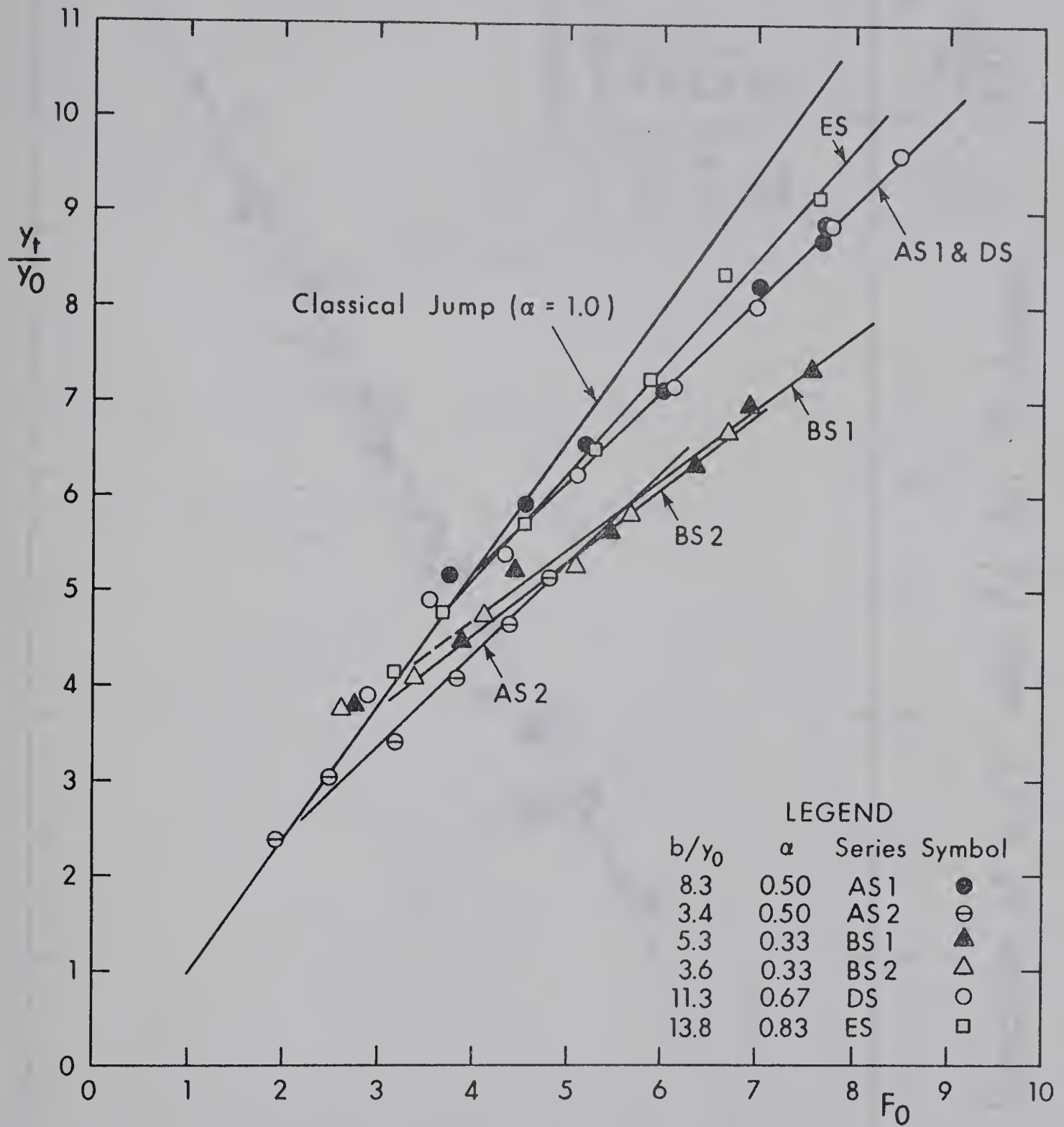


Fig. VI-10. Study of the Ratio y_t/y_0 for S-Jump

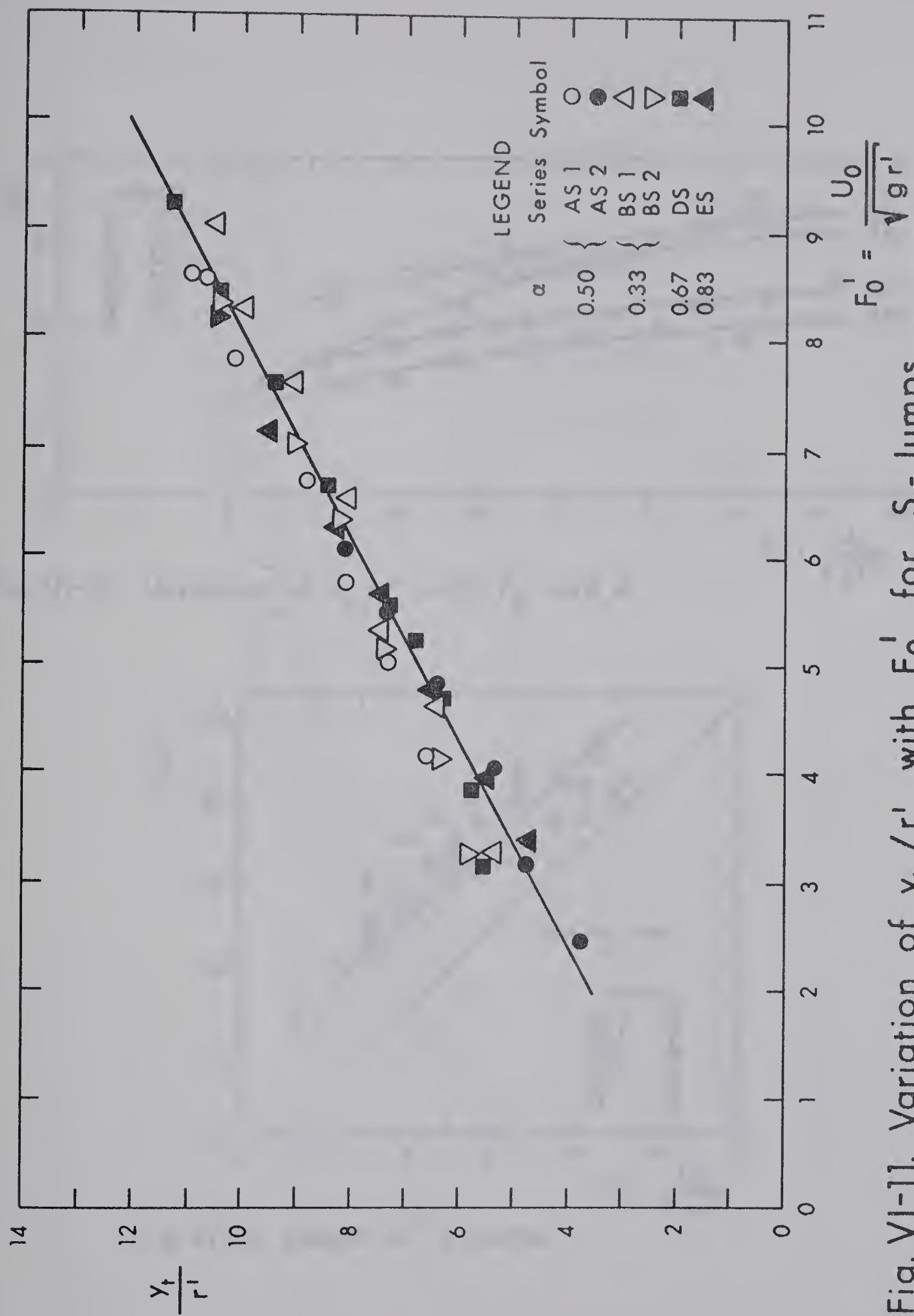


Fig. VI-11. Variation of γ_t / r' with F_0' for S-Jumps

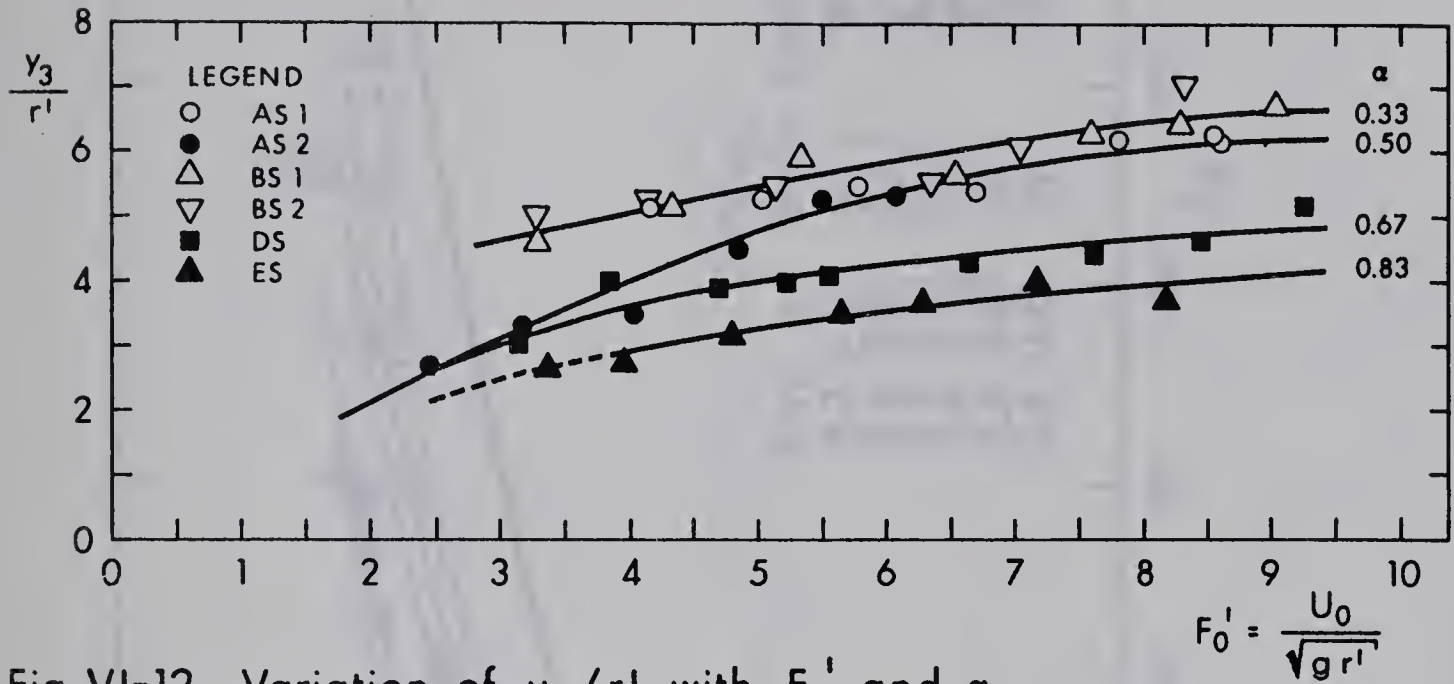


Fig. VI-12. Variation of y_3/r' with F_0' and α

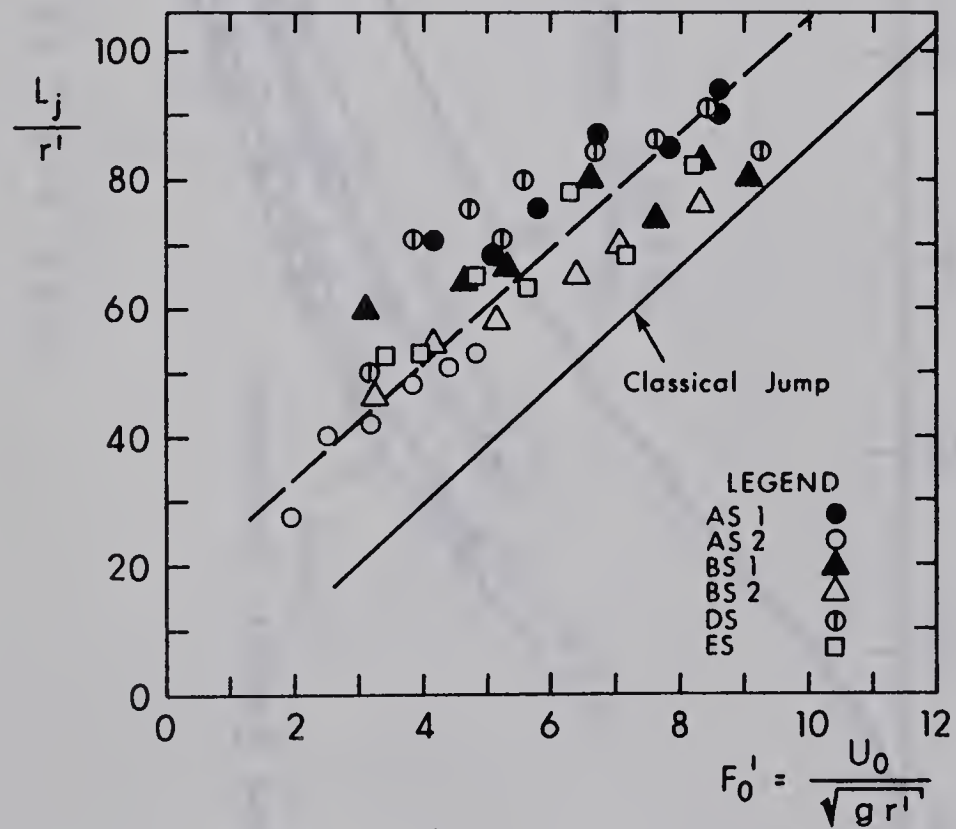


Fig. VI-13. Length of S-Jump

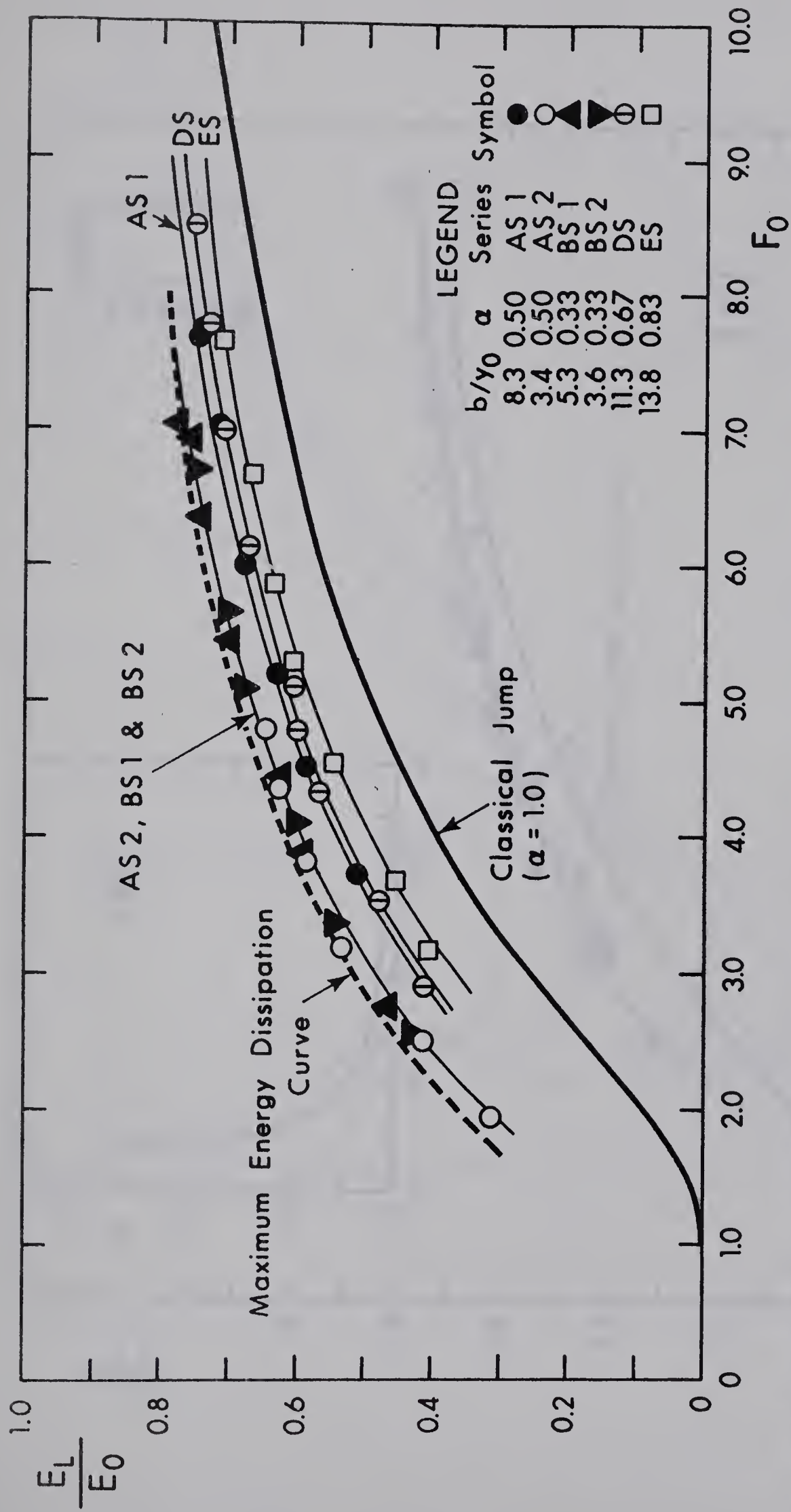


Fig. VI-14. Energy Dissipation - S - Jumps

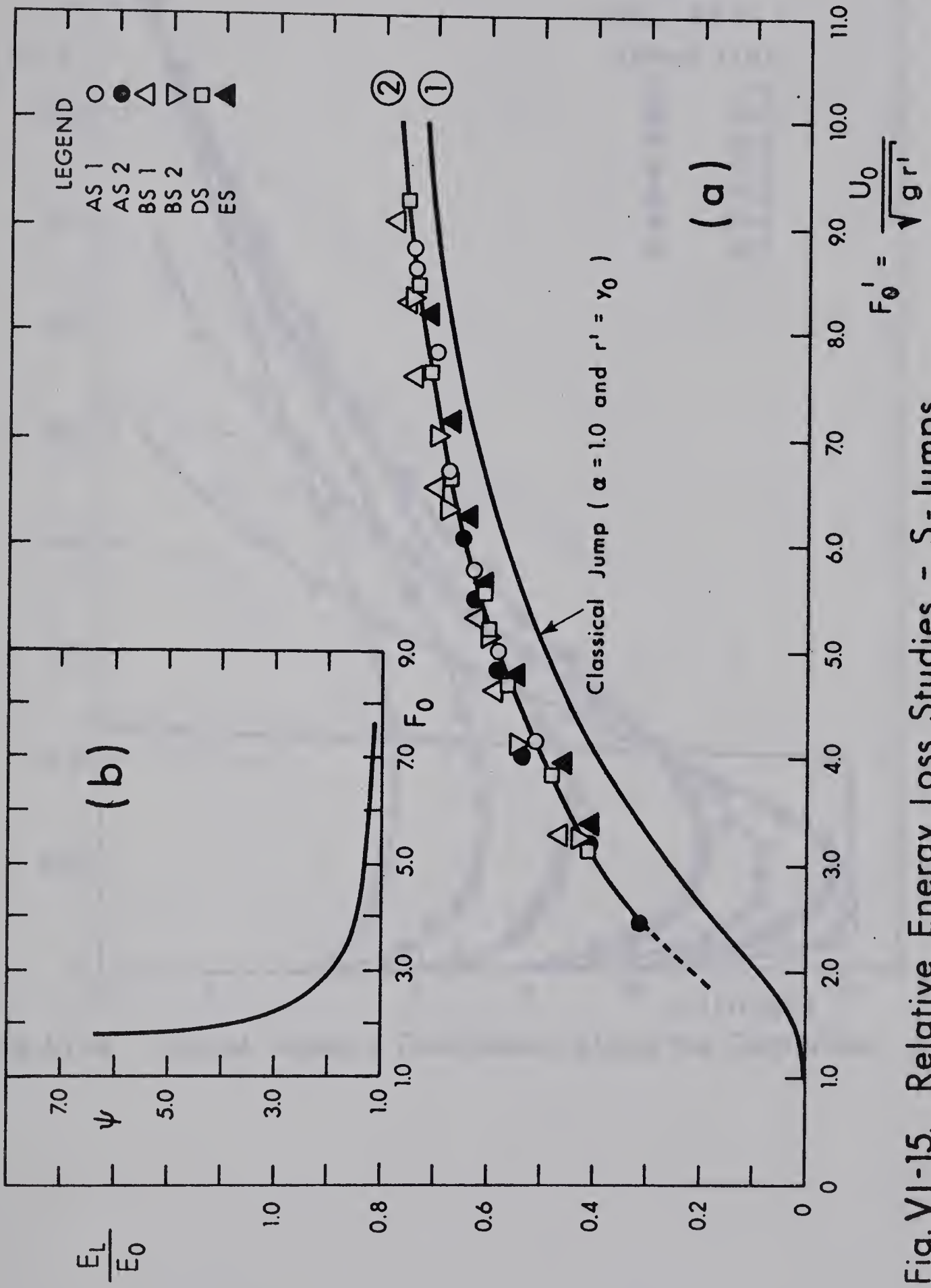


Fig. VI-15. Relative Energy Loss Studies - S-Jumps

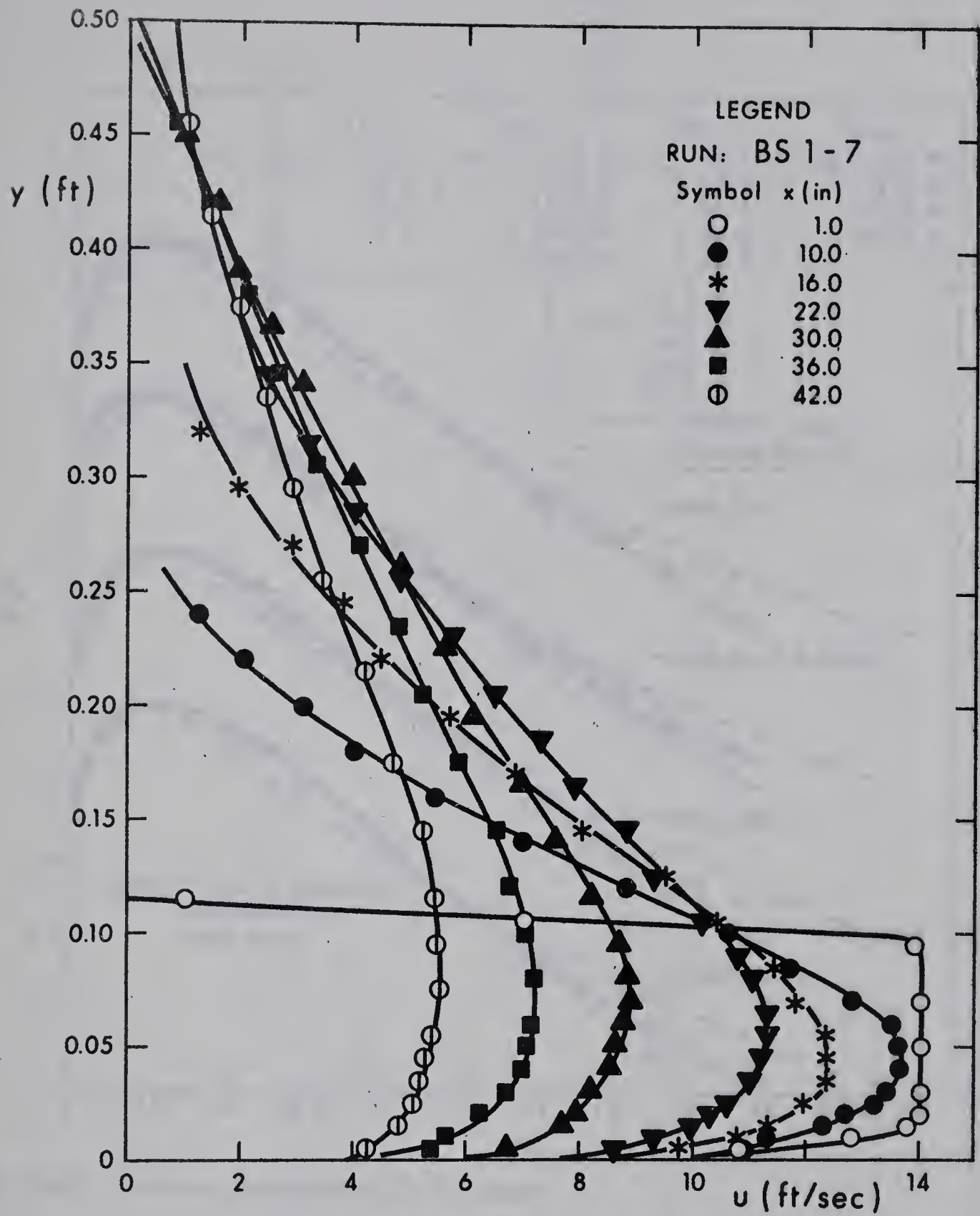


Fig. VI-16. Typical Velocity Distribution along the Centerline

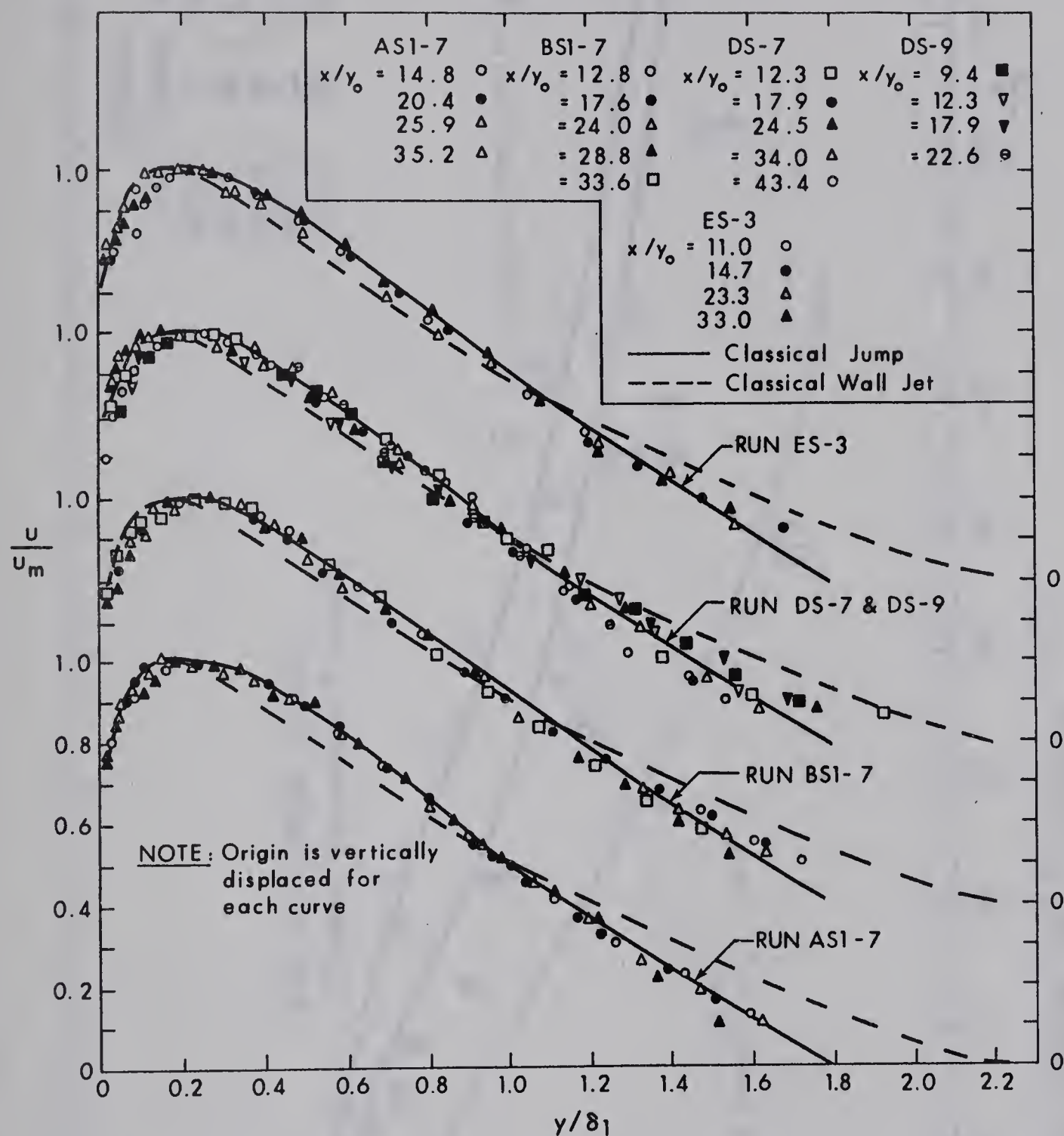


FIG. VI-17. Velocity Distribution in S - Jumps

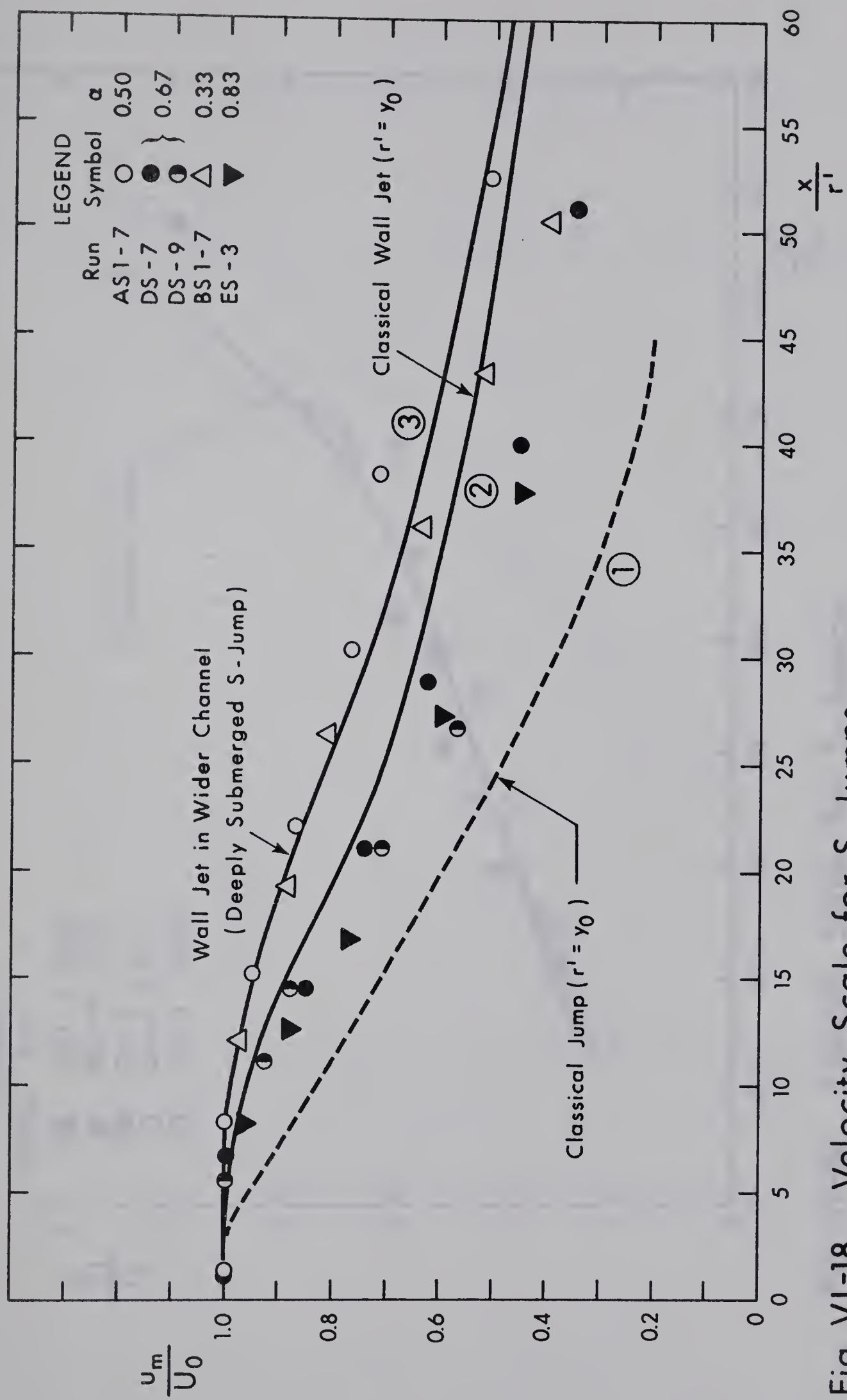


Fig. VI-18. Velocity Scale for S-Jumps

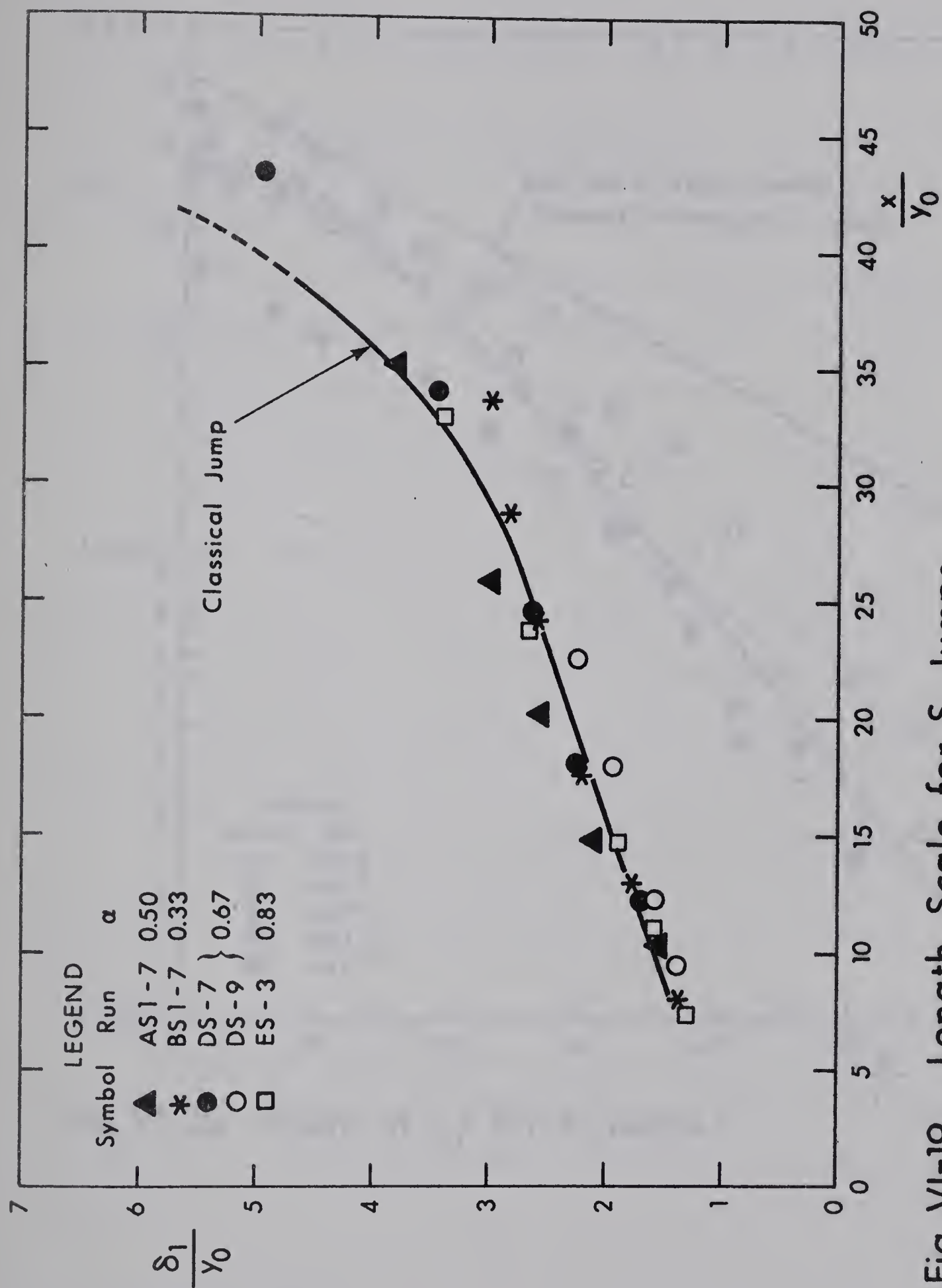


Fig. VI-19. Length Scale for S-Jumps

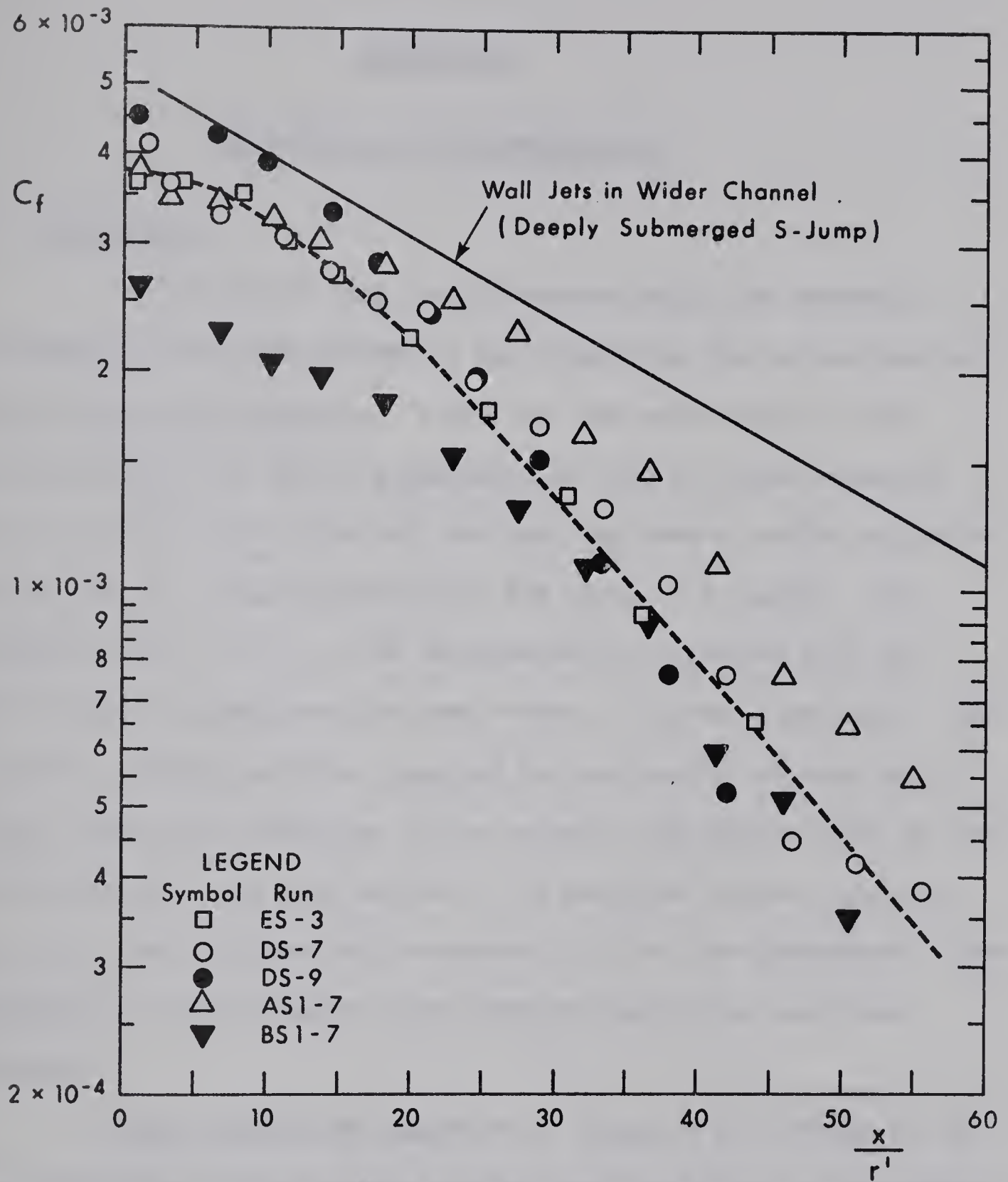


Fig. VI-20. Study of C_f for S-Jumps

CHAPTER VII

CONCLUSIONS AND RECOMMENDATIONS

7.1 Conclusions

As an initial step towards understanding the mechanics of submerged flow from outlets, a few simplified flow situations have been studied experimentally. These are, the water wall jet, the reattached wall jet due to submerged flow from an outlet situated over an abrupt drop in the bed, and the flow from an outlet situated on the bed at a sudden expansion in the width of a channel. The classical wall jet, i.e., the two-dimensional turbulent wall jet, with infinite submergence has been chosen as a basic flow model. The velocity profiles have been analysed for similarity and when similarity exists the variations of the velocity and length scales of the similarity plot have been studied. The bed shear stress variation data have been obtained and correlated with the flow parameters. Some information on the boundary layer characteristics has also been obtained.

These studies are described in Chapters III through VI and the conclusions of the various studies have been given in the respective chapters. The significant conclusions are collected together in this section.

7.1.1 Water Wall Jet

In the study of the deeply submerged water wall jet it has

been found that in the zone of established flow the velocity profiles are similar and the similarity profile, the maximum velocity decay and the variation of the bed shear stress are the same as in a corresponding classical wall jet. The length scale, however, is found to grow about 40% faster than in the classical wall jet and the presence of a finite recirculation zone over the water wall jet is believed to be responsible for this deviation.

7.1.2 Reattached Wall Jet

The study of the submerged flow from an outlet situated over a drop revealed that after a certain distance downstream of the reattachment line, the velocity profiles in the reattached wall jet are similar and the similarity profile is the same as that of the classical wall jet. The decay curve of the maximum velocity in the reattached wall jet is composed of two distinct regions, viz., the characteristic decay region and the classical wall jet decay region.

The bed shear profiles could be reduced to one dimensionless similarity plot, in which the non-dimensional shear stress and length scales depend only on the relative height of the drop.

7.1.3 Wall Jet into Wider Channel

The centerline velocity profiles in the free mixing region of a wall jet, resulting from a finite-sized slot jet diffusing into a wider channel at a sudden expansion, are similar and the similarity profile is the same as that of the corresponding classical wall jet. The length scale of this similarity plot, of the free mixing region, varies linearly with the longitudinal distance from the outlet, and

depends upon the contraction ratio, b/B .

The characteristic length of the outlet, r' , which is its hydraulic radius neglecting the bottom (Sec. 5.2.5), is found to be very effective in correlating the maximum velocity decay and bed shear stress variation data for various outlet shapes.

The velocity distribution in the boundary layer region can be expressed as a power law, with the value of the exponent varying from $1/10$ to $1/12$ depending on the contraction ratio, b/B .

7.1.4 Hydraulic Jumps below Abrupt Symmetrical Expansions

The study of the repelled jump (R-jump) indicated that Kuznetsov's equation, cannot satisfactorily predict the sequent depth. An empirical equation for the sequent depth, based on the present study, (Eq. 6.6), is presented.

Regarding the stable jump (S-jump), the characteristic length of the outlet, r' , is found to be very effective in correlating most of the gross characteristics. A simple empirical formula for the sequent depth of S-jumps is developed, (Eq. 6.20).

The centerline velocity profiles, in S-jumps, are found to be similar, at least in the free-mixing region. The similarity plot and the variation of the length scales are essentially the same as in a classical jump. However, the decay of maximum velocity in a S-jump is slower than in a classical jump.

7.2 Recommendations for Further Study

The following topics are recommended for further study:

- 1) The backward flow region in a water wall jet.

- 2) The effect of the initial non-uniformity of the velocity profile--as, for example, the flow from a conduit outlet--on the diffusion characteristics of the water wall jet.
- 3) The initial region of a jet issuing from over a drop, i.e., the curved free jet.
- 4) Lateral distribution of forward velocities and bed shear stress in a diverging wall jet.
- 5) Limits of application of r' in the S-jump and lateral distribution of forward velocity.

LIST OF REFERENCES

1. Abramovich, G.N., "The Theory of Turbulent Jets," M.I.T. Press, Cambridge, Mass., 1963.(English Translation).
2. Albertson, M.L., Dai, Y.G., Jensen, R. A., and Rouse, H., "Diffusion of Submerged Jets," Trans., ASCE, Vol. 115, 1950.
3. Anwar, H.O., "Application of the Principle of Extremum to a Submerged Discharge," Nature, London, England, pp. 287-289, April 16, 1966.
4. Bakhmeteff, B.A., and Matzke, A.E., "The Hydraulic Jump in Terms of Dynamic Similarity," Trans. ASCE., Vol. 101, pp. 630-680, 1936.
5. Bourque, C., and Newman, B.G., "Reattachment of a Two-Dimensional Incompressible Jet to an Adjacent Flat Plate," Aero. Quarterly, Vol. XI, Aug. 1960.
6. Benjamin, T.B., "On the Flow in Channels when Rigid Obstacles Are Placed in the Stream," J. of Fluid Mech., Vol. 1, pp. 227-248, 1955.
7. Chow, V.T., "Open Channel Hydraulics," McGraw-Hill Book Co., Inc., N.Y., 1959.
8. Curtis, D.D., Martinez, J.E., and Vazquez, V., "Coefficient of Contraction for a Submerged Jet," Proc. ASCE., J. of Hyd. Div., Vol. 82, No. HY 4, Aug. 1956.

9. Escande, L., "Etude de quelques écoulements comportant la formation d'une veine de courant--Vannes de fond, barrages--devers--oires, piles de points," Publications Scientifiques et Techniques du Ministère de l'Air, Paris, No. 163, 1946.
10. Eskinazi, S., and Kruka, V., "Mixing of a Turbulent Wall Jet in to a Free Stream," Proc. ASCE., J. of Engg. Mech. Div., Proc. paper, 3106, April 1962.
11. Eskinazi, S., and Kruka, V., "The Wall Jet in a Moving Stream," J. of Fluid Mech., Vol. 20, 1964.
12. Forthmann, E., "Turbulent Jet Expansion," NACA., TM 789, March 1936. (English Translation).
13. Gartshore, I. S., "Jets and Wall Jets in Uniform Streaming Flow," McGill University Mech. Engg. Res. Lab. Report No. 64-4, 1964.
14. Glauert, M.B., "The Wall Jet," J. of Fluid Mech., Vol. 1, 1956.
15. Girerd, H., and Guienne, P., "Nouvelles Sondes de Pression Statique pour Mesures Aérodynamiques," Comptes Rendus, Institut de France, Paris, Vol. 228, 1949.
16. Gupta, N.K., Dis. on proc. paper 4482, J. of Hyd. Div., HY 3, May 1966.
17. Henderson, F.M., "Open Channel Flow," The Macmillan Co., N.Y., 1966.
18. Henry, H.R., "A Study of Flow from a Submerged Sluice Gate," M.Sc. Thesis, State Univ. of Iowa, Iowa, Feb. 1950.
19. Iwagaki, Y., and Tsuchiya, Y., "Boundary Layer Growth in Wall Jets Issuing from a Submerged Outlet," Proc. 9th Japan National Congress for App. Mech., pp. 256-264, 1959.

20. Jaeger, C., "Engineering Fluid Mechanics," Blakie and Son, Ltd., London, 1957.
21. Johnston, J.P., "On the Three-Dimensional Turbulent Boundary Layer Generated by Secondary Flow," J. of Basic Engg., Trans. ASME., March 1960, (a).
22. Johnston, J.P., "The Turbulent Boundary Layer at a Plane of Symmetry in a Three-Dimensional Flow," J. of Basic Engg., Trans. ASME., Sept. 1960, (b).
23. Kuznetsov, S.K., "Free Horizontal Spread of the Stream Flow in the Tailwater of Hydro Structures," pp. 346-349, in "Soviet Hydro Engineering"--Israel Program for Scientific Translations, Jerusalem, 1964. (English Translation).
24. Lau, L., "Flow Characteristics of Wall Jets on Smooth, Rough, and Porous Walls," M.A.Sc. Thesis, Dept. of Mech. Engg., Univ. of Toronto, Toronto, 1963.
25. Liu, H.K., "Diffusion of Flow from a Submerged Sluice Gate," M.Sc. Thesis, State Univ. of Iowa, Iowa, Feb. 1949.
26. Moore, W.L., "Energy Loss at the Base of a Free Overfall," Trans. ASCE., Vol. 108, pp. 1343-1392, 1943.
27. Myers, G.E., Schauer, J.J., and Eustis, R.H., "The Plane Turbulent Wall Jet--Part I: Jet Development and Friction Factor," Tech. Report 1, Dept. of Mech. Engg., Stanford Univ., Stanford, June 1961.
28. Newman, B.G., "The Deflection of Plane Jets by Adjacent Boundaries--Coanda Effect," Chap. "Boundary Layer and Flow Control," Vol. 1, Ed. by Lachman, G.V., Pergamon Press, N.Y., 1961.

29. Ortiz, N.V., "Hydraulics of B-Jumps at Abrupt Drops," M.Sc. Thesis, Dept. of Civil Engg., Univ. of Alberta, Edmonton, 1966.
30. Patel, V.C., "Calibration of the Preston Tube and Limitations on Its Use in Pressure Gradients," J. of Fluid Mech., Vol. 23, 1965.
31. Preston, J.H., "The Determination of Turbulent Skin Friction by Means of Pitot Tubes," J. of Roy. Aero. Soc., London, Vol. 58, 1954.
32. Rajaratnam, N., "Some Studies on Hydraulic Jump," Ph.D. Thesis submitted to the Indian Institute of Science, Bangalore, India, 1961.
33. Rajaratnam, N., "Submerged Hydraulic Jump," Proc. ASCE., J. of Hyd. Div., No. HY 4, July 1965, (a).
34. Rajaratnam, N., "The Hydraulic Jump as a Wall Jet," Proc. ASCE., J. of Hyd. Div., No. HY 5, Sept. 1965, (b).
35. Rajaratnam, N., "Flow below a Submerged Sluice Gate as a Wall Jet Problem," Proc. 2nd Australasian Conf. on Hyd. and Fl. Mech., Auckland, New Zealand, Dec. 1965, (c).
36. Rajaratnam, N., "Plane Turbulent Wall Jets on Rough Boundaries," Water Power, London, April, May, and June 1967.
37. Rosenhead, L., "Laminar Boundary Layers," Clarendon Press, Oxford, England, 1963.
38. Rouse, H., (Ed.), "Engineering Hydraulics," John Wiley and Sons, Inc., N.Y., 1950.
39. Rouse, H., Siao, T.T., and Nagaratnam, S., "Turbulence Characteristics of the Hydraulic Jump," Trans. ASCE., Vol. 124, pp. 926-966, 1959.

40. Sananes, F., and Fortey, J.W.,--Discussion on proc. paper No. 4482, J. of Hyd. Div., HY 3, pp. 117-119, May 1966.
41. Sawyer, R.A., "The Flow Due to a Two-Dimensional Jet Issuing Parallel to a Flat Plate," J. of Fluid Mech., Vol. 9, 1960.
42. Sawyer, R.A., "Two-Dimensional Reattaching Jet Flows Including the Effects of Curvature on Entrainment," J. of Fluid Mech., Vol. 17, 1963.
43. Schubauer, G.B., and Tchen, C.M., "Turbulent Flow," Princeton Univ. Press, Princeton, N.J., 1961.
44. Schlichting, H., "Boundary Layer Theory," McGraw-Hill Book Co., Inc., N.Y., 1960.
45. Schwarz, W.H., and Cosart, W.P., "The Two-Dimensional Turbulent Wall Jet," J. of Fluid Mech., Vol. 10, 1961.
46. Sforza, P.M., Steiger, M.H., and Trentacoste, N., "Studies on Three-Dimensional Viscous Jets," J. of AIAA, Vol. 4, Pt. 2, 1966.
47. Sharma, H.D., "The Spatial Jump and Its Problems," J. of Central Board of Irrigation and Power, New Delhi, India, pp. 431-440, Oct. 1966.
48. Sigalla, A., "Experimental Data on Turbulent Wall Jets," Aircraft Engg., Vol. 30, May 1958, (a).
49. Sigalla, A., "Measurement of Skin Friction in a Plane Turbulent Wall Jet," J. of Roy. Aero. Soc., London, Vol. 62, Dec. 1958, (b).
50. Sridhar, K., and Tu, P.K.C., "Effects of an Initial Gap on the Flow in a Turbulent Wall Jet," Tech. Note, J. of Roy. Aero. Soc., London, Vol. 70, June 1966.

51. Tani, I., Iuchi, M., and Komoda, H., "Experimental Investigation of Flow Separation Associated with a Step or a Groove," Aero. Res. Inst., Univ. of Tokyo, Japan, Report No. 364, April 1961.
52. Trentacoste, N., and Sforza, P.M., "An Experimental Investigation of Three-Dimensional Free Mixing in Incompressible Turbulent Free Jets," Polytechnic Institute of Brooklyn, Brooklyn, PIBAL Report No. 871, March 1966.
53. Unny, T.E., "The Spatial Hydraulic Jump," Proc. Xth IAHR Congress, Belgrade, pp. 32-42, 1961.
54. Viets, H., and Sforza, P.M., "An Experimental Investigation of a Turbulent, Incompressible, Three-Dimensional Wall Jet," Polytechnic Institute of Brooklyn, Brooklyn, PIBAL Report No. 968, April 1966.
55. Woycicki, K., "The Hydraulic Jump and Its Top Roll and the Discharge of Sluice Gates," U.S. Bureau of Reclamation, Tech. Memo. 435, 1934. (English Translation).
56. Yevdjevich, V.M., "Diffusion of Slot Jets with Finite Orifice Length-Width Ratios," Hydraulics Papers No. 2, Colorado State Univ., Fort Collins, March 1966.
57. Zijnen, B.G. Van der Hegge, "Measurement of the Velocity Distribution in Plane Turbulent Jet of Air," Appl. Sci. Res., Sec. A, Vol. 7, 1957.

APPENDIX A

FLOW IMMEDIATELY BELOW A SUBMERGED SLUICE GATE

APPENDIX A

FLOW IMMEDIATELY BELOW A SUBMERGED SLUICE GATE

A.1 Introduction

Flow below a vertical sluice gate in a rectangular channel of the same width could be divided into two groups as free flow and submerged flow. Fig. A-1(a) shows free flow, where "a" is the gate opening, H_1 is the depth of approaching flow and H_0 is the corresponding total energy. As the water flows out of the sharp-edged gate opening, the free surface contracts to a minimum section known as the vena contracta. If Y_{of} is the depth of flow at the vena contracta, it is normally written as $y_{of} = C_c a$, where C_c is known as the coefficient of contraction. It is generally believed that the vena contracta occurs at a distance roughly equal to "a" from the gate.

A number of analytical attempts have been made to study the form of the free surface and hence to predict C_c . As shown by Benjamin (1955), C_c is a function of only a/H_0 , if viscous effects are neglected. Further, the variation of C_c with a/H_0 is very small, and for practical purposes a value of 0.61 has been recommended by Henderson (1966). Experimental observations of Woycicki (1934) and Benjamin (1955) have shown that the measured values of C_c are in general much higher than the analytically determined values, and the boundary layer on the bed has been assumed to be responsible for this deviation (Benjamin, 1955).

Considering the case of deeply submerged flow, Fig. A-1(b), it is generally assumed that a coefficient of contraction occurs in the submerged flow also. Woycicki (1936), Liu (1949) and Henry (1950) have defined C_c for the submerged flow in different ways, for the purpose of writing a discharge equation. Anwar (1966), with the use of some rather doubtful assumptions, obtained analytically a value of $C_c = 0.61$ for the submerged case.

However, there appears to be no experimental investigation of C_c for submerged flow. Also, no information is available on the nature of velocity distribution and pressure distribution in the region of $x/a \leq 3.0$. Hence an experimental investigation was undertaken with the primary object of studying the submerged stream leaving the sluice gate and to define the so-called coefficient of concentration. The investigation, which included the study of the velocity distribution in the accelerating region, the diffusion region and the boundary layer on the bed, was confined to the immediate neighbourhood of the sluice gate, i.e., $x/a \leq 3.0$.

A.2 Experiments

Experiments were conducted in Flume A. A special traverse, which could position the instruments with an accuracy of 0.005 ft. in the horizontal direction, was used. Extensive measurements were made for 3 runs, III-A-2, B and C, and only exploratory measurements were made in Run III-A-1. The experimental details are given in Table A-1.

A.3 Pressure Distribution

From the static pressure measurements, it was found that in

TABLE A-1

FLOW IMMEDIATELY BELOW A SUBMERGED SLUICE GATE

Summary of Experimental Data

Run	a in.	B in.	Q cfs	H ₁ in.	H ₂ in.	ΔH in.	H ₁ /a	H ₂ /a	y _t in.
III-A-1	2.0	18.0	1.184	31.90	19.80	12.10	15.95	9.90	20.80
III-A-2	2.0	18.0	1.192	34.80	22.80	12.00	17.40	11.40	23.40
III-B	3.0	18.0	1.400	29.00	21.40	7.60	9.67	7.13	22.40
III-C	1.5	18.0	1.088	35.30	17.90	17.40	23.50	11.93	19.36

the submerged jet, in the vicinity of the gate, the pressure distribution is far from hydrostatic. At any point at a height y above the bed, if h is the piezometric head and if H is the depth of flow at that section, the variation of h/H with y/a for various values of x/a , for one typical run (III-A-2) is shown in Fig. A-2. It is seen that at $x/a = 0$, the deviation from the hydrostatic distribution is very large, as expected. The deviation becomes smaller as x/a is increased and becomes essentially zero for $x/a \approx 2.25$. Further, if p is the pressure at any point and p_0 = the corresponding hydrostatic pressure, and if $\Delta p = p - p_0$, the variation of the dimensionless excess pressure $\Delta p / (\rho U_0^2 / 2)$ with x/a and y/a is shown in Fig. A-3. In Fig. A-3, the excess pressure on the bed could be obtained by a small extrapolation. This was done for all four runs and the variation of the dimensionless excess pressure on the bed with x/a is shown in Fig. A-4. It decreases rapidly from 0.5 at $x/a = 0$ to about 0.02 at $x/a = 2.0$ and appears

to approach zero asymptotically with increase in x/a . The corresponding curve for free flow, as obtained from Rouse (1950), is seen to be considerably lower than the variation in the present case.

A.4 Coefficient of Contraction

Fig. A-5 shows the velocity distribution obtained in a typical run, III-B. It is seen that the emerging stream is being accelerated as x/a increases from zero and the maximum velocity becomes equal to $U_o = \sqrt{2g(H_1 - H_2)}$ at a particular section. With further increase in x/a , the region of constant maximum velocity U_o --i.e., the portion of y over which $u = U_o$ at any section--increases, reaches a maximum value, and then begins to decrease. This region of maximum velocity U_o , is called the potential core. Due to friction of the bed, there is a boundary layer on the bed. On the top of the potential core is a region of turbulent diffusion, in which the turbulent mean velocity decreases from core velocity to zero velocity. For reasons of continuity, a region of return flow is formed on the top of the forward flow zone. (The return flow was not measured).

Using y_f for the depth of forward flow at any section, the variation of y_f/a with x/a is shown in Fig. A-6. It is seen that y_f/a decreases from unity at $x/a = 0$ to a minimum value and then increases almost linearly as x/a increases further.

Regarding the coefficient of contraction for the submerged sluice gate flow, it is logical to define the contracted stream as that which carries a forward flow equivalent to the flow entering at the gate. That is, if at any section, q_f , the total forward flow per unit width,

is written as

$$q_f = \int_0^{y_f} u \, dy \quad . \quad . \quad . \quad . \quad . \quad . \quad (A-1)$$

and if y_o is the depth such that

$$\int_0^{y_o} u \, dy = q \quad . \quad . \quad . \quad . \quad . \quad . \quad (A-2)$$

in which q = the discharge intensity entering the flume, then y_o = the depth of the contracted stream.

Using the measured velocity profiles, y_o was calculated and the variation of y_o/a with x/a is shown in Fig. A-7. It is seen that a single curve could easily be drawn, for which y_o/a decreases from 0.687 at $x/a = 0.25$ to a minimum of about 0.61 at $x/a = 1.15$ and increases for larger values of x/a . At $x/a = 3.0$, y_o/a is about 0.648.

The section at which y_o/a is a minimum can be considered the vena contracta. It is interesting to note that C_c is about 0.61 for the entire practical range of the free flow.

In this connection, it should be mentioned that, in the case of a submerged circular orifice, Curtis et al. (1956), defined the contracted stream in a similar manner and obtained comparable results.

A.5 The Free Jet Boundary Problem

Before taking up a detailed discussion of the free mixing

region of the jet issuing from the sluice gate, a very brief summary of the free jet boundary problem is given to build up the method of analysis.

Fig. A-8 is a schematic representation of the free jet boundary problem in which a jet with a velocity of U_0 and large depth flows tangentially over the same fluid at rest. As a result of the intense mixing at the interface there is a retardation of the uniform stream and a consequent acceleration of the ambient fluid. If δ_3 is the depth in which the mean longitudinal velocity decreases from U_0 to zero, then δ_3 is taken as the depth of the mixing region.

The free jet boundary problem was first solved by Tollmien (Schlichting, 1955) and Tollmien's solution has been found to agree satisfactorily with the experimental data of Albertson et al. (Abramovich, 1963). Another solution of the free jet boundary problem using the concept of constant eddy viscosity was accomplished by Goertler (Schlichting, 1955).

A.5.1 Analysis of the Free Mixing Region

The free mixing region on the top of the contracted stream could be treated as the free jet boundary problem with an initial boundary layer, i.e., with a region of non-uniform velocity distribution. Since the jet is appreciably curved for smaller values of x/a , the present analysis is initially limited to values of $x/a \geq 1.15$, i.e., beyond the vena contracta.

With reference to Fig. A-9, the contracted stream at the vena contracta could be imagined as a jet with an initial boundary layer of thickness δ_3 on the top and the boundary layer on the bed does not enter

into this analysis up to the end of the potential core. Using the present velocity distribution data, an attempt was made to find as to whether the velocity distribution in the free mixing region is similar and if so whether it agrees with the theoretical solutions given respectively by Tollmien and Goertler. In Fig. A-10, the velocity distribution in the free mixing region is plotted for the different sections of all the three runs in a non-dimensional form as u/u_m against $\bar{\eta} = \left[\frac{y - \delta_p}{\delta_1} \right]$ in which u = velocity at a distance of y from the bed, u_m = maximum velocity in the potential core at that vertical section, δ_p = distance of the uppermost point of the maximum velocity from the bed, δ_1 = length scale, i.e., the distance between the depths at which $u/u_m = 1.0$ and 0.50 . It is seen that points for the sections located downstream of the vena contracta do indeed dictate a single curve which agrees well with Tollmien's solution and with Goertler's solution for $\bar{\eta}$ up to about unity. It is of course well known that Goertler's solution predicts somewhat higher velocities in the outer region.

A close examination of Fig. A-10 reveals that points for some sections located upstream of the vena contracta also lie along the mean curve. Only for sections with $x/a \leq 0.50$, the points lie away from the mean curve.

For the free mixing region, the length scale δ_1 could be more accurately determined experimentally than δ_3 , the depth of the mixing region. For Tollmien's solution

$$\delta_1/x = 0.120 \quad . \quad . \quad . \quad . \quad . \quad (A-3)$$

The present results for the three runs III-A-2, B and C are shown plotted in Fig. A-11 and A-12. From Fig. A-11, it is found that beyond the vena contracta δ_1 increases linearly with x . In Fig. A-12, for $x/a \geq 1.15$, δ_1/x is essentially a constant but the values are different for each run. Further, these values are much larger than that given by Eq. (A-3). It is believed that the non-uniformity of the velocity profile at the reference section, vena contracta, is responsible for the deviation. The Reynolds number written as $R_o = q/\nu$ appears to be a parameter, but the present data are not sufficient to establish this conclusively.

A.5.2 Other Length Characteristics

Regarding δ_p , one could write

$$\delta_p = \beta y_o - \Delta \delta_p \quad . \quad . \quad . \quad . \quad (A-4)$$

$$= \beta a C_c - \Delta \delta_p \quad . \quad . \quad . \quad . \quad (A-5)$$

where β is an empirical coefficient and $\Delta \delta_p$ is the change in δ_p . Because of the linear spreading characteristic of the mixing region,

$$\Delta \delta_p \propto x \quad . \quad . \quad . \quad . \quad (A-6)$$

$$\text{Hence } \delta_p/x = (a/x) \beta C_c - C_1 \quad . \quad . \quad . \quad . \quad (A-7)$$

When the experimental results are plotted with δ_p/x against a/x as shown in Fig. A-13, in the region for a/x less than 0.87 and greater than 0.24 (this lower limit being obtained from the known length of the potential core), three different lines could be drawn with the same

slope, as indicated by equation (A-7) and it is seen that β is essentially the same for the three runs with different values of C_1 . The values of C_1 for the runs III-A-2, B and C are 0.175, 0.20 and 0.13 respectively. It is seen that equation (A-7) applies even in the region with $a/x > 0.87$. Assuming an average value of 0.17 for C_1 as a first approximation, the equation (A-7) could be rewritten as

$$\delta_p/x = 0.66 (a/x) - 0.17 \quad . \quad . \quad . \quad (A-8)$$

Regarding the depth of forward flow y_f , it could be written as

$$y_f = y_{fo} + C_2 x \quad . \quad . \quad . \quad . \quad (A-9)$$

where y_{fo} is the depth of the forward flow at the vena contracta.

$$\text{Thus } y_f/x = y_{fo}/x + C_2 = \left(\frac{y_{fo}}{a}\right) \left(\frac{a}{x}\right) + C_2 \quad . \quad (A-10)$$

Assuming that y_{fo}/a is a constant at the vena contracta, equation (A-10) becomes

$$y_f/x = C_3 (a/x) + C_2 \quad . \quad . \quad . \quad . \quad (A-11)$$

When the experimental data are plotted with y_f/x versus a/x as shown in Fig. A-14, it is found that a single straight line could be drawn, in the limited region of $0.24 < a/x < 0.87$, which describes the data well, even beyond the upper limit. Equation (A-11) could be written for preliminary use as

$$y_f/x = 0.81 a/x + 0.23 \quad . \quad . \quad . \quad . \quad (A-12)$$

TABLE A-2
FLOW IMMEDIATELY BELOW A SUBMERGED SLUICE GATE--VELOCITY PROFILE CHARACTERISTICS

Run	x/a	δ_p , in feet	y_f , in feet	δ_3 , in feet	δ_1 , in feet	δ_p/a	y_f/a	δ_3/a	δ_1/a	δ_1/x	δ_3/x	u_m/u_o
III-A-1	0.25	0.110	0.160	0.050	0.029	0.660	0.960	0.300	0.174	0.696	1.200	0.895
	0.375	0.115	0.155	0.040	0.023	0.690	0.930	0.240	0.138	0.368	0.640	0.920
	0.625	0.100	0.160	0.060	0.029	0.600	0.960	0.360	0.174	0.279	0.590	0.985
III-A-2	0	0.130	0.167	0.037	0.0275	0.780	1.000	0.220	0.165	0	0	0.790
	0.25	0.113	0.155	0.042	0.0300	0.678	0.930	0.252	0.180	0.720	1.010	0.890
	0.50	0.110	0.150	0.040	0.0220	0.660	0.900	0.240	0.132	0.264	0.480	0.962
	0.75	0.100	0.165	0.065	0.0263	0.600	0.990	0.390	0.158	0.209	0.520	0.995
	1.00	0.085	0.175	0.090	0.039	0.510	1.050	0.540	0.234	0.234	0.540	1.000
	1.25	0.078	0.188	0.110	0.042	0.468	1.130	0.660	0.252	0.202	0.530	1.000
	1.50	0.070	0.195	0.125	0.052	0.420	1.170	0.750	0.311	0.208	0.500	1.00
	2.00	0.055	0.215	0.160	0.074	0.329	1.290	0.961	0.444	0.222	0.480	1.00
	2.25	0.050	0.225	0.175	0.077	0.300	1.350	1.050	0.462	0.205	0.467	1.00
III-B	0.167	0.180	0.235	0.055	0.038	0.720	0.940	0.220	0.152	0.912	0	0.905
	0.333	0.156	0.234	0.078	0.039	0.624	0.936	0.312	0.156	0.468	0.936	0.960
	0.583	0.139	0.246	0.107	0.055	0.556	0.984	0.428	0.220	0.378	0.735	0.950
	0.833	0.124	0.266	0.142	0.058	0.496	1.064	0.568	0.232	0.278	0.685	1.000
	1.250	0.115	0.290	0.175	0.076	0.460	1.160	0.700	0.304	0.243	0.560	1.000
	1.750	0.090	0.320	0.230	0.105	0.360	1.280	0.920	0.420	0.240	0.525	1.000
	2.500	0.060	0.346	0.286	0.152	0.240	1.384	1.144	0.608	0.243	0.458	1.000
	3.000	0.050	0.380	0.330	0.160	0.200	1.520	1.320	0.640	0.213	0.440	1.000
III-C	0.25	0.060	0.110	0.050	0.0445	0.480	0.880	0.400	0.356	1.43	1.600	0.900
	0.667	0.080	0.109	0.029	0.0140	0.640	0.872	0.232	0.112	0.168	0.348	0.972
	1.333	0.064	0.120	0.056	0.0230	0.512	0.960	0.448	0.184	0.148	0.336	1.000
	1.667	0.059	0.135	0.076	0.0310	0.472	1.080	0.608	0.248	0.149	0.367	1.000
	2.330	0.049	0.160	0.111	0.0450	0.392	1.280	0.888	0.360	0.154	0.382	1.000
	3.000	0.035	0.175	0.140	0.0675	0.280	1.400	1.120	0.540	0.180	0.373	1.000

The experimental data concerning all the important flow parameters are collected together in Table A-2.

A.6 Boundary Layer

From a study of the velocity distribution diagram (Fig. A-5) and Fig. A-4, it could be seen that the boundary layer is growing under an appreciable favourable pressure gradient for x/a up to about 2.0. If δ denotes the boundary layer thickness at any section, the variation of δ with x for sections downstream of vena contracta is given in Table A-3. If δ^* is the displacement thickness, the ratio δ^*/a is also given in Table A-3. If δ_o^* is the displacement thickness at the

TABLE A-3

FLOW IMMEDIATELY BELOW A SUBMERGED SLUICE GATE
BOUNDARY LAYER CHARACTERISTICS

Run	x/a	δ (ft)	δ^* (ft)	δ^*/a	δ/a
III-A-2	1.25	0.040	0.00123	0.00736	0.240
	1.50	0.028	0.0011	0.00660	0.167
	2.00	0.025	0.00125	0.00750	0.150
	2.25	0.020	0.00124	0.00742	0.120
III-B	1.25	0.055	0.00162	0.0065	0.220
	1.75	0.035	0.00130	0.0052	0.140
	2.50	0.032	0.00120	0.0048	0.128
	3.00	0.032	0.00126	0.0050	0.128
III-C	1.333	0.030	0.00115	0.0092	0.240
	1.670	0.023	0.00115	0.0092	0.184
	2.330	0.025	0.00105	0.0084	0.200
	3.000	0.035	0.00200	0.0160	0.280

vena contracta, then the ratio δ^*/a is about 0.0075 for all the three runs. This is very small compared with $y^0/a = 0.61$. Thus the effect of the bottom boundary layer on the value of the coefficient of contraction appears to be negligible.

The velocity distribution data in the boundary layer are plotted in Fig. A-15. It seems fuller than that given by one-seventh power law. The data indicate that, in any preliminary work, the velocity distribution could be assumed to follow the power law with the power $n \approx 12.0$

A.7 Conclusions

The following conclusions are drawn based on the experimental study of the flow immediately below a deeply submerged sluice gate;

- 1) If the contracted stream is defined as a stream carrying a discharge intensity equal to the entrant discharge, then it is possible to define a vena contracta similar to the free flow case. This vena contracta occurs at $1.15 a$ from the gate with a depth equal to $0.61 a$.
- 2) The region of free mixing can be analysed as a free jet boundary problem. The velocity distribution in the diffusion region at $x/a \approx 0.50$ has been found to be similar and agrees well with Tollmien's solution. The length scales grow linearly with the longitudinal distance but with rates differing from those of the free jet boundary with a uniform velocity distribution.
- 3) The boundary layer on the bed grows initially, under favourable pressure gradient and the displacement thickness at the vena contracta is very small compared to the depth of the contracted stream at that section.

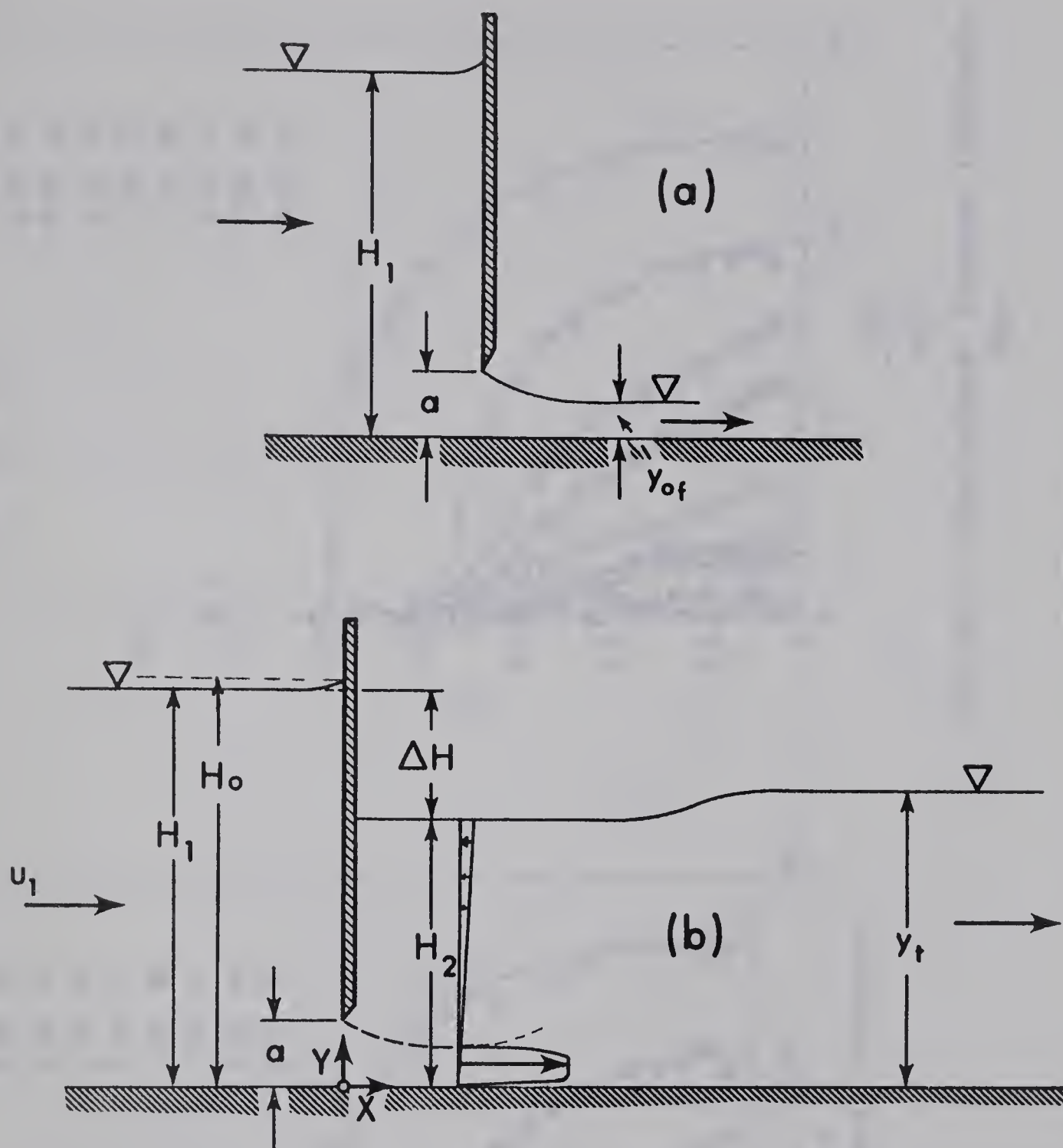


FIG. A-1. —(a) Free Flow and (b) Submerged Flow below a Sluice Gate.

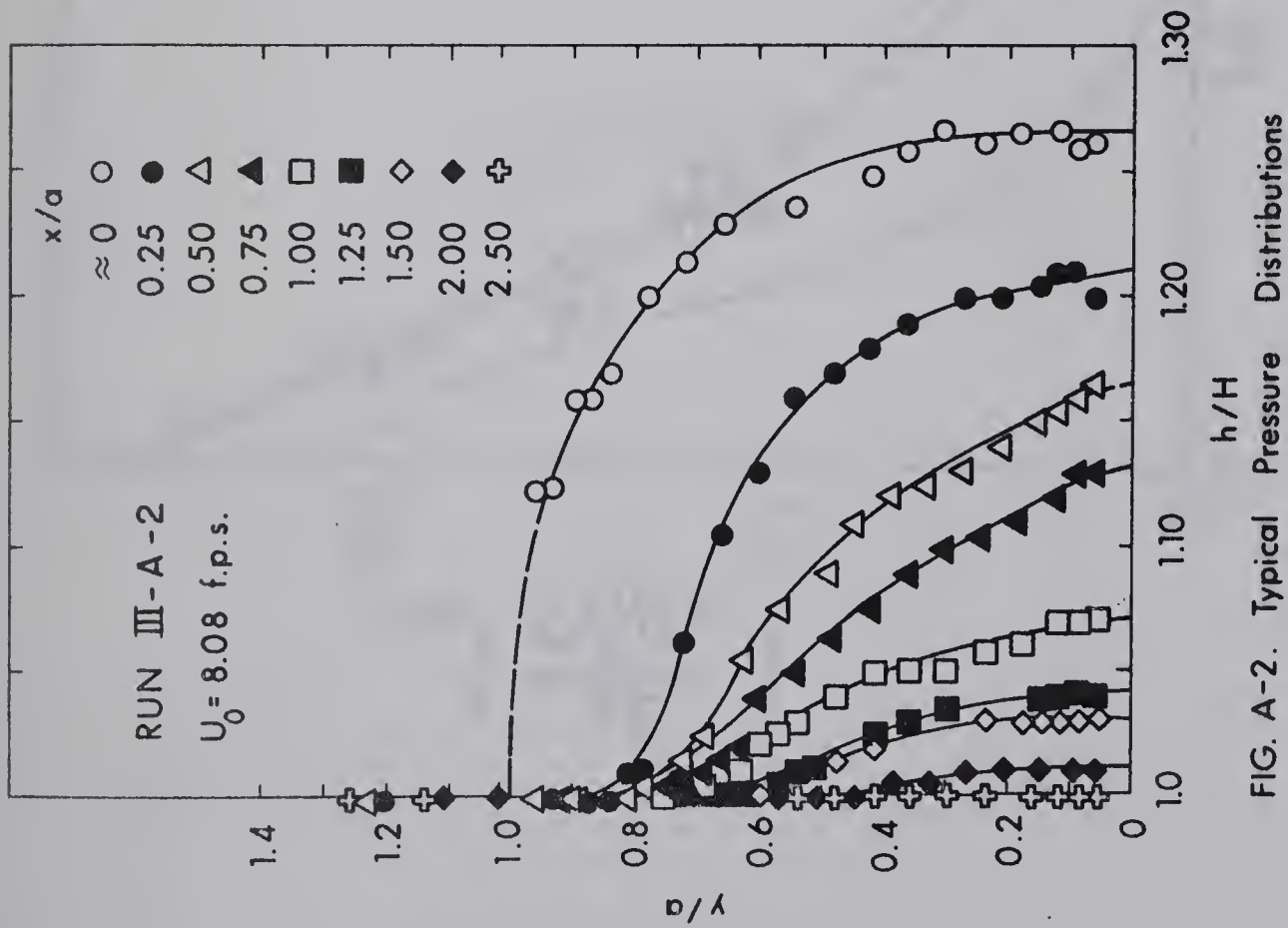


FIG. A-2. Typical Pressure Distributions

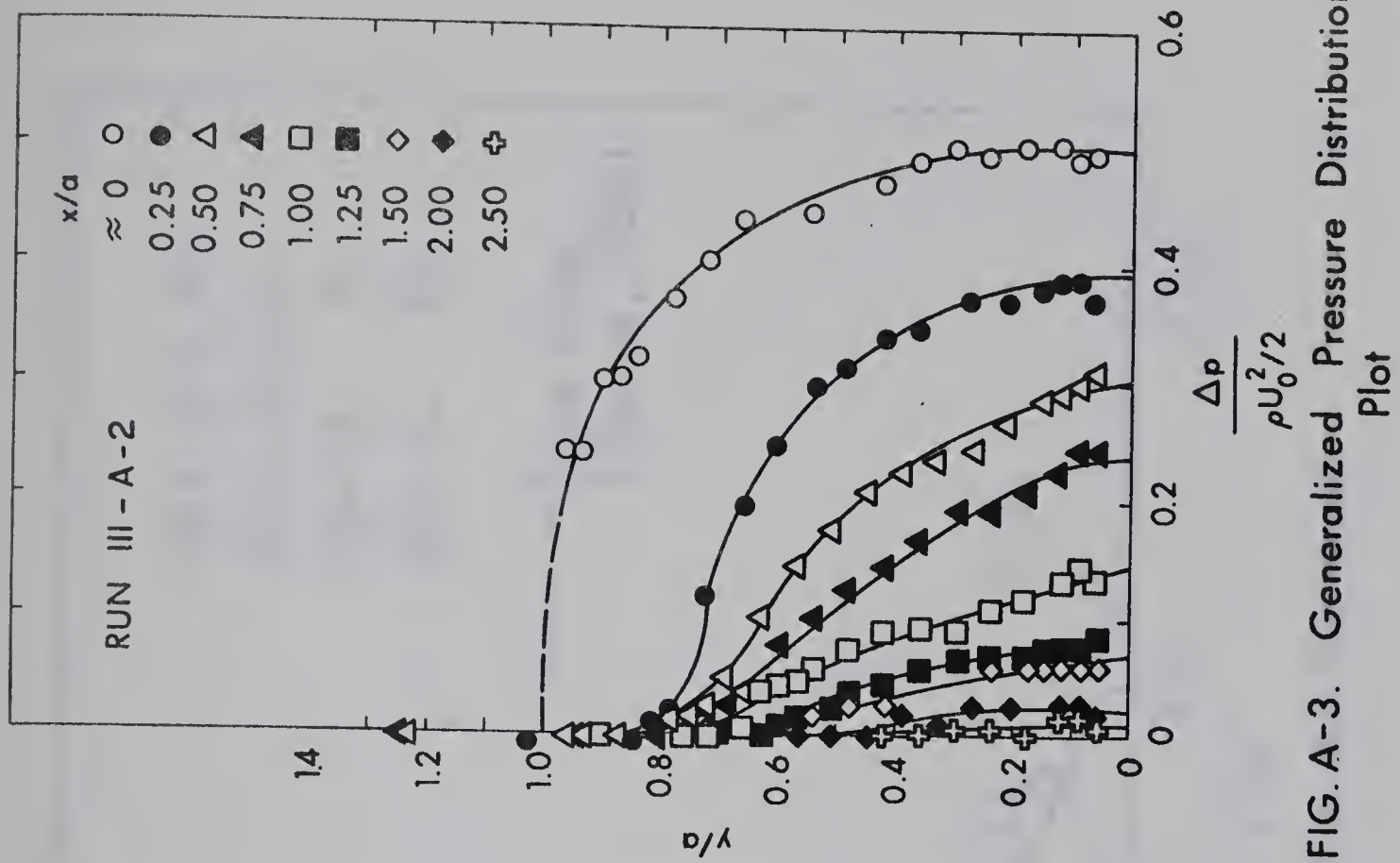


FIG. A-3. Generalized Pressure Distribution Plot

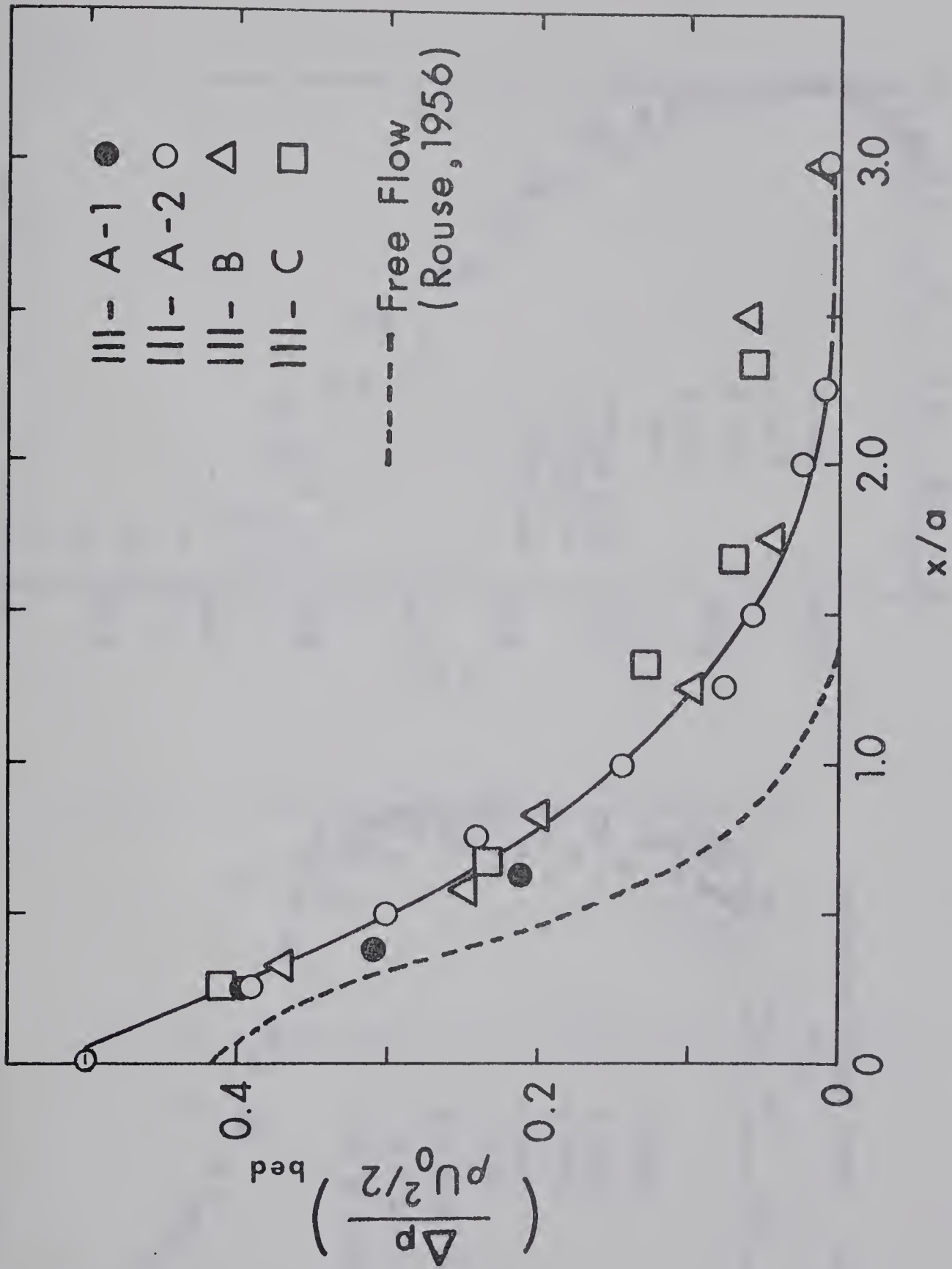


Fig. A-4. Excess Pressure on the Bed

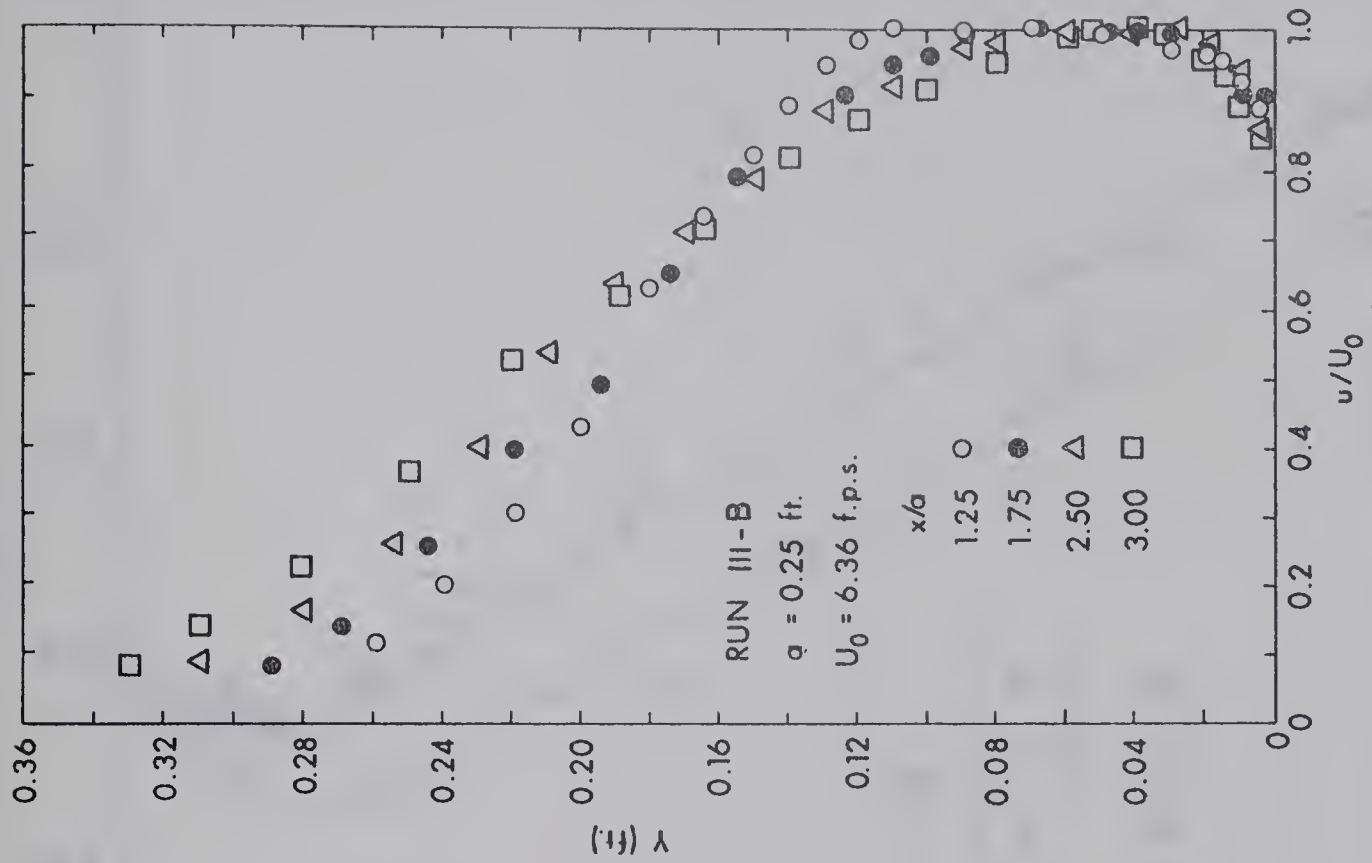


FIG. A-5 Continued

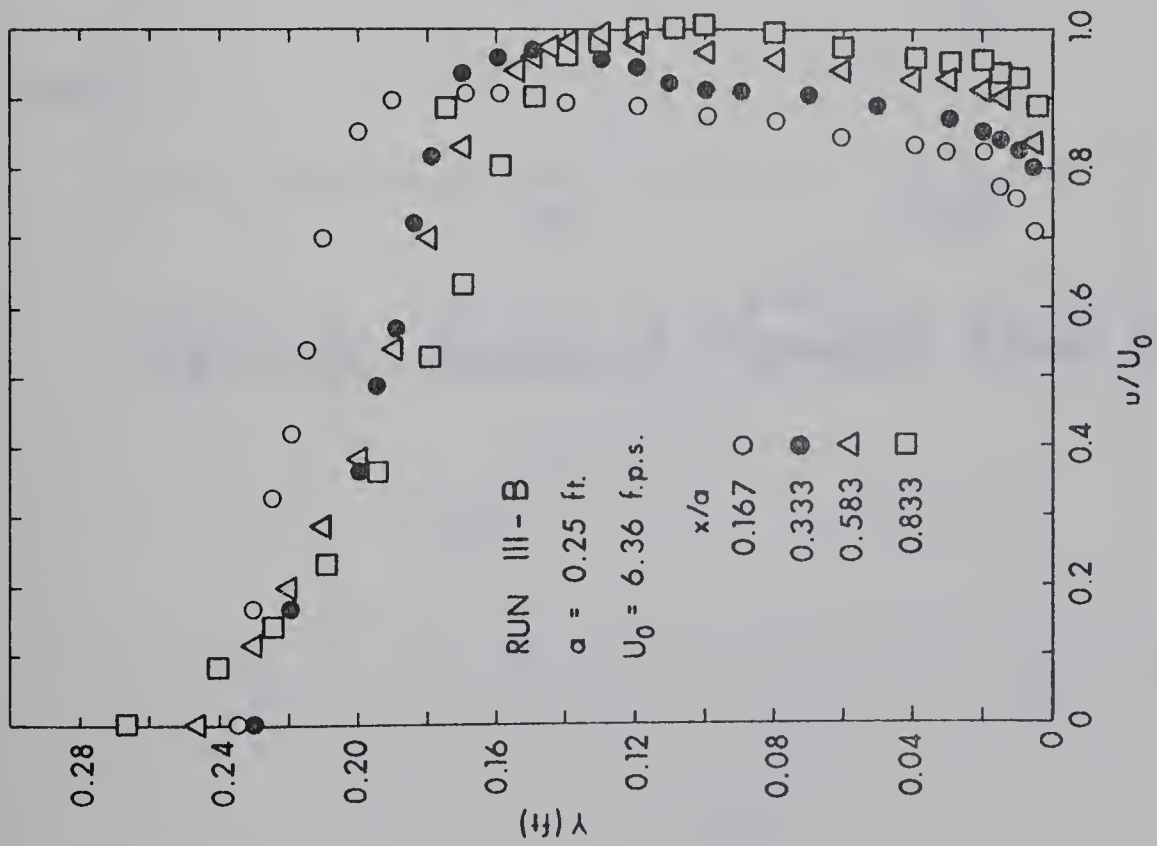


Fig. A-5 Typical Velocity Distributions

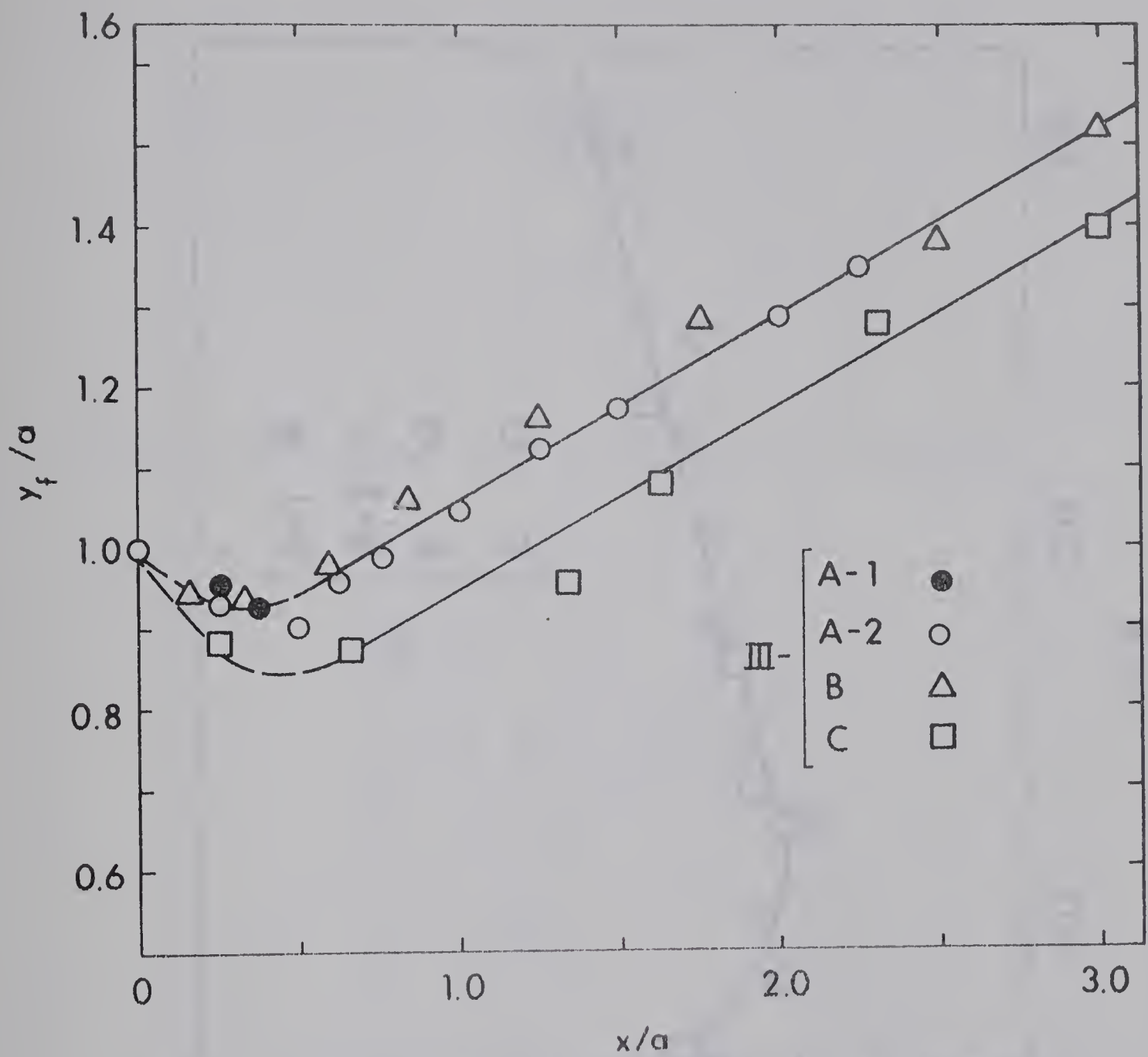


FIG. A-6. Study of Forward Flow Depth



FIG. A - 7. - VENA CONTRACTA FOR SUBMERGED FLOW

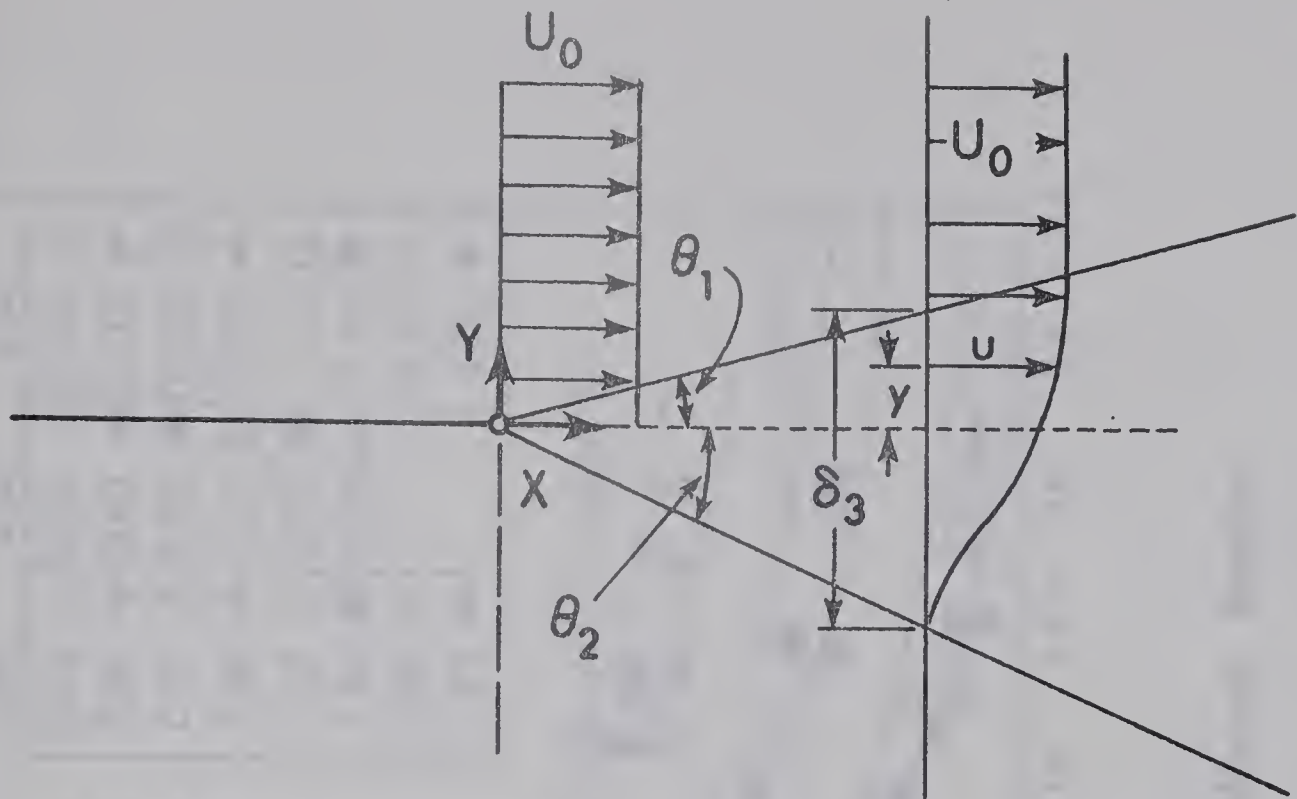


FIG. A-8. Free Jet Boundary Problem

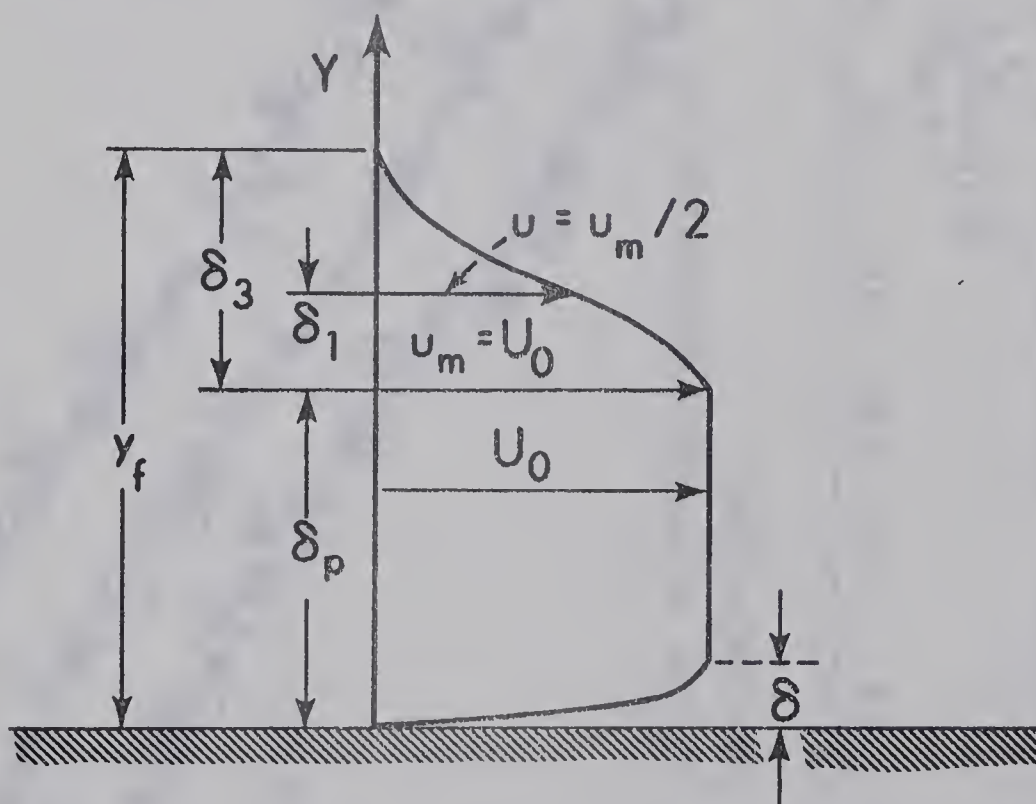


FIG. A-9. DEFINITION SKETCH

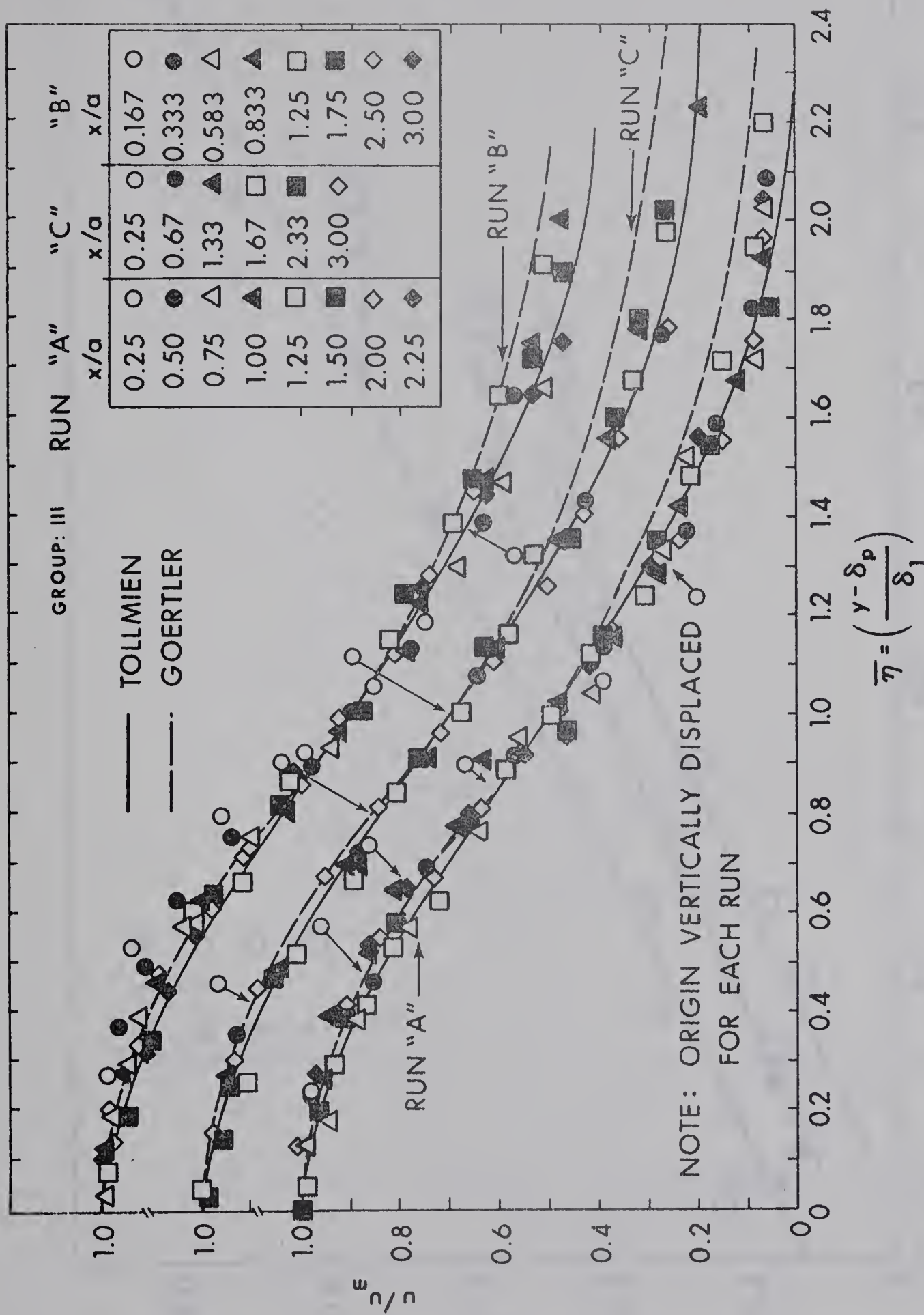


FIG. A-10. Velocity Distribution in the Free Mixing Region

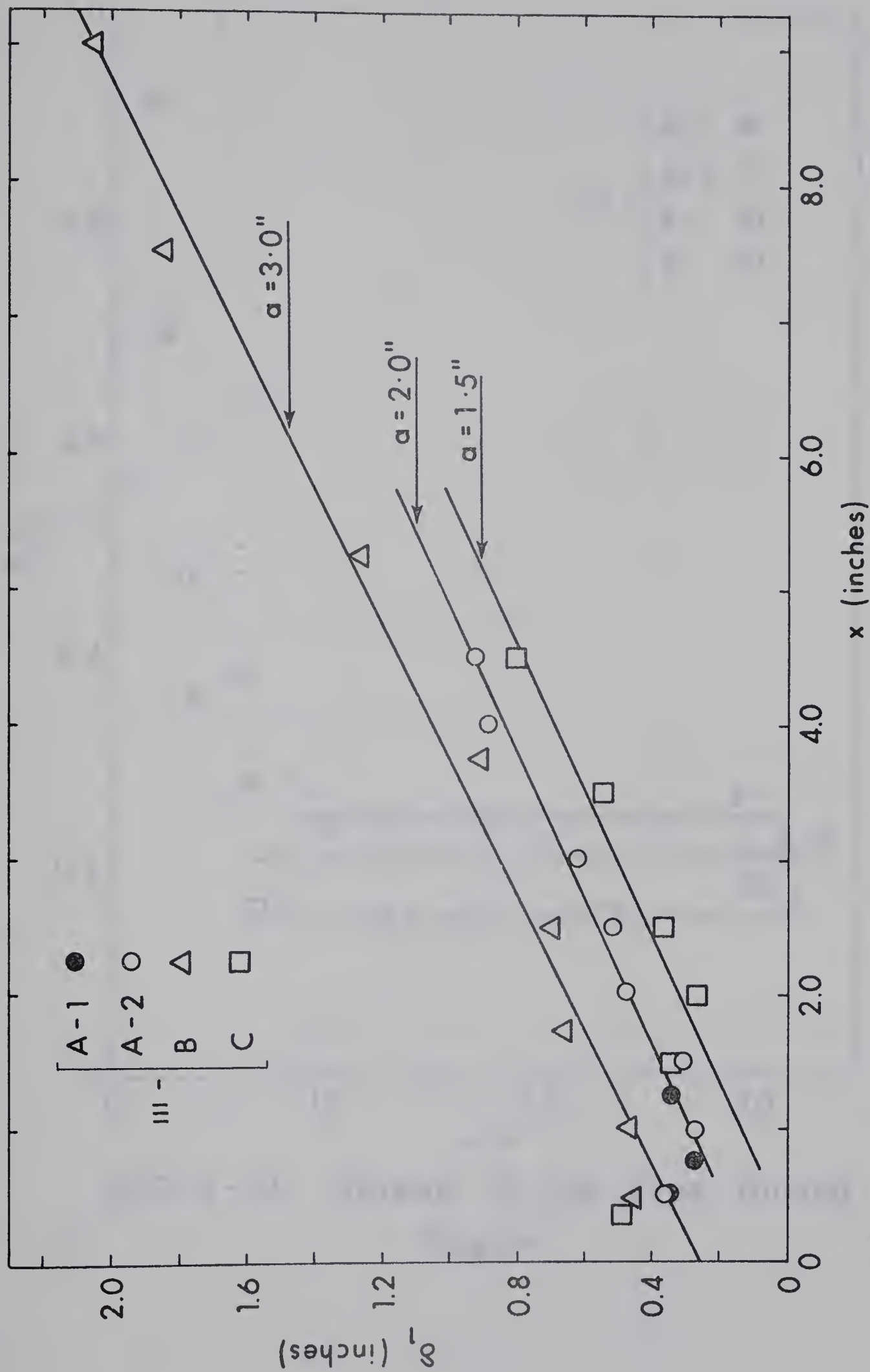


FIG. A-11. Study of the Length Scale

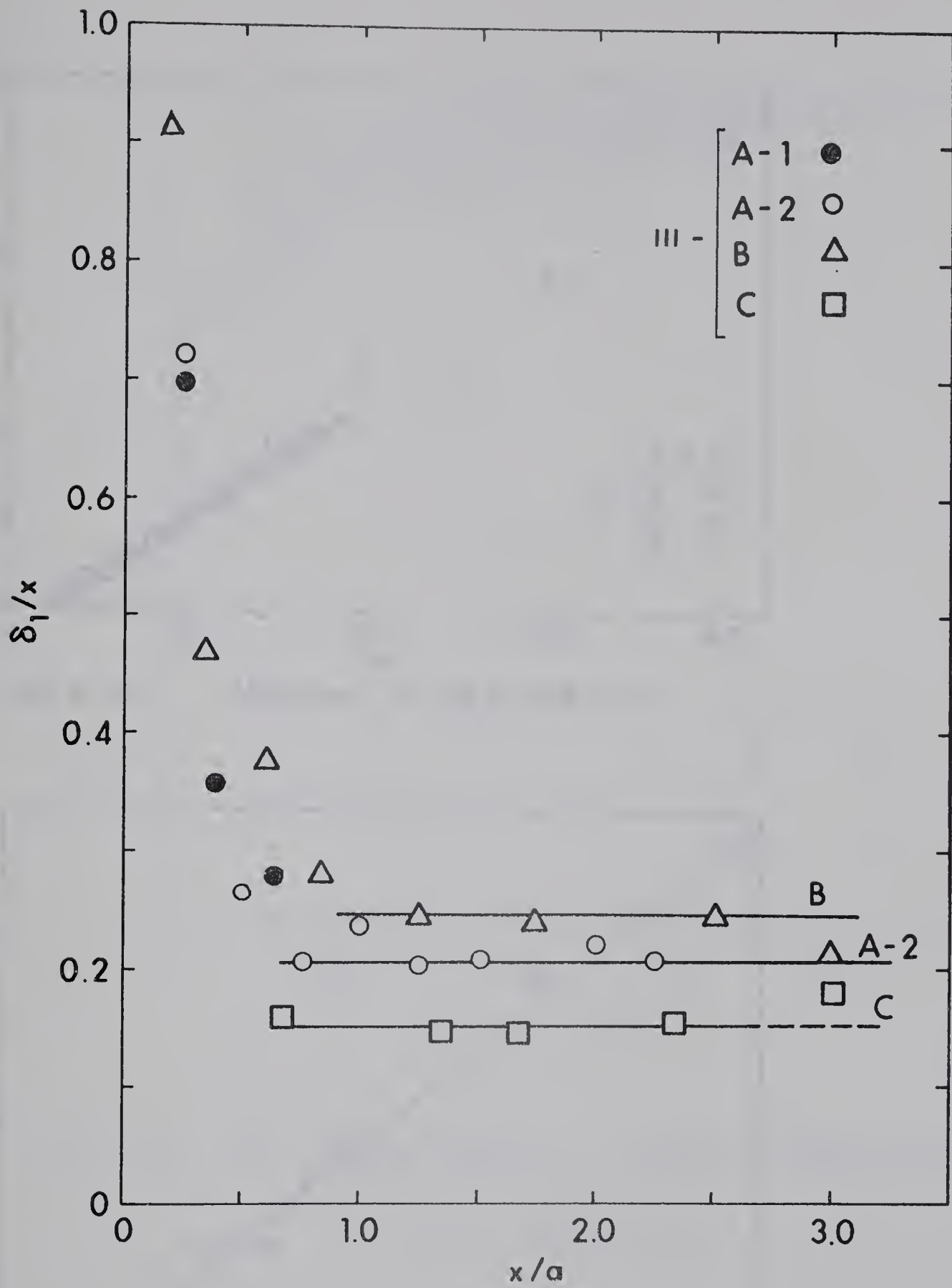


FIG. A-12. Spread of the Free Mixing Region

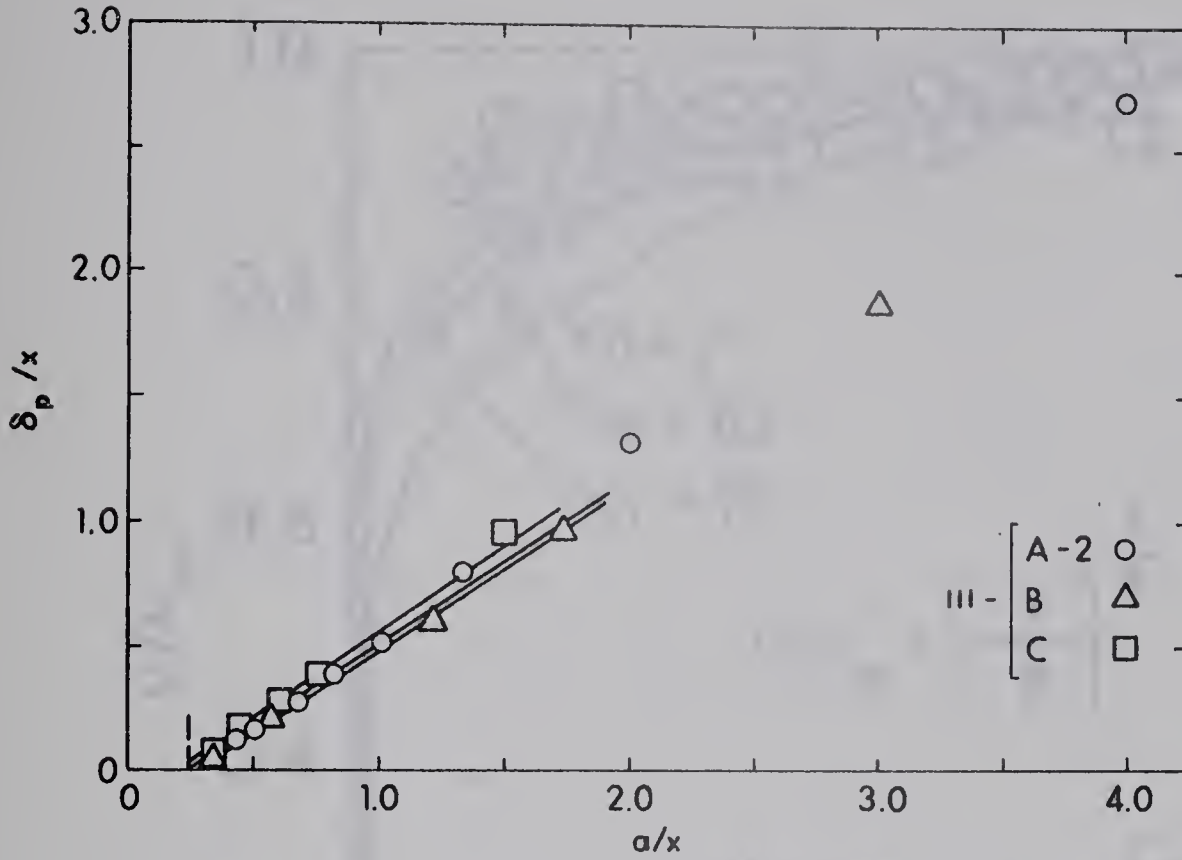


FIG. A-13. Variation of δ_p/x with a/x

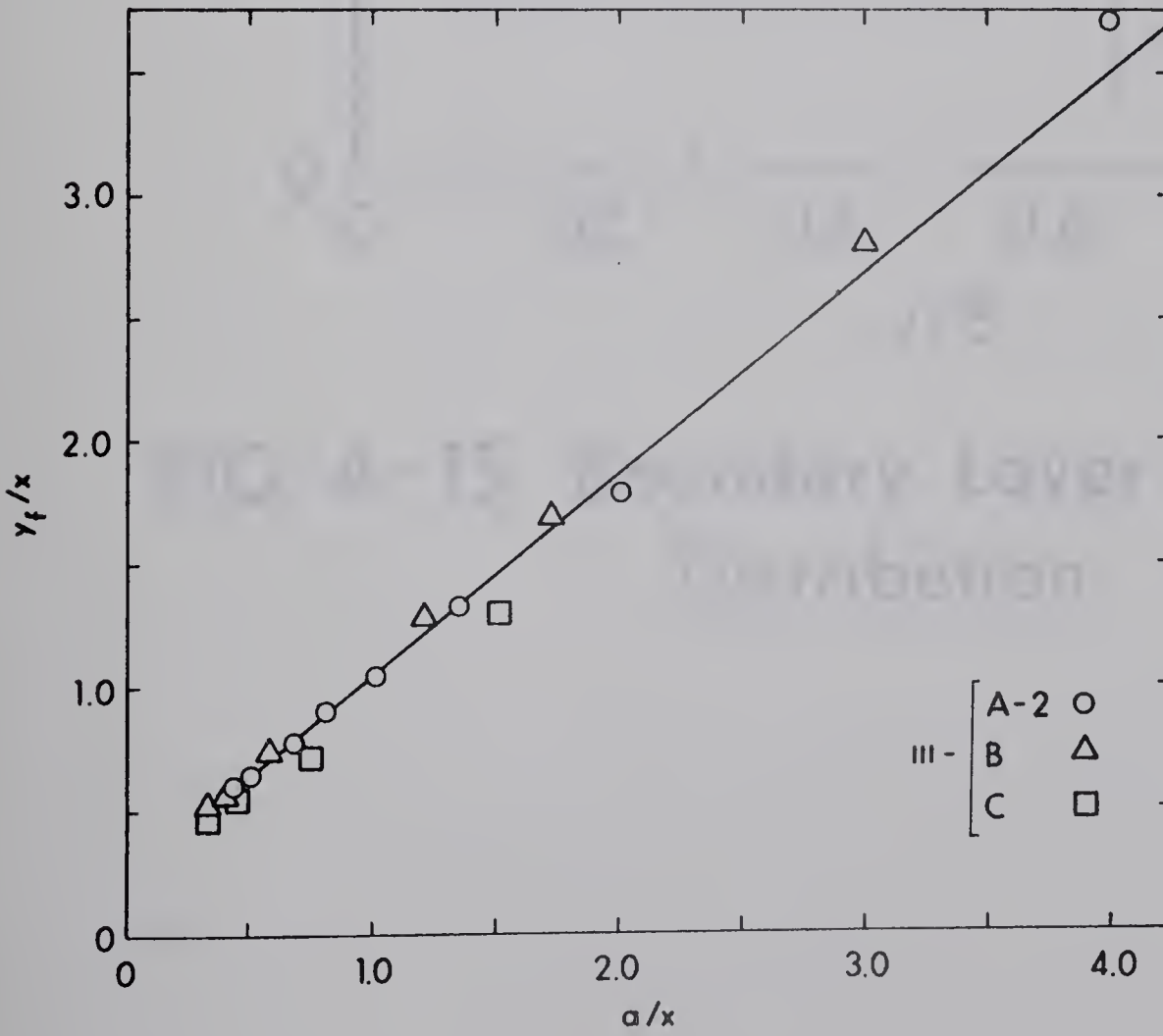


FIG. A-14. Variation y_f/x with a/x

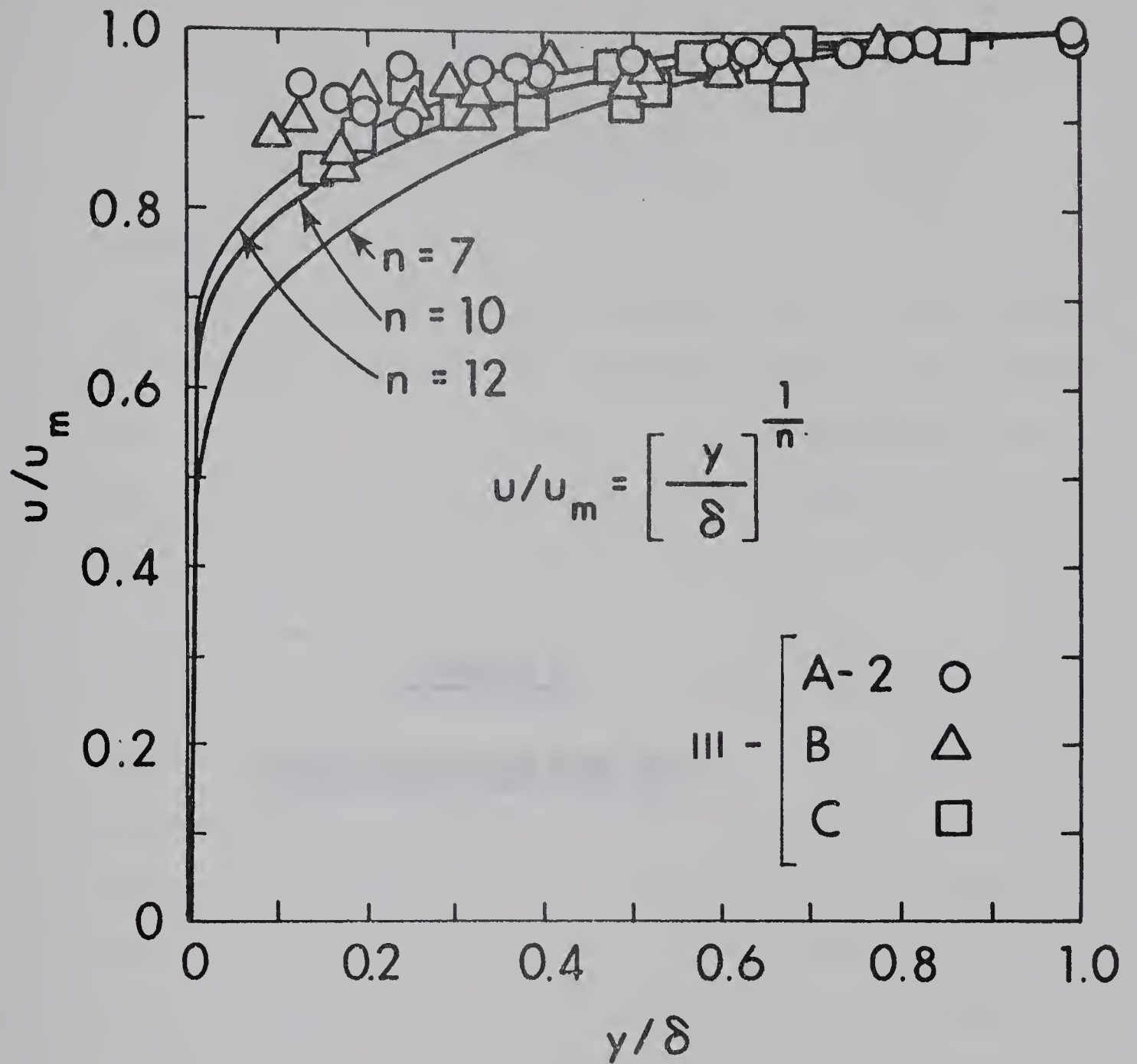


FIG. A-15. Boundary Layer Velocity Distribution

APPENDIX B

THREE-DIMENSIONAL FREE JETS

APPENDIX B

THREE-DIMENSIONAL FREE JETS

B.1 Introduction

Fairly elegant semi-empirical theories are available for predicting the turbulent diffusion of axisymmetric and plane jets (Schlichting, 1960; Abramovich, 1963). However, there are relatively few investigations on the non-axisymmetric free jets, herein denoted as three-dimensional jets. The extensive investigation conducted at the Polytechnic Institute of Brooklyn (Trentacoste and Sforza, 1966, and Sforza et al., 1966) on three-dimensional jets have shown that the flow field is characterised by three distinct regions; the potential core, the characteristic decay (C.D) region and the axisymmetric decay (A.D) region. In the C.D region the velocity profiles in the direction of the minor axis are similar but the maximum velocity decay curves are different for different shapes. In the A.D region the flow characteristics are similar to that of an axisymmetric free jet. Yevdjovich (1966) has recently conducted an investigation on rectangular jets.

The conventional way of representing the maximum velocity decay gives different lines for different shapes of the orifices. Thus, it is difficult to predict the bulk characteristics of jets of different shapes. A convenient method of predicting the velocity and length scales of three-dimensional jets of different shapes, but of small aspect ratio, is presented here.

B.2 Velocity Scale

Fig. B-1 shows the velocity decay of three-dimensional jets, plotted in the conventional way. The ordinate is u_m/U_o , where U_o = uniform initial velocity and u_m = maximum velocity of the jet. The abscissa is x/d , where x = longitudinal distance from the face of the orifice and d = characteristic linear dimension of the initial section of the jet. Usually d is taken as the height of the orifice; thus d is taken as the diameter for circular jets, the length of the minor axis for rectangular and elliptical jets and the height for equilateral triangular jets. In Fig. B-1, Curve 1 is the mean line for the circular jets (Trentacoste and Sforza, 1966) given by the equation

$$u_m/U_o = 7.0/(x/d) \quad . \quad . \quad . \quad . \quad (B-1(a))$$

and Curve 2 is that for the plane jet (Albertson et al., 1950) given by

$$u_m/U_o = 2.28/\sqrt{x/d} \quad . \quad . \quad . \quad . \quad (B-1(b))$$

The characteristic length of the outlet, which was useful in correlating the data on wall jets in wider channels, (Chapter V), is tested for its applicability to three-dimensional jets. For the present case, the characteristic length is designated as " r " and is defined as $r = \frac{\text{area}}{\text{perimeter}}$ of the jet at $x = 0$. Thus, for example, for a rectangular free jet

$$r = \frac{bd}{2(b + d)} \quad . \quad . \quad . \quad . \quad (B-2)$$

Using the length r , instead of d , the data of Fig. B-1 are replotted as u_m/U_o against x/r , in Fig. B-2. It is seen that

the data for square, triangular and rectangular orifices of aspect ratio less than 5.0 , fall on the curve for circular jets. The data for rectangular jets with larger aspect ratios deviate progressively outwards towards the curve of the plane jet. Thus the characteristic length of the outlet, r , appears to be an adequate characteristic length to represent jets of various geometric shapes, with aspect ratio less than about 5.0 , and for such jets, the curve 1 of Fig. B-2, can be used to predict the velocity decay.

B.3 Length Scale

Regarding the length scale Abramovich (1963) has indicated that the circular jet and plane jet data are well described by one common equation

$$\delta_1/d = 0.097 \, x/d \quad . \quad . \quad . \quad . \quad (B-3)$$

where δ_1 = normal distance from the plane of maximum velocity to that at which the velocity is half the maximum. Hence, it is to be expected that the length scale data for all three-dimensional jets will fall on a single line. Fig. B-3 is a plot of the available data (as taken from the mean line of respective investigation), and it is seen that they indeed agree with Eq. B-3.

B.4 Conclusion

From this study of the available data on three-dimensional free jets, it is concluded that the characteristic length of the outlet, r , is a useful parameter in correlating velocity decay characteristics of free jets of various shapes but of small aspect ratio.

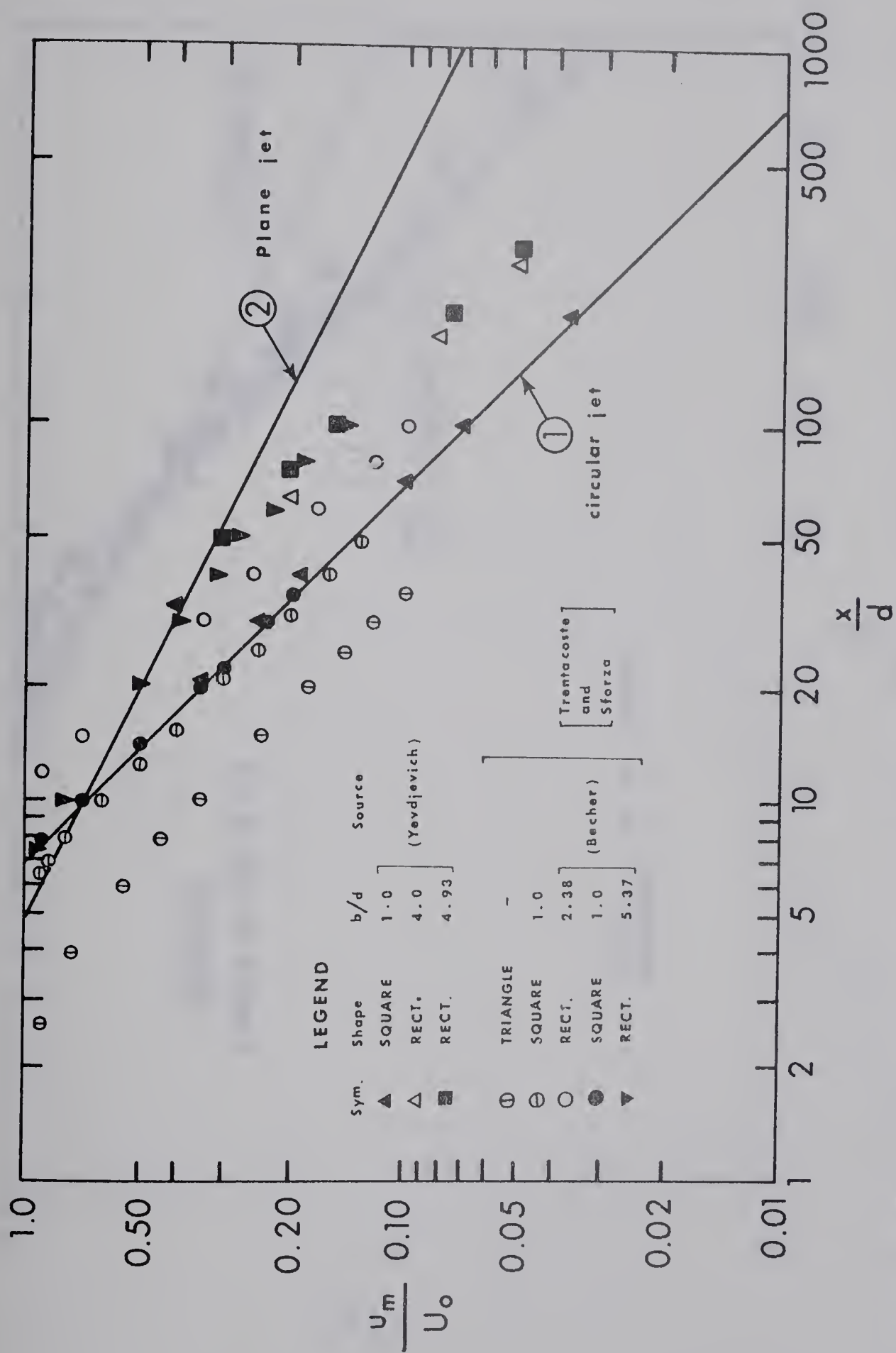
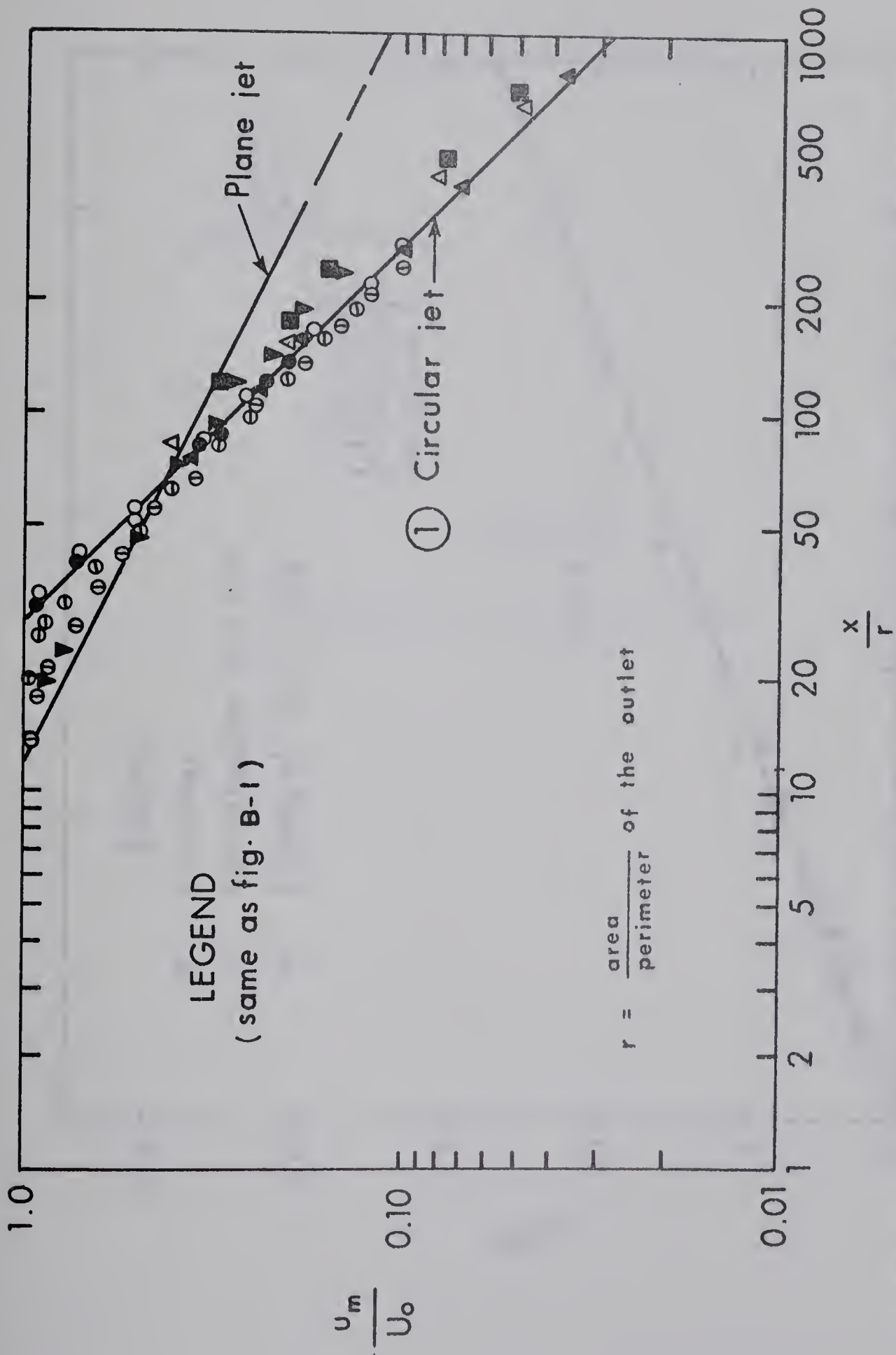
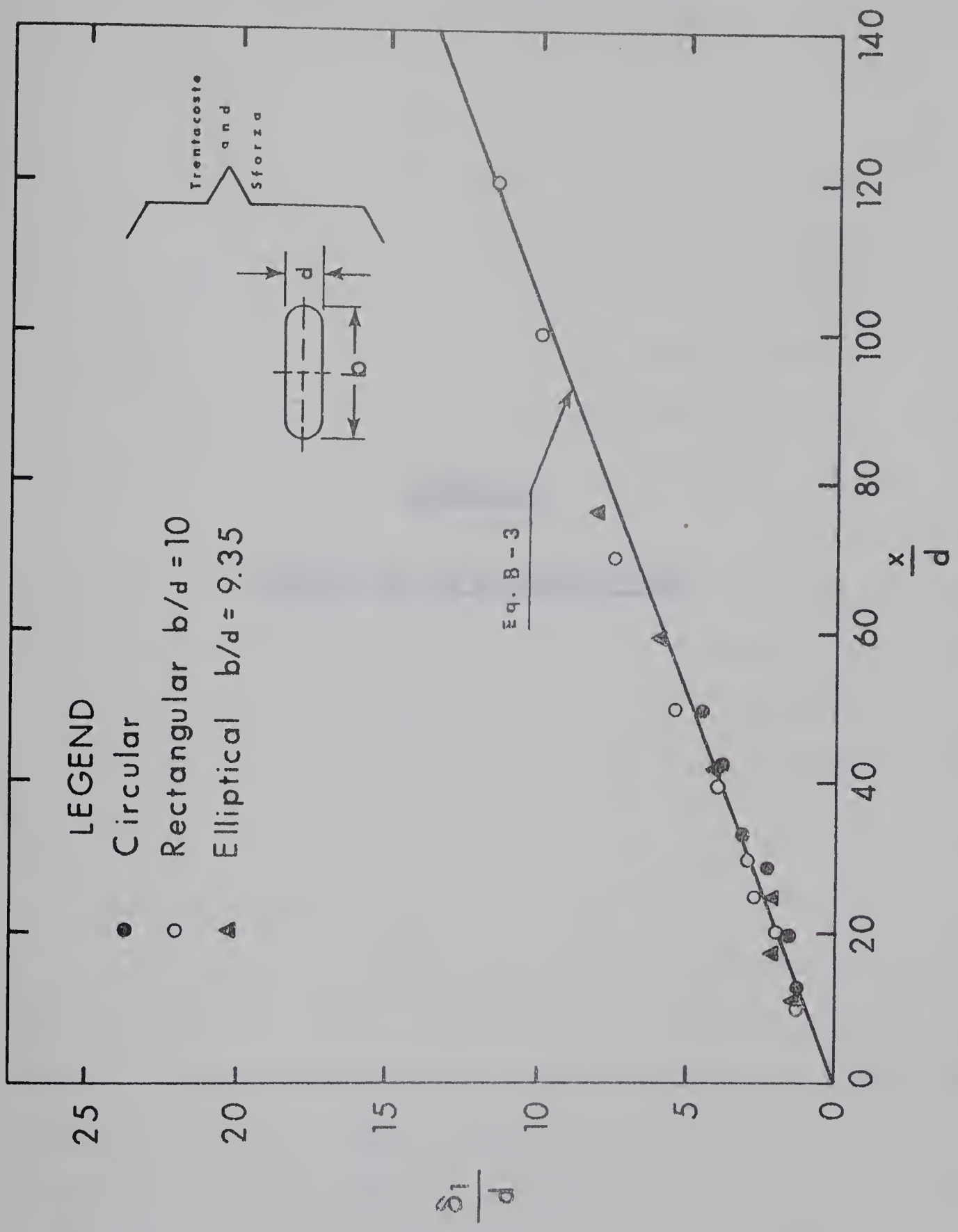


FIG. B-1. VELOCITY DECAY FOR TURBULENT JETS—
CONVENTIONAL PLOT



FIG·B-2· VELOCITY DECAY OF TURBULENT JETS —ALTERNATE PLOT



FIG·B-3· LENGTH SCALE OF TURBULENT JETS

APPENDIX C

PROFILE OF THE HYDRAULIC JUMP

APPENDIX C

PROFILE OF THE HYDRAULIC JUMP

C-1 Introduction

Consider a hydraulic jump in a rectangular channel as in Fig. C-1. If y_1 and U_1 are respectively the depth and mean velocity before the jump, and the supercritical Froude number $F_1 = \frac{U_1}{\sqrt{gy_1}}$, the sequent depth y_2 is given in terms of y_1 and F_1 , fairly satisfactorily, by the well known Belanger equation. Also, the geometrical configuration of the jump is specified by y_1 and F_1 .

A knowledge of the surface profile of the jump is useful in the economic design of stilling basin side walls, and information on the bed pressure profile would be useful in the design of stilling basin floors laid on permeable foundations. A study of the similarity of the jump profiles, using the available data, is presented in the following sections.

C.2 Review of Previous Works

Bakhmeteff and Matzke (1936) plotted their data on water surface profiles of jumps in a dimensionless form with $\frac{y}{y_2 - y_1}$ against $\frac{x}{y_2 - y_1}$, where x and y are the coordinates of the profile as shown in Fig. C-1. This procedure gave a different profile for each F_1 and their results are reproduced in Fig. C-2. Moore (1943) has also plotted the water surface data of his study on jumps below drops in the dimensionless form adopted by Bakhmeteff and Matzke (1936).

Rajaratnam (1961), by using his data on bed pressure profiles in jumps with F_1 from 3.50 to 11.30, developed the equation for the bed pressure profile for $F_1 \geq 5.0$

$$\text{as } y/y_2 = A_1 (x/y_2) + A_2 (x/y_2)^2 \quad . \quad . \quad (C-1)$$

where A_1 and A_2 are coefficients which depend upon F_1 . Recently, another method has been suggested by Rajaratnam (1965-b).

Gupta (1966) has written the following equation for the profile of the jump

$$\left[1 - \frac{y}{(y_2 - y_1)} \right] = \left[\frac{1}{L_j/(y_2 - y_1)} \right] \left[\frac{L_j}{(y_2 - y_1)} - \frac{x}{(y_2 - y_1)} \right]^2 \quad . \quad . \quad (C-2)$$

where L_j is the length of the jump, for which a logarithmic form of equation is written.

C.3 Present Study

It is known that even though the pressure distribution is not hydrostatic in the complete body of the jump, the pressure head profile on the bed is essentially the same as the mean water surface profile, except in a small portion near the toe where the pressure profile is somewhat higher (Rajaratnam, 1965-b). In the present study the water surface profile is considered the same as the bed pressure head profile in all portions of the jump. The profile of the jump is analysed for similarity in a manner analogous to the study of the velocity and bed shear profiles studied in Chapter IV.

In the non-dimensionalised similarity plot of the profile,

the vertical scale is referred to as Y and the corresponding horizontal scale as X . In the selection of these, normally the first choice would be $Y = y_2 - y_1$ and $X = L_j$. But, in this choice the flat nature of the surface profile towards the end of the jump causes large personal errors in the determination of $X = L_j$ and hence errors in the similarity profile. Writing $Y = \alpha (y_2 - y_1)$, if α is small, the reference section is located rather too close to the fluctuating toe of the jump. With this in view and after a study of a number of choices, it was decided to take $Y = 0.75 (y_2 - y_1)$ and $X =$ the value of x at which $y = 0.75 (y_2 - y_1)$.

Rajaratnam's 1965 data are plotted in Fig. C-3 as $\zeta = y/Y$ versus $\lambda = x/X$. It is seen that for runs with $F_1 \geq 4.0$, a single curve is indeed justified. A mean curve through data with $F \geq 4.0$ is drawn and is considered as the similarity curve of the jump profile. Table C-1 gives the co-ordinates of this curve. For the similarity curve the Y scale is known when y_1 and F_1 are specified. Regarding the

TABLE C-1

COORDINATES OF THE SIMILARITY PROFILE OF THE HYDRAULIC JUMP

λ	ζ	λ	ζ	λ	ζ	λ	ζ
0	0	0.60	0.655	1.40	1.180	2.60	1.333
0.05	0.185	0.70	0.736	1.50	1.215	2.80	1.333
0.10	0.245	0.80	0.820	1.60	1.240	3.00	1.333
0.15	0.280	0.90	0.920	1.80	1.285		
0.20	0.320	1.00	1.000	2.00	1.315		
0.30	0.405	1.10	1.060	2.20	1.320		
0.40	0.485	1.20	1.105	2.40	1.325		
0.50	0.570	1.30	1.140	2.50	1.333		
							$\lambda = x/X$ $\zeta = y/Y$

X scale, the variation of X/y_1 with F_1 is studied in Fig. C-4. It is seen that data are well correlated by a straight line,

$$X/y_1 = 5.08 F_1 - 7.82 \quad . \quad . \quad . \quad . \quad (C-3)$$

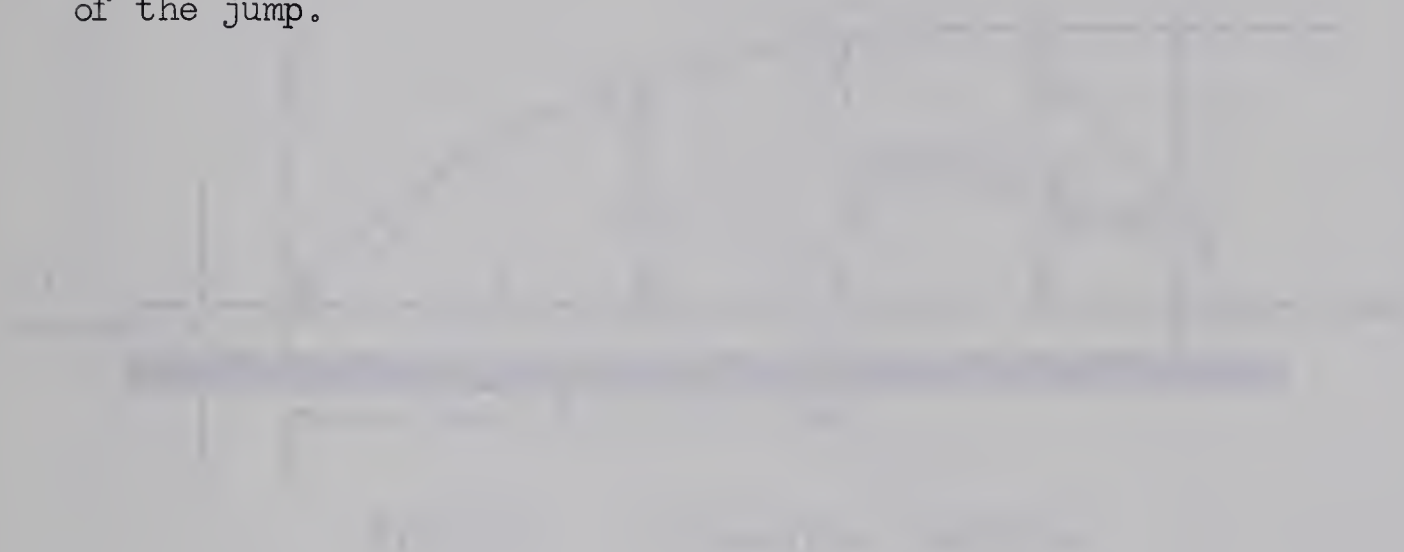
The similarity profile and the variation of the horizontal scales developed above were tested with the other available data. In Fig. C-5, Rajaratnam's 1961 data are plotted as ζ versus λ . In Fig. C-6, the data of Bakhmeteff and Matzke (1936), Moore (1943), Rouse et al. (1959), Henry (1950), and Sananes and Fortey (1966) are all plotted in terms of dimensionless similarity coordinates. It is seen that in these two figures the agreement of the plotted points with the similarity curve of Fig. C-3 is very good. The horizontal scale corresponding to data plotted in Figs. C-5 and C-6 are plotted in Fig. C-4. It can be seen that the data are represented well by Eq. (C-3).

C.4 Profiles of Another Type of Jump

To test whether the similarity profile developed above is applicable to other types of jumps, the data of Ortiz (1966), on a particular B-type of jump at abrupt drop, were tested. Fig. C-7 gives a plot of ζ against λ . It is surprising to note the good agreement of the data with the present curve. The scale factor X/y_1 when plotted against F_1 , in Fig. C-8, however, is seen to depend on the relative height of the drop, h/y_1 , also. There are not sufficient data available to predict the variation of X/y_1 with F_1 and h/y_1 , for this type of jump.

C.5 Conclusion

The study of the available data indicates that the profiles of the hydraulic jump in a rectangular channel are similar. The similarity curve (Table C-1) together with the variation of the horizontal scale (Eq. C.3) provide a simple means of predicting the profile of the jump.



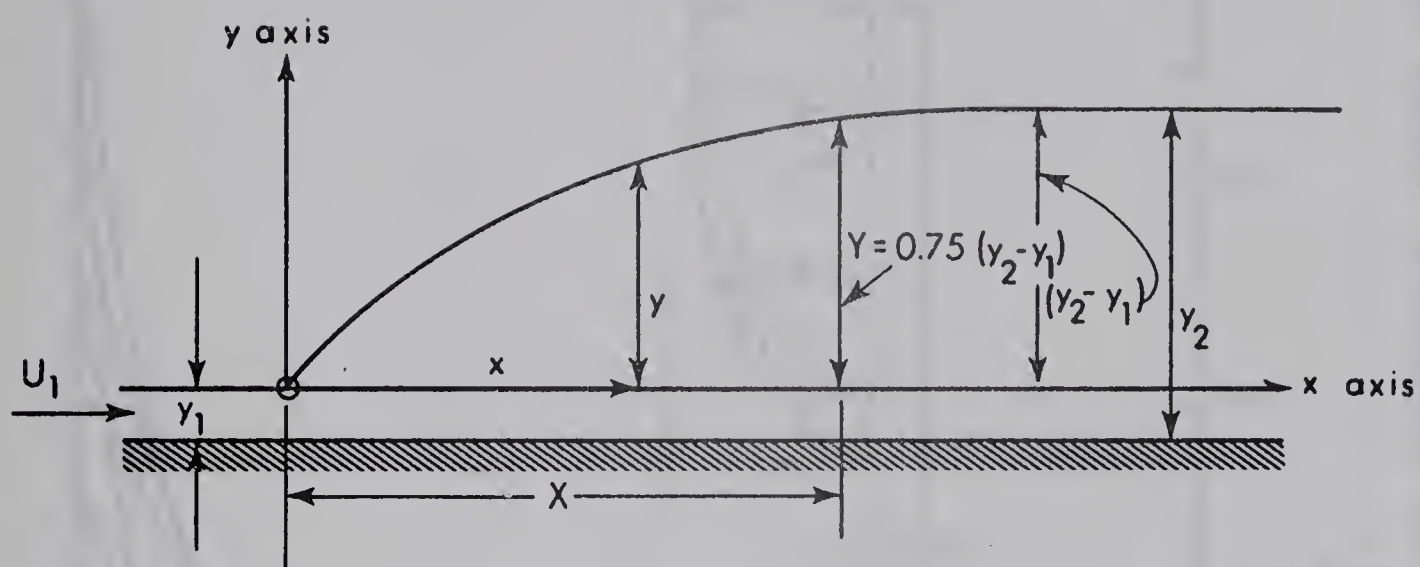


FIG. C-1. DEFINITION SKETCH

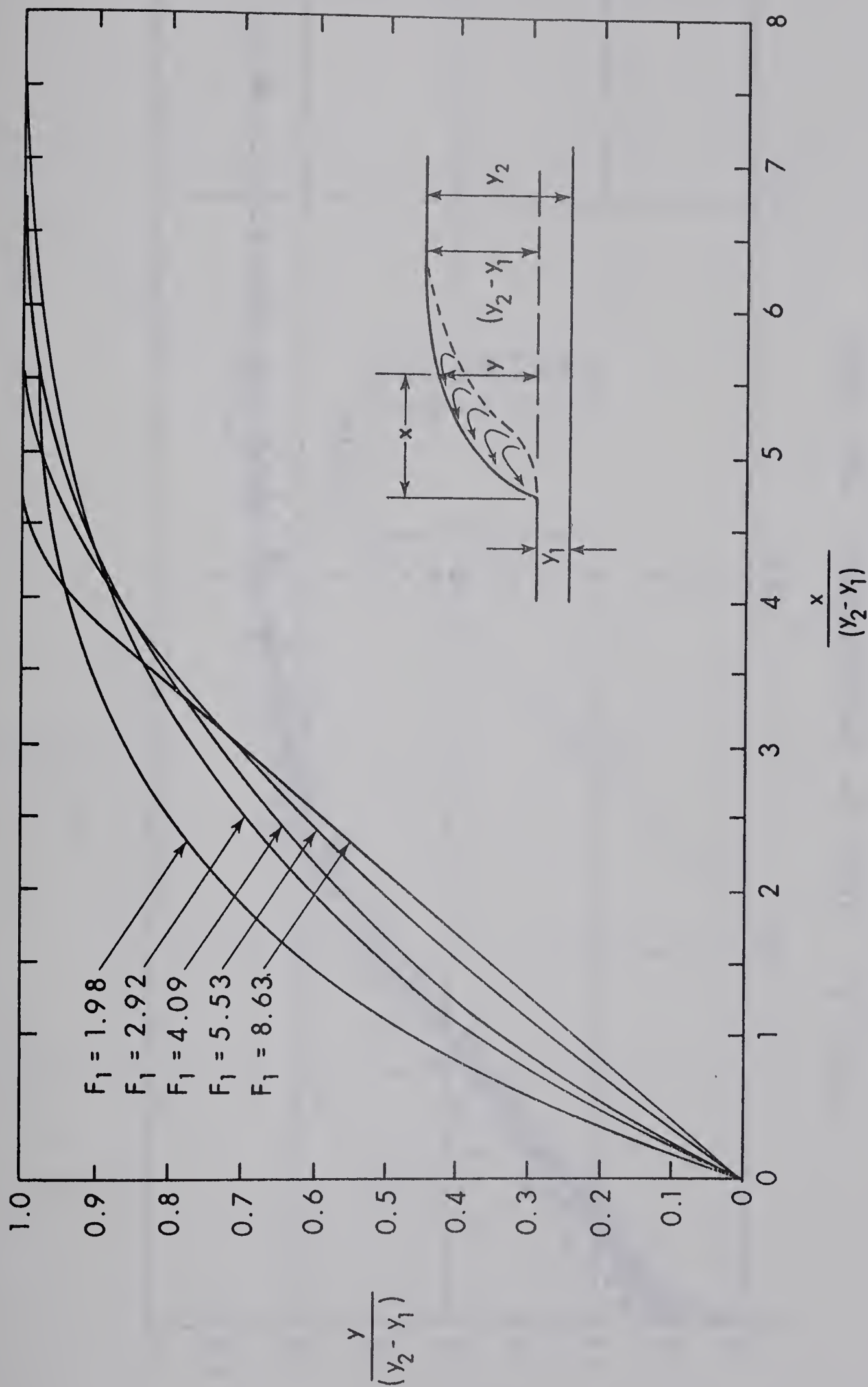


FIG. C-2. DIMENSIONLESS SURFACE PROFILES OF HYDRAULIC JUMPS IN HORIZONTAL CHANNELS. [Bakhmeteff - Matzke]

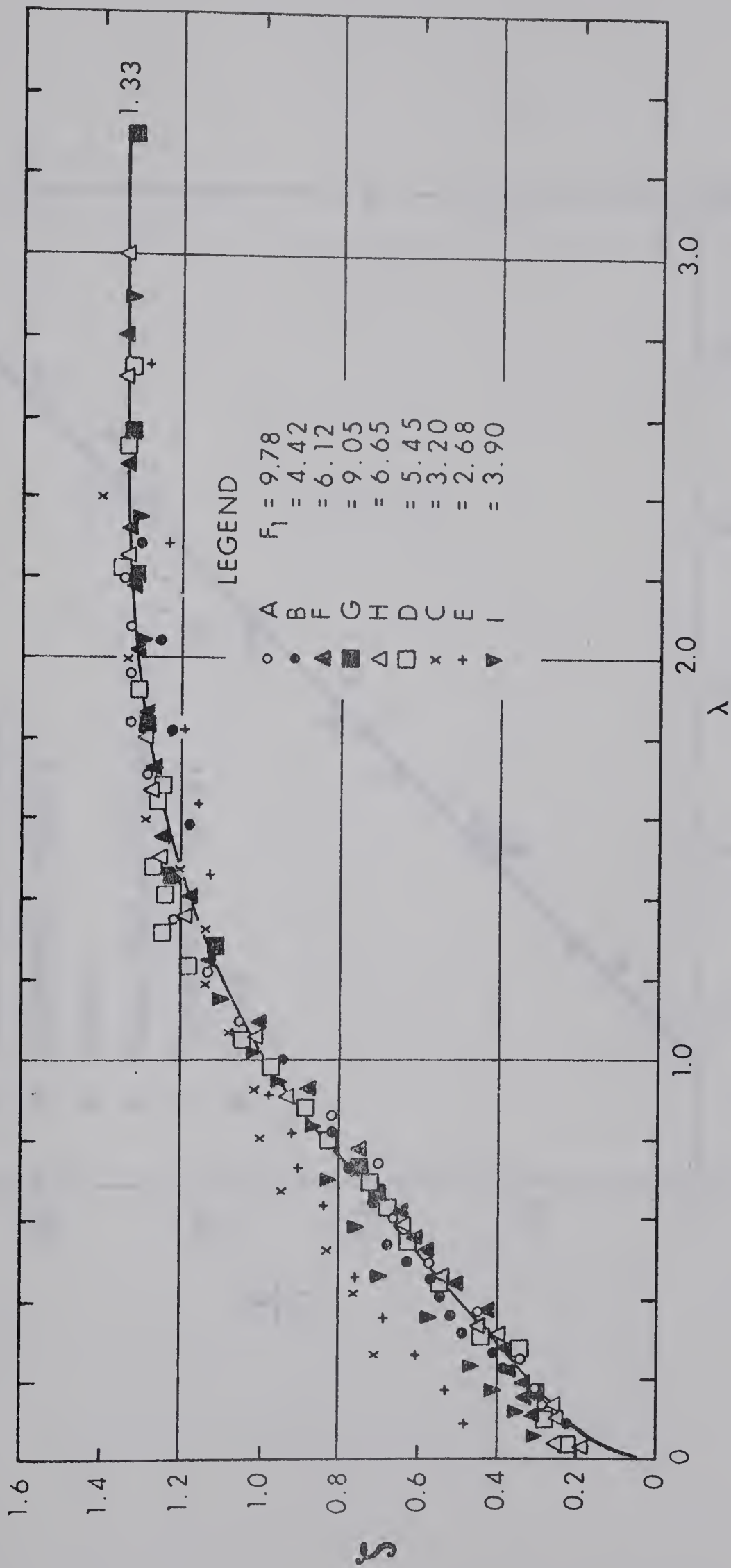


FIG-C-3. STUDY OF RAJARATNAM'S 1965 DATA

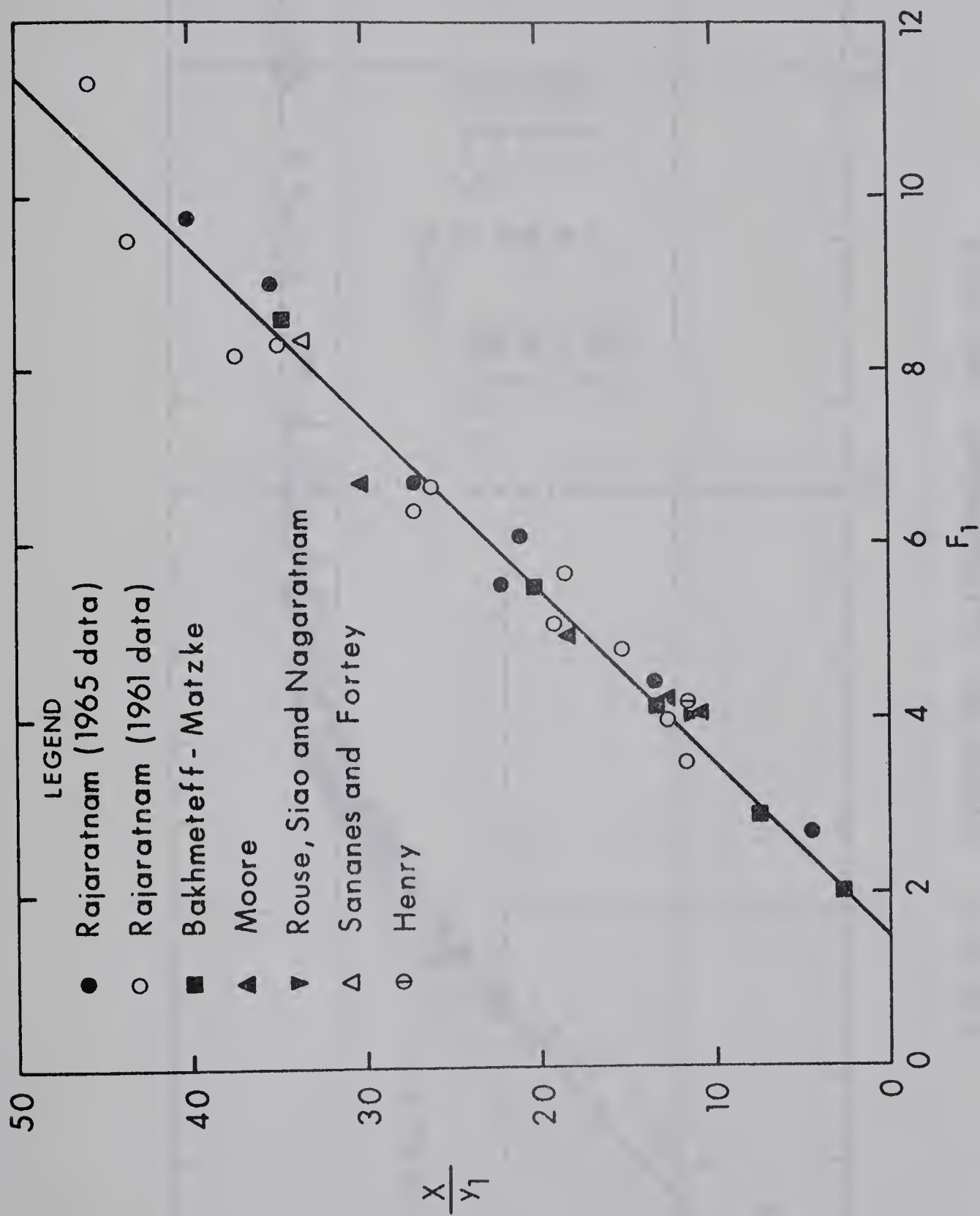


FIG-C-4. STUDY OF THE SCALE FACTOR, X/y_1

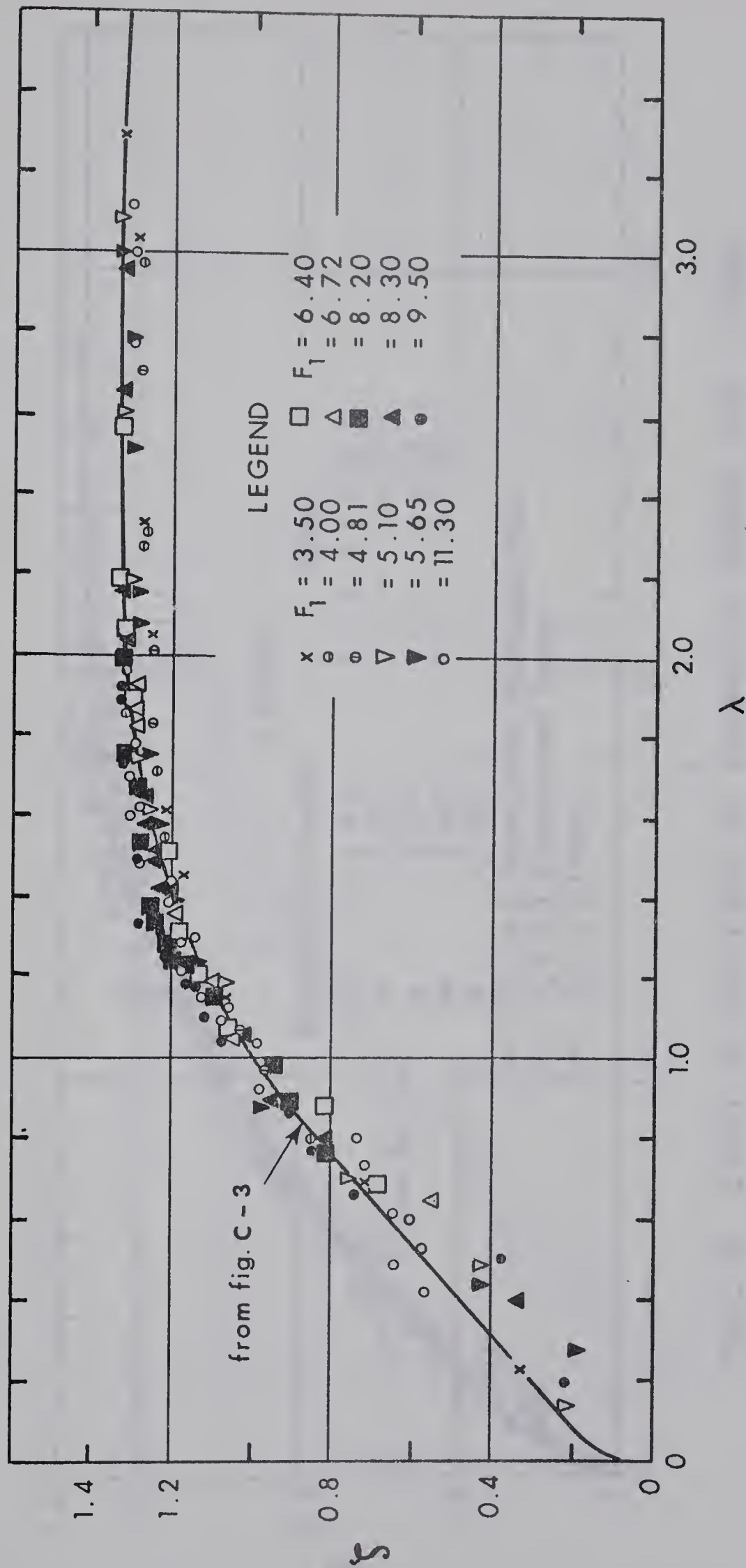


FIG-C-5. STUDY OF RAJARATNAM'S 1961 DATA

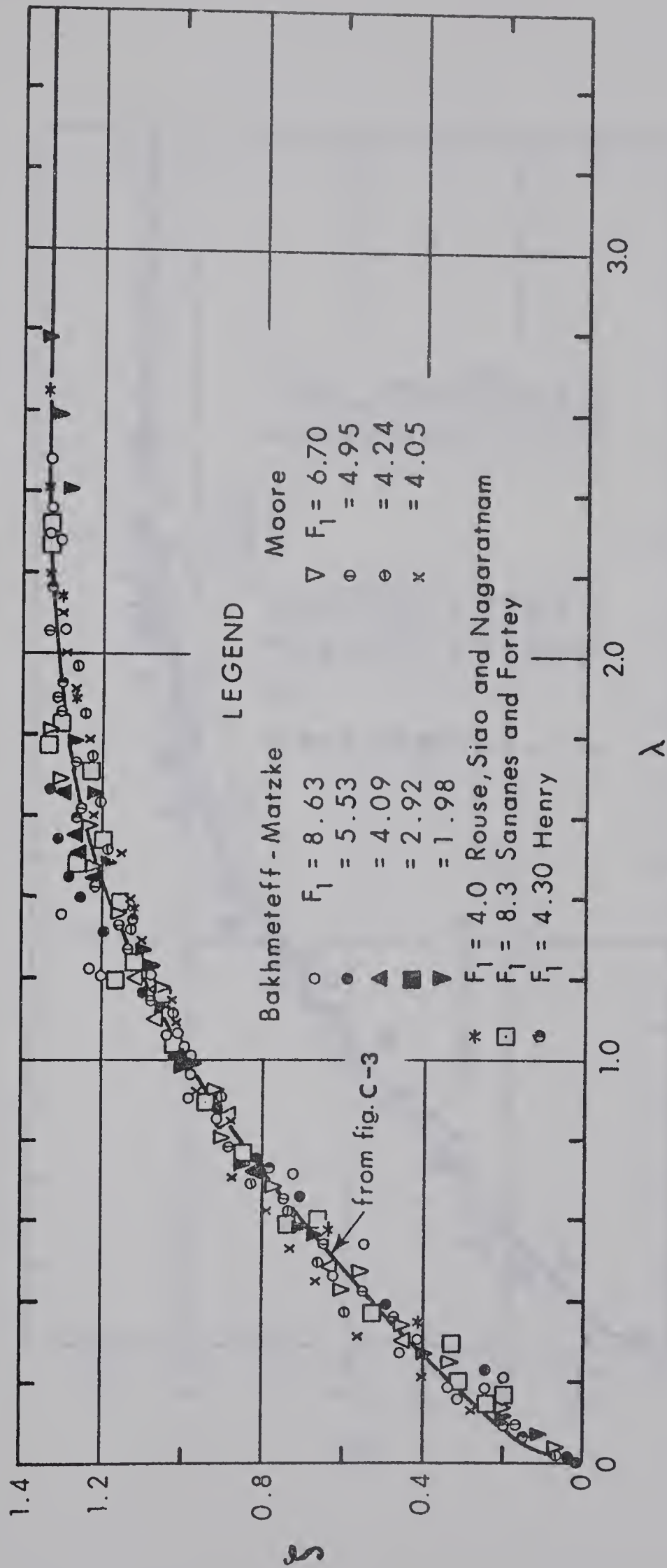
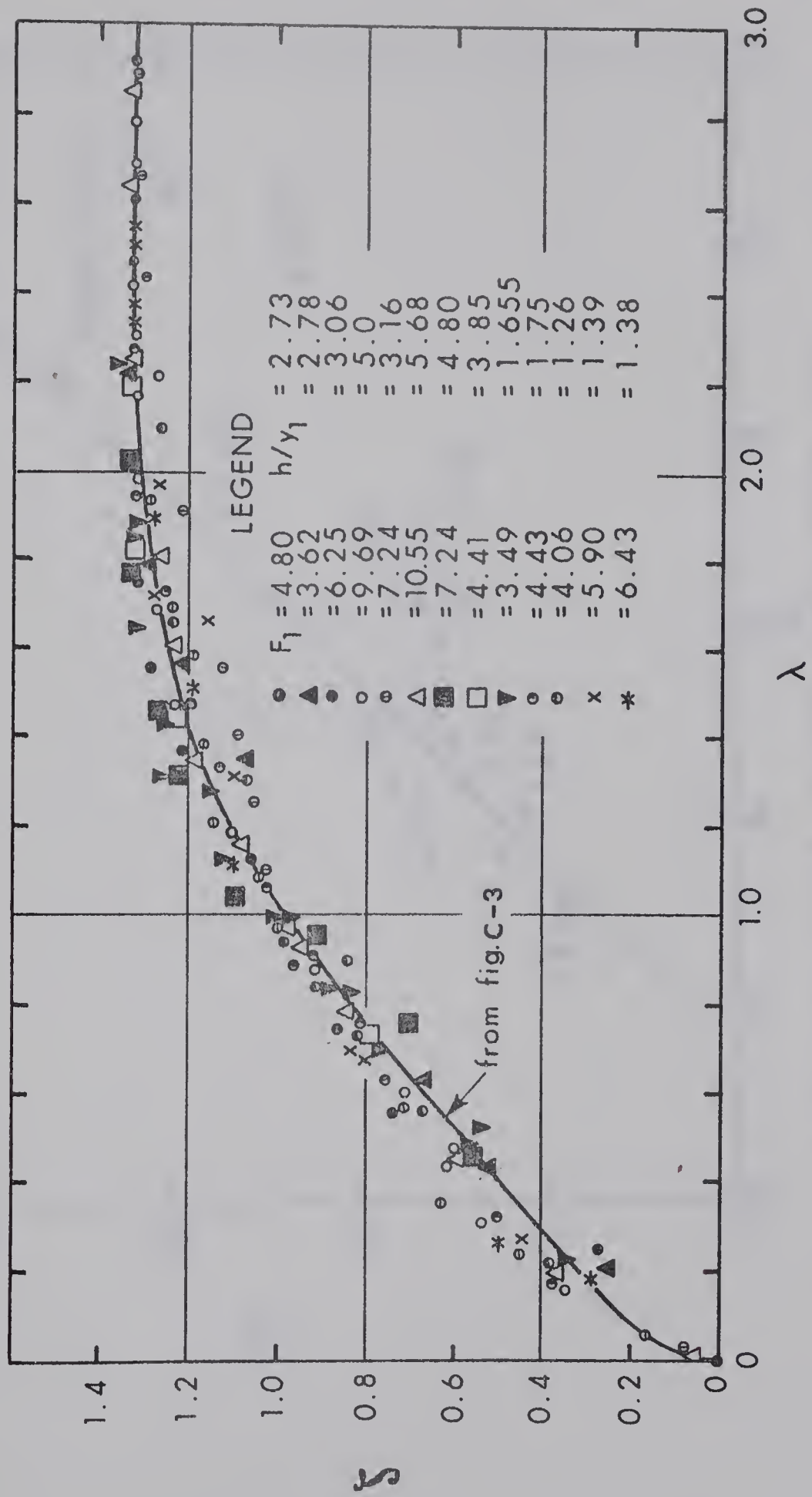


FIG-C-6. STUDY OF THE DATA OF BAKHMETEFF - MATZKE AND OTHERS



FIG·C-7. STUDY OF ORTIZ DATA (B JUMPS AT ABRUPT DROPS)

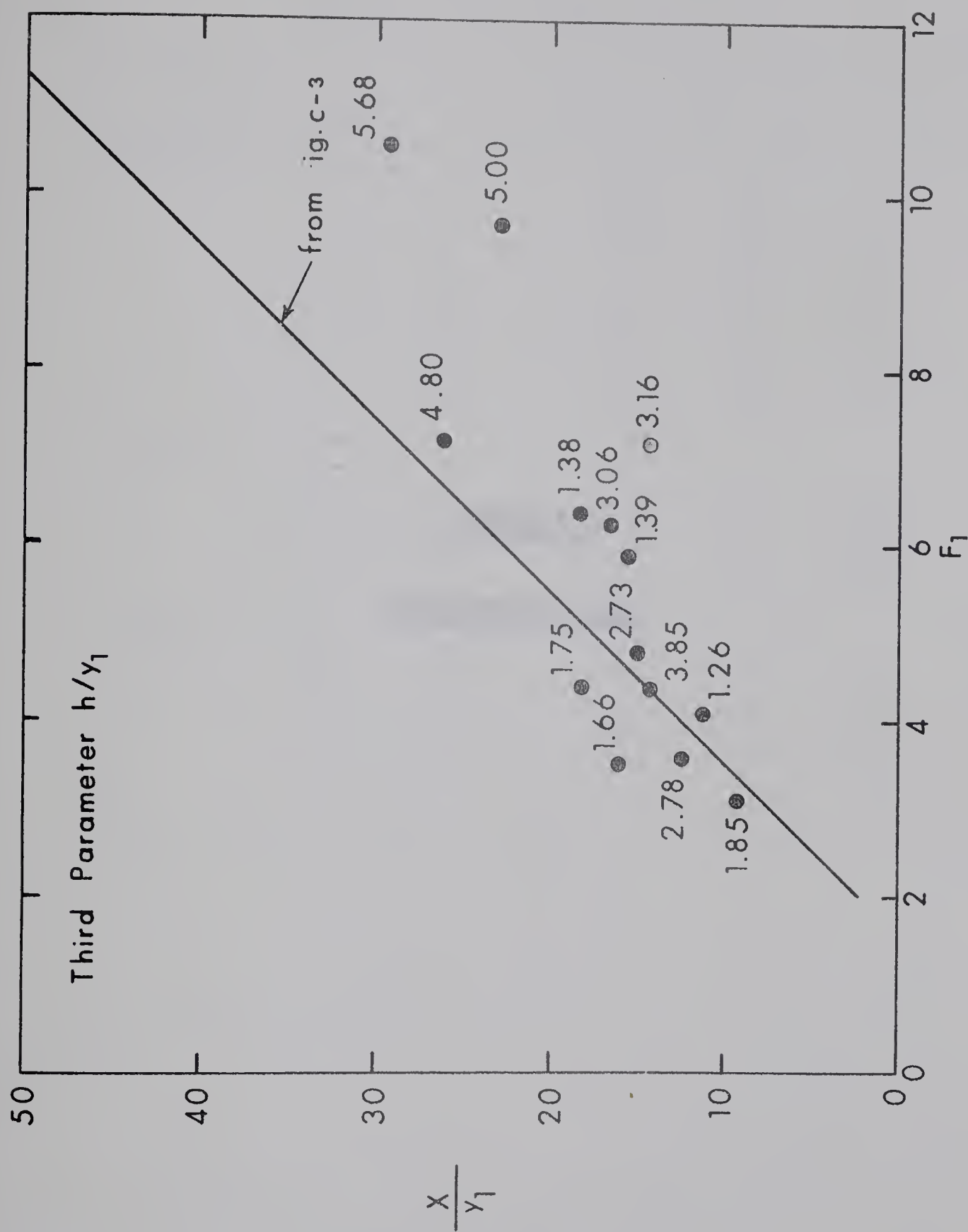


FIG. C - 8. SCALE FACTOR FOR ORTIZ DATA

APPENDIX D

EXPERIMENTAL DATA

TABLE D-1

WATER WALL JET DATA

Velocity Profile Characteristics

Run	x inches	x/y_o	u_m/U_o	δ_1/y_o	δ/y_o
II-E-1	2.0	1.88	1.00	--	--
	10.6	10.0	0.930	1.56	0.40
	16.0	15.0	0.835	2.04	0.40
	21.3	20.0	0.765	2.60	0.53
	26.6	25.0	0.710	3.00	0.51
	31.9	30.0	0.665	3.58	0.63
	36.2	34.0	0.630	3.83	0.63
	42.5	40.0	0.590	4.08	0.68
	47.8	45.0	0.546	4.60	0.57
I-E-1	1.0	0.73	1.00	--	--
	13.0	9.5	0.952	1.57	0.305
	26.0	18.9	0.830	2.52	0.350
	42.0	30.6	0.705	3.60	0.568
	58.0	42.2	0.610	4.63	0.785
I-E-2	1.0	1.15	1.00	--	--
	14.0	16.0	0.820	2.26	0.480
	22.0	25.0	0.690	3.29	0.520
	32.0	36.6	0.600	4.32	0.617
	44.0	50.2	0.524	5.60	0.755
	54.0	61.6	0.471	7.00	1.09

TABLE D-2
WATER WALL JET DATA

Variation of C_f

Run: I-E-1		Run: I-E-2		Run: II-E-1	
x/y_o	$C_f \times 10^3$	x/y_o	$C_f \times 10^3$	x/y_o	$C_f \times 10^3$
1.0	3.50	2.0	3.57	1.88	3.67
5.0	3.50	4.0	3.57	10.63	3.83
7.3	3.57	6.9	3.57	15.0	3.00
9.5	3.57	9.2	3.22	20.0	2.89
11.6	3.40	11.4	3.14	25.0	2.69
14.8	3.24	14.9	3.08	30.0	2.22
16.0	3.07	18.3	2.83	35.0	1.97
18.9	2.86	21.7	2.50	40.0	1.50
21.8	2.72	25.2	2.24	45.0	1.41
24.7	2.50	29.7	2.04	51.6	1.17
27.6	2.33	34.3	1.79		
30.6	2.17	39.0	1.62		
33.4	2.03	43.4	1.49		
36.3	1.86	48.0	1.32		
39.2	1.70	52.5	1.17		
42.2	1.62	57.0	1.09		
45.0	1.57	62.0	0.93		
48.0	1.49	66.0	0.83		
51.0	1.34	71.0	0.73		
		75.5	0.685		
		80.0	0.63		

TABLE D-3
RE-ATTACHED WALL JET (NOZZLE OUTLET)

Velocity Profile Characteristics

Run	x/y_o	u_m/U_o	δ_1/y_o	Run	x/y_o	u_m/U_o	δ_1/y_o
I-A-2	1.5	1.000	--	I-C-1	1.0	1.000	--
	3.5	0.997	--		5.3	0.932	--
	7.0	0.764	--		8.0	0.766	--
	9.5	0.523	--		13.3	0.680	--
	12.0	0.520	--		18.7	0.690	--
	16.0	0.608	--		24.0	0.658	3.76
	19.5	0.603	3.56		29.4	0.622	3.84
	25.0	0.584	3.84		34.7	0.600	4.67
	32.0	0.561	4.26		40.0	0.570	4.97
	40.0	0.522	4.56	I-D-1	0.9	1.000	--
I-A-3	1.0	1.000	--		3.4	0.967	--
	7.0	0.775	--		4.5	0.910	--
	13.0	0.545	--		7.9	0.845	--
	22.0	0.635	3.66		12.0	0.775	--
	35.0	0.546	4.58		17.9	0.755	2.78
	45.0	0.510	4.80		23.9	0.725	3.13
	55.0	0.463	5.28	I-D-2	0.7	1.000	--
	65.0	0.411	5.74		19.4	0.766	3.31
I-B-1	0.9	1.000	--		37.3	0.625	4.16
	4.6	0.981	--		46.3	0.555	5.10
	12.7	0.628	--	I-E-1	0.7	1.000	--
	15.5	0.445	--		9.5	0.952	1.57
	36.4	0.474	6.87		18.9	0.830	2.52
	45.5	0.468	7.68		30.6	0.705	3.60
	54.5	0.440	8.08		42.2	0.610	4.63
	72.6	0.392	9.15	I-E-2	1.1	1.000	--
I-B-2	0.9	1.000	--		16.0	0.820	2.26
	7.3	0.802	--		25.0	0.690	3.29
	10.9	0.610	--		36.6	0.600	4.32
	23.6	0.436	--		50.2	0.524	5.60
	41.8	0.441	6.98		61.6	0.471	7.00
	60.0	0.404	8.08				
	78.0	0.358	9.20				

TABLE D-4

RE-ATTACHED WALL JET (SLUICE GATE OUTLET)

Velocity Profile Characteristics

Run	x/y_o^*	u_m/U_o	δ_1/y_o^*	Run	x/y_o^*	u_m/U_o	δ_1/y_o^*
I(S)-A-1	0.584	1.00	--	I(S)-C	1.55	1.00	--
	2.34	0.99	--		6.21	0.790	--
	4.67	0.875	--		9.32	0.615	--
	7.00	0.834	--		15.50	0.706	2.40
	10.50	0.807	1.43		24.80	0.645	2.72
	14.00	0.770	1.69		35.70	0.525	3.34
	18.70	0.762	2.06		46.60	0.476	3.83
	23.40	0.729	2.38				
	35.00	0.615	3.22				
	44.40	0.535	3.58				
I(S)-A-2	1.17	1.00	--	I(S)-D	0.926	1.00	--
	2.94	0.965	--		1.850	1.00	--
	4.70	0.926	--		3.71	0.97	--
	8.22	0.904	1.49		6.01	0.80	--
	12.90	0.865	1.69		8.34	0.82	--
	18.70	0.790	1.97		13.90	0.80	1.84
	25.80	0.695	2.60		20.40	0.745	2.19
	32.80	0.625	3.10		27.80	0.672	2.78
	41.10	0.556	3.71		33.40	0.635	3.06
I(S)-B	0.78	1.00	--				
	1.94	0.992	--				
	3.49	0.962	--				
	6.20	0.946	1.42				
	10.85	0.906	1.68				
	15.50	0.845	1.96				
	20.90	0.745	2.48				
	27.10	0.695	2.85				

TABLE D-5
RE-ATTACHED WALL JET

Bed Shear Stress Distribution Data

Outlet	Expt.	τ_{om} lbs/sft	$C_{fm} = \frac{\tau_{om}}{\rho U_o^2 / 2}$ $\times 10^3$	θ_1 in.	θ_1/h	y_o/h	h/y_o
Nozzle	I-A-2	0.142	2.17	43.25	13.10	0.302	3.31
	I-A-3	0.205	2.24	41.25	12.40	0.302	3.31
	I-B-1	0.131	1.67	27.00	8.15	0.166	6.02
	I-B-2	0.155	1.35	32.50	9.82	0.166	6.02
	I-C-1	0.240	2.55	33.50	24.90	0.559	1.79
	I-D-1	0.211	3.03	44.00	32.70	1.00	1.00
	I-D-2	0.193	3.11	46.00	34.20	1.00	1.00
	I-E-1	0.250	3.59	--	--	0	0
	I-E-2	0.250	3.59	--	--	0	0
Sluice Gate	I(S)-A-1	0.265	4.05	23.25	17.30	0.636	1.57
	I(S)-A-2	0.375	3.88	23.50	17.50	0.633	1.58
	I(S)-B	0.220	4.40	34.00	25.30	0.961	1.04
	I(S)-C	0.243	3.00	18.00	5.40	0.194	5.15
	I(S)-D	0.260	3.61	30.25	9.15	0.327	3.06

TABLE D-6

WALL JETS IN WIDER CHANNELS

Centerline Velocity Distribution Characteristics

Run	x	δ_1	δ	x/r'	x/y_o	u_m/U_o	$(\delta_1 - \delta)$	δ/x
	in.	ft.	ft.				y_o	
II-A-1	2.0	--	--	2.44	1.78	1.00	--	--
	5.0	0.135	0.048	6.07	4.42	0.99	0.93	0.115
	10.0	0.168	0.065	12.2	8.89	0.96	1.06	0.078
	15.0	0.195	0.055	18.3	13.30	0.87	1.49	0.044
	20.0	0.204	0.040	24.4	17.75	0.79	1.74	0.024
	25.0	0.252	0.055	30.5	22.20	0.715	2.10	0.0265
	35.0	0.300	0.060	42.7	31.10	0.623	2.56	0.0206
II-A-2	2.00	--	--	2.44	1.78	1.00	--	--
	5.00	0.105	0.040	6.07	4.42	0.997	0.69	0.0963
	11.25	0.150	0.035	13.7	10.0	0.935	1.22	0.0374
	16.9	0.185	0.040	20.6	15.0	0.840	1.55	0.0284
	22.5	0.255	0.060	27.4	20.0	0.745	2.08	0.0320
	33.8	0.305	0.075	41.2	30.0	0.626	2.46	0.0267
	45.0	0.370	0.042	55.0	40.0	0.507	3.52	0.0107
	50.6	0.460	0.060	61.7	45.0	0.422	4.27	0.0142
II-A-3	2.0	--	--	2.44	1.78	1.0	--	--
	5.73	--	--	6.86	5.00	1.0	--	--
	11.25	0.152	0.040	13.7	10.0	0.935	1.21	0.0430
	16.9	0.203	0.050	20.6	15.0	0.832	1.61	0.0355
	22.5	0.237	0.050	27.4	20.0	0.748	2.00	0.0267
	28.2	0.280	0.055	34.3	25.0	0.676	2.41	0.0231
	33.7	0.292	0.055	41.2	30.0	0.617	2.54	0.0193
	39.4	0.320	0.050	48.0	35.0	0.548	2.89	0.0150
II-B-1	2.50	--	--	2.38	1.54	1.00	--	--
	19.5	0.241	0.070	18.5	12.0	0.90	1.27	0.0431
	26.0	0.282	0.065	24.7	16.0	0.827	1.61	0.0301
	32.5	0.310	0.065	30.9	20.0	0.738	1.82	0.0241
	39.0	0.335	0.055	37.0	24.0	0.681	2.07	0.0169
	45.5	0.348	0.060	43.2	28.0	0.618	2.14	0.0158
II-E-1	2.00	--	--	--	1.88	1.00	--	--
	10.63	0.138	0.035	--	10.0	0.930	1.16	0.040
	15.95	0.180	0.035	--	15.0	0.835	1.64	0.0263
	21.25	0.230	0.047	--	20.0	0.765	2.07	0.0265
	26.60	0.265	0.045	--	25.0	0.710	2.49	0.0204
	31.90	0.316	0.055	--	30.0	0.665	2.95	0.0210
	36.20	0.338	0.055	--	34.0	0.630	3.20	0.0184
	42.50	0.360	0.060	--	40.0	0.590	3.40	0.0170
	47.80	0.405	0.050	--	45.0	0.546	4.03	0.0127

TABLE D-6 (continued)

Run	x in.	δ_1 ft.	δ ft.	x/r'	x/y _o	u _m /U _o	$\frac{(\delta_1 - \delta)}{y_o}$	δ/x
II-F-1	2.00	--	--	2.32	1.88	1.00	--	--
	10.65	0.140	0.038	12.3	10.0	0.965	1.13	0.045
	13.90	0.162	0.045	16.1	13.1	0.906	1.32	0.039
	21.25	0.225	0.045	24.6	20.0	0.800	2.04	0.0255
	26.60	0.270	0.055	30.8	25.0	0.745	2.44	0.0248
	31.80	0.307	0.060	37.0	30.0	0.685	2.80	0.0226
	37.2	0.329	0.050	43.1	35.0	0.645	3.17	0.0166
	42.5	0.360	0.060	49.3	40.0	0.600	3.39	0.0170
II-F-2	2.00	--	--	2.32	1.88	1.00	2.32	--
	9.6	0.130	0.035	11.1	9.00	0.975	11.1	0.0445
	15.9	0.172	0.045	18.5	15.0	0.875	18.5	0.0340
	23.4	0.240	0.055	27.1	22.0	0.767	27.1	0.0282
	29.8	0.282	0.055	34.5	28.0	0.710	34.5	0.0221
	36.1	0.332	0.050	41.9	34.0	0.645	41.9	0.0168
	44.6	0.400	0.055	51.7	42.0	0.586	51.7	0.0148
	53.0	0.450	0.085	61.6	50.0	0.515	61.6	0.0192
II-B-2	2.50	--	--	2.38	1.54	1.000	--	--
	14.6	0.210	0.065	13.9	9.0	0.948	1.075	0.0534
	22.8	0.267	0.075	21.6	14.0	0.866	1.415	0.0496
	30.9	0.310	0.055	29.3	19.0	0.760	1.890	0.0214
	40.7	0.336	0.050	38.6	25.0	0.675	2.110	0.0148
	50.5	0.439	0.085	47.8	31.0	0.565	2.614	0.0202
	56.8	0.480	0.095	54.0	35.0	0.502	2.800	0.0212
II-C-1	1.75	--	--	2.67	1.55	1.00	--	--
	9.00	0.130	0.055	13.8	8.00	0.967	0.80	0.0735
	13.5	0.150	0.055	20.6	12.00	0.885	1.01	0.0490
	18.0	0.184	0.052	27.6	16.0	0.784	1.36	0.0346
	22.5	0.205	0.065	34.5	20.0	0.675	1.49	0.0348
	27.0	0.230	0.055	41.3	24.0	0.605	1.87	0.0245
	31.5	0.255	0.055	48.2	28.0	0.540	2.13	0.0210
II-C-2	2.00	--	--	2.73	1.78	1.00	--	--
	11.25	0.138	0.050	17.4	10.0	0.927	0.93	0.0535
	16.90	0.175	0.055	25.8	15.0	0.815	1.28	0.0391
	22.50	0.220	0.065	34.5	20.0	0.681	1.65	0.0347
	28.30	0.235	0.060	43.1	25.0	0.600	1.76	0.0300
	33.75	0.268	0.040	51.7	30.0	0.495	2.43	0.0143
	39.90	0.284	0.055	60.2	35.0	0.440	2.45	0.0168

TABLE D-6 (continued)

Run	x in.	δ_1 ft.	δ ft.	x/r'	x/y_o	u_m/U_o	$\frac{(\delta_1 - \delta)}{y_o}$	δ/x
II-D-1	2.00	--	--	5.56	1.78	1.00	--	--
	6.75	0.103	0.045	18.8	6.00	0.92	0.54	0.080
	10.13	0.107	0.035	28.1	9.00	0.815	0.77	0.0415
	13.50	0.130	0.040	37.5	12.00	0.665	0.97	0.0355
	18.00	0.154	0.040	50.0	16.00	0.526	1.21	0.0266
	22.50	0.170	0.040	62.5	20.00	0.430	1.38	0.0213
II-D-2	2.00	--	--	5.56	1.78	1.00	--	--
	5.63	0.102	0.040	15.6	5.00	0.930	0.66	0.085
	9.00	0.105	0.030	25.0	8.00	0.850	0.84	0.040
	11.3	0.110	0.030	31.2	10.00	0.750	0.86	0.032
	15.8	0.125	0.030	43.8	14.0	0.600	1.01	0.0228
	20.0	0.145	0.030	56.2	18.0	0.490	1.23	0.0168
	24.8	0.153	0.040	68.7	22.0	0.440	1.23	0.0195
	29.2	0.188	0.030	81.2	26.0	0.340	1.70	0.0123

TABLE D-7

EXPERIMENTAL DATA FOR R-JUMPS

No.	y_o (in)	b (in)	U_o (ft/sec)	F_o	$\alpha = \frac{b}{B}$	y_t (in)	$\frac{y_t}{y_o}$	L_r (in)	L_j (in)	L_o (in)	L_l (in)
AR-1	1.08	9.0	7.05	4.13	0.50	3.70	3.43	14.0	26.0	10.0	26.0
-2	1.08	9.0	9.28	5.45	0.50	4.90	4.54	17.0	26.0	15.0	31.0
-3	1.08	9.0	10.80	6.33	0.50	5.70	5.28	17.0	35.0	18.0	35.0
-4	1.08	9.0	12.00	7.02	0.50	6.60	6.11	19.0	53.0	20.0	35.0
-5	1.08	9.0	13.65	8.00	0.50	7.30	6.76	20.0	56.0	22.0	40.0
-6	1.08	9.0	15.10	8.88	0.50	8.20	7.60	28.0	70.0	26.0	42.0
-7	1.08	9.0	4.10	2.40	0.50	2.40	2.22	6.0	15.0	7.0	17.0
-8	1.08	9.0	5.00	2.94	0.50	2.70	2.50	9.0	15.0	8.5	19.0
-9	1.08	9.0	7.85	4.60	0.50	4.20	3.89	15.0	32.0	13.0	28.0
BR1-1	1.25	6.0	6.20	3.38	0.33	2.90	2.32	9.0	44.0	12.0	26.0
-2	1.25	6.0	8.30	4.52	0.33	3.80	3.04	11.0	65.0	16.0	32.0
-3	1.25	6.0	10.40	5.78	0.33	4.60	3.68	14.0	41.0	19.5	44.0
-4	1.25	6.0	12.80	6.97	0.33	5.80	4.64	22.0	47.0	26.0	46.0
-5	1.25	6.0	14.70	8.00	0.33	6.40	5.11	24.0	43.0	29.0	50.0
-6	1.25	6.0	15.10	8.22	0.33	6.70	5.35	26.0	41.0	30.0	52.0
-7	1.25	6.0	9.22	5.02	0.33	4.20	3.36	16.0	46.0	19.0	34.0
-8	1.25	6.0	7.10	3.88	0.33	3.20	2.56	10.0	23.0	14.0	27.0
BR2-1	3.10	6.0	7.20	2.53	0.33	5.50	1.78	12.0	36.0	9.0	18.0
-2	3.10	6.0	8.92	3.14	0.33	6.90	2.22	14.0	34.0	11.5	20.0
-3	3.10	6.0	10.60	3.73	0.33	8.30	2.68	21.0	38.0	14.5	24.0
-4	3.10	6.0	12.30	4.32	0.33	9.30	3.00	24.0	55.0	16.0	30.0
BR3-1	1.63	6.0	4.62	2.20	0.33	2.50	1.54	6.0	30.0	9.0	16.0
-2	1.63	6.0	6.75	3.22	0.33	3.60	2.21	10.0	34.0	12.0	24.0
-3	1.63	6.0	9.00	4.29	0.33	4.90	3.01	14.0	30.0	14.0	28.0
-4	1.63	6.0	11.00	5.25	0.33	5.80	3.56	19.0	32.0	18.0	36.0
-5	1.63	6.0	14.50	6.91	0.33	7.30	4.48	24.0	49.0	26.0	49.0
-6	1.63	6.0	12.60	6.01	0.33	6.40	3.92	20.0	47.0	22.5	46.0
CR-1	1.25	3.0	5.36	2.92	0.17	1.40	1.12	4.0	26.0	13.5	28.0
-2	1.25	3.0	6.74	3.67	0.17	1.60	1.28	4.0	22.0	16.0	36.0
DR-1	1.06	12.0	4.32	2.56	0.67	2.40	2.26	4.0	21.0	5.5	13.0
-2	1.06	12.0	6.50	3.86	0.67	3.80	3.59	8.0	35.0	7.0	15.0
-3	1.06	12.0	8.15	4.84	0.67	4.90	4.62	15.0	70.0	9.0	20.0
-4	1.06	12.0	9.40	5.58	0.67	5.60	5.28	19.0	56.0	10.5	22.0
-5	1.06	12.0	10.30	6.11	0.67	6.20	5.85	22.0	58.0	12.0	24.0
-6	1.06	12.0	11.40	6.76	0.67	6.90	6.50	22.5	57.0	13.0	25.0
-7	1.06	12.0	12.70	7.54	0.67	7.70	7.26	30.0	60.0	14.0	25.0
-8	1.06	12.0	14.50	8.61	0.67	8.70	8.20	28.0	68.0	16.5	30.0
-9	1.06	12.0	5.79	3.44	0.67	3.40	3.20	8.0	26.0	7.0	16.0
ER-1	1.09	15.0	4.73	2.77	0.83	3.20	2.93	8.0	16.0	--	6.0
-2	1.09	15.0	6.28	3.67	0.83	4.20	3.85	12.0	43.0	--	7.0
-3	1.09	15.0	7.80	4.56	0.83	5.40	4.95	17.0	53.0	--	9.0
-4	1.09	15.0	8.95	5.24	0.83	6.20	5.69	20.0	48.0	--	9.5
-5	1.09	15.0	10.35	6.05	0.83	7.20	6.60	26.0	50.5	--	11.5
-6	1.09	15.0	11.80	7.02	0.83	8.30	7.62	36.0	70.0	--	12.0
-7	1.09	15.0	13.50	7.90	0.83	9.60	8.80	42.0	77.5	---	12.5

TABLE D-8

EXPERIMENTAL DATA FOR S-JUMPS

No.	y_o (in)	b (in)	U (ft/sec)	F _o	$\alpha = \frac{b}{B}$	y_t (in)	r' (in)	$\frac{y_t}{r'}$	F' _o	$\frac{b}{y_o}$	L _j (in)	y ₃ (in)
AS1-1	1.08	9.0	7.70	4.51	0.50	6.40	0.872	7.35	5.02	8.33	60.0	4.60
-2	1.08	9.0	8.85	5.19	0.50	7.10	0.872	8.15	5.78	8.33	66.0	4.80
-3	1.08	9.0	10.25	6.01	0.50	7.70	0.872	8.84	6.70	8.33	76.0	4.70
-4	1.08	9.0	12.00	7.02	0.50	8.90	0.872	10.20	7.82	8.33	74.0	5.40
-5	1.08	9.0	13.30	7.71	0.50	9.60	0.872	11.00	8.60	8.33	82.0	5.40
-6	1.08	9.0	6.35	3.73	0.50	5.80	0.872	6.65	4.16	8.33	62.0	4.50
-7*	1.08	9.0	13.10	7.69	0.50	9.40	0.872	10.75	8.56	8.33	78.0	5.50
AS2-1	2.65	9.0	5.20	1.94	0.50	6.30	1.665	3.78	2.45	3.40	46.0	4.50
-2	2.65	9.0	6.70	2.50	0.50	8.00	1.665	4.80	3.16	3.40	66.0	5.60
-3	2.65	9.0	8.50	3.18	0.50	9.00	1.665	5.40	4.02	3.40	70.0	5.80
-4	2.65	9.0	10.20	3.82	0.50	10.70	1.665	6.42	4.84	3.40	80.0	7.50
-5	2.65	9.0	11.70	4.36	0.50	12.3	1.665	7.38	5.50	3.40	85.0	8.80
-6	2.65	9.0	12.80	4.80	0.50	13.6	1.665	8.16	6.06	3.40	88.0	8.90
BS1-1	1.25	6.0	5.03	2.75	0.33	4.70	0.882	5.32	3.27	5.33	52.0	4.00
-2	1.25	6.0	7.07	3.86	0.33	5.60	0.882	6.35	4.60	5.33	56.0	4.50
-3	1.25	6.0	8.14	4.44	0.33	6.50	0.882	7.35	5.30	5.33	58.0	5.15
-4	1.25	6.0	10.00	5.46	0.33	7.00	0.882	7.92	6.50	5.33	60.0	4.90
-5	1.25	6.0	11.60	6.35	0.33	7.90	0.882	8.95	7.55	5.33	64.0	5.50
-6	1.25	6.0	12.70	6.94	0.33	8.70	0.882	9.85	8.25	5.33	72.0	5.60
-7*	1.25	6.0	13.80	7.55	0.33	9.20	0.882	10.40	8.98	5.33	70.0	5.90
BS2-1	1.69	6.0	5.56	2.61	0.33	6.30	1.08	5.83	3.26	3.56	50.0	5.40
-2	1.69	6.0	7.05	3.38	0.33	6.90	1.08	6.40	4.13	3.56	58.0	5.70
-3	1.69	6.0	8.75	4.11	0.33	8.00	1.08	7.40	5.13	3.56	62.0	5.90
-4	1.69	6.0	10.80	5.10	0.33	8.90	1.08	8.23	6.35	3.56	70.0	6.00
-5	1.69	6.0	12.00	5.65	0.33	9.80	1.08	9.06	7.05	3.56	76.0	6.60
-6	1.69	6.0	14.20	6.70	0.33	11.30	1.08	10.47	8.32	3.56	82.0	7.60
DS-1	1.06	12.0	5.95	3.54	0.67	5.20	0.900	5.78	3.85	11.30	64.0	3.60
-2	1.06	12.0	7.17	4.32	0.67	5.70	0.900	6.33	4.70	11.30	68.0	3.50
-3	1.06	12.0	8.60	5.10	0.67	6.60	0.900	7.33	5.55	11.30	72.0	3.70
-4	1.06	12.0	10.30	6.12	0.67	7.60	0.900	8.45	6.65	11.30	76.0	3.90
-5	1.06	12.0	11.80	7.00	0.67	8.50	0.900	9.45	7.61	11.30	78.0	4.00
-6	1.06	12.0	13.10	7.77	0.67	9.40	0.900	10.42	8.45	11.30	82.0	4.20
-7*	1.06	12.0	14.30	8.50	0.67	10.20	0.900	11.32	9.25	11.30	76.0	4.70
-8	1.06	12.0	4.78	2.90	0.67	4.10	0.900	4.56	3.15	11.30	45.0	2.75
-9*	1.06	12.0	8.06	4.79	0.67	6.15	0.900	6.83	5.21	11.30	64.0	3.60
ES-1	1.09	15.0	5.40	3.16	0.83	4.50	0.952	4.72	3.39	13.75	50.0	2.50
-2	1.09	15.0	6.30	3.70	0.83	5.20	0.952	5.46	3.96	13.75	50.0	2.60
-3*	1.09	15.0	11.40	6.67	0.83	9.10	0.952	9.56	7.16	13.75	66.0	3.80
-4	1.09	15.0	7.80	4.55	0.83	6.20	0.952	6.50	4.80	13.75	62.0	3.00
-5	1.09	15.0	9.05	5.29	0.83	7.10	0.952	7.45	5.65	13.75	60.0	3.30
-6	1.09	15.0	10.05	5.87	0.83	7.90	0.952	8.30	6.28	13.75	74.0	3.50
-7	1.09	15.0	13.10	7.65	0.83	10.00	0.952	10.50	8.19	13.75	78.0	3.60

B29879